UNIVERSITAT POLITÈCNICA DE CATALUNYA

DOCTORAL PROGRAMME:

AUTOMATIC CONTROL, ROBOTICS AND COMPUTER VISION (ARV)

DOCTORAL THESIS

HEAT PUMP CONTROLS TO EXPLOIT THE ENERGY FLEXIBILITY OF BUILDING THERMAL LOADS

SUPERVISORS
Dr. Jaume Salom
Dr. Ramon Costa-Castelló

PHD STUDENT
Thibault Q. Péan

NOVEMBER 2019

Heat pump controls to exploit the energy flexibility of building thermal loads

Doctoral thesis

by

Thibault Q. Péan

Acknowledgments

Multilingual and non-exhaustive!

Carrying out a PhD is a long and sometimes difficult process, and this accomplishment could never have been possible without the presence of a number of great people to which I would like to express my gratitude in these few words.

En primer lloc, vull adreçar el meu més sincer agraïment als meus supervisors: Jaume Salom del IREC per guiar-me en aquests darrers tres anys i per sempre darme feedback complet i bons consells, i Ramon Costa Castelló de la UPC per la seva ajuda en qualsevol moment que necessitava il·luminació sobre el món del control. Tots dos heu contribuït a fer d'aquesta tesi el que és avui y a ferme créixer professional- y personalment.

Muchas gracias a todos los colegas pasados y presentes en IREC, Joana, Paolo, Ramon, Joaquim para las ayudas con los modelos de TRNSYS, las discusiones interesantes y sobre todo el buen ambiente de trabajo! También agradezco mucho al equipo de SEILAB en Tarragona, Elena, Ivan y Paco, sin quien la parte experimental del proyecto nunca se podría haber llevado a cabo. Vuestros conocimientos técnicos y capacidades en troubleshooting han sido preciosos cada vez que caía un ensayo (y esto pasó...). Gracias a los estudiantes que han realizado sus trabajos de fin de master con nosotros y que he parcialmente supervisado o simplemente ayudado: Riccardo, Jalomi, Bismark y Antonio.

I should also thank the European Union for providing funding for this research, through the Horizon 2020 research and innovation programme under the Marie Skłodowska-Curie grant agreement No 675318 (INCITE). The Marie Curie actions provided me with great opportunities of collaborations, training, secondments and possibilities to attend high level conferences around the world, for which I am very grateful. Thanks to Marta and my 14 fellow INCITErs, it has always been a pleasure to gather with you all twice a year! Thanks also to Roel de Coninck at 3E and Gowri Suryanarayana at VITO/EnergyVille who welcomed me in their institutions during the two external stays that I carried out in Belgium during this project.

I have had the chance to coincide during my PhD with the IEA EBC Annex 67 about Energy Flexible Buildings, which gave me a lot of possibilities of collaboration with the most renowned experts from all around the world working on topics closely related to my thesis. This was a unique opportunity to be confronted to the latest research on the subject of energy flexibility in buildings and I made sure to fully benefit from it and participate actively in several tasks and working meetings. Thanks also for the collaborations that emerged from the Annex to Kyriaki, Christian, John, Anjukan and Kun. Lidt tilbage i tiden vil jeg gerne sige tak til dem i Danmark der delte deres passion for forskning, og der introducede mig til denne verden, Bjarne, Ongun, Luca, Lefteris, alle kolleger af den International Center for Indoor Environment and Energy på DTU.

Finally, thank you to all my friends of Barcelona, Copenhagen, Angers and anywhere else, un grand merci aux 2000, y darle las gracias especialmente a Alfonso el mejor compi y amigo que me ha aguantado durante los periodos de estrés que cualquier tesis supone. Pour finir, merci infiniment à ma famille, mes parents et frère et soeur qui ont posé les bases d'une éducation et d'une curiosité du monde nécessaire à tout travail de recherche, qui m'ont toujours soutenu dans mes choix et permis de suivre des études supérieures, même si cela supposait de vivre loin, comme je le fais maintenant depuis de nombreuses années. Merci !

Abstract

Urgent actions are required to mitigate climate change and global warming. Decarbonizing our energy systems represents an important step in that direction. For the power grid, this means integrating larger share of renewable sources (RES), such as solar and wind power. Due to their variability and unpredictability, these sources however pose some challenges to the grid if they constitute the main electricity supply: possible supply-demand mismatch, consequent necessity to curtail RES production or to use peak fossil-fueled plants, grid congestions due to prosumers and decentralization, inviability of the other peak power plants without subsidies. Demand-side management (DSM), which consists in increasing the flexibility of the demand-side, constitutes a promising set of solutions to help manage the operation of the grid with high shares of RES. In particular, buildings and their embedded thermal mass can be regarded as thermal storage, and heat pumps represent one of the most ideal means to couple such storage with the power grid and cover the heating, cooling and hot water loads in a more flexible manner.

Smart controls for heat pumps are required to harness the full energy flexibility potential of building thermal loads. A thorough literature review revealed that most strategies used for this purpose can be classified in two categories: rule-based control (RBC) and model predictive control (MPC). RBC is made of simple rules of the form "if a condition is verified, then take an action". MPC is a more advanced strategy that makes use of models and forecasts the behaviour of the systems in the near future in order to find the optimal plan of action. It requires the prior development of models, and the solving of an optimization problem at regular time intervals. For this reason, its development and operating costs are higher, although it outperforms RBC strategies in most cases. Both RBC and MPC can use external signals (named penalty signals in this thesis) to prompt their actions. The price of electricity is most often used for this purpose, leading to strategies that aim to reduce the costs. It was suggested to use also other signals, for this purpose a CO_2 emissions signals was developed and used. This signal was derived from a new methodology presented in this work, and represents the marginal emissions of the grid (MEF): it thus gives a more accurate estimation of the potential impacts of DSM actions in terms of carbon footprint.

In the mark of this thesis, both an RBC and an MPC controllers were developed as supervisory controls for an air-to-water heat pump supplying the heating, cooling and hot water needs of a residential building. The RBC strategy consists in modulating the set-points in the indoor space and in a hot water tank, using the penalty signal as trigger for the modulation. The MPC strategy consists in minimizing the overall summed penalties due to the heat pump use, while balancing with comfort constraints and a proper operation of the systems. Two versions of these controllers were produced: one using the electricity price as penalty signal, the other using the marginal emissions. The MPC controller in particular required the development of a simplified model of the building envelope (resistance-capacitance grey-box model) and of the heat pump performance, both adjusted differently for heating or cooling operation. The MPC included several novelties in its configuration, such as the mixed-integer formulation, the heat pump simplified model based on experimental data and the consideration of its computational delay.

The developed controllers were then tested, firstly in an experimental setup. This laboratory setup applies the hardware-in-the-loop concept, with a real heat pump installed in the laboratory facilities, and connected to thermal benches that emulated the thermal loads from a building model running in real time. The study case was a residential flat representative from the Mediterranean area of Spain, and the boundary conditions therefore also were taken from this location (weather and grid data for

a summer period and a winter period). Implementing the control strategies on a real heat pump enabled to highlight some practical challenges such as model mismatch in the MPC, communication issues, interfacing and control conflicts with the heat pump local controller. These observations also form part of the valuable output of the thesis.

Further than the experimental setup, a simulation-only framework was also developed to test other configurations of the controllers. In that case, the real heat pump was replaced by a detailed model which was specially developed for this purpose, since such model did not previously exist in the considered simulation framework. The detailed model is based on static tests performed in the laboratory, and therefore reproduces the dynamic behavior of the heat pump with high fidelity. The co-simulation framework uses TRNSYS as the main dynamic building simulation tool, coupled with MATLAB for the implementation of the MPC controller, and can be used to perform numerous simulations with the same boundary conditions, enabling repeatability and comparison across cases.

The results from experimental and simulation studies revealed the ability of both types of controllers to shift the building loads towards periods where the electricity was either cheaper or less CO_2-emitting. These two objectives were in fact contradictory, a cost reduction leading to an increase in emissions and vice-versa. In the cases where the reference thermostat control presented a large margin for improvements, the RBC and MPC controllers performed equally and provided important savings: around 15% emissions savings in heating mode, and 30% cost savings in cooling mode. In the cases where the reference control already performed close to optimally, the RBC controller failed to provide improvements, while the MPC benefitted from its stronger optimization and prediction features, reaching 5% cost savings in heating mode and 10% emissions savings in cooling mode.

The research carried out in the framework of this thesis covered many aspects of energy flexibility in buildings: creation of input penalty signals, graphical representation of flexibility, development of controllers, performance in realistic experimental setup, fitting of appropriate models and compared performance in heating and cooling. The development efforts and barriers hindering the deployment of MPC controllers at large scale for building climate control have additionally been discussed. The performance of the developed controllers was evidenced in the thesis, proving their potential for load-shifting incentivized by different penalty signals: they could become a strong asset to unlock demand-side flexibility and *in fine*, help integrating a larger share of RES in the grid.

Keywords: *heat pumps, model predictive control, building model, rule-based control, energy flexibility, HVAC control, smart grid, mixed-integer MPC formulation, energy-flexible building.*

Resumen

La situación de emergencia climática en la que se encuentra nuestro planeta requiere de acciones urgentes e inaplazables para mitigar los efectos del cambio climático. Una de las importantes estrategias que se están adoptando en esta dirección es la descarbonización de los sistemas energéticos, desde el transporte a la industria pasando por la edificación. En el caso de la red eléctrica, la estrategia pasa por integrar una mayor proporción de fuentes de energía renovables, con la intención de reducir al máximo o a cero la producción de electricidad basada en combustibles fósiles. Debido a su variabilidad y su dependencia meteorológica, la alta penetración de fuentes de energía renovables como la energía solar o eólica plantea una serie de desafíos tecnológicos al sistema de producción, transmisión y distribución eléctrica. Entre estos desafíos a solucionar podemos citar: el posible desequilibrio entre la demanda y la producción eléctrica, la consecuente necesidad de restringir la producción basada en energías renovables en ciertos momentos, o de recurrir a centrales de generación que usan combustibles fósiles para puntas de demanda, la potencial congestión de las redes de distribución por la descarbonización de ciertos consumos energéticos, la proliferación de sistemas de generación renovable descentralizada y de los prosumidores. La gestión de la demanda (DSM del inglés Demand Side Management) define un conjunto de estrategias cuyo objetivo es aumentar la flexibilidad en los puntos de demanda para contribuir de forma eficiente a la gestión de una infraestructura eléctrica con un alto nivel de penetración de energías renovables. En particular, los edificios y su masa térmica incorporada tienen una capacidad de almacenamiento térmico y pueden ser activados como fuentes de flexibilidad para el sistema eléctrico. El uso de bombas de calor y su gestión inteligente para cubrir las demandas de climatización y agua caliente sanitaria en la edificación representan una herramienta ideal para poder gestionar los edificios como un activo flexible para el sistema eléctrico.

Para aprovechar de forma adecuada todo el potencial de flexibilidad energética de las cargas térmicas en los edificios equipados con bombas de calor se requiere de sistemas de control inteligente. Una extensa revisión bibliográfica ha revelado que la mayoría de las estrategias de gestión utilizadas para esta finalidad pueden ser clasificadas en dos categorías: control predictivo en base a modelos (MPC, del inglés Model Predictive Control) o control en base a reglas (RBC, del inglés Rule-based control). RBC se basa en reglas simples de la forma "si una condición se cumple, entonces realiza una acción". La gestión tipo MPC constituye una estrategia más avanzada que utiliza modelos y previsiones para predecir el comportamiento de los sistemas en el futuro cercano y encontrar un plan de acción óptimo. Los sistemas MPC requieren el desarrollo preliminar de modelos y la resolución de un problema de optimización cada cierto paso de tiempo. Por esta razón, su desarrollo y sus costes de operación son más elevados, aunque generalmente funcionan mejor que las estrategias tipo RBC. Ambos sistemas, tanto RBC como MPC, pueden utilizar señales externas de gestión dinámicas (llamadas señales de penalización en esta tesis) para fundamentar sus decisiones. El precio de la electricidad es utilizado de forma habitual como señal de penalización en estrategias que tienen como objetivo la reducción del coste económico, aunque la utilización de otro tipo de señales es posible. En el marco de esta tesis también se han utilizado señales de penalización basadas en las emisiones de CO_2. Para ello, se ha desarrollado una nueva metodología que permite definir una señal de las emisiones marginales de CO_2 basada en la información del sistema eléctrico, con el objetivo de tener en cuenta con más precisión el impacto en términos de huella de carbono de las estrategias de gestión de la demanda implementadas.

En el marco de esta tesis, se han desarrollado controles para sistemas de bombas de calor aire-agua de capacidad variable que cubren las demandas de calefacción, refrigeración y agua caliente sanitaria

en el ámbito residencial. Se han desarrollado estrategias basadas en controladores tipo RBC y MPC. La estrategia RBC consiste en modular las temperaturas de consigna en la zona de la vivienda y en el tanque de almacenamiento de agua caliente, respondiendo a la forma de la señal de penalización. La estrategia MPC consiste en minimizar las penalizaciones totales del sistema al mismo tiempo que se consideran las restricciones operativas de los equipos y las derivadas del confort térmico de los ocupantes de la vivienda. Se han desarrollado y testeado dos versiones de ambos controladores usando el precio de la electricidad y las emisiones marginales de CO_2 como señales de penalización. En particular, el controlador tipo MPC ha requerido el desarrollo de modelos simplificados, llamados de caja-gris, para predecir la demanda del edificio y el rendimiento de la bomba de calor, tanto en modo calefacción como en modo refrigeración, que presentan avances significativos en su aproximación metodológica. Otras novedades añadidas en la configuración del MPC son la formulación entera mixta, y la consideración del retraso debido al tiempo de cómputo.

Un aspecto altamente relevante de este trabajo es que los controladores fueron testeados en primer lugar en un entorno experimental semi-virtual. Este entorno basado en el concepto "hardware-in-the-loop" posibilita el test de una bomba de calor real instalada en un laboratorio conjuntamente con los sistemas de control desarrollados, conectados a unos bancos térmicos que emulan en tiempo real y de forma dinámica las cargas térmicas de un edificio modelizado mediante un software especializado. El caso testeado corresponde a una vivienda residencial representativa de la región mediterránea de España, y las condiciones de contorno (datos meteorológicos, ocupación de la vivienda, condiciones de la red eléctrica, etc.) se han seleccionado para reproducir periodos significativos de invierno y verano. Los resultados obtenidos en el entorno experimental han permitido poner de manifiesto algunos retos prácticos en la implementación de las estrategias de control, tales como la discrepancia en el modelo del MPC y conflictos de comunicación, de interconexión y de control con el controlador local de la bomba de calor. Estas observaciones forman parte de los resultados de la tesis al aportar conocimientos valiosos en la implementación práctica del control de bombas de calor de capacidad variable y sobre los beneficios esperados de las diferentes estrategias implementadas.

De forma complementaria al entorno experimental, un entorno completo de co-simulación ha sido creado con el objetivo de testear y analizar diversas configuraciones de los controladores. Para ello, se ha desarrollado un modelo altamente detallado de la bomba de calor, basado en ensayos de caracterización realizados en laboratorio, que reproduce el comportamiento dinámico de la bomba de calor con alta fidelidad. El entorno de co-simulación usa TRNSYS como la herramienta de simulación principal acoplada con MATLAB para la implementación del controlador MPC. El entorno ha sido validado con los resultados experimentales y ha sido utilizado para realizar simulaciones que permiten la comparación entre casos y el análisis del impacto de variaciones en la formulación de los controladores.

Tanto los resultados experimentales como los simulados han revelado la capacidad de los dos tipos de controladores de desplazar las cargas del edificio en el tiempo hacia periodos donde la electricidad era más barata o había menos emisiones de CO_2. Por la forma de las señales de penalización, estos dos objetivos presentaban, de hecho, impactos contradictorios, ya que una reducción del coste económico producía un aumento de emisiones y viceversa. En los casos donde el control de referencia con termostato y control por sonda exterior presentaba un amplio margen de mejora, los controladores RBC y MPC han demostrado la capacidad de actuar eficientemente y proveer ahorros importantes: alrededor de un 15% de emisiones en modo calefacción y de un 30% de coste económico en modo frío. En aquellos casos testeados en los que el control de referencia actuaba de forma cercana a la óptima, los controladores RBC no han sido capaces de actuar eficientemente y aportar mejoras significativas, mientras que las estrategias basadas en MPC han demostrado la capacidad de conseguir ahorros de un 5% de coste económico en modo calefacción y de un 10% de emisiones en modo frío, gracias a su formulación basada en optimización y predicción.

La investigación realizada en esta tesis ha abarcado amplios aspectos de la flexibilidad energética en los edificios: la generación de señales de penalización, la representación gráfica del potencial de flexibilidad energética de los edificios residenciales, el ajuste de modelos simplificados y detallados para este análisis, el desarrollo de controladores y ensayo tanto en un entorno experimental como en un entorno de simulación, con la consecuente evaluación de su rendimiento comparado tanto en periodos de invierno con predominancia de cargas de calefacción como en verano con cargas de

refrigeración. Las conclusiones extraídas en el proceso de desarrollo e implementación práctica han permitido discutir las ventajas y potencial impacto del despliegue de controladores RBC y MPC a gran escala, así como las barreras que dificultan su implementación. Finalmente, la tesis ha evidenciado el rendimiento de los controladores desarrollados si se formulan de forma adecuada, demostrando su potencial para el desplazamiento del consumo eléctrico en la edificación residencial con sistemas de bomba de calor respondiendo a diferentes señales de penalización. En conclusión, los sistemas propuestos pueden ser elementos muy valiosos para favorecer la necesaria flexibilidad de la demanda térmica en la edificación y posibilitar la integración de sistemas de generación renovables en la red.

Palabras clave: *bombas de calor, control predictivo, modelización de edificios, control basado en reglas, flexibilidad energética, control de climatización y refrigeración, red inteligente, formulación de MPC mixta entera, edificio de energía flexible.*

Contents

Nomenclature

Abbreviations

ADR	Active Demand Response
$ASHRAE$	American Society of Heating, Refrigeration and Air-Conditioning Engineers
COP	Coefficient of Performance
CR	Capacity Ratio at part-load
$CTSM$	Continuous Time Stochastic Modelling
DHW	Domestic Hot Water
DR	Demand Response
DSM	Demand-Side Management
EBC	Energy in Buildings and Communities programme
EER	Energy Efficiency Ratio
EF	Average CO_2 Emissions Factor
$EHPA$	European Heat Pump Association
$EMPC$	Economic Model Predictive Control
$EPBD$	Energy Performance of Buildings Directive
EV	Electric Vehicle
FCU	Fan-Coil Unit
FF	Flexibility Factor
$GSHP$	Ground Source Heat Pump
HiL	Hardware-in-the-loop
$HVAC$	Heating, Ventilation & Air Conditioning
HX	Heat Exchanger
IEA	International Energy Agency
IEQ	Indoor Environmental Quality
$IPCC$	Intergovernmental Panel on Climate Change
$IREC$	Institut de Recerca en Energia de Catalunya
ITN	Innovative Training Network

KPI	Key Performance Indicator
MEF	Marginal CO_2 Emissions Factor
$MILP$	Mixed-Integer Linear Programming
MPC	Model Predictive Control
$MSCA$	Marie Sklodowska-Curie Actions
$NRMSE$	Normalized Mean Root Square Error
$NRPE$	Non-renewable Primary Energy
$nZEB$	Nearly-Zero Energy Building
OCP	Optimal Control Problem
PCM	Phase Change Materials
PEF	Primary Energy Factor
PID	Proportional Integral Derivative controller
PLF	Part-Load Factor
PMV	Predicted Mean Vote (comfort index)
PPD	Percentage of People Dissatisfied
$PRBS$	Pseudo Random Binary Signal
PV	Photovoltaic
$PVPC$	Precio Voluntario para el Pequeño Consumidor, or voluntary price for small consumers (electricity tariff in Spain)
RBC	Rule-Based Control
RC	Resistance-Capacitance model
RES	Renewable Energy Sources
$RMSE$	Root Mean Square Error
SB	Standby mode
SC	Space Cooling
SH	Space Heating
SOC	State of Charge
SP	Set-point
SPF	Seasonal Performance Factor
$TABS$	Thermally Activated Building System
TES	Thermal Energy Storage
ToU	Time-of-Use tariff
TSO	Transmission System Operator
UPC	Universitat Politècnica de Catalunya
$VSHP$	Variable Speed Heat Pump

Parameter symbols

$\alpha_{\Delta u}$	Weighting coefficient of the smoothing objective	$[-]$
α_{ε}	Weighting coefficient of the comfort objective	$[-]$
α	Weighting coefficient within the multi-objective function	$[-]$
ΔQ_{th}	Thermal energy difference in the building between a final and an initial state	kWh
ΔT	Temperature lift $T_{sup} - T_{ret}$	$°C$
δT	Amplitude of the set-point modulation	$°C$
δ	Vector of binary on-off variables	$[-]$
δ_S	On-off binary variable for the SH/SC circuit	$[-]$
δ_{TES}	On-off binary variable for the TES circuit	$[-]$
$\dot{m}$	Water mass flow rate	kg/h
η_{ADR}	Storage efficiency of the ADR event	
$\overline{Q_{SC}}$	Upper constraint of heat pump capacity for space cooling	kW
$\overline{Q_{SH}}$	Upper constraint of heat pump capacity for space heating	kW
$\overline{Q_{TES}}$	Upper constraint of heat pump capacity for DHW	kW
$\overline{T_{int}}$	Upper constraint for room temperature	$°C$
$\overline{T_{TES}}$	Upper constraint for tank temperature	$°C$
σ	Binary indicator of the change of HP status	
θ_{occ}	Occupancy factor	$[-]$
$\underline{Q_{SC}}$	Lower constraint of heat pump capacity for space cooling	kW
$\underline{Q_{SH}}$	Lower constraint of heat pump capacity for space heating	kW
$\underline{Q_{TES}}$	Lower constraint of heat pump capacity for DHW	kW
$\underline{T_{int}}$	Lower constraint for room temperature	$°C$
$\underline{T_{TES}}$	Lower constraint for tank temperature	$°C$
ε	Slack variable (for relaxing comfort constraints)	$°C$
A	Matrix of the state-space model (associated with the states x). An optional superscript 'd' indicates the discrete form of the matrix. A tilde indicates the transformed version of the matrix to include the delay.	$[-]$
a_i	Coefficients of fitted model	$[-]$
B_e	Matrix of the state-space model (associated with the inputs e). An optional superscript 'd' indicates the discrete form of the matrix. A tilde indicates the transformed version of the matrix to include the delay.	$[-]$
b_i	Coefficients of fitted model	$[-]$
B_u	Matrix of the state-space model (associated with the control inputs u). An optional superscript 'd' indicates the discrete form of the matrix. A tilde indicates the transformed version of the matrix to include the delay.	$[-]$

C	Matrix of the state-space model (associated with the outputs y). An optional superscript 'd' indicates the discrete form of the matrix. A tilde indicates the transformed version of the matrix to include the delay.	$[-]$
C	Thermal capacity	kWh/K
c	General notation for the cost vector	$[-]$
C_c	Degradation coefficient for the heat pump performance	$[-]$
c_g	Cost of natural gas	EUR/kWh
c_i	Cost of energy carrier i	EUR/kWh
c_p	Peak demand cost	u/kW
c_p	Specific heat	$kJ/kg.K$
c_Σ	Summed costs or penalties	
c_ε	Cost of comfort constraints violations	$1/K$
C_{ADR}	Active Demand Response Capacity	kWh
C_{dis}	Thermal capacity of the distribution circuit node	kWh/K
C_{eff}	Effective thermal capacity	kWh/K
$c_{el,\Sigma}$	Summed electricity costs	EUR
$c_{el,max}$	Upper value of electricity price	EUR/MWh
c_{el}	Price of electricity	EUR/MWh
C_{eq}	Equivalent thermal capacity of the building $C_{int} + C_w$	kWh/K
c_{high}	High penalty threshold	$[-]$
C_{int}	Thermal capacity of the internal node	kWh/K
c_{low}	Low penalty threshold	$[-]$
$c_{MEF,\Sigma}$	Summed marginal emissions	$kgCO_2$
$c_{MEF,max}$	Upper value of the MEF	$kgCO_2/kWh$
c_{MEF}	Marginal emissions factor as a penalty signal	$kgCO_2/kW$
$c_{PEF,\Sigma}$	Summed primary energy use	kWh
c_{PEF}	Primary energy factor as a penalty signal	$[-]$
C_{TES}	Thermal capacity of the tank water	kWh/K
C_w	Thermal capacity of the walls node	kWh/K
COP	Instantaneous coefficient of performance	$[-]$
COP_{avg}	Average COP over a period	$[-]$
CR	Capacity Ratio	$[-]$
e	Vector of non-controllable exogenous inputs. A tilde indicates the transformed version of the vector to include the delay.	$[-]$
EER	Instantaneous energy efficiency ratio	$[-]$
EER_{avg}	Average EER over a period	$[-]$

f	Compressor frequency	Hz
F_{target}	Flexibility target to track	kWh
FF_p	Flexibility factor for penalty signal p	$[-]$
FF_{CO_2}	CO_2 flexibility factor	$[-]$
FF_{cost}	Cost flexibility factor	$[-]$
gA	Aperture area	m^2
h	Computational delay	s
I_H	Total horizontal solar irradiation	kW/m^2
J	Objective function	$[-]$
J_d	Comfort objective (set-point tracking)	$[-]$
J_f	Flexibility objective	$[-]$
J_p	Objective of peak shaving	$[-]$
J_q	Primary energy minimization objective	$[-]$
$J_{\Delta u}$	Smoothing objective	$[-]$
J_ε	Robustness objective / Comfort objective (slack variable)	$[-]$
J_{CO2}	CO_2 emissions minimization objective	$[-]$
J_{cost}	Cost objective	$[-]$
J_{en}	Thermal energy minimization objective	$[-]$
J_{obj}	Main flexibility objective of the MPC	$[-]$
k	Time step	$[-]$
K_p	Proportional gain (PID controller)	$[-]$
L	System load	GW
L_{down}	Minimum down-time constraint	$[-]$
L_{up}	Minimum up-time constraint	$[-]$
N	Prediction horizon of the MPC (in number of time steps)	$[-]$
$P_{el,\Sigma,hp}$	Summed electricity use in high penalty periods	kWh
$P_{el,\Sigma,lp}$	Summed electricity use in low penalty periods	kWh
$P_{el,\Sigma,mp}$	Summed electricity use in medium penalty periods	kWh
$P_{el,\Sigma}$	Summed electrical energy use of the heat pump	kWh
$P_{el,det}$	Detailed model of the heat pump electricity use	kW
$P_{el,FCU}$	Electricity use of the FCU	kW
$P_{el,simpl}$	Simple model of the heat pump electricity use	kW
P_{el}	Electrical power of the heat pump	kW
$P_{FCU,on}$	Constant of the electricity use of the FCU when on	kW

PLF	Part-Load Factor	$[-]$
Q	Thermal power	kW
Q_S	Thermal power for the SH/SC circuit	kW
Q_{DHW}	Thermal power of the DHW extractions	kW
Q_{extr}	Thermal energy of the DHW extractions	kWh
Q_{losses}	Thermal losses of the DHW tank	kWh
Q_{occ}	Occupants internal gains	kW
Q_{TES}	Thermal power for the TES circuit	kW
$Q_{th,\Sigma}$	Summed thermal energy of the HP	kWh
$Q_{th,ADR}$	Thermal power of the ADR event	kW
$Q_{th,det}$	Detailed model of the heat pump thermal power	kW
$Q_{th,FL}$	Thermal capacity of the heat pump at full load	kW
$Q_{th,ref}$	Thermal power of the reference case	kW
$Q_{th,use}$	Thermal energy use, including the HP production and the thermal energy difference	kWh
Q_{th}	Thermal power of the heat pump	kW
R	Thermal resistance	K/kW
r	Modulation factor for the set-point	$[-]$
R_{dis}	Thermal resistance of the distribution circuit node	K/kW
R_{eq}	Equivalent thermal resistance of the building $R_{int} + R_w$	K/kW
R_{int}	Thermal resistance of the internal node	K/kW
R_{TES}	Thermal resistance of the tank node	K/kW
R_w	Thermal resistance of the walls node	K/kW
RES	RES Percentage	$\%$
T	Temperature	$°C$
t	Time	s
t_d	Derivative time constant (PID controller)	h
t_i	Integral time constant (PID controller)	h
t_s	Sampling time	h
t_{ADR}	Duration of the ADR event	$[h]$
T_{amb}	Ambient temperature	$°C$
T_{dis}	Distribution circuit temperature	$°C$
T_{env}	Temperature of the environment surrounding the tank	$°C$
$T_{i,fin}$	Temperature of the state T_i at the end of the simulation	$°C$
$T_{i,init}$	Temperature of the state T_i at the start of the simulation	$°C$

$T_{int,SP}$	Room temperature set-point	$°C$
T_{int}	Indoor zone temperature	$°C$
T_{ret}	Return temperature	$°C$
$T_{sup,SP}$	Supply temperature set-point	$°C$
T_{sup}	Supply temperature	
$T_{TES,SP}$	Water tank temperature set-point	$°C$
T_{TES}	Water tank temperature	$°C$
u	Vector of control inputs (thermal powers in the MPC)	$[kW]$
v	Vector of the delayed control inputs	$[-]$
x	Vector of states. A tilde indicates the transformed version of the vector to include the delay.	$[-]$
y	Vector of outputs. A tilde indicates the transformed version of the vector to include the delay.	$[-]$

Chapter I

Introduction and motivations

1 Motivations

1.1 Urgency of climate change mitigation

The work developed during this thesis is largely driven by the general emergency of the climate crisis and of the global warming situation. It certainly does not come as fresh news, but the Earth is warming up at an unprecedented pace in the known history of our planet. The latest report of the Intergovernmental Panel on Climate Change (IPCC) establishes clearly that the Earth has already warmed on average by 1°C compared to pre-industrial levels, and that global warming will certainly reach at least 1.5°C by 2030 due to manmade activities [1]. A constant flow of new science and information tells us every day how urgent is the situation, and how global warming has already become a reality.

July 2019 was the hottest month recorded on Earth. It followed June 2019 which was the warmest June ever measured globally [2]. All previous records also belonged to recent years. The Greenland ice sheet broke records on 1 August 2019 by losing more water volume in 1 day than on than any other day since records began in 1950, shedding 12.5 billion tons of water into the sea [3]. This extreme event is only a manifestation of the constant decline in the Arctic sea ice extent, with a rate of 7.3% every decade. In the Arctic circle, temperatures almost 10°C higher than the 1980-2010 average have caused unprecedented wildfires in large parts of Siberia, releasing 50 Mt CO_2 in June 2019 only. These few pieces of news are only a sample taken from this summer, and there is no doubt that the remaining of the year 2019, until this thesis will be defended, will bring its own lot of alarming news and sad records.

Although the assessment of the global situation is now clear and consensual, insufficient actions are being implemented to counteract global warming and decrease the rate of emissions due to mankind activities. As proof of the global awareness on this matter, 935 jurisdictions have already declared officially a climate emergency as of the 13th of August 2019, including for instance the cities of Paris and London or the regional government of Catalonia in Spain [4]. Acknowledging the problem represents a first step, however the governing bodies should not stop there, and actually put policies into action in order to mitigate the climate crisis and its effects on the planet.

To avoid a global warming beyond 1.5°C and the catastrophic consequences related to such an important climate change, an inflection of the human-made emissions curve is urgently needed [1]. The acknowledgement of the climate phenomenon has been delayed for decades because of counterforces such as lobbies, industries and politics. There is now little time left for action to avoid reaching the tipping point which would completely deregulate the Earth's climate. For this reason, the emissions must be drastically reduced in the very near future. However, the current predictions rather anticipate a constant increase of the global emissions, although probably at a slower pace or reaching a plateau if some measures are taken.

Even though the current policies clearly lack ambition in terms of climate change mitigation, sev-

eral initiatives are being taken in the good direction. At the global level, the Paris agreement accorded at the end of the COP21 conference in 2015 led to the outline of an overall plan for actions at an international level [5]. However the text was not binding and the USA have unfortunately withdrawn from the agreement afterwards. In Europe, the Commission has enforced its latest package on energy in mid-2019 [6]. Called the "Clean energy for all Europeans", this package contains the targets for the European Union for 2030: 40% cuts in greenhouse gas emissions, 32% of renewables in the energy consumption, and 32.5% energy efficiency. The Member States must implement these targets into their national law in the upcoming 1 or 2 years.

1.2 Penetration of renewable energies in the power grid

The first two goals of the Clean energy for all Europeans package can be partly reached by increasing the proportion of renewable energies in the energy mix of the EU countries. The IPCC also calls among other recommendations for a deep and fast decarbonization of our energy systems [1]. In particular, we focus here on the power grid, hence not considering directly thermal networks or the transport sector, which also form a great proportion of the overall energy systems.

Decarbonizing the power systems will require an ever increasing proportion of energy coming from renewable sources (RES). Achieving 100% of RES in the grid remains a very challenging goal towards which we must aim, the current goal of the EU for 2030 being 32%, as a reminder. Hydropower already contributes significantly to the penetration of RES in several countries, but this resource is geographically limited to a few sites where it is mostly already exploited [7]. Nowadays, the fastest growing RES sectors consist of solar and wind power: the rapid decline in the cost of these technologies has made them cost-competitive against other fossil or nuclear fuels, and has led to their accelerated deployment [8]. Figure I.1 shows the installed capacity of wind and solar power plants, over the period 2006 - 2018, based on data from [9], [10]. In a little bit more than a decade, the capacity of these two technologies has been multiplied by 10. The capacity of solar plants was almost nonexistent in 2006, and has now reached more than 500 GW in the world in 2018.

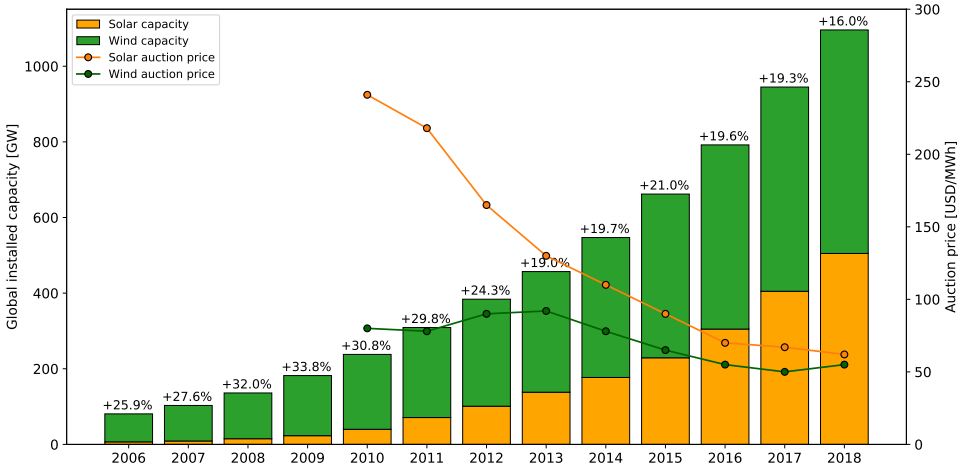

Figure I.1. Global installed capacity of wind and solar power in the period 2006-2018, and auction prices for PV and wind plants in the period 2010-2018. The percentages show the increase in the total installed capacity (wind and PV) from one year to the next. Sources: REN21 and IRENA reports [9], [10].

Figure I.1 also displays the evolution of the auction prices for new power solar and wind power plants over the years 2010 to 2018. The price has only slightly decreased for new wind farms, reaching the level of 55 USD/MWh, since this technology was already mature in 2010. On the other hand, photovoltaic (PV) technology has seen its auction price decreased significantly, almost divided by 5 between 2010 and 2018, from 241 to 62 USD/MWh. New record low prices are often beaten, the latest to date being 14.67 €/MWh (around 16 USD/MWh) in Portugal in July 2019 [11]. These constantly declining costs have been the driving force behind the rapid growth of these technologies, which are

now entirely competitive against other non-renewable sources of energy, even without subsidies.

The situation is not uniform across the globe, with China for instance still building new coal plants - the most emitting source of energy. Overall, the rapid growth of RES still constitutes a satisfactory trend for all states committed to reduce their greenhouse gas emissions. However, the inherent intermittency of solar and wind power also poses certain threats to the stability of the electricity grids. Indeed, these two power sources highly depend on climatic conditions, which can result in possible mismatch between this variable production and the demand when the penetration of RES is high. This energy transition might thus provoke challenges and instability in the electricity grids, if non-dispatchable sources such as solar and wind become predominant. Some regions already experience the effects of a high penetration of renewable energy sources (RES): in Germany for example, where the share of solar energy is high, prices can become negative at times of high production. In such cases, curtailment of the RES constitutes an easy solution, but basically consist in wasting free available energy, like these days of December 2012 where 300 MW of wind power were curtailed [12].

A high proportion of RES can have different adverse effects. As already mentioned, at some times of the day, it can happen that the production surpasses the demand, because of the high availability of these sources. At other times, the production from renewables might be insufficient to cover the demand, and other peak power plants must be activated. These plants must be easily dispatchable and often rely on coal or natural gas as their main source of energy. Such peak power plants must be maintained all year round to ensure an availability of their power capacity at times where the production from solar and wind would be insufficient. Some economical problems then occur regarding their profitability: they would be activated only during few hours of the year, only when RES are not available. If there is enough RES, gas or coal cannot compete, since the marginal costs of solar or wind is virtually null (they do not consume any fuel, contrary to a gas or coal plant). In these conditions, owning, investing or running a gas or coal plant is not anymore profitable on a yearly basis. However, these peak power plants are still needed to guarantee a power supply in case of low RES availability all year round. Their financial viability is thus challenged by a high RES penetration.

Another challenge raised by the emergence of cleaner sources of energy is the possible emergence of congestion problems in the grid. The current power grid was built under the assumption of a very centralized system, with large power plants at the core of the system, and a ramified distribution system dispatching the electricity until the end-users. RES are by essence often decentralized, and spread over the territory. Consumers can now become prosumers by installing small scale PV panels or windmillls, and also inject power into the grids. The power lines have not been dimensioned to support such large power flows, and this could cause congestions in the grid. The most famous example about this issue is the "duck curve" in California: this American state has had a very high penetration of solar energy in its grid in recent years. For this reason, the residual load (load minus production of RES) is rather low during midday hours, when solar production is at its maximum: this is the belly of the duck. However in the evening, the sun sets and the PV panels stop producing, causing all users to switch from their PV production to the grid supply. In a very short time, the residual load increases at a high pace (it is the neck of the duck), potentially provoking congestions, and requiring other power sources which must ramp very fast to supplant the solar supply every evening. This is another illustration of adverse effects provoked by a high penetration of variable RES.

To summarize, increasing the share of renewable sources in our energy mix is an absolute necessity if we are to decarbonize our energy systems and reduce our greenhouse gas emissions. Solar and wind power show a good potential to achieve these goals, since they provide electricity with a low carbon footprint. However, their introduction in a high proportion can pose some challenges:

- They are variable and weather-dependant, therefore they are not controllable like conventional power plants.
- Because of this weather dependency, they are more difficult to manage since their production output is unpredictable.
- Since they cannot be controlled, mismatch can occur between production and demand. Both a surplus or a lack of energy are problematic.
- The recent decline in costs of solar and wind plants can lead to the traditional gas or coal peak

plants becoming financially non-viable. Since these plants are still needed to ensure a continuity of supply at times of low RES availability, important subsidies would have to be put into place to keep them afloat.

- The emergence of decentralized RES means of productions and prosumers can lead to congestion problems within the grid.

These challenges can be overcome, as will be explained later, and should not constitute obstacles to the deployment of solar and wind power, given their enormous benefits as providers of low-carbon electricity. To manage high penetration levels of these RES sources, better ways of matching the supply and the demand will thus be needed. Overall, the traditional vision where the "production follows the demand" needs a paradigm shift towards a concept where the "demand follows the production".

1.3 Demand-side management

Some solutions have already been developed and implemented to solve the problems raised by a high penetration of variable RES:

- Curtailment, as already mentioned, consists in interrupting some power plants in case of overproduction to preserve the stability of the grid, but this involves dumping renewable electricity that is available, and it also impacts the return on the investments realized in these plants.
- The surplus of electricity occurring at certain times can be absorbed by storage to be used later on. However, storage technologies are so far not enough cost-efficient to perform such operation on the large-scale of the power grid. Storage can take multiple forms, such as pumping water over hydroelectric dams, batteries of electric vehicles (EVs), thermal storage, hydrogen production etc.
- Supply-side flexibility can be activated to compensate for a lack of renewable energy production, but it requires the all-year maintenance of power plants used only punctually, and these peaking plants are based on fossil fuels, which goes against the overall goal of decarbonization.
- The voltage or frequency of the grid can also be deviated from their nominal points to absorb part of the supply-demand mismatch, but this is only possible within narrow limitations and it degrades the quality of the electricity delivered to the end users.
- Transmission lines can be upgraded to enable the higher short-term peaks and variations in the grid caused by the increasing number of prosumers and decentralized RES sources. These transmission lines are however costly and their building process is very long and complex, since they cross large parts of the land territory.
- Transmission lines can also increase the possibilities of electricity import/export with neighboring countries which have a different energy mix, but these are costly to build and require cooperation among nations. The idea can even be pushed until the establishment of a global grid [13], where for example the solar production of the Sahara could be supplied to Northern Europe during daytime, while the windfarms of the Baltic Sea would cover the nighttime demand of the Southern hemisphere.
- The prediction models for the production of wind and solar plants are becoming more accurate, therefore managing their operation and the overall grid becomes a more manageable task. Furthermore, the predictions enable to anticipate the variations in RES production and to act accordingly, for instance by starting other types of power plants before a predicted drop in solar or wind production. Even with the recent advances, predictions will however never be perfect.
- To compensate for the low profitability of peak power plants against the ever cheaper renewables, subsidies can be put into place by governing bodies in order to maintain their needed availability, but these measures are of course costly.

None of these existing solutions is therefore ideal, even though they can be used to support the grid operation. It should be stressed that all of them can partly contribute to solving the problem. For such a large-scale and complex issue, there won't be a single technology which will miraculously emerge as a single powerful solution, but rather a multiple set of solutions which will each help in improving certain aspects, each to its own proportion.

This situation also calls for new and better solutions, and notably for an increase in the flexibility of the demand side. The momentum towards a more flexible electricity system based on RES is increasing [14] and it has definitely become a "hot topic", given the large amount of literature recently published on the matter [12]. Through an increased flexibility, energy systems could have inherent capabilities to accommodate a larger share of variable RES without requiring massive new investments. In particular, treating thermal and electrical systems as a whole could offer major new opportunities [12]. Increasing the flexibility of the loads rather than that of the supply-side represents a whole set of methods, grouped under the denomination of Demand-Side Management (DSM) or Demand Response (DR).

DSM has been identified as a promising solution to help balance energy production and demand at any time [15], [16]. DSM generally consists in adapting the demand loads to the grid requirements; and this demand profile can be made flexible in different ways: load-shifting, peak shaving, reduction of energy use or valley filling. DSM has historically been applied with larger energy consumers such as industries or factories, which can be subject to load shedding or rolling blackouts in exchange for monetary compensation. Recently, more research has focused on the DSM potential of smaller users, aggregated or not. In the present work, attention is drawn to DSM applied to buildings and their embedded systems.

Demand response can be activated in different manners for the end-consumers. Two categories are normally distinguished: explicit and implicit demand response. With explicit demand response, also called "incentive-based", the consumers receive direct payments in retribution for changing their consumption pattern upon request. They can receive the payments directly or through the intermediary of an aggregator. With implicit demand response, also called "price-based", the consumers react to a dynamic signal, which is often a time-varying price [17]. Those two types of DR are not exclusive and could both be enabled in a certain geographic area. The present thesis focuses on the specific case of Spain. In this country, explicit DR schemes are not possible so far with small consumers, since aggregators are still not legal. For large industrial consumers, interruptible load programmes do exist, but are limited to emergency situations. On the other hand, implicit demand response is more advanced in Spain, since it was the first country to set its default electricity price as an hourly price based on the spot market. Implicit DR is also facilitated by the large rollout of smart meters in Spain, which reached 99.1% of the consumers of less than 15 kW contracted in the end of of 2018 [18]. Smart meters enable a direct communication, notably sending the hourly prices to the consumers and receiving their hourly consumption. For this reason, this thesis focuses on implicit demand response schemes rather than on explicit ones.

1.4 Buildings as energy flexibility assets

Buildings represent interesting subjects for DSM, first and foremost because they account for approximately 40% of the total energy consumption in the EU, and around 36% of the total CO_2 emissions, as stated in the Energy Performance of Buildings Directive (EPBD) [19]. For this reason, the building stock represents a great potential as flexibility provider [20] if made available for demand response. The trend for increasing the energy flexibility of the demand side will thus soon reach the building sector. The European Union already requires its member states to only construct nearly zero energy buildings (nZEB) by 2020, which means they should achieve a nearly annual zero energy balance [19]. In the future, buildings not only will need to be energy-efficient and reach the nZEB target, they will also have to be energy-flexible. In fact, buildings are becoming micro-energy hubs, including production units, storage, demand response possibilities, and flexible loads. Taking into account this evolution, the nZEB 2.0 of the future will be an interactive player in the energy grids and could even play an important role as such in the transformation of the European energy market [21]. The EU has even impulsed the development of a Smart Readiness Indicator for buildings to make the level of

building smartness more tangible for different stakeholders [22].

Following this trend, enhancing the flexibility of buildings energy use has concentrated an important amount of research in recent years. It lead to the creation of the "Annex 67 - Energy-flexible buildings" project of the International Energy Agency - Energy in Buildings and Communities (IEA - EBC) programme [23]. The experts participating in this work have defined energy flexibility of a building as the *"ability to manage its demand and generation according to local climate conditions, user needs and grid requirements"*. Local climate conditions and user needs have long been considered when

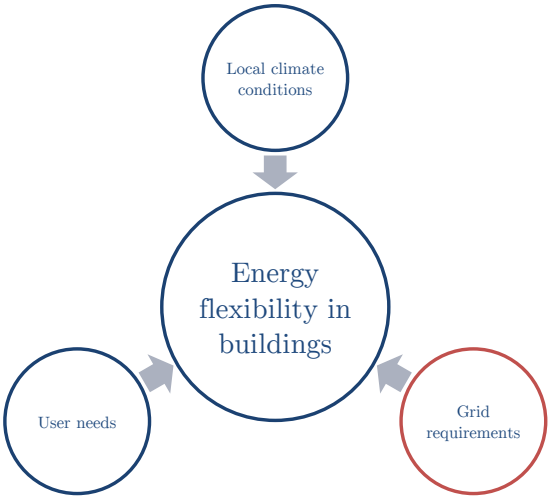

Figure I.2. Principle of energy flexibility in buildings.

Several components of a building energy use can be considered for the activation of flexibility. The control of smart appliances has been notably investigated for that purpose, but heating and cooling loads have maybe concentrated the most interest, because they are the major entry in a building's energy use. Heating, Ventilation and Air Conditioning (HVAC) systems operate inherently shiftable loads which can contribute to the energy flexibility of a building. Furthermore, buildings possess an intrinsic thermal mass which can be regarded as a storage means and activated by appropriate control strategies [24]. Additional storage options such as water tanks or embedded phase-change materials can also be valued as Thermal Energy Storage (TES) means for that purpose [25].

This project has received funding from the European Union's Horizon 2020 research and innovation programme under the Marie Skłodowska-Curie grant agreement No 675318.

In particular, the present thesis focuses on two types of TES: water storage tanks and the proper building thermal mass. Water is one of the best storage mediums for low temperature applications, it is widely available and at low cost, therefore water stratified tanks represent a promising source of TES [26]. Furthermore, small tanks for Domestic Hot Water (DHW) are already installed in a significant share of residential buildings, representing a large storage potential where flexibility can be activated. The air and structural mass of a building can also be exploited for short-term energy storage: they are highlighted as a key technology for implementing DSM [27] because they are readily available and do not require further equipment investment. Both water tanks and thermal mass show promising potential to enhance the energy flexibility of buildings [23]. Numerous studies have already proven that they can effectively be used with that purpose, for example by means of load-shifting [28], storing excess energy from an on-site RES plant [29], and resulting more cost-effective than batteries [30].

Another reason of the recent interest towards energy flexibility in buildings is the current electrification of dwellings. This trend has notably been pushed by governmental decisions: for instance, the recast of the EPBD [19] obliges its member states to only build nZEBs from 2020. The definition of nZEB has long been difficult to clarify with a wide consensus [31], but Sartori et al. proposed a framework definition in 2012 [32]. Its basic principles consist in reducing the energy use of the build-

ing while providing the remaining with renewable sources, aiming to achieve an annual zero energy balance. So far, the most promising nZEBs seem to be all-electrical [33], with a photovoltaic system for the production of the renewable energy part, and a heat pump for the heating or cooling supply. This combination is up until now the most simple and effective way to reach the nZEB target, and is the most implemented in real cases, as seen for example in the prototype houses presented regularly during the Solar Decathlon competitions [34], [35]. In fact, the markets for both types of systems (PV and heat pump) have seen an important increase over the last years, and this trend is bound to continue. The electrification of residential households also includes the rapid deployment of electric vehicles, which can also be considered as a source of flexibility.

For all these reasons, buildings are deemed worthy of further investigations with regards to their potential for energy flexibility. They can become active elements in the energy grids, providing flexibility services when needed.

1.5 Heat pumps as a coupling means between thermal storage and power grid

To sum up, it appears we have on the one hand upcoming challenges in the power grid, with an increased penetration of variable RES. On the other hand, the loads from buildings show a good potential for demand-side flexibility thanks to their integrated thermal storage, and are becoming more and more electrified. To bridge the gap, heat pump technologies represent an ideal tool to couple the electrical grids with thermal storages and to provide demand-side management [36].

Heat pumps provide heating and cooling from electricity through a highly efficient thermodynamic cycle. Their efficiency is characterized by a coefficient of performance (COP), which usually takes values higher than 2, meaning that for every kWh of electricity used, they produce more than 2 kWh of heat or cold. Supplied by renewable electricity, heat pumps are a 100% renewable and emission-free solution. They can thus deliver major economic, environmental and energy system benefits, notably by decarbonising heating and cooling [37]. Furthermore, a heat pump transfers heat from a low-temperature energy source to a higher temperature energy sink, therefore it can either provide heating or cooling, or both at the same time. This is particularly relevant in locations where both heating and cooling demand are present, and given that the global energy demand for cooling is steadily increasing. In fact, cooling is the fastest-growing end use in buildings, notably because of global warming and the rising of the living conditions across the globe. Energy demand for cooling has more than tripled from 1990 to 2018, reaching 2000 TWh of electricity last year [38].

Although the heat pump concept has been around for more than 150 years, it is still not widely adopted, even though the market shows interesting dynamics [40]. Figure I.3 shows the sales of heat pumps in Europe per country and per heat pump type in 2016, retrieved from the European Heat Pump Association (EHPA) website [39]. The market has grown of 12% that year in all the continent, with reversible air-to-air units as the predominant technology. France leads by the number of units

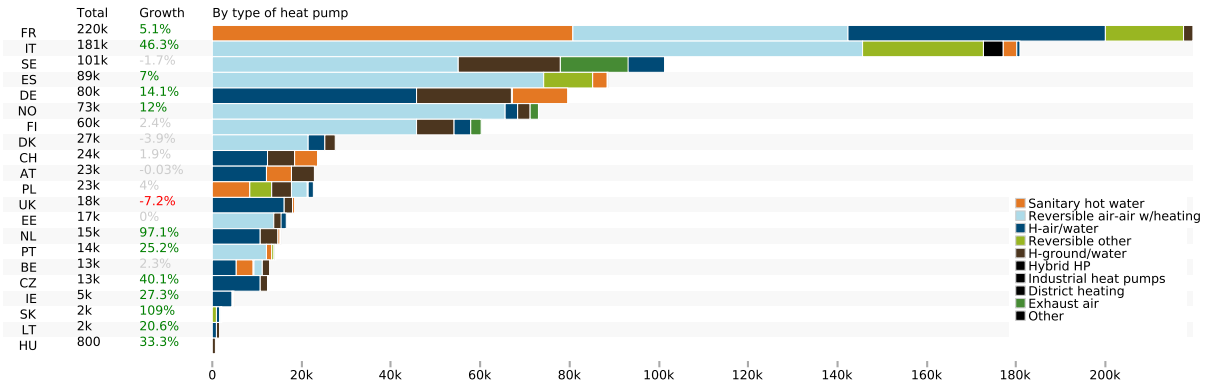

Figure I.3. Sales of heat pumps in Europe in 2016, per country and heat pump type. Source: EHPA [39].

sold, with 220k, while if normalized by the number of households in the country, Norway performs best, with 3.3 heat pumps per 100 households (0.76 in France for instance). The Italian market has seen a considerable growth with +46.3% over the previous year. In Spain, 89k units were sold, which represents 0.48 heat pumps per 100 households and a market growth of 7%. With a current electricity to gas price ratio around 3, heat pumps face a hard competition with gas boilers, which are the predominant technology for space and water heating in Spanish households, given their cheaper price compared to heat pump units. There is thus an important potential for the heat pump sector to increase its share in the market.

This increase in the share of heat pumping technologies for heating and cooling will be completely necessary to cope with ambitious climate change mitigation targets. This statement is illustrated and supported by Figure I.4. The Energy Technology Perspectives 2017 report [41] from the IEA states that electric heat pumps must increase from roughly 3% of installed heating equipment in buildings today to nearly 50% of the total heating stock in 2060, so as to reach its most ambitious B2DS scenario (i.e. where global warming is kept below 2°C). At the same time, the average energy performance of heat pumps in buildings, with COPs of around 2 to 2.5 today, must double by 2060 to achieve average COPs of 4 to 4.5 or greater [41]. As an illustration that this transition has already started, most heat pump manufacturers have now developed new models with R32 as a refrigerant instead of the most common R410A used so far; they claim higher COPs, and less refrigerant needed to operate the heat pump. Furthermore, R32 has a lower greenhouse potential than R410A, which limits the overall impact of installing heat pumps, when considering potential leaks.

As a summary, heat pumps represent a very efficient and necessary technology to both decarbonise heating and cooling, and enable their demand-side flexibility. Since heat pumps still remain to this day n[illegible] their fossil-fuelled counterparts, policy-makers must act consequently to guide i[illegible] such kinds of emission-free technologies.

Figure 3.12 Evolution of heating equipment in buildings to 2060

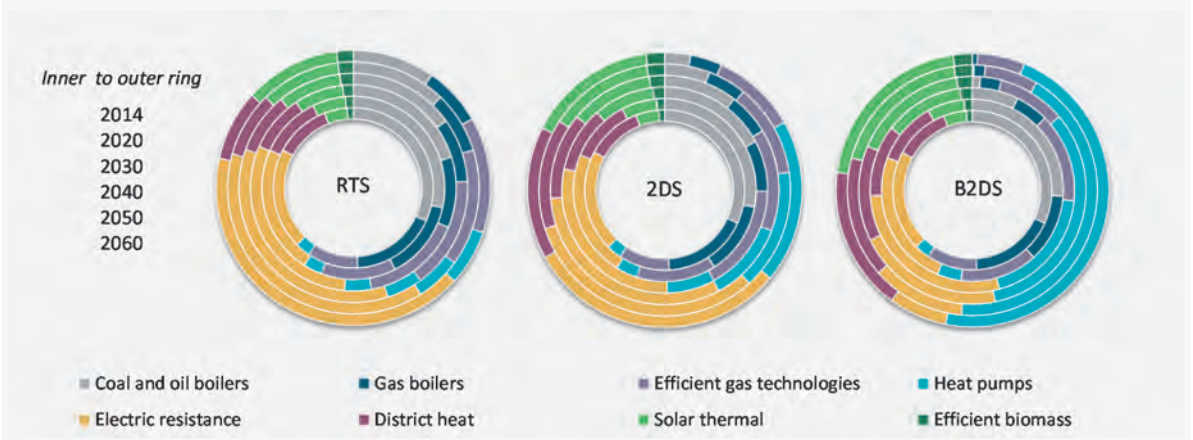

Notes: Heating in buildings represents space and water heating; it excludes cooking and other end uses. Efficient gas technologies include gas condensing boilers, gas instantaneous equipment and gas heat pumps. Traditional use of solid biomass is not included.

Key point *The B2DS represents a strategic shift away from fossil fuel equipment to high-efficiency and renewable technologies, such as heat pumps, solar thermal and modern district energy.*

Figure I.4. Evolution of heating equipment in buildings to 2060. The Reference Technology Scenario (RTS) reflects the world's current ambitions in terms of climate policies, while the scenarios 2DS and B2DS consider more ambitious plans to reduce global warming by maximum 2°C or below 2°C, respectively. Source: IEA Energy Technology Perspectives 2017 [41].

30. Further information can be found at www.cleanenergyministerial.org/Our-Work/Initiatives/Energy-Access.
31. Further information can be found at www.efficiency4access.org/about/.
32. Efficient biomass heaters, such as high-performance fireplaces, masonry stoves and pellet stoves, can achieve burn efficiencies of as much as 90% or more, while maintaining high temperatures over long periods of time (IEA, 2013b).
33. Deployment of solar thermal technology in buildings has slowed down in the last two years due to less rapid growth in China. See Chapter 2, "Tracking clean energy progress".

1.6 Need for adequate control strategies

To exploit the thermal storage of buildings and unlock the flexibility potential of heat pumps, appropriate control strategies are however needed. The flexibility of heating or cooling loads can be controlled in different manners. The first group of methods consists of simple rule-based controls (RBC),

which aim at avoiding peak periods with fixed schedules [42], reducing the peak power exchange between buildings and the grid [43], reducing the energy cost [44] or increasing the consumption of RES [45]. More advanced control strategies revolve around model predictive control (MPC), which consists of an optimization problem, most commonly used for decreasing the energy bills when variable electricity tariffs are applied [46]–[48]. However, the implementation of this second group of control strategies remains more complex due to the prior need of models to forecast the behavior of the systems in the future, and the high computation efforts required to solve the resulting optimization problem [49].

Supervisory control for improving demand-side flexibility with heat pumps has largely been investigated in recent literature [50]. Both RBC and MPC present advantages as well as drawbacks for improving the energy flexibility of heating and cooling loads. However, there is still a lack of knowledge in certain aspects of these types of controllers, notably regarding their development, tuning and testing in realistic setups. The present thesis thus intends to address these lacks and produce scientific knowledge about the performance of these controllers and the contexts in which they can be used. This knowledge will be useful to help performing a successful transition towards smarter and more energy-flexible buildings and more sustainable integration of heating and cooling demands.

2 Research questions and objectives of the thesis

2.1 General objective

The final aim of this doctoral thesis consists in facilitating the integration of RES in the energy mix by enhancing the energy flexibility of buildings in the future context of the smart grids. To this end, innovative control strategies for building energy systems such as heat pumps should be designed, which make use of short-term heat storage within the building thermal mass or within water tanks. The main research question can thus be formulated as follows: *which control strategies can be implemented to improve the energy flexibility of a building equipped with a heat pump, and thus to help manage the smart grid of the future?*

2.2 Research gaps and specific objectives

The general objective of the thesis is then declined into several specific sub-objectives, according to the identified research gaps.

Although energy flexibility has become a trending research topic in recent years, the role that buildings can play as flexible assets in the energy grids might still not be evident for the utilities. Energy flexibility is still not an absolute and immediate need, or it is still confined to certain specific geographic areas, which explains why the exploitation of energy-flexible buildings is yet very timid or even nonexistent. Research in this area is still mainly restricted to academia or theoretical studies, and too few on-site implementations have been carried out so far. However, the constant increase of variable renewable energies in the grid will soon make the need for energy-flexible buildings a more tangible and urgent reality. For this reason, the research in this domain must be brought one step further, with tests in experimental or field setups, so as to prove their viability and performance in more realistic contexts.

The existing research on energy flexibility in buildings has often focused on how to exploit the heating loads for this purpose, sometimes the cooling loads, but seldom for both with the same building. However, some regions such as the Mediterranean area have mild climates where the cooling peaks in summer might be of similar amplitude than the heating peaks in winter. In this context, energy flexibility might present an interest in both seasons to support the operation of the grid. The constraints are nevertheless different, with the cooling demand peaking in the afternoons, while the heating demand generally peaks in the mornings and evenings. Consequently, the peak demand matches differently for instance with the peak of solar energy production, according to the season. To the knowledge of the author, little research has been carried out on this topic, and the adaptations potentially needed

to exploit a single building for its energy flexibility in a heating or cooling context are still little known, as well as the differences of flexibility resources in different seasons.

Regarding the type of controllers that can be utilized to exploit the energy flexibility of buildings, a detailed state-of-the-art is reported in chapter II. They can mostly be classified between rule-based controllers and predictive controllers. Their formulation, and more particularly their declared objectives have been investigated in the existing literature. They usually intend to enhance the energy flexibility in different ways, but these are not necessarily specific to heat pump systems. Especially in MPC formulations, the representation of the heat pump is often simplified drastically and does not take into account practical constraints that apply to a real pump functioning in an actual building. A lack of suitability of the controllers to the particularities of heat pumps was thus observed and should be addressed. Regarding the MPC in particular, it is known that such controllers have high development costs compared to simpler strategies, but there exists little previous work that puts into perspective their development costs with the benefits they can achieve when operational. Further than that, there is also a lack a comprehensive comparisons between MPC and RBC operated in a controlled environment with the exact same boundary conditions: such studies would be very beneficial to help inform decisions on what type of controller can be used for energy flexibility in buildings.

In the state-of-the-art of chapter II, the flexibility objectives declared in existing studies often consist in reducing the operational costs. Few other objectives than the economic one have been studied, although recent studies have chosen to go in this direction. In particular, since the final aim is to decarbonize our energy systems, other objectives should be tested, especially the reduction of the CO_2 emissions related to the heating and cooling of buildings. The carbon footprint of the electricity from the grid must thus be known precisely, and the impact of the flexibility strategies in terms of emissions should be studied.

The specific objectives that stem from these identified research gaps are explained hereafter.

- A first goal of the PhD thesis consists in developing and obtaining supervisory controllers for heat pumps, capable to enhance the energy flexibility of the heating and cooling demand. Both RBC and MPC controllers will be developed. For the RBC controller, the development steps are rather straightforward:

  a) Choosing the input data and the type of rules which makes up the RBC.
  b) Tuning the parameters present in the RBC to obtain the best performance.

  For the MPC, which is a more complex controller, the methodology requires more prior work. The most important steps to develop the MPC are:

  a) Obtaining and validating reduced-order models of buildings and of the heat pump for the controller. The MPC solving will notably be influenced by the linearity of those models.
  b) The implementation of the cost function. Since Economic MPC has already been largely investigated in the context of building energy management, other MPC configurations should be tested, notably introducing the carbon footprint in the objective.
  c) The optimization and tuning of the MPC configuration, especially taking into accounts constraints representative of the real operation of heat pump systems.

  The thesis should thus answer the following: *which are the best parameters to include in an energy flexibility controller? How does changing the objectives or constraints affect the performance of said controller? What are the pros and cons of different RBC or MPC configurations? How can flexibility controllers be better adapted to the particularities and operational constraints of heat pump systems? For MPC, how does the required modelling and formulation affect the performance of the controller?*

- The thesis shall also demonstrate the benefits of using innovative control strategies for managing energy in buildings. If new control strategies are developed, they should present some advantages for the grid side (for example reducing the peak demand, shifting loads to non-peak periods, or more generally enabling a larger integration of renewable energy) and for the user side (regarding comfort or energy bills for instance). In this regard, *which criteria should be used for*

the evaluation of the control strategies? Using these criteria, what are the improvements brought by MPC or RBC compared to traditional controls? Are these improvements worth the efforts in development and implementation required by these new smart controllers?

- Few real implementations of flexibility controllers for heat pump systems have been realized so far. The performance of the control strategy could be subject to variations between simulation and on-site implementation, due to external disturbances, inaccuracies in the modelling or in the forecasting. Especially for MPC, the operation on a physical device in real conditions should be carried out, to answer the following questions: *how do the MPC strategy and the heat pump perform in a more realistic setup such as a semi-virtual environment or in a real building? Is the performance coherent with the expected behavior reported in simulations? What are the observed differences and by which factors can they be explained?*

- The geographical context and the type of buildings can also impact the efficiency of the considered control strategies. In particular, several parameters such as the climate, characteristics of the grid or the energy mix can be used as input for the developed control strategies. In order to address some of these issues, the following questions will be researched: *especially focusing on the Mediterranean context, can we use reversible heat pumps for energy flexibility both in the heating and the cooling season? What differences does it make in the formulation and in the results? What is the expected performance of energy-flexibility controllers in the Mediterranean context for residential buildings?*

3 Framework and structure of the thesis

3.1 Framework

This PhD project forms part of the INCITE Innovative Training Network (ITN) described below, in which the training of the PhD candidates constitutes an important objective, aside from the production of valuable scientific research. Training includes the attendance to several technical courses (summer schools, master courses at the UPC) to acquire specific knowledge, as well as complementary skills courses (project management, responsible conduct in research etc.). The aim is to enhance the career prospects of the candidate in the R&D field through a complete and inter-disciplinary training. The candidate was also exposed to multi-sectoral and international work environments which enabled him to start building a professional network. In addition, the PhD candidate is involved in the activities of IEA EBC Annex 67. Those different entities which form the framework of the PhD are described in the following paragraphs. In addition, the PhD candidate also performed two external stays in international institutions: one in 3E, a consulting company based in Brussels, and the second one in EnergyVille, an entity of VITO, the Flemish Research Institute, dedicated to energy research and located in Genk, Belgium.

INCITE ITN The PhD project has been fully financed by INCITE, a European project that received funding from the Horizon 2020 Research Programme of the European Union. The project has the format of an Innovative Training Network (ITN) of the Marie Sklodowska-Curie Actions (MSCA), which means that several PhD fellows (14) were hired simultaneously in different European countries (7) to work on a common topic, with each his/her individual research project. INCITE focuses on developing innovative controls for the integration of renewable sources into smart energy systems. As an ITN, the project offers networking opportunities among the member institutions and with the other fellows, network-wide courses and seminars (twice a year) and secondment possibilities in non-academic institutions. More information on the project can be found on the following website: www.incite-itn.eu.

IEA EBC – ANNEX 67 The International Energy Agency (IEA) and its programme on Energy in Buildings and Communities (EBC) organize several transnational projects named 'annexes'. The Annex numbered 67 focuses on the Energy Flexibility of Buildings, which is therefore totally in the scope of

the present project. The aim is to increase the knowledge on this specific topic and to demonstrate the potential that buildings possess with regards to energy flexibility. Spain and IREC in particular are involved in this Annex 67, which includes the participation in the bi-annual expert meetings and different work subtasks. Specifically, the present PhD project contributed to the Subtask B.3 about control strategies and algorithms, and to the writing of different deliverables and reports. More information on the project can be found on the following webpage: http://annex67.org.

3.2 Publications and outreach activities

In the mark of the thesis, several publications were written for international journals and conferences. The thesis is partly based on those contributions. They are referenced here, firstly listing the ones where the PhD candidates was the first author: 4 journal articles, and 6 papers in international conference proceedings. The PhD candidate has also been involved in other publications, such as reports and deliverables of the IEA EBC Annex 67, or as co-author of journal articles and conference papers. These are listed as other contributions. Furthermore, several outreach activities also contributed to disseminating the knowledge related to this PhD thesis to a broader and more general audience.

Journal articles:

- T. Péan, J. Ortiz, and J. Salom, "Impact of Demand-Side Management on Thermal Comfort and Energy Costs in a Residential nZEB," *Buildings*, vol. 7, no. 2, p. 37, 2017, ISSN: 2075-5309. DOI: 10.3390/buildings7020037 [51].

  Impact factor: not indexed in JCR, CiteScore 2018 from Scopus: 2.28 (#7/111 Q1 in Engineering Architecture)

- T. Péan, J. Salom, and R. Costa-Castelló, "Review of control strategies for improving the energy flexibility provided by heat pump systems in buildings," *Journal of Process Control*, vol. 74C, Special Issue on Efficient Energy Management, pp. 35–49, Apr. 2019, ISSN: 09591524. DOI: 10.1016/j.jprocont.2018.03.006 [50].

  Impact factor: 3.316 (2018 JCR, Q2: #38/138 in Chemical Engineering, Q2: #21/62 in Automation & Control Systems)

- T. Péan, R. Costa-Castello, E. Fuentes, and J. Salom, "Experimental testing of variable speed heat pump control strategies for enhancing energy flexibility in buildings," *IEEE Access*, vol. 7, no. 1, pp. 37 071–37 087, 2019, ISSN: 2169-3536. DOI: 10.1109/ACCESS.2019.2903084 [52].

  Impact factor: 4.098 (2018 JCR, Q1: #24/148 in Computer science & information systems, Q1: #48/260 in Electrical and electronic engineering, Q1: #19/87 in Telecommunications)

- T. Péan, R. Costa-Castelló, and J. Salom, "Price and carbon-based energy flexibility of residential heating and cooling loads using model predictive control," Sustainable Cities and Society, vol. 50, Oct. 2019, ISSN: 22106707. DOI: 10.1016/j.scs.2019.101579 [53].

  Impact factor: 4.624 (2018 JCR, Q1: #6/63 in Construction & Building Technology, Q1: #25/103 in Energy & Fuels, Q2: #10/35 in Green & Sustainable Science & Technology)

Conference papers:

- T. Péan, J. Ortiz, and J. Salom, "Potential and optimization of a price-based control strategy for improving energy flexibility in Mediterranean buildings." in *Proceedings of CISBAT 2017 International Conference – Future Buildings and Districts – Energy Efficiency from Nano to Urban Scale*, Lausanne, Switzerland, 2017 [54].

- T. Péan, E. Fuentes, J. Ortiz, and J. Salom, "Performance of a gas boiler under dynamic operation conditions: experimental studies in semi-virtual environment," in *Proceedings of COBEE2018 - Conference On Building Energy & Environment*, Melbourne, Australia, 2018.[55]

- T. Péan, B. Torres, J. Salom, and J. Ortiz, "Representation of daily profiles of building energy flexibility," in *Proceedings of eSim 2018, the 10th Conference of IBPSA-Canada*, Montréal (QC), Canada, 2018, pp. 153–162, ISBN: 9782921145886 [56]

- T. Péan, J. Salom, and J. Ortiz, "Environmental and Economic Impact of Demand Response Strategies for Energy Flexible Buildings," in *Proceedings of BSO 2018 Building Simulation and Optimization*,11-12th September 2018, Cambridge, United Kingdom, 2018, pp. 277–283 [57].

- T. Péan, J. Salom, and R. Costa-Castelló, "Configurations of model predictive control to exploit energy flexibility in building thermal loads," in *Proceedings of the 57th IEEE Conference on Decision and Control*, Miami Beach, FL, USA, 2018 [58].

- T. Péan, I. Bellanco and J. Salom, "Impact of the weather forecast on a predictive controller performance: experimental studies with a residential heat pump for space cooling", in *Proceedings of the 13th IEA Heat Pump Conference* (Jeju, Korea), May 2020 (abstract accepted 16 August 2019).

Other contributions:

- T. Péan and J. Salom, "Laboratory facilities used to test energy flexibility in buildings - A technical report from IEA EBC Annex 67 Energy Flexible Buildings," IEA EBC Annex 67, Tech. Rep., 2019. . Available from: http://annex67.org/media/1708/laboratory-facilities-used-to-test-energy-flexibility-in-buildings-2nd-edition.pdf [59].

- R. Toffanin, T. Péan, J. Ortiz, and J. Salom, "Development and Implementation of a Reversible Variable Speed Heat Pump Model for Model Predictive Control Strategies," in *Proceedings of Building Simulation 2019 - 16th IBPSA International Conference*, Rome, Italy, 2019 [60].

- C. Finck, P. Beagon, J. Clauß, T. Péan, P. Vogler-Finck, K. Zhang, and H. Kazmi, "Review of applied and tested control possibilities for energy flexibility in buildings - A technical report from IEA EBC Annex 67 Energy Flexible Buildings," International Energy Agency - Energy in Buildings and Communities, Tech. Rep., 2018, 61 p. [Online]. Available from: http://annex67.org/media/1551/review-of-applied-and-tested-control-possibilities-for-energy-flexibility-in-buildings-technical-report-annex67.pdf [61].

- J. Salom and T. Péan, "Experimental facilities and methods for assessing energy flexibility in buildings -Deliverable of the Annex 67 - Energy Flexible Buildings," International Energy Agency - Energy in Buildings and Communities, Tech. Rep., 2019, 111p. [62].

- K. Foteinaki, R. Li, T. Péan, C. Rode, J. Salom, "Evaluation of energy flexibility of low-energy residential buildings connected to district heating", Submitted to *Energy and Buildings* (revision requested 05 September 2019)

Outreach activities

- Participation in the 1st BCN Science Slam, 3rd March 2017 in Bar Mau Mau, Barcelona (Spain), following a science communication workshop.

  Video: https://www.youtube.com/watch?v=qMsR5oYx8y4

- Organization and presentation during the workshop "Energy-flexible buildings" for the IEA EBC Annex 67 6th working meeting, 26th March 2018 in Palau Robert, Barcelona (Spain).

- Participation in the UPC institutional final of the competition "Tesis en 4 minuts" organized by the Fundació Catalana per a la Recerca i la Innovació (FCRi), 16th May 2019, UPC campus in Barcelona (Spain).

3.3 Structure of the thesis

Following this introductory chapter, the remaining of the thesis is structured as follows.

Chapter II relates the state-of-the-art of heat pump controls for energy flexibility, by performing a thorough review of the existing literature on this topic. In particular, the objectives utilized by different authors in RBC and MPC controllers are analyzed in details.

Chapter III groups all the methodology needed to analyze the energy flexibility of buildings and the performance of the developed controllers. Firstly, the simulation and experimental frameworks used to test the controllers are explained. Then the Key Performance Indicators (KPIs) and input data used to enhance the energy flexibility are detailed. The next section of this chapter relates the characterization and modelling of the studied heat pump system, while the last one relates the modelling of the building study case.

Chapter IV reports the development of the energy-flexibility controllers. It starts by the development of the RBC controller and its tuning. The MPC controller is then detailed, and in particular also its formulation and the tuning of its different parameters.

Chapter V concerns the results of the experimental studies carried out in the mark of this thesis with a real heat pump system. Using the controllers developed in the previous chapter and the methodology of Chapter III, the performed experiments are analyzed in details, bringing practical insights on the performance of the controllers operating with a real heat pump.

Chapter VI then describes the results of simulation-only studies. Learning from the experiments, some adjustments are made and the results from the controllers operating in a simulated framework are analyzed and compared with the experimental ones, providing a further validation of the models.

Finally, Chapter VII concludes the thesis by summarizing the learnings from both the experiments and the simulations. The performance results of the RBC and MPC controllers is summed up, discussions are drawn regarding the practical implementation of such controllers, and an outlook on potential further research is proposed.

Several appendices complete the body of the thesis; they give additional details on some aspects which were not required within the main text.

Chapter II

State of the art in heat pump controls

Buildings equipped with heat pumps are deemed worthy of further investigations with regards to their potential for energy flexibility. They can become active elements in the energy grids, providing flexibility services when needed [63]. A quite extensive amount of research and articles has been published on these topics in the recent years. Because of the relatively new interest shown on energy flexibility with heat pumps, a clear overview is still lacking in this field. Several reviews on close topics have nevertheless been published: Afram and Janabi-Sharifi [64] reviewed MPC techniques applied to HVAC systems, but their study did not focus on heat pumps specifically. Atam and Helsen [65] studied modelling challenges and control techniques, but only for ground-source heat pumps. Fischer and Madani [36] recently published a review on the use of heat pumps within smart grid contexts, but their study did not go in depth into the different control strategies used in the studied literature. Based on this assessment, the present chapter proposes a detailed review of the control strategies used for activating energy flexibility with heat pumps, detailing in particular the different objectives claimed and the constraints included.

In the reviewed publications, a scheme similar to the one presented in Figure II.1 was generally observed. The control strategies presented here are acting at the supervisory level, assuming the presence of local controllers within the heat pump, which enable a proper operation of the different components (compressor, pumps, defrost...). The supervisory controller receives information from different sensors in the building (room temperature, temperature in a storage tank, PV production, net power exchange with the grid etc.) as well as data on weather and energy tariffs. Based on this information, the control algorithm defines a strategy for operating the system, and sends the corresponding signal to the local controller in the heat pump.

The control strategies reviewed have been classified in two distinct categories: rule-based controls (RBC) and Model Predictive Control (MPC), because of their conceptual difference. Rule-based controls are simple heuristic methods which generally have the form "if (condition is verified), then (action is triggered)". RBC usually rely on the monitoring of a specific "trigger" parameter (PV power, room temperature for example) on which a threshold value has been fixed. When the threshold is reached, the operation of the heat pump is changed, according to the predefined strategy. On the other hand, Model Predictive Control is a more complex strategy, which relies on a model of the building to project its behavior in the future. MPC is an optimization problem, therefore it intends to find the best solution for the management of the heat pump operation, over a certain time horizon and within certain constraints. Further than this classification between RBC and MPC, the reviewed papers have been sorted by the objective that the control strategy aims for.

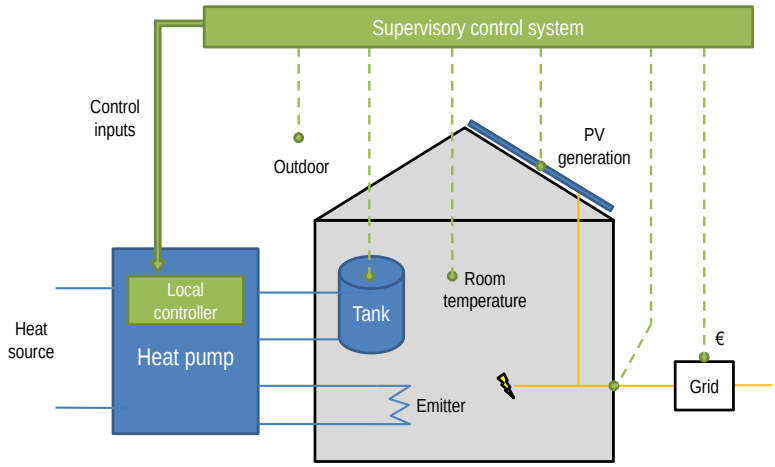

Figure II.1. General scheme of supervisory control systems for heat pumps. The supervisory control receives information from different sources, and defines a control input which is then sent to the heat pump.

1 Common characteristics

1.1 Control inputs

The control strategies act upon certain parameters, which are called control inputs (or manipulated variables). No major differences were found for the control inputs between RBC and MPC. In the reviewed papers, the following control inputs have been identified:

- **Temperature set-points**: several control strategies modulate the temperature set-points, whether in the room thermostats [66], [67], the supply of the systems [68], or in a water storage tank [66], [69].
- **Power of the heat pump**: this variable can be binary, which means the heat pump is completely switched on/off depending on the control algorithm decisions [70]. If the heat pump is inverter-controlled, the power of the heat pump can be modulated by regulating the speed of the compressor [71], therefore the control input can vary between the minimum and the maximum available power of the heat pump. This is easily done in simulations, however in practice, this modulation can also be achieved indirectly by adjusting the set-points, like previously mentioned [43].

1.2 Sensors

A supervisory control system usually receives measurement data from different sensors. The most common sensors encountered in the literature are the following:

- **Temperatures**: the indoor temperature is normally the main parameter monitored to ensure comfort. Usually the operative temperature is considered, which is an average between the air temperature and the mean radiant temperature (taking into account the radiation effects from the surrounding surfaces)[72]. When using radiant systems for cooling, the relative humidity must be measured as well to calculate the dew point and thus avoid condensation on the surfaces. In the case of a storage tank, a sensor can measure the water temperature inside it, which is sometimes converted into a "state of charge" of the tank [43], [73].
- **Power measurements**: when applicable, the energy consumption of the building can be monitored, through a simple electricity meter for example. If a production unit like PV is present,

the production can usually be retrieved from the inverter. Specific control strategies rely on the measurement of other parameters like the voltage level at the distribution feeder [45].

- **Outside conditions**: when weather compensation is utilized (see subsection 1.3), a probe needs to measure the outside temperature to adapt the system supply temperature consequently.

1.3 Reference weather compensation control

The simplest type of rule-based control for a heat pump consists in applying a target set-point to its supply temperature. The set-point is then tracked with traditional PID or hysteresis controller [68]. The main objective is therefore to provide the necessary comfort to the end-user, by reaching this set-point. No flexibility is intended at this stage, only the users' needs and the local climate constraints are taken into account, that is why such strategies are normally used as reference cases. As there is no need for supervisory control, a low-level controller integrated in the heat pump is sufficient for the operation of such simple strategies.

Rather than applying a constant set-point, the use of 'heating curves' (also known as 'weather compensation') has become state of the art in most of the heat pumps available on the market. A heating curve enables to adapt the water supply temperature set-point according to the outdoor temperature, and consequently to reduce the energy consumption in part-load conditions. Some parameters are needed as input for the heating curve (conditions at design outdoor temperature and threshold when heating is not anymore needed), which are often determined in practice by trial and error [67].

Several authors mention the use of weather compensation control in the reference case of their publications [43], [46], [68], [73], [74]. The set-point obtained from the heating curve can be applied in a water storage tank or directly in the water circulated into the heating circuit of a building (radiators, floor heating). A room thermostat is then necessary to control the water flow (either from the tank or directly from the heat pump) or heat pump activation and deliver the proper amount of heat to the building zone, according to the occupancy.

2 Rule-based controls

2.1 Classification of rule-based controls

When the building's designers intend to provide some flexibility from the building side, further than only comfort, they usually define certain objectives to reach. Especially in RBC, these objectives are not always mentioned explicitly, but most of the time a clear goal can still be identified. In the present review, the following objectives have been identified: load shifting with fixed scheduling, peak shaving, reduction of energy cost and increasing the consumption of renewables. These are summarized in Table II.1 and detailed in subsection 2.2. Most of these rule-based controls follow the same principle: a trigger parameter is monitored (time, power, energy price, residual load) and associated with predefined threshold values. When the threshold is reached, it triggers a control action on the heat pump (start/stop or change in set-point among others).

2.2 Flexibility objectives

Load shifting with fixed scheduling is maybe the most evident form of rule-based control for energy flexibility. Daily peak periods can usually be identified in a national electricity grid. The controller can therefore try to avoid or force the operation of the heat pump during fixed hours. For instance, Lee et al. use set-point modulation to reduce the use of the heat pump during the grid peaks (14:00 to 17:00 in summer and 17:00 to 20:00 in winter) [66]. They achieved a reduction in the energy consumption during peak hours of 80% and 64% in cooling and heating respectively (Figure II.2a). In the study by Carvalho et al., the heat pump was forced to stop during peak hours (9:00 to 10:30 and 18:00 to 20:30)[42], reducing the energy cost by 17 to 34% (Figure II.2b). Fixed scheduling can also be used to

Table II.1. Classification of rule-based controls according to their objectives and trigger parameters.

Flexibility objectives	References with rule-based controls (RBC)	Trigger
Load shifting with fixed scheduling	Lee et al. (2015)[66]; Carvalho et al. (2015)[42]; De Coninck et al. (2010)[73]; De Coninck et al. (2014)[45]	Time
Peak shaving, reduction of peak power exchange	Dar et al. (2014)[43]; De Coninck et al. (2010)[73]; De Coninck et al. (2014)[45]	Power
Reduction of energy cost	Schibuola et al. (2015)[44]; Le Dréau and Heiselberg (2016)[75]	Electricity price
Increase consumption of renewables	Dar et al. (2014)[43]; Schibuola et al. (2015)[44]; De Coninck et al. (2014)[45]; Reynders et al. (2013)[74]; Miara et al. (2014)[69]; Hong et al. (2012)[67]	PV power, voltage deviation, residual load

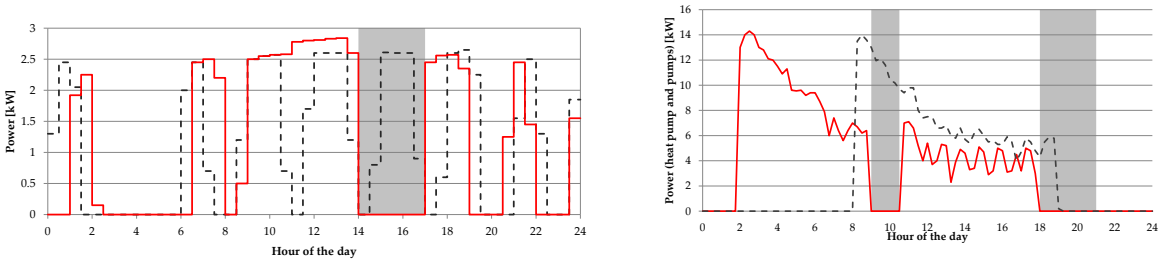

(a) **(b)**

Figure II.2. Examples of fixed scheduling strategies from [66](a) and [42](b). The peak periods (identified in grey) are constant, and the control strategies thus aim to avoid the heat pump operation (red lines) during these fixed periods. In both cases, this objective is reached. The dashed lines show the profile of the heat pump operation prior to the implementation of the control.

force the charging of a thermal energy storage (TES) tank: for instance, De Coninck et al. used this strategy to charge a tank from 12:00 to 19:00 every day, benefitting from the higher Seasonal Performance Factor (SPF) of the heat pump during daytime [73]. In another study they used clock control, raising the Domestic Hot water (DHW) heating set-point from 12:00 to 16:00 in order to force the heat pump operation during this period, and achieving best results than more advanced rule-based controls [45]. Overall, fixed scheduling strategies are simple and easy to implement, and they can already achieve a substantial performance. Even though the schedule can be changed seasonally as for instance in Lee et al. [66], this method is not dynamic enough since the fixed schedule does not adapt to the real conditions.

Another objective targeted by RBC strategies is *peak shaving*, i.e. the reduction of the demand peak, in order to support the grid operation. In these cases, the monitored parameter is the power exchange of the building with the grid. Thresholds can be defined both for the export and in the import powers, or only in one of them. For instance, Dar et al. set an import limit of 2500 W and an export limit of 5000 W in a nZEB equipped with a PV system [43]. When the building is consuming more than the import threshold, the heat pump is switched off. Conversely, if the building injects more power in the grid than the export thresholds, the heat pump is started. This control method results in a reduction of the import hours (over the threshold limit) down to 41-108 hours, compared to 346 hours for the reference case. De Coninck et al. present a similar “grid-load strategy”, with both consumption and injection thresholds set at 3500 W [73]. This method could reduce the number of peaks by up to 50% and the one percent peak power (mean power of the one percent highest quarter hourly peaks) by up to 20%. However, the highest peaks could not be eliminated, since they were not caused by the

heat pump nor the PV systems, but by non-controllable loads such as domestic appliances. In a later study, De Coninck et al. investigated a similar approach [45], but applied to a cluster of 33 buildings instead of a single one. When the power injection in the grid surpasses the predefined limit, the set-points for the DHW tanks are raised, thus increasing the self-consumption from the PV systems. This strategy reduces effectively the curtailing losses, though not as much as the fixed scheduling strategy also investigated in [45] (because the latter is active every day and not only during sunny days). To sum up, peak shaving control strategies enable to support the grid by limiting the peak demand or injection of the building. Another conclusion drawn from the review is that the threshold values should be chosen with precaution, since their setting will highly influence the outcome of the control strategy.

Certain control strategies rely on the variations of energy price in time with the objective of *reducing the energy costs* for the end-users. As evidenced notably by [76], [77], time-varying price structures produce incentives for the consumers to shift their loads or reduce their peak demand, while reducing their energy budget. It is therefore profitable for both parties, the grid side and the consumer side. In this case, the controller monitors the electricity price and takes action when the price becomes too high or too low. The main differences in the reviewed papers therefore consist in the definition of the high and low price thresholds. Schibuola et al. propose two different approaches [44]: the first one analyzes the price data of two entire years (2012 and 2013), and fixes thresholds based on this distribution. The second approach compares the current electricity price with the forecasted price over the next 12 hours, hence relying on prediction data rather than on past data. Both methods enabled to reduce the yearly electricity costs of around 15%. Le Dréau and Heiselberg also based their approach on recorded past data [75]: their thresholds were calculated using the first and the third quartiles from the price distribution of the two weeks prior to the current moment. Changes of ± 2 K in the heating set-points were then implemented when the current electricity price reached the thresholds. A high flexibility was thus obtained and the cost savings ranged from 3 to 10%. This type of price-based control is bound to grow in the coming years with the increasing development of smart-grids, where dynamic pricing can easily be sent to the end-users. The performance of the controls then highly depends on the processing of this price data and the definition of the threshold parameters.

The last category of rule-based controls reviewed here aims at *improving the consumption of renewable energy sources (RES)*. This can be done at the scale of the building, which means a local generation unit is present and the objective consists in improving its self-consumption. It can also be done at the scale of the overall electricity grid, which means the control relies on the analysis of the residual load calculated at a national level. The residual load equals the power demand less the power generation from fluctuating RES (solar and wind), hence representing the electricity demand not covered by renewables. In the study by Dar et al. [43], the building is equipped with a PV system. The controller starts the heat pump when the PV production exceeds the non-heating loads. This method leads to an improvement of the load cover factor from 19.6 to 26-32%, hence a better coincidence between photovoltaic generation and electricity consumption of the heat pump. A similar approach is presented by Schibuola et al. [44], but with a more straightforward method: the heat pump is simply forced to switch on when the PV panels are generating electricity, regardless of the current loads. This method enabled to reduce the electricity exported by up to 12% and the electricity imported by up to 22%, thus improving the self-consumption. De Coninck et al. use a different trigger for the activation of DSM: voltage measurement [45]. Their study assumes that an excess PV production induces an increase of voltage of the distribution feeder. The voltage is therefore monitored, and when it surpasses a defined value (around 250 V), the set-point for the DHW tank is raised in order to utilize more electricity and avoid the PV inverter shutdown. This method enables to reduce the curtailing losses by up to 74%. The residual load at a national scale has been identified by [78] as a potential input signal for DSM control of heat pumps. Miara et al. make use of this residual load profile to design their own Time of Use (ToU) signal [69]. This technique enables an efficient load shifting: the percentage of energy spent during the most profitable periods (e.g. with high residual load) is increased from 30% to around 60% in the best case. To summarize, the improvement of RES consumption can be realized by monitoring different trigger parameters: voltage at the distribution feeder, PV production, residual load at the local or global scale, but it remains difficult to compare these approaches since they use different evaluation criteria.

2.3 Interaction with the constraints

Rule based controls also need to deal with additional constraints, to account for the comfort of users or the physical limitations of the systems. Similarly than the control objective, the constraints are more difficult to identify in the case of RBC, since they are not always formally identified. For instance, setting a threshold on the grid power exchange as presented in [43], [45], [73], could be considered as a constraint on this parameter (or alternatively as a peak shaving objective, as mentioned previously). Control inputs are usually constrained by construction, therefore these constraints are normally always satisfied. For instance, the temperature set-points are obviously chosen within the desired comfort boundaries during occupancy periods. It is however more difficult to ensure that the constraints on the control outputs will always be formally fulfilled. In the case of building climate control, the control outputs almost always include the room temperature. For instance in [42], a preheating strategy is implemented and the heat pump is switched off during peak hours. The authors do not mention a backup control strategy for ensuring comfort during this switched off period. Even though the preheating strategy is specially designed to avoid discomfort, such punctual inconveniences could occur. In several publications, a buffer storage is present. Such device enables to decouple the zone heating circuit from the buffer heating circuit. In this way, the fulfilment of the constraints on the zone temperature is less affected by the flexibility-oriented RBC: the zone heating circuit operates normally, retrieving thermal energy from the storage, while the flexibility strategy is applied directly on the storage. In this case, additional constraints can be applied to maintain a minimum or maximum state of charge (SOC) in the storage [43], [69], [73]. In general, constraints in RBC can be seen as additional rules which are given priority over the rule defining the flexibility objective. The physical integrity and the satisfaction of users must normally be met at all times, and the flexibility can be improved only once these constraints are satisfied. This principle is well illustrated in the form of a flow chart in [67]: the algorithm first checks if the zone temperature lies between the upper and lower comfort boundaries. If and only if this condition is satisfied, the flexibility strategy can be started. Even if favorable conditions appear (i.e. high production of renewables) while comfort is not guaranteed, the controller will still operate the system normally to promptly return within the defined temperature boundaries, before to consider the activation of flexibility. Several RBC strategies use modulation of temperature set-points as the main driver for energy flexibility [51], [66], [75]. If these set-points are always chosen within the desired comfort boundaries (considering the dead-bands too), the output temperature should also stay within these boundaries (unless the system is badly dimensioned or has too much inertia). With this technique, the comfort constraints are fulfilled while the loads are shifted in time. To sum up, in the case of RBC, the fulfilment of constraints is difficult to guarantee, given the lack of tools to formally analyze the system behavior. Furthermore, rule-based controls do not allow to balance the satisfaction of the constraints with the desired objective (and thus to allow for instance small constraint violations if it provides greater benefits for the achievement of the objective). However, the rules are normally designed to guarantee constraints fulfilment and thus ensure a satisfactory performance of RBC.

2.4 Conclusions and limits of RBC

In view of the presented papers and their respective conclusions, it is observed that rule-based controls can yield significant performance with regards to improving the energy flexibility. Applying simple heuristic algorithms enables for example to delay the use of a heat pump for several hours, or to realize significant cost savings by reorganizing its operation schedule. The good performance of the heuristic control strategies obviously depends a lot on the good choice of the thresholds values placed on the “trigger” parameters [79]. It is therefore crucial to draw some attention on the tuning of these values, as highlighted also by [80]. Another advantage of RBC resides in its simplicity. No complex models are required, neither computationally demanding algorithms. Most of the reviewed papers consider algorithms of the form “if condition is fulfilled” then “send a signal to the heat pump”. This simplicity could consequently facilitate the potential implementation of such controls at a larger scale, having a greater impact ultimately. However, rule-based controls also feature several lacks, usually concerning their poor dynamics. The fact that the trigger parameters or threshold values are fixed makes it difficult for this kind of control to adapt to changing external conditions. For instance, the

study [66] uses fixed scheduling because the peaks in the grid are identified between 17:00 and 20:00 in winter days. However, this assumption is based on the analysis of previous data and rules of thumb, but it could very well happen that the peaks occur outside this time window. This will become truer and truer in the future, as the penetration of variable renewable energies increases in the overall mix: Klein et al. [78] predicted that the variability of the residual load will be substantially higher in 2030. In particular in Spain, the calculated standard deviation of the residual load was very high compared to other countries, which means that the profile of this residual load could vary drastically from one day to the next. For this reason, the performance of fixed-rule controls appears rather limited, and better control strategies are needed in order to react faster to rapid changes in the grid conditions. Finally, rule-based controls lack the possibility to anticipate and optimize the heat pump operation over a certain time horizon. This deficiency is clearly visible when analyzing the result graphs from [67] presented in Figure II.3: the rule-based control implemented here results in a better fit of the demand power curve to the supply power curve (wind turbine), which is a good example of demand flexibility. However, a peak of electricity generation occurs just before the start of the heating system, but it is not exploited by the controller. A more optimal strategy would have preheated the building before, benefitting from the availability of electricity at that moment, and limiting the impact on the occupants' comfort afterwards. Another example of these deficiencies is given by [74] in mid-season: their control strategy charges the thermal mass of the building in the morning, because the local PV system produces electricity at that time. The building therefore reaches the upper limit of temperature comfort, and when the solar gains (unanticipated by the control strategy) later enter the room, overheating occurs. With this review, the performance and simplicity of rule-based controls have been highlighted, as well as the importance of a good design in the choice of the parameters defining the rule. It should be mentioned that it remains difficult to evaluate the performance of RBC, since they usually do not define an explicit cost a priori. Furthermore, their lacks in dynamics, adaptation and anticipation call for better control strategies based on optimization methods, as will be presented in the next section.

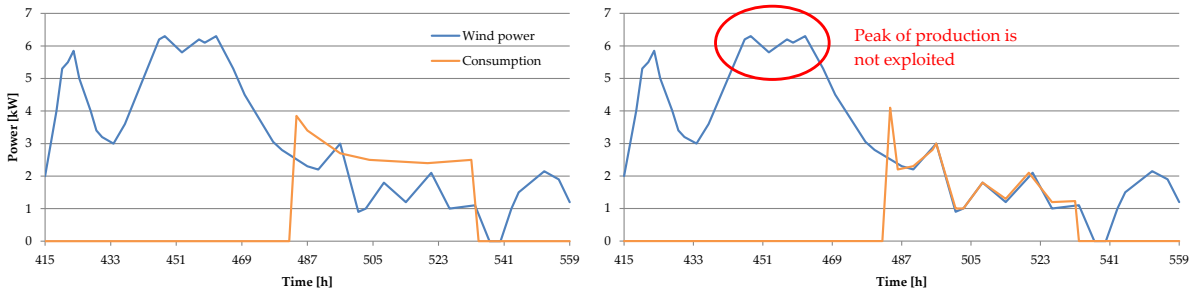

Figure II.3. Results extracted from the rule-based control algorithm proposed by [67]. The reference case is presented on the left and the rule-based control on the right. The rule-based control clearly provides a flexibility of the demand, since the consumption (orange line) adapts to the production (blue line). However, it does not optimize the energy management: the production peak before the activation of the heat pump is not exploited for storing energy, since the rule-based control is unable to make anticipated decisions.

3 Model predictive controls

3.1 Classification of MPC and decomposition of the different objective functions

Even though rule-based controls can already yield significant improvements with regards to demand response and flexibility, MPC is expected to produce further improvements but it also requires more investments and is more complex due to the prior need of a model [45]. As recalled by [81], model predictive control covers a wide range of different control techniques. They have in common to "make explicit use of a model of the process to estimate a future control signal by minimizing an

objective function" over a receding horizon N. At each time step k, the best sequence of future control inputs is calculated by the optimizer, and only the first one is then applied to the actual systems. The case of an application of MPC to building climate control with MPC is presented schematically in Figure II.4. The first applications of MPC to building climate control intended to enhance the energy efficiency and reduce the energy consumption [82], without too much focus on flexibility or demand-side management. Recently, more research has been developed for the use of MPC within smart-grids, with emphasis on flexibility. In this regard, MPC is an ideal framework to use weather and price predictions in order to make use of the thermal storage of a building appropriately [79]. In MPC (and contrary to RBC), the objective of the controller is relatively simple to identify due to the presence of an explicit cost function. Its expression represents the quantity that the control should optimize, for instance the energy cost. In general, this function contains multiple terms that represent multiple objectives, which are balanced with appropriate weights. The optimal values of the weighting factors are usually computed using Pareto fronts, such as mentioned in [83]. Table II.2 summarizes the objective terms used in the referenced papers (see also detailed table in the Appendix A), and indicates whether the studies rely on simulation or experimental work. It can thus be observed that few articles have validated the performance of their control strategies through experimental implementation; most of them only rely on computer simulations.

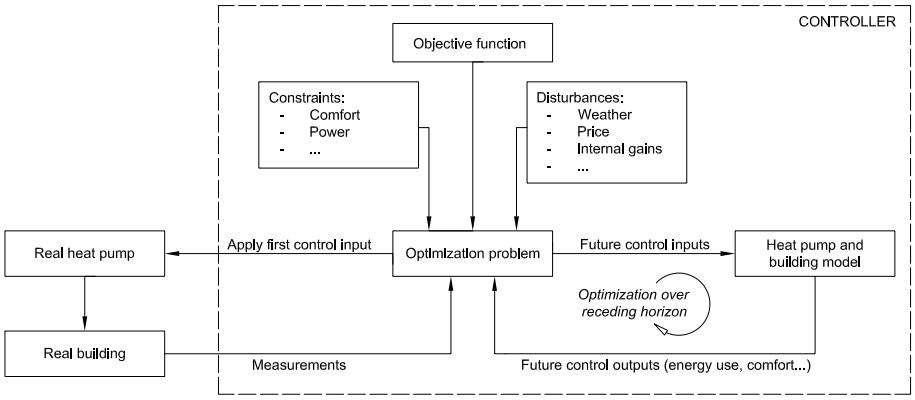

Figure II.4. Principle of MPC applied to building climate control with heat pumps, partially derived from [79] and [84]. The controller finds the sequence of future control inputs that will minimize the objective function over the receding horizon, taking into account the constraints, disturbances, and behavior of the model. The first control input is then applied to the real system.

3.2 Economic MPC

In the reviewed literature, one sort of MPC clearly stands out: Economic MPC (EMPC), where the objective is to *reduce monetary costs*. This cost optimization relies on time-varying energy prices. The objective function J_{cost} has in most of the cases indexed in Table II.2 the following form:

$$J_{cost} = \sum_{k} \left[P_{el}(k) \cdot c_{el}(k) + \sum_{i} P_i(k) \cdot c_i(k) \right] \tag{II.1}$$

Where k is every time step from 0 to the receding horizon N, P_{el} is the control input (the heat pump power in this case), c_{el} is the electricity price (varying in time according to different tariffs). When several energy carriers are present, their respective price c_i and consumption P_i are also taken into account. The optimization process then must minimize this cost function over the receding horizon, logically leading to monetary savings. Even though the claimed objective is to reduce the costs, this method will normally result in load shifting towards periods of lower energy prices. Depending on how the price profile is constructed, this load shifting can constitute an interesting form of energy flexibility, and therefore a more general objective. The price profiles tested either have a day/night

Table II.2. Decomposition of the objective functions in MPC strategies. A more detailed version of this table can be found in the Appendix, with the mathematical formulations of the different terms. Furthermore, it is indicated in the left column if the MPC strategy has been tested with simulations, experimentally, or both.

Reference	Economic term	Energy term	Peak shaving term	CO_2 term	Robustness term slack variable	Flexibility term	(Dis)comfort term
SIMULATIONS							
Masy et al. (2015)[46]	X						X
Tahersima et al. (2012)[85]	X						X
Li and Malkawi (2016)[86]	X						X
Verhelst et al. (2012)[83]	X						X
Pedersen et al. (2013)[87]	X						X
Kajgaard et al. (2011)[88]	X				X		X
Halvgaard et al. (2012)[47]	X				X		
Santos et al. (2016)[89]	X				X		
Bianchini et al. (2016)[90]	X					X	
Knudsen and Petersen (2016)[91]	X			X			
Sichilalu et al. (2015)[92]	X						
Mendoza-Serrano et al. (2014)[93]	X						
Salpakari and Lund (2015)[94]	X						
Toersche et al. (2012)[95]			X				
BOTH SIMULATIONS AND EXPERIMENTS							
Ma et al. (2014)[48]	X		X				
Sturzenegger et al. (2013)[96]		X					
Oldewurtel et al. (2013)[97]		X					
EXPERIMENTS							
De Coninck et al. (2016)[98]	X					X	X
Vana et al. (2014)[99]	X				X		X

structure [46], [71], [86], [92], [98], or an hourly variation corresponding to the spot prices on the day-ahead market (often the Nordpool market for instance)[45]–[47], [88], [90], [91]. Masy et al. use EMPC precisely to compare three different electricity tariffs [46]: flat rate, day-night tariff and ToU (see Figure II.5a). Constraints are implemented for the output temperature range and the maximum power of the heat pump. It is clear from the middle graph of Figure II.5a that the electricity consumption of the heat pump is shifted to low-price hours when a time-varying price is applied. At the optimum, this load shifting reaches 80%, while the procurement costs are reduced by up to 15%. However, an increase in the overall energy consumption of 20% is observed.

De Coninck et al. used a very similar method [98]. A major difference is that the building here is equipped with a gas boiler and a heat pump, therefore the system can alternate between both sources, depending on their cost. In the summation of J_{cost}, the cost of gas is implemented through the additional term $P_g(k) \cdot c_g(k)$, with P_g the gas consumption and c_g the constant price of natural gas (similar method in [86]). Furthermore, this study is experimental and measures the effects of the control strategy on a real building. A reduced-order model and a day-night electricity tariff were used. Compared to RBC, the MPC enabled to reduce the costs by 30-40%, and the primary energy by 20-30%, which is an additional benefit since this parameter is not included in the objective function. To achieve this result, the MPC controller tends to preheat the building with the heat pump during the night at a lower supply temperature, and enhances the use of the heat pump as a priority over the gas boiler.

Halvgaard et al. also present an EMPC scheme [47]. The studied house is heated by floor heating supplied by a ground-source heat pump (GSHP) which is linked to a storage tank, and is represented by a single zone state-space model. The EMPC strategy minimizes the electricity cost while keeping

constraints of indoor temperature, by acting on the power used by the compressor of the heat pump. The method resulted in 35% economic savings, compared to a case with constant electricity price. The energy consumption is clearly shifted towards low-price periods as can be seen in Figure II.5b.

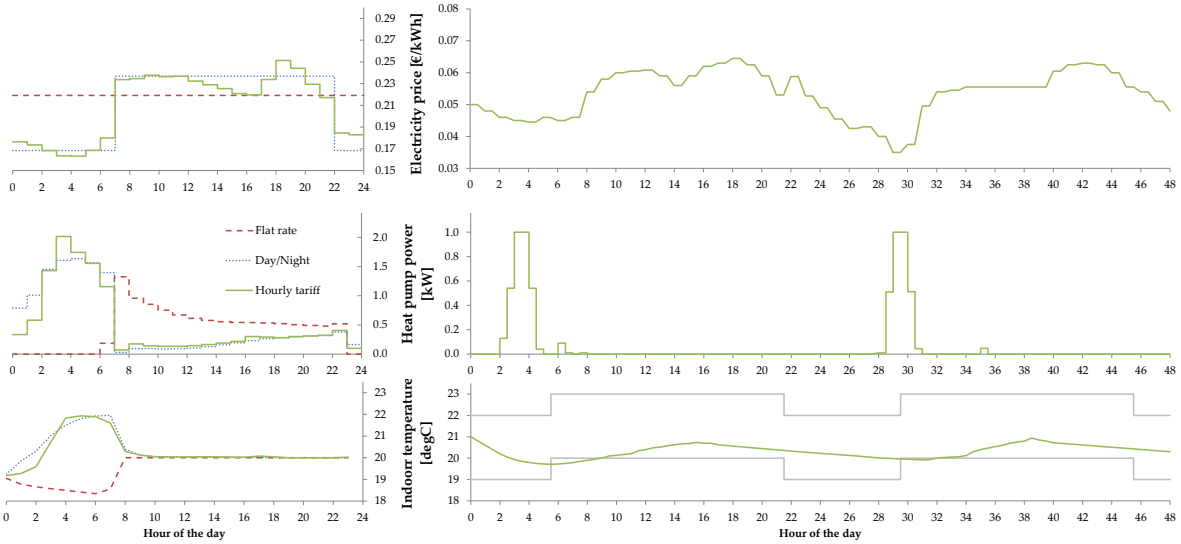

Figure II.5. EMPC examples from (a) Masy et al. (2015)[46] and (b) Halvgaard et al. (2012)[47]. The top graphs show the electricity price variations (on the left, three different tariffs were tested). The middle graphs show the resulting heat pump power profiles, and on the bottom graphs, the resulting indoor temperature profiles. A coincidence is observed between the utilization of the heat pump and the periods of lower energy price.

3.3 Other flexibility objectives

Aside from EMPC, MPC has sometimes been used with other flexibility objectives than the sole monetary one. For instance, Sturzenegger et al. used an MPC strategy to control a Swiss office building's HVAC systems (including thermal slab, ventilation and blinds)[96]. The goal of the objective function is to *minimize the non-renewable primary energy (NRPE) consumption*, through the following formulation:

$$J_q = \sum_k c(k) \cdot u(k) \tag{II.2}$$

Where $u(k)$ is the vector of the control inputs and $c(k)$ is a vector representing the conversion factors ("cost") of each control input, depending on the systems efficiency. MPC used 17% less NRPE energy (including lighting and equipment energy consumption) compared to an RBC strategy, most savings occurring during the heating season. Reynders et al. used a model-based predictive control approach [74], but not formulated explicitly as an optimization problem. The controller defines the heating set-point $T_{int,SP}$ according to the following equation: $T_{int,SP} = \underline{T_{int}} + \frac{1}{C} \cdot \int_0^N Q_{pred}(t)dt$, where $\underline{T_{int}}$ is the minimum temperature for comfort, and C is the thermal storage capacity of the building. The model and prediction aspects of the controller are present within the term $Q_{pred}(t)$ which is the predicted heating demand, computed using detailed building model simulation, assuming perfect prediction of weather and future internal gains. The aim of the set-point calculation is to preheat the building taking into account the future energy demand, thus avoiding overcharging. In this way, the electricity use of the heat pump during peak period is reduced by 47 to 88%, depending on the cases.

Few articles use a term for *peak shaving* within their objective function. Notably Ma et al. [48] present the following formulation:

$$J_p = c_p \cdot \max_k P_{el}(k) \tag{II.3}$$

Where c_p represents the peak demand cost. In this way, the peak power is penalized in the objective function, therefore the MPC will try to reduce it, leading to peak shaving. Unfortunately in [48], the authors do not analyze the results in terms of peak shaving. [95] use a different formula, where the objective function is the difference in heat pump power between time steps k and $k+1$, summed over the control horizon. By minimizing it, the power curve is smoothed, resulting in 25% lower peaks.

Reducing the CO_2 intensity is an alternative objective implemented in MPC. Dahl Knudsen et al. [91] notably use the same formulation than J_q in Equation II.2, except that the cost vector $c(k)$ here represents the prediction of the CO_2 intensity associated with the electricity production. An MPC solely aiming at minimizing this term reaches effectively a reduction of CO_2 emissions, but only reduces costs marginally and can potentially increase consumption in peak hours, in contrast to an EMPC.

Other terms can be introduced in the objective function to increase the robustness of the control. They do not represent a flexibility objective in their own, but enable a smoother operation of the systems. Santos et al. for example introduce the following term [89]:

$$J_\varepsilon = \sum_k c_\varepsilon \cdot \varepsilon(k) \tag{II.4}$$

Where c_ε is a penalty factor and $\varepsilon(k)$ a slack variable [84]. The constraint on the room temperature is then formulated as follows: $\underline{T_{int}} - \varepsilon(k) \leq T_{int} \leq \overline{T_{int}} + \varepsilon(k)$. Without the slack variable, the MPC cannot find a solution if the output T_{int} accidentally exceeds the constraint boundaries $\left[\underline{T_{int}}; \overline{T_{int}}\right]$. Introducing the slack variable enables to soften the constraints imposed on the output, and thus the optimizer can find a solution outside the strict range, although at the cost of a certain penalty [47], [99]. It therefore enlarges the feasible range of the problem.

In one article by De Coninck et al. [98], the authors introduce directly a term for energy flexibility in the objective function:

$$J_f = \left(\sum_{k=k_i}^{k_e} P_{el}(k) \cdot k - F_{target} \right)^2 = (F - F_{target})^2 \tag{II.5}$$

Where the optimizer should track a pre-defined energy consumption F_{target} during a specified flexibility interval $[k_i; k_e]$. In this scenario, a third party (energy provider for example) requires the activation of energy flexibility during a certain period $[k_i; k_e]$. If the required flexibility consists in increasing the energy consumption, F_{target} can be set to a high value, while if it consists in limiting the energy consumption during the time interval, F_{target} can be set to zero.

Finally, it is important to mention that these different objectives are usually combined in a single objective function. Most papers use linear combinations of the different J terms, setting different weights to put more emphasis on certain aspects of the optimization. For instance, De Coninck et al. [98] present a global objective function of the form $J = J_{cost} + \alpha_d \cdot J_d + \alpha_f \cdot J_f$, which is an EMPC but also taking into account a discomfort term J_d with weight α_d and a flexibility term J_f with weight α_f. The MPC controller then tries to minimize the total J over the receding horizon, taking into account the constraints of the problem. Some terms like J_d are not linear (because of the maximum function) and therefore require more numerical efforts for solving.

3.4 Accounting for comfort

Accounting for the users' comfort is a crucial aspect when designing HVAC control strategies, because it will eventually affect the acceptance and thus the viability of such methods. It was observed in the literature that comfort can be included in the MPC toolchain either as a constraint, or as an objective.

As a *hard constraint*, the comfort requirements take the form of a temperature range in which the indoor temperature (control output) should stay: for example, 22-25°C in winter and 22-27°C in summer mentioned by [96], 21-24°C in [48], 20-22°C in [46]. The constraints can be relaxed during

non-occupancy periods: in [46], outside the time frame [7:00 – 22:00], the problem is unconstrained. Halvgaard et al. change the constraint at night, with a minimum output temperature of 18°C, while this lower bound is set to 21°C during daytime [47]. The temperature range constraint can also be applied into storage tanks when applicable, for instance when using DHW that needs to be kept warm enough to avoid Legionnaire's disease.

Constraining the optimization problem in such a way makes it impossible to find an explicit solution (numerical methods must be used)[84]. Furthermore, it can happen that the optimizer does not find a solution that respects these constraints (because of the dynamics of the building for example). For these reasons, many authors prefer to integrate the *comfort as a term in the objective function*: in this way, violations of the comfort requirements are always possible, but they are penalized. This term can take the following form:

$$J_d = \sum_k \theta_{occ}(k) \cdot (T_{int}(k) - T_{int,SP}(k))^2 \tag{II.6}$$

With θ_{occ} a binary occupancy factor, T_{int} and $T_{int,SP}$ respectively the actual zone temperature and set-point. The controller thus has to track the reference set-point $T_{int,SP}$. The temperature error $T_{int} - T_{int,SP}$ is here considered as squared, which means that large temperature deviations will be more penalized than small ones, but some papers only consider the absolute value of this error. Another remark raised by [48] concerns the use of unconstrained temperature range in real building applications: it might cause problems because the actuators (room thermostats) might have a specific acceptable range of temperature set-points.

Li and Malkawi [86] propose an original approach, using the *Predicted Mean Vote (PMV)*. This indicator reflects the thermal sensation of the occupants and varies from -3 (too cold) to +3 (too hot), while 0 corresponds to a neutral sensation. Aiming to achieve this optimal (neutral) comfort with $PMV = 0$, the comfort term in the objective function is expressed as in Equation II.7

$$J_d = \sum_k (\theta_{occ}(k) \cdot PMV(k))^2 \tag{II.7}$$

This method enables to keep the PMV within the limits recommended by ASHRAE standard ($-0.5 < PMV < 0.5$)[100] for most of the occupancy time. However, this approach requires a high computation demand (around 3 hours to solve the optimization problem with detailed building simulation), given the complex calculation of the PMV which depends on the occupants' clothing and metabolic rate as well as the indoor temperature and air velocity [101].

3.5 Other constraints

Accounting for comfort mainly leads to constraining the control output (indoor temperature), which must be anticipated beforehand by the controller. However, some constraints should also be set to the control inputs, to account for the physical limitations of the devices in use. For instance, Dahl Knudsen et al. [91] bounds the power of the heating system to [0 – 0.5 kW], and Masy et al. [46] to [0 – 3 kW], which corresponds to the devices used in their respective studies. The MPC controller can then pick a thermal power within this interval at every time step. In the studies [96], [97], the MPC also controls blinds or ventilation in addition to the heat pump, therefore constraints are also imposed on these systems (minimum and maximum air supply temperature, only non-closed position for the blinds during occupancy hours to guarantee some daylight). A minimum air ventilation flow rate is also implemented as a constraint for health reasons, to guarantee air renewal indoors. Sometimes, constraints are also imposed on the changes in the control inputs $u(k+1) - u(k)$, to avoid frequent cycling behavior or steep ramping, and increase the controller robustness, like in [47] or [89].

3.6 Challenges in modelling

One of the greatest challenges residing within MPC is obtaining the model used in the controller. It remains a difficult task to create an accurate model for every building, yet simple enough to limit

the computation effort for the controller. Indeed, detailed models (developed for energy calculations for instance) are not commonly used for MPC applications since they drastically increase the computation time required by the optimization solver (example: 3 hours in [86] for the total solving of the optimization problem with EnergyPlus and Genopt). Instead, simplified RC-models (resistance-capacity, analog to electrical models) are utilized in the great majority of the reviewed cases, but they provide less accurate description of the heat dynamics of the building. RC-models have the general form presented in Equation II.8 [99]:

$$C_n T_n = \sum_j \frac{T_j - T_n}{R_{j,n}} + \sum_l Q_l \tag{II.8}$$

Where j is the j-th node with temperature T_j, $R_{j,n}$ is the thermal resistance between points j and n, C_n and T_n are respectively the thermal capacity and temperature of the point of interest, and Q_l represents the different additional heat fluxes. This form of model is therefore linear and corresponds to a network of thermal capacities and resistances, which can either be assigned to the real elements of the building (interior air, walls, furniture etc...) or be lumped into a reduced order model. Santos et al. [89] experimented the use of non-linear models, expressing some of the thermal resistances $R_{j,n}$ with power laws in function of the wind speed. This non-linear controller proved to be more efficient, especially when the weather conditions are determinant and the non-linearity of the models become essential to describe the dynamics of the system.

Some of the issues related to modelling in MPC are related by [98]. For example, the model of MPC can require a lot of meta-information (like room sizes, insulation level etc.), but these data are often not available. The authors of [98] therefore suggest creating simpler models, so that the method is applicable in a larger number of cases. This can cause some problems: the identification dataset used for the model of [61] was retrieved in January/February, therefore the solar radiation was discarded as a significant input. This situation is not true anymore in the summer season, hence the control model is mainly valid for winter season and this becomes problematic. Several attempts at solving the model inaccuracy issues have been reported in the literature. Masy et al. used a simplified model for the controller, which induced some error [46]. Therefore a feedback loop was implemented from a more detailed emulator, to introduce a correction for the possible mismatch between the simplified model and the emulator.

For obtaining easily a model adapted to a specific building, De Coninck et al. created a specific toolbox [49]. Its toolchain facilitates and automates the different steps in the system identification procedure like data-handling, model selection, parameter estimation and validation. It was tested for a single-family dwelling for which measured data was available for validation. One experiment showed poorer results and the authors identified a poor information content in the identification dataset as the likely reason. To create a dataset sufficient for the identification process, [102] proposed a method based on the excitation of the building by a pseudo-random binary sequence signal. This signal applied to the heating system reveals and facilitates the creation of suitable models representing the heat dynamics of buildings. To analyze the obtained time series, the CTSM tool (Continuous Time Stochastic Modelling) has been proposed by Juhl et al. [103]. It enables to identify grey-box models using multivariate time series data, and to identify the embedded parameters (thermal resistances and capacities for example).

3.7 Disturbances

An MPC controller usually simulates the response of the building model to several external disturbances, not only to the control inputs. The most common disturbances taken into account by MPC are the *outside weather conditions*, since they will affect the most the heating or cooling needs of the building. The external temperature is considered in the model of almost all the reviewed papers. A notable exception is the paper [48], where the authors found out that the outside temperature did not have as much influence on the output as the set-points or the heating power, and therefore neglected it. The articles [92], [96]–[98] only consider the external temperature when accounting for weather conditions. Several papers additionally consider the solar irradiation [47], [90], [91], [99]. Besides the external temperature and the solar irradiation, [89] and [46] also take into account the effects of wind

speed. In many cases, it is assumed that the forecast of these disturbances is perfect. When the MPC is implemented in a real building, weather forecast is retrieved from external services or derived from a local measurement.

Another major source of disturbance is the *internal heat gains*. They group the heat gains from occupants, appliances and equipment. Most commonly, a deterministic approach is applied, with a fixed schedule representing these internal gains [46], [90], [99]. When the MPC is implemented in real buildings, other methods can be employed: an occupancy sensor like in [92], or deriving the internal gains from measurements of the plug and lighting electricity circuits [98].

For all the EMPC strategies relying on cost optimization, the *time-varying price of energy* constitutes an additional cost signal to be taken into account by the controller. Time-of-use electricity tariffs are applied most often, with different values for peak periods and off-peak periods, and sometimes with an additional medium price in-between. In other papers, hourly tariffs are applied, reflecting day-ahead prices on the spot market.

Regarding the *prediction of the disturbances*, different concepts are found in the literature. Several publications consider a perfect knowledge of the future (in the case of simulations), which corresponds to the highest achievable performance of MPC. Most of the time, a forecast of the electricity price and weather for the next 24 hours can be retrieved, which is an imperfect prediction. This solution is implemented in most of the studied papers, especially when the MPC is applied to a real building. Finally, the MPC can also be left without any knowledge of the future, and therefore needs to build its own disturbances' forecast. To this end, one can utilize black-box models using past data. In the case of energy price and weather, an oscillatory behavior with a period of one day is observed. Shaping filters on historic data can be applied, considering a 24 hours period and adding white noise to account for the stochastic behavior. Pawlowski et al. [104] present different time-series methods for estimating disturbance forecasts to be used in MPC. In [93], the authors compare the three approaches (full, imperfect or zero knowledge about the future). With perfect predictions, the EMPC achieves cost reduction of 31%, while with perfect ignorance of the future, the cost reductions amount to 27%. The performance thus improves with a better forecast, but the margin remains relatively small.

4 Thermal energy storage

When studying the potential flexibility offered by buildings, the thermal energy storage plays a key role, since it enables to stock energy for later use, hence shifting the loads in time. In general for DSM with heat pumps, two fundamentally different types of thermal storage are considered [24]: building thermal mass and water buffer storage tanks, which are sometimes combined together. In some reviews, the first type is called passive storage whereas the second one is referred to as active storage [105]. Many other types of thermal storage do exist, such as Phase Change Materials (PCM), thermo-chemical or ice storage [106] but most of the studied cases in the present work rely on existing thermal mass and water storage tanks for activating flexibility.

When their storage losses are neglected [93], [107], [108], water tanks are found to provide greater flexibility. However when these losses are considered [44]–[46], [66], [73], larger water tanks induce a degradation in the system efficiency due to these increased thermal losses. Furthermore, water storage tanks are costly in monetary terms and in terms of space occupied within the building.

On the other hand, thermal mass does not require prior investment since it is already available within the construction of the building. However, the comfort constraints are more restrictive because of the limited temperature variations allowed in the occupied zones, while less problematic in a water tank. Building thermal mass has been identified and tested by several studies as a good storage means for demand-side management and flexibility initiatives [74], [75], [109], [110], but its potential highly depends on the type of building [46], [74], [75]. Further investigations are needed since the existing literature contains some lacks in this regard [75], [111].

5 Discussions and conclusions

To summarize, even though RBC strategies can yield significant improvements, they do not achieve the optimal performance. For this reason, MPC has shown strong advantages over classical control, but some challenges remain concerning its implementation. The largest one resides in obtaining a satisfactory building model for the controller, which is a costly and complicated process. A trade-off needs to be found between the accuracy of the model and its simplicity. To tackle this issue, several methods have been developed to facilitate the obtaining of building models to be used by MPC controllers [49], [102], [103]. Furthermore, it would be relevant for further studies to include the computation times, so that the efficiency of different modelling approaches can be evaluated.

Another challenge consists in realizing the connection of MPC with different data services. It might result difficult to realize a connection to weather forecast services from a third party; and even if it is realized, the closest forecast might not be adapted to the local conditions. The automatic access to the day-ahead electricity price (in case it is variable) might not either be straightforward. However, the upcoming large implementation of smart meters (the EU aims to replace at least 80% of electricity meters with smart meters by 2020 wherever it is cost-effective to do so [112] and by 2018 in Spain [113]) could facilitate this communication between the end-consumer and the grid. Moreover, the numerous examples of smart grid projects usually already consider that the users have access to electricity price data.

Despite these potential barriers, MPC has been identified as a very powerful tool to activate energy flexibility and optimize heat pump operation. Globally, MPC overcomes the limitations encountered by simpler rule-based controls and outperforms them [80], [114]. MPC projects the behavior of the system in the future, and thus optimizes the heat pump operation over a certain control horizon, for instance storing energy at times where it is more profitable, and releasing it afterwards when needed. The lack of dynamics and anticipation of RBC are therefore clearly surmounted by MPC. From their review about optimal design and control of GSHP, [65] deduced that model-based control methods are better by far than any other approaches and that RBC is suboptimal compared to MPC.

Among the different studies reviewed on MPC, a large majority resorted to Economic Model Predictive Control (EMPC). The primary objective of such strategy is thus to minimize the energy cost. This objective is generally achieved, with reductions of up to 40% in the reviewed papers and without jeopardizing thermal comfort, compared to conventional heating curve (or cooling curve) control strategies [36]. Reduction of energy use or improvement of the comfort can also occur with EMPC even though they are not formally identified as an objective. In this regard, it would be interesting if further research would analyze the effects of EMPC further than the reduction of the energy cost (which some articles also do). In particular, the correlation of the variable electricity price with the primary energy factors or the CO_2 emissions should be studied, so that EMPC can be used for more global objectives than the sole monetary one. In this way, the EMPC framework can be kept, but by adapting the price profile to the desired effect, one can instead achieve a reduction of the primary energy use or the CO_2 emissions.

Along the same lines, it should be mentioned that few articles were found with MPC strategies that considered other objectives than the reduction of the energy costs. EMPC seems the most common way to provide energy flexibility, but it has been extensively studied, therefore the research efforts should now concentrate on other aspects. In particular, other objective terms should be integrated in the MPC framework, such as the heat pump COP (coefficient of performance), flexibility indicators or primary energy use. The study [114] notably compares different MPC objectives, concluding that the reduction of the energy use or the maximization of renewable energy use are the most interesting options. If energy flexibility is bound to become the new target for energy efficient buildings [115], then it should be integrated directly as an objective in the optimization problem through different indicators [116], to maximize this flexibility. Furthermore, it would be relevant to include multi and contradictory objectives in the same MPC, and evaluate the trade-off made by the controller. For instance, it could seem like a good strategy to operate a heat pump at night to benefit from traditionally lower electricity prices, but the COP is also reduced at night because of lower outdoor temperature (in heating case). These two aspects need to be balanced by the MPC, and it should be noted that rule-based controls can only deal with such issues in an intuitive (non-optimal) manner.

Overall, despite its complexity and the identified challenges residing in the modelling and the implementation of such control, MPC strategies are bound to be increasingly used in the future. Oldewurtel et al. put forward several reasons for this foreseen development [79]: drastic increase in computational power, standardized use of simulation tools, increase in the quality of weather forecasting, rising of energy costs and the desire to handle time-varying electricity prices (within smart grids for instance). However, the existing work on MPC for heat pump control primarily relies on simulations; few implementations in real buildings have been realized [45] (see also Table II.2). Now that this technology is mature enough, it should be deployed and studied in more realistic environments. In particular, the heat pump functioning in real-time, its efficiency, the part-load conditions, the interactions between supervisory and local controls, the comparison between simulation and experiments have rarely been mentioned in the literature, and thus constitute interesting paths for new investigations that steered the present thesis. Furthermore, the studied articles often focus on a single heat pump system in one building. Energy flexibility has much greater potential when aggregated for numerous buildings, therefore this aspect should also be studied: multiple MPC algorithms that collaborate to reach a common goal, aggregation potential and drawbacks, impact of market penetration. Several works have already been published on these topics [45], [117], but more research is needed.

Based on this review of the state of the art, the following conclusions have led the work later developed for this thesis:

- Both an RBC controller and an MPC controller have been developed. These two types of controller were tested in the same framework, enabling a thorough comparison of their performance. Furthermore, the development of the MPC controller and the production of the needed control models has been detailed, so as to put into perspective the development efforts with the achieved performance for such complex controllers.
- The developed controllers (RBC as well as MPC) have been declined with several objectives, so as to study different flexibility goals than the cost reduction. In particular, the reduction of the CO_2 emissions was targeted to reduce the environmental impact of heating and cooling.
- The developed control strategies have been tested experimentally on a real heat pump. This process enabled to give more realistic results of the system performance, and highlighted practical issues encountered during the implementation.
- Along the same line, models of heat pump were developed, validated using experimental data. These more accurate models provide a better representation of the heat pump dynamics and operation, while the existing literature often relied on very simplified models, e.g. a constant COP. Using more realistic models enabled to evaluate the performance of the control strategies in a more tangible manner and to put the claimed savings into perspective.

The work developed following the outcome of this review is described in the following chapters, starting from the methodology to evaluate the flexibility and followed by the development of the two controllers.

Chapter III

Methodology for the analysis of energy flexibility in buildings

1 Co-simulation and experimental frameworks for testing

To test the controllers described in chapter IV, different frameworks were developed. Firstly, a simulation-only configuration is presented in subsection 1.1. In that scheme, the controller is tested on a detailed model of heat pump. Secondly, a semi-virtual environment setup is described in subsection 1.2. In that case, the heat pump model is replaced by a real heat pump system operated in a laboratory, and managed by the tested controller.

1.1 Co-simulation framework

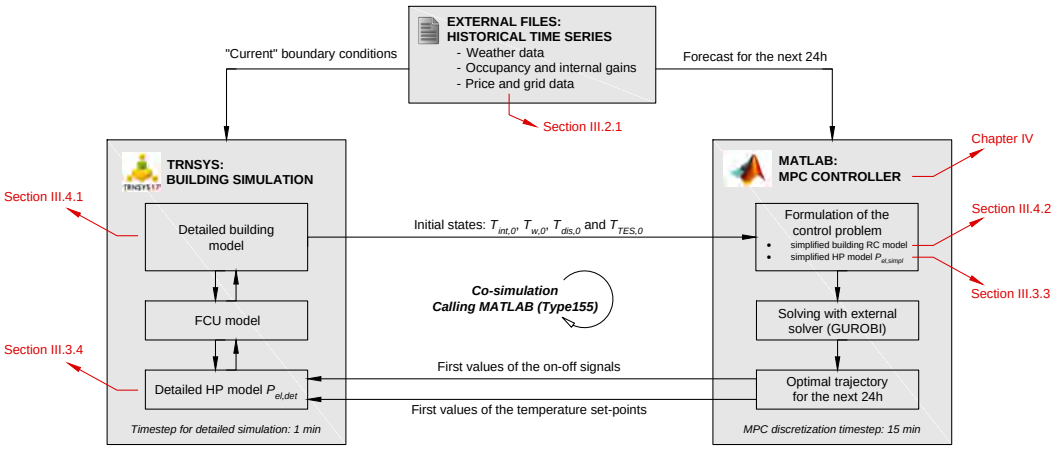

Figure III.1. Co-simulation scheme between TRNSYS and MATLAB (case of an MPC controller).

This testing scheme relies entirely on dynamic simulations, with different software interacting, hence the "co-simulation" designation. The scheme of the co-simulation and the exchange of variables is presented in Figure III.1, and relies on TRNSYS as the main software. TRNSYS is a transient systems simulation program [118] that enables to perform dynamic simulations of most commonly found thermal, electrical and control systems. It has a modular structure, with blocks called "Types" available from existing libraries, and which are connected with each other (e.g. the air-source heat pump model is Type941).

The detailed model in TRNSYS here serves as the "real building", in other words it constitutes a virtual plant with which the control strategies can be tested. This principle is commonly known as "hardware-in-the-loop" (HiL) and enables to run a great quantity of simulations to test the controller, without the costs of performing actual physical tests in a real building. The details of the model and the building study case used for this purpose are described in section 4. The TRNSYS simulation runs using the necessary inputs (weather, occupancy, DHW tapping profiles, grid etc...) from external files. Considering perfect predictions, these external files also provide the forecasts necessary for the MPC to project the future behavior of the systems. Part of the intelligence for the flexibility exploitation actually originates from the design of the input signals such as the price or emissions of the power grid: the analysis of these signals is detailed in subsection 2.1.

In the case of an RBC controller, the control can be implemented directly in TRNSYS (classic thermostat control). In the case of MPC, TRNSYS does not contain suitable tools for optimization, therefore the MPC calculation must be externalized in another software, MATLAB in the present case, similarly to the method applied by Alibabaei et al. [119]. When the MPC controller in MATLAB is called, it is provided with the necessary input, namely the initial values of the states and the forecasts for the next 24h, taken from the same files. The control problem is formulated in MATLAB with the YALMIP tool [120] and solved with GUROBI [121]. To limit the computation efforts, the MPC controller requires simplified or low order models of the building envelope and the heat pump performance: these are detailed respectively in subsection 4.2 and subsection 3.3. From the optimal control trajectory calculated over the horizon of the next 24 hours, the first values are sent to TRNSYS, before a new computation of the MPC is carried out and new values are obtained. The MPC controller is called every 15 minutes, while the detailed TRNSYS simulations runs with a finer resolution of 1 minute, so as to better observe the intrasampling behavior of the systems within one control action. In practice, the Type155 of TRNSYS enables to establish the connection between both software. It should be noted that for clarity, the term "detailed" generally refers to the TRNSYS framework, while the term "simplified" refers to the MPC framework, since the models and time steps of these two frameworks are notably distinct. The results from the co-simulation studies performed in this framework are later presented in chapter V.

1.2 Semi-virtual environment laboratory framework

The performed tests presented in chapter V were carried out in a semi-virtual environment experimental setup. The main difference with the co-simulation framework resides in the real heat pump system, which replaces the heat pump model. The schematic of the control and communication setup is presented in Figure III.2. The Labview interface centralizes all the commands and exchanges of variables between the different pieces of software. The TRNSYS simulation, set to a calculation time step of 1 minute, calculates the energy loads of the real building, and thus still serves as the virtual plant that enables to try the different control strategies, following the HiL concept. HiL allows for the testing of a complex real-time embedded system [122]. In this case, the controller is interfaced with its related systems which are partly real (the heat pump), and partly virtual (the mathematical representation the building dynamics, also called the "plant simulation").

Similarly, the MPC controller is implemented externally in MATLAB to benefit from its optimization features, and the external files containing time series data of weather, occupancy and grid variables provide the necessary input for TRNSYS. The same weather conditions are emulated dynamically in the laboratory climate chamber in which the heat pump is placed. The data acquisition system saves the measured data at a sampling time of 10 s, while it updates the control set-points for the laboratory every minute.

The mechanical schematic of the experimental laboratory setup is represented in Figure III.3. It illustrates the concept of semi-virtual environment, where a real device (a heat pump in the present case) is coupled with a virtual simulation software (building simulation in TRNSYS in the present case). Such setup is used in many laboratories where energy flexibility of buildings is tested [59]. The air-to-water heat pump is installed as shown in the photographs of Figure III.4: the outdoor unit is placed into a climate chamber, and the floor standing indoor unit containing the DHW tank is placed outside the chamber in the laboratory space room. Both units are connected through a refrigerant fluid circuit. The walk-in climate chamber is a 45 m^3 room space, where the air properties can be con-

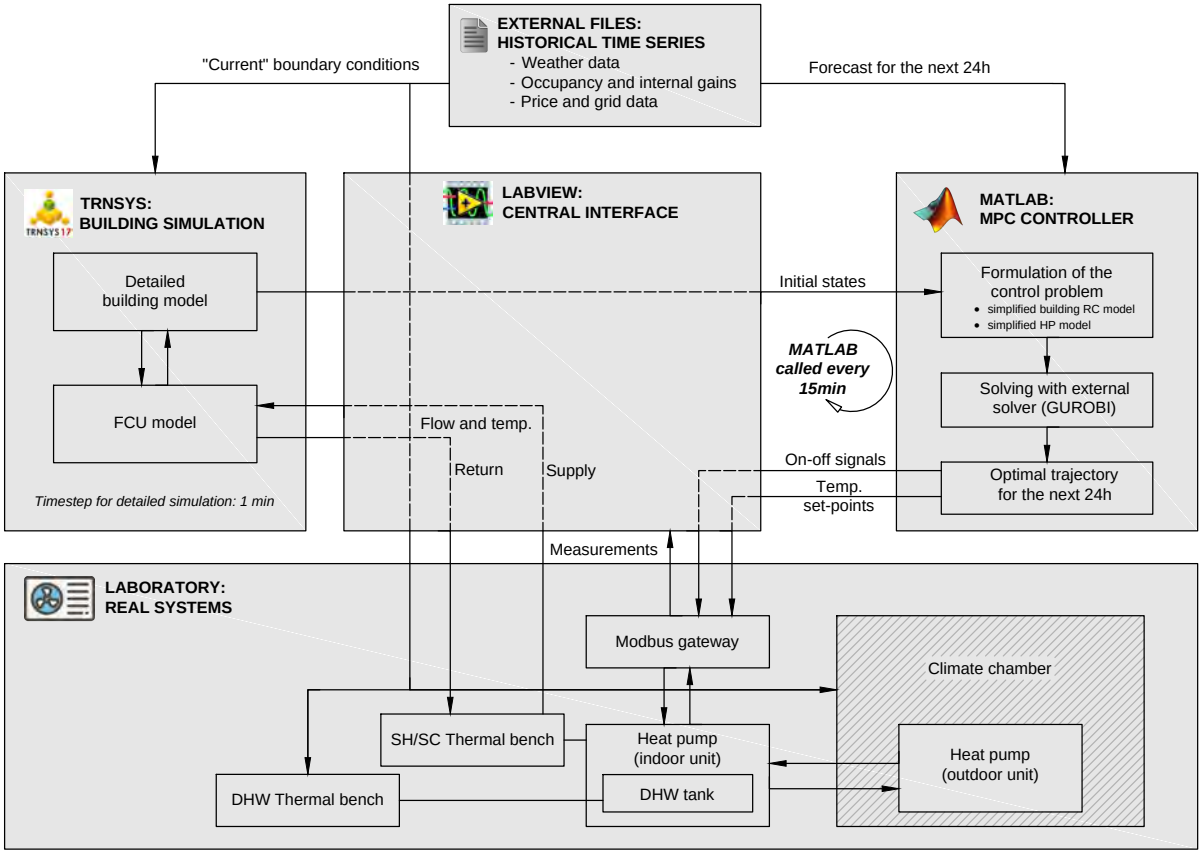

Figure III.2. Schematic of the co-simulation and the software environment in the experimental setup.

trolled in a temperature range of -30 to +60°C and a relative humidity range of 15 to 98%, enabling to recreate a wide spectrum of climatic conditions. In the reported experiments, this climate chamber is used to emulate dynamically the outdoor conditions of the chosen location. Such setup enables to perform repetitive experiments with the exact same boundary conditions and thus to ensure reproducibility and a valid comparison between the different control configurations.

The coupling between the virtual building and the heat pump is done by means of two thermal benches. The first thermal bench emulates the space heating or cooling load from the building emission system (here Fan-Coil Units or FCU): when the heat pump runs in this mode, its output water flow and supply temperature are recorded in the laboratory. These measurements are sent to the TRNSYS building model, which calculates the corresponding return temperature considering the dynamics of the building. This return temperature is emulated with the thermal bench that extracts or delivers heat to the water flow by means of a heat exchanger to reproduce the thermal load of the building.

In all the presented experiments, the water flow in the heat pump circuit is kept at a constant value of 26 l/min for the space heating/cooling loop and 33 l/min in the internal DHW tank charging loop, both in the normal range of operation of the machine.

A second thermal bench allows reproducing the DHW tapping profiles of the building occupants. Following a predefined daily tapping schedule derived from the standard [123], a water flow is drawn from the top of the DHW tank, so as to deliver 45°C at the tapping point. A buffer tank with cold water (1000 liters) is used to provide water at the temperature of the mains network during the DHW extractions. This tank is kept at a temperature of 10°C in the winter cases, and 19°C in the summer cases. The water from the bottom of this cold tank is circulated into the heat pump DHW tank during each tapping event. The water flow during the DHW extractions is controlled with the 3-way valves and a flow controller loop in the corresponding test bench.

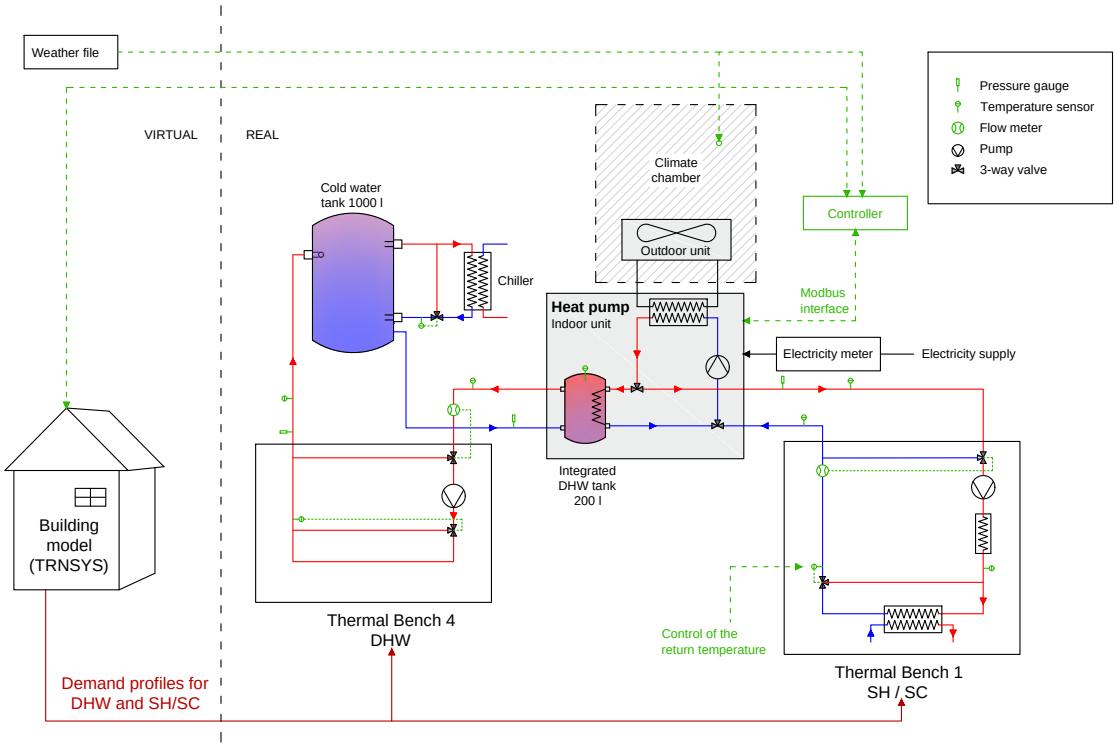

Figure III.3. Schematic of the mechanical and control systems, illustrating the principle of the semi-virtual environment, with the separation between the real systems and the plant simulation.

Several sensors are placed in the laboratory to measure the status of the different components in the circuit. The main logged variables are the following, with their respective accuracies:

- **Supply temperature** T_{sup}: measured on the output pipe of the heat pump with a PT100 sensor that has a precision of $\pm$ 0.25 K
- **Return temperature** T_{ret}: measured on the input pipe of the heat pump, also with a PT100 sensor of the same precision (thus for the temperature difference in the water loop, the precision is $\pm$ 0.5 K).
- **Water mass flow meter** $\dot{m}$: measured in the water loop circuit with an induction flow meter which has a high precision of $\pm$ 0.2 to 0.5%, which makes its error negligible. The thermal power Q_{th} can be deduced from the three previous measurements (see later Equation III.16).
- **Power used by the heat pump** P_{el}: measured by a power meter where the heat pump is plugged to the grid, with a precision of $\pm$ 1%.
- **Air temperature** T_{amb}: measured throughout the climate chamber by 10 temperature sensors which are arithmetically averaged.
- **Frequency of the compressor** f: measured by the internal sensors of the heat pump and retrieved through its Modbus interface, with a resolution of 1 Hz.
- **Temperature in the DHW tank** T_{TES}: measured by the internal temperature sensor of the heat pump placed outside the tank in the middle of its height, with a resolution of 1 K.

(a) **(b)**

Figure III.4. Photograph of the laboratory with the floor standing indoor unit of the heat pump, and the outdoor unit in the climate chamber which is closed in (a) and open in (b).

2 Energy flexibility: inputs and indicators

2.1 Input penalty signals

The control strategies presented in this thesis belong to the class of indirect control, or implicit demand response: in these cases, the controller receives external signals as inputs, also called penalty signals [124], and can then choose whether or not to react to them. On the other hand, in an explicit demand response scheme, the controller would receive an order from an external party (e.g. an aggregator) to modify the energy consumption of the building for a certain period, and would be required to comply with this plan in exchange for a reward. The only explicit demand response programmes available in Spain are reserved for large consumers and are only activated to curtail the load in emergency situations. Explicit demand response for smaller consumers is not possible so far in this country, since aggregation is still not legal [17], [125], therefore explicit demand response strategies have been discarded in the present research.

In implicit demand response schemes, the input penalty signal for the controller (often a price signal) constitutes one of the most important elements. A large part of the intelligence actually comes from the design of the signal, since this will determine to which periods the end-users are incentivized to shift their loads. The signal must therefore be constructed to solve a specific problem. A famous example is the "duck curve" case in California [126] in recent years, the share of solar energy in the grid of this American state has increased in an important manner. As a result, the residual load presents a valley during the day hours, while in the early evening, all customers shift from their PV supply and connect to the grid at the same time, causing an important ramping during a short period, which the grid has to sustain. To respond to this specific issue, the grid operators designed time-of-use (ToU) rates to increase the electricity tariff in the evening hours, and thus spread the connection of the users to the grid on a larger period.

Time-varying electricity prices constitute the great majority of penalty signals used in implicit demand response programmes; the ones used for this research are detailed in section 2.1.1. Given the urge to decarbonize our energy systems, the use of signals representing the carbon footprint of the grid has gained interest in recent research: the construction of such signals is detailed in section 2.1.2. These are the two signals tested in the present thesis. Following this method, penalty signals based on other criteria could easily be constructed for use in the same control framework, without changing the nature of the control problem. For instance, the residual load of the grid (total load less the RES production)[69], [78] or the non-renewable primary energy factor constitute interesting alternatives of penalty signal.

2.1.1 Price signals

When a certain controller is designed to minimize the energy costs, it must be supplied with a signal of the time-varying price of energy. As seen in the literature review, a majority of the existing research on MPC for energy flexibility relied on this type of economic optimization. The price profiles used either have a day/night structure [46], [71], [86], [92], [127], or an hourly variation corresponding to the spot prices on the day-ahead market (often the Nordpool market for instance)[45]–[47], [88], [90], [91]. In Spain, different time-varying tariffs are also available for small customers, in fact it was the first country in the world where the default price for households was based on hourly spot prices [17]. In the absence of explicit demand response programmes in this country, this policy supposes a large roll-out of hourly electricity tariffs in the country, and thus an important potential for implicit demand response.

To exploit the energy flexibility of buildings to their full potential, the end users must have a direct access to the hourly prices in advance. This is made possible with smart meters, which enable easy communication with the grid operators and facilitate this data collection. In fact, the European Union plans to replace at least 80% of electricity meters by smart meters by 2020 wherever it is cost-effective to do so [112], and in Spain this deployment has been achieved in 2018 [113]. The rollout reached 99.14% of all the meters for customers of less than 15 kW contracted, which corresponds to

28.6 millions of meters replaced, as of the 31st of December 2018 [18]. The direct access to the varying electricity price profiles is therefore considered as given (the prices are usually published at 22:00 for the next day). Moreover, the numerous examples of smart-grid projects usually consider that the users already have access to electricity price data.

The Spanish hourly tariffs are named PVPC (Precio Voluntario para el Pequeño Consumidor, or Voluntary Tariff for Small Consumers) and are targeted for small consumers with a contracted power of less than 10 kW. These prices are indexed on the spot price of the Spanish market and determined with information from the Spanish TSO, Red Eléctrica de España [128]. Three different tariffs exist, as illustrated in Figure III.5 for a sample week of March 2019. The default PVPC tariff follows the evolution of the spot market price, but at a higher level since it is aimed for end-consumers. The "2-periods PVPC" tariff also varies hourly, but presents a clear peak/off-peak structure: the price is higher during daytime (from 11:00 to 21:00) and lower during the rest of the day. This is the preferred tariff when used in an implicit demand response configuration, since the large variations between peak and off-peak prices make more room for optimizing the energy costs and shift the loads to the cheapest hours. Finally, the PVPC tariff for EV is only applied for electric vehicles and show approximately the same pattern than the 2-periods tariff. The three available tariffs include an energy term for the access tolls, the charges and the cost of production, but exclude taxes.

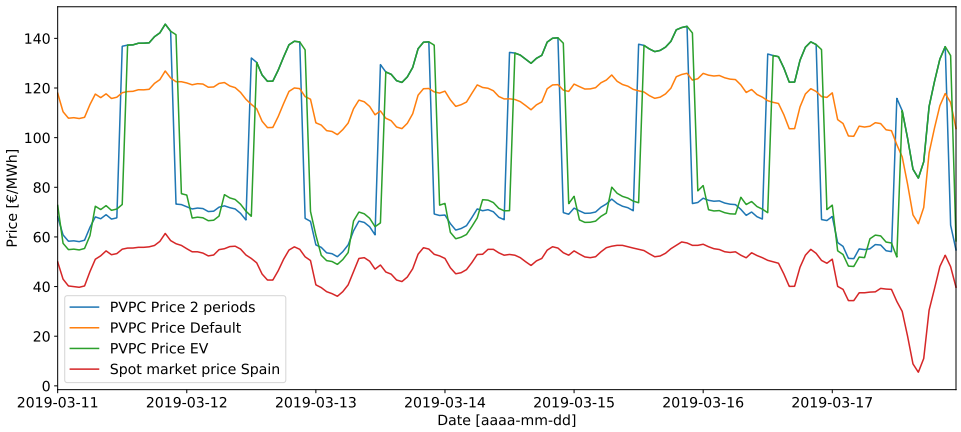

Figure III.5. Sample of the different electricity tariffs existing in Spain, for one week of March 2019 (week 11).

It is observed on the last day in Figure III.5 (Sunday March 17th) that around midday, the spot price presents an important drop: this is due to the coincidence of high solar energy availability and a low load, typical on a Sunday when industrial activities are stopped. All the other tariffs also reflect this price drop. It is expected that in the future, with the increase penetration of RES, the volatility of the prices will increase, making the research on demand-side flexibility particularly relevant. Negative prices have for example already been observed for some hours in regions like Germany or California where the penetration of solar energy is particularly important.

2.1.2 Carbon intensity signals

Given the urgent need to decarbonize our societies, it was suggested earlier that other objectives than cost minimization could be studied, since the ultimate goal is actually to reduce the carbon footprint of our energy use. An alternative approach thus consists in using the carbon intensity of the grid as an input penalty signal for the controller. In this way, the main objective of the controller would consist in minimizing the CO_2 emissions due to the energy use of the building. This concept has gained a lot of interest in recent years, with several articles reporting the use of CO_2-based signals in their control strategies [52], [53], [91], [129], [130].

Moreover, when the impacts in terms of carbon footprint are evaluated, the CO_2 emissions are usually calculated with average values. In this work, we propose a novel approach, by calculating the *marginal* CO_2 emissions, instead of the average emissions of the grid. The marginal emissions con-

sider the merit order in which the production plants are activated in a given grid, and thus the emissions savings are meant to be calculated more accurately. For instance, if a demand-side management action triggers a reduction of the energy use, this will not affect a base plant like nuclear, which is too slow to start and stop for balancing the grid. Instead, this variation will be compensated for example by a gas turbine, and therefore the resulting marginal emissions saved will be greater. The Marginal Emissions Factor (MEF) will thus be used in this study, as it gives a more accurate representation of the environmental impact of DSM actions. The calculation methodology for the MEF is based on the statistical analysis of historical data obtained from the grid operator [57] and is detailed hereafter.

The MEF highly depends on the national context and the energy mix of a country [131]. It is calculated here at the national scale for Spain and represents the quantity of CO_2 emissions which are avoided for every kWh of electricity saved at a certain moment in that context. To calculate the MEF, the following steps have been followed: firstly, the hourly data of the energy mix have been retrieved from the Transmission System Operator (TSO) [132]. The data contains the breakdown of the electricity production for every hour, detailed per energy source. Considering the CO_2 emission coefficients of each energy source [133], the average CO_2 emission factor (EF, in $kgCO_2/kWh$) can be computed for every hour of the year. Secondly, two time series are calculated: the difference in the system load and the difference in the average CO_2 emissions, from one data point to the next. These data are represented as a scatter plot in Figure III.6a.

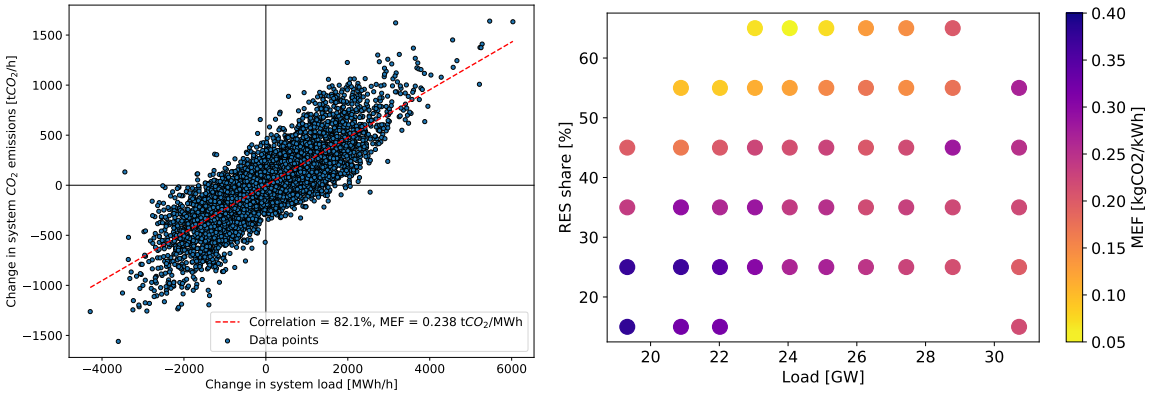

Figure III.6. (a) Average MEF (0.238 tCO_2/MWh) in the Spanish electricity mix, based on hourly data from 2016. (b) MEF calculated per clusters of RES share and system load (data for Spain from 2016).

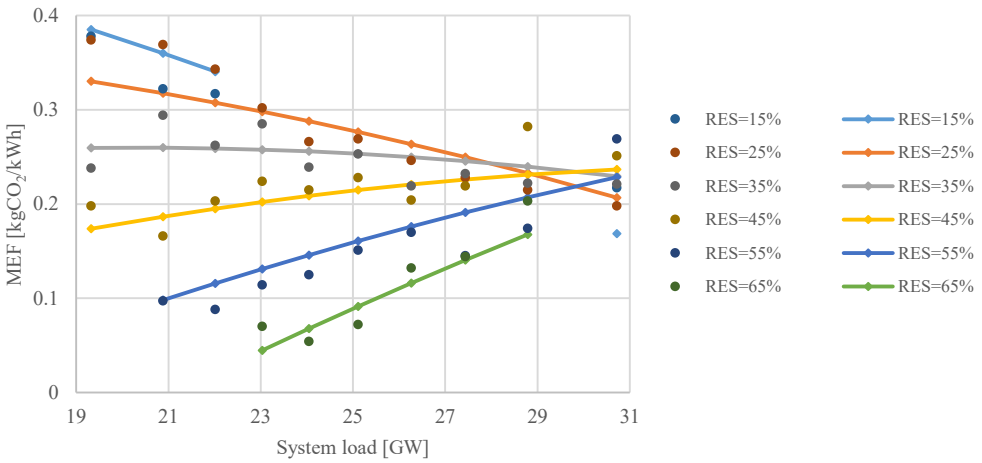

Figure III.7. Quadratic model of the MEF in function of the RES share and the system load. The data points (same than Figure III.6b) are only shown as dots, while the model is represented with solid lines of a similar colour.

From this figure, the overall MEF can be derived: it corresponds to the slope of the linear regression, here 0.238 $kgCO_2/kWh$ (for comparison, the average MEF found by Hawkes [131] for Great Britain was 0.69 $kgCO_2/kWh$) . However, it is observed in Figure III.6a that the data points are relatively scattered. In fact the MEF varies substantially at different scales, both seasonally and according to the system load, the time of the day or the proportion of renewable energy sources (RES) in the energy mix. For this reason, the data points of Figure III.6a have been clustered according to the following rules:

- First the data are clustered per ascending system load, into 10 clusters of equal size (same number of data points),
- Inside these 10 datasets, the data are then clustered per proportion of RES (from 10% to 70% and with steps of 10%), with at least 50 points.
- For the data points of each obtained cluster, a linear regression similar to the one presented in Figure III.6a is realized, to obtain the MEF of the cluster.

The resulting MEF values are plotted in Figure III.6b with colour mapping, in function of both the average system load and the RES share of the clusters. These MEF values have been obtained with an average correlation coefficient of 76% in the different clusters, thus the linear regression results are considered reliable. Figure III.6b clearly demonstrates the dependency of the CO_2 MEF with the RES share and the national load. When both the RES and the load are low, the MEF reaches higher values, because the remaining base load must be covered with CO_2 emitting sources. At middle load levels and high RES share, the MEF displays its lowest values: at these points, there is enough margin to increase the load and benefit from the high availability of renewable sources. Finally, when the load is high, the dependency of the MEF on the RES share tends to disappear. To obtain a more direct expression of the MEF, a quadratic fit is derived from the data points presented in Figure III.6b. The equation of this model is shown in Equation III.1, with L the system load (GW), RES the RES share (%) and a_i the fitting coefficients. The comparison between the model and the data points is represented in Figure III.7. The model is fitted by minimizing the root mean square error (RMSE), which reaches

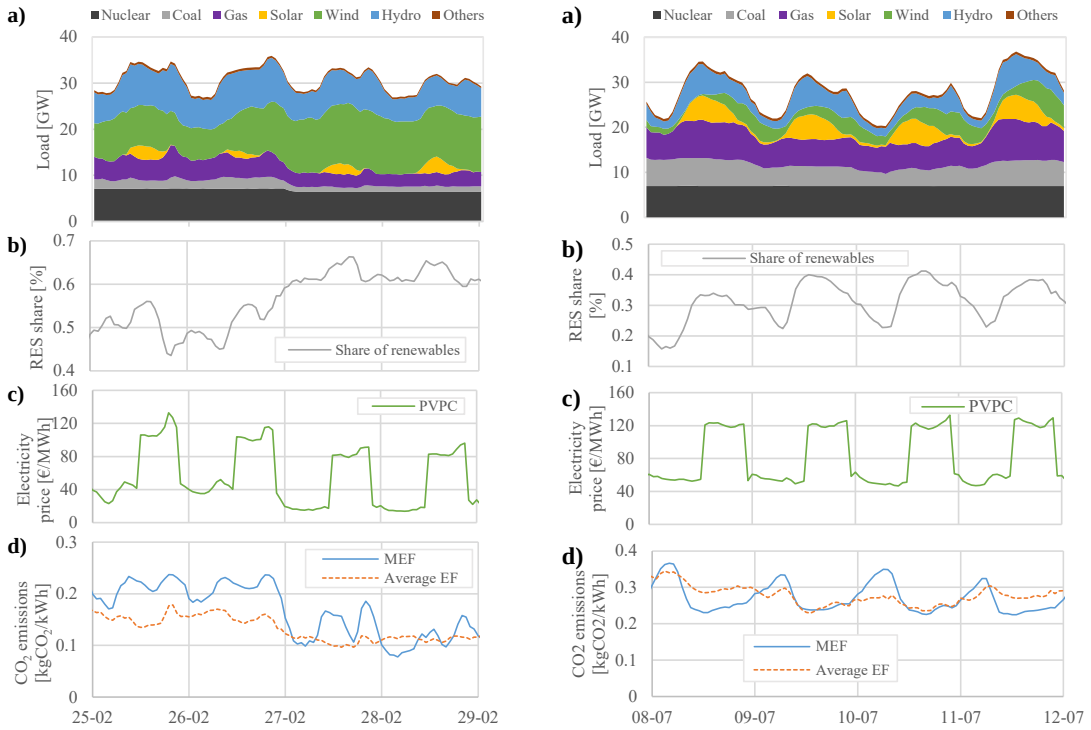

Figure III.8. Time series of the system load, the RES share, the electricity price and both the CO_2 EF and MEF, for a few days of February 2016 (left) and August 2016 (right).

the value of RMSE=0.00062 $kgCO_2/kWh$ or as a normalized value: NRMSE=0.28%.

$$MEF = a_0 + a_1 RES + a_2 L + a_3 RES^2 + a_4 L^2 + a_5 RES \cdot L \tag{III.1}$$

When analysing a particular period of time, the MEF can then be obtained by applying Equation III.1 to the time series of the power grid. An example is represented in Figure III.8: the system load (a) and the RES share (b), enable to calculate the MEF (d) thanks to the quadratic fit equation. The MEF and the average EF curves (compared in Figure III.8 (d)) globally follow the same trends. However, the MEF displays variations of larger amplitude than the average EF, and therefore leaves more room for optimization, which is the main reason behind the whole MEF signal calculation.

To interpret the curves, it should be reminded that a low MEF corresponds to a favourable case to use electricity, since the related CO_2 emissions will be lower, while a high MEF will trigger higher emissions. The MEF signal and the price signal (the latter being more traditionally used as an input signal for load-shifting) show a rather similar behaviour, although the price signal (PVPC) has a clear day/night discrepancy by construction. It should be noted that for instance, the MEF signal shows a clear valley around midday, which is also present, but less evident in the PVPC signal. This situation is foreseen to amplify in the future: Klein et al. [78] have analysed the energy mix of Spain in 2030 and deduced that it will be more profitable to use energy during day hours for a grid-optimal scenario, i.e. when the residual load is negative, due to the importance of solar-based energy. These statements are highly dependent on the country (see observed differences between Spain and Great Britain for the average MEF), the energy mix, and the dispatching of the energy sources within the grid. The operation of the grid also influences greatly the MEF calculation: for instance, it seems from Figure III.8 that mainly hydropower and gas are used to absorb the daily load fluctuations, while another management strategy would probably lead to different results in terms of marginal emissions.

2.2 Quantification - Key Performance Indicators

To evaluate the control strategies discussed in this thesis, it is necessary to pre-establish certain Key Performance Indicators (KPIs) to quantify the controller performance in different areas. Firstly, integrated values of energy and other quantities are calculated: they constitute the most intuitive KPIs that one would usually compute (section 2.2.1). Secondly, indicators specific to the context of energy flexibility are defined (section 2.2.2). Those mostly come from recent literature reviews on this topic. Thirdly, the control strategies must not jeopardize the comfort of the users, therefore some comfort indicators are also utilized (section 2.2.3).

2.2.1 Integrated energy values

The first indicators to observe when acting on HVAC control are the integrated energy values. In chapters IV and V, simulations and experiments of three days duration are reported. One can naturally calculate the integrated values over these three days: thermal energy delivered, electrical energy used, primary energy, costs or emissions due to the use of the heat pump. These primary KPIs already give a first indication about the performance of the controller.

Thermal energy The integrated thermal energy delivered by the heat pump $Q_{th,\Sigma}$ simply corresponds to the integral of the thermal power Q_{th} over the considered period, as shown in Equation III.2. When dealing with relatively short simulations (like three days in the present case), it is also important to consider the overall energy balance: between the final state and the initial state of the simulation, some energy has also been charged or discharged from the thermal storage (building mass and water tank), and the building is not left in the exact same state where it was found at the beginning of the simulation. To quantify this gap between initial and final state, the quantity ΔQ_{th} is computed, according to Equation III.3. For every state of the model T_i associated with the capacitance C_i, we calculate the difference of energy content between the final state $T_{i,fin}$ and the initial state $T_{i,init}$. ΔQ_{th} provides an approximate calculation of the difference of energy content of these states. The overall

thermal energy used $Q_{th,use}$ is then calculated with Equation III.4 and enables to consider both the energy produced by the heat pump and the energy charged/discharged in the building. Note that in the case of cooling, the sign of ΔQ_{th} is reversed, but Q_{th} is always counted positive, whether as heating or cooling thermal power.

$$Q_{th,\Sigma} = \int Q_{th}(t)dt \tag{III.2}$$

$$\Delta Q_{th,SH/SC} = \sum_{i \in \{states\}} C_i(T_{i,fin} - T_{i,init}) \quad \text{and} \quad \Delta Q_{th,TES} = C_{TES}(T_{TES,fin} - T_{TES,init}) \tag{III.3}$$

$$Q_{th,use} = \begin{cases} Q_{th,\Sigma} + \Delta Q_{th,TES} + \Delta Q_{th,SH} & \text{in heating mode} \\ Q_{th,\Sigma} + \Delta Q_{th,TES} - \Delta Q_{th,SC} & \text{in cooling mode} \end{cases} \tag{III.4}$$

Electrical energy The electrical power used by the heat pump P_{el} is integrated over the considered period, as shown in Equation III.5. To get a more complete picture, the consumption of other elements can also be included in the integral, such as the consumption of the FCU, additional pumps or valves, or even of the other electric loads of the building. However in this thesis, the focus lies on the operation of the heat pump, therefore we only consider the electricity use of the heat pump alone (including all its components).

$$P_{el,\Sigma} = \int P_{el}(t)dt \tag{III.5}$$

Efficiency (COP) To understand how efficiently the heat pump has operated over a certain period, an average COP value can be computed, as shown in Equation III.6. It simply consists in the ratio between the thermal energy produced by the heat pump and its electrical consumption. This quantity would correspond to the Seasonal Performance Factor (SPF) if calculated over an entire year. As mentioned in Equation III.5, the power consumption includes all the components of the heat pump (compressor, fan, controller, pump), but excludes any exterior device (FCUs for instance), so as to consider the COP of the heat pump only.

$$COP_{avg} = \frac{Q_{th,\Sigma}}{P_{el,\Sigma}} \tag{III.6}$$

Penalties - Cost, emissions and primary energy The objectives of the control strategies studied in this thesis often consist in minimizing the monetary costs, energy use or emissions due to the heat pump use. To evaluate if these goals have been reached, the integrated penalties are computed as described in the general formulation of Equation III.7. Considering a time-varying penalty c (price, emissions or primary energy factor PEF), the electricity use is multiplied by this penalty at every time step. The obtained c_Σ correspond to the integrated penalties. The specific formulation is shown in Equation III.8 for the energy costs with the electricity price c_{el}, and in Equation III.9 for the primary energy with the primary energy factor c_{PEF}. The time-varying PEF is defined for every kind of primary energy (coal, nuclear, solar etc.)[134], and the overall PEF for Spain is calculated every hour, according to the breakdown of its energy mix. The PEF, expressed in kWh_{prim}/kWh_{el}, takes into account resource extraction, transport and conversion of energy carriers, the use of fuels in power plants and the auxiliary energy use.

In the case of the marginal emissions, the general calculation must be slightly adapted, since such savings must be calculated considering a difference of energy use in comparison with a reference case. This calculation is reported in Equation III.10. $c_{MEF,\Sigma}$ corresponds to the marginal CO_2 emissions saved compared to the reference case (not to the global emissions of the considered case).

$$c_\Sigma = \int P_{el}(t) \cdot c(t)dt \tag{III.7}$$

$$c_{el,\Sigma} = \int P_{el}(t) \cdot c_{el}(t)dt \tag{III.8}$$

$$c_{PEF,\Sigma} = \int P_{el}(t) \cdot c_{PEF}(t)dt \tag{III.9}$$

$$c_{MEF,\Sigma} = \int [P_{el}(t) - P_{el,ref}(t)] \cdot c_{MEF}(t)dt \tag{III.10}$$

2.2.2 Flexibility indicators

Since energy flexibility applied to buildings is a relatively recent research topic, there does not exist a clear consensus about how to quantify this potential. Several recent reviews published in the frame of the IEA EBC Annex 67 have revealed the variety and numerous approaches in attempting to quantify the energy flexibility of buildings [116], [135], [136]. Most of them take into account one or several of these quantities to characterize the energy flexibility: power, energy, time or costs. Other articles attempted to define new indicators or methods, such as the standardized building assessment for demand response by Oldewurtel et al. [97], the flexibility factor by Le Dréau and Heiselberg [137], the quantification with cost curves by De Coninck and Helsen [138] or the flexibility function developed by Grønborg-Junker et al. [124].

The work of Reynders et al. [27], [139] exposes a distinction between two types of flexibility assessment: an evaluation beforehand, which would correspond to a prediction of the flexibility potential that one could obtain from a given building in the future, and an evaluation a posteriori, where a certain flexibility strategy has already been implemented and one wants to assess its performance afterwards. The first approach is more useful in an explicit demand response scheme, where for example an aggregator wants to know how much flexibility it can expect from its building portfolio and make biddings based on this prediction. It often relies on a comparison with a theoretical reference case where no flexibility is activated, which questions the choice of a standard reference case. The second approach is more relevant in implicit demand response scheme, where a signal is for example sent to the individual buildings, and the evaluation focuses on how much energy flexibility actually occurred with the considered controller. In this case, the indicators are often related to the strategy implemented (e.g. which input penalty signal was used), which limits their generalization.

This thesis focuses on implicit demand response, therefore an indicator able to quantify the performance of the load-shifting was chosen (the Flexibility Factor from [137]) and is presented in the next section. A set of indicators for explicit demand response was also chosen (the ADR indicators from [27]) and used in the later subsection 2.3 about the representation of flexibility.

Flexibility factor One major goal of implementing energy flexibility control strategies consists in shifting the loads towards periods of lower electricity price or lower CO_2 emissions from the grid. To quantify this shifting, the flexibility factor (FF) as defined in [137] is utilized. This indicator is calculated both with regards to the electricity price (FF_{cost}) and the CO_2 marginal emissions input signal (FF_{CO2}). In a generic formulation, p refers to the penalty signal being used (price or emissions), with hp, mp and lp respectively the high, medium and low penalty periods[1]. One can then compute the sum of electricity use during each one of these periods: $P_{el,\Sigma,hp}$, $P_{el,\Sigma,mp}$ and $P_{el,\Sigma,lp}$, which already gives a first quantification of the load shifting. The flexibility factor is then defined as in Equation III.12: FF_p varies between -1 (all the electricity use occurs during hours of high price/emissions) and 1 (all the electricity use occurs during hours of low price/emissions).

$$P_{el,\Sigma,lp} = \int_{lp} P_{el}(t)dt \quad , \quad P_{el,\Sigma,mp} = \int_{mp} P_{el}(t)dt \quad and \quad P_{el,\Sigma,hp} = \int_{hp} P_{el}(t)dt \tag{III.11}$$

[1]The method to obtain the thresholds for low and high penalty is discussed later in chapter IV about the development of the rule-based controller.

$$FF_p = \frac{P_{el,\Sigma,lp} - P_{el,\Sigma,hp}}{P_{el,\Sigma,lp} + P_{el,\Sigma,hp}} = \frac{\int_{lp} P_{el}(t)dt - \int_{hp} P_{el}(t)dt}{\int_{lp} P_{el}(t)dt + \int_{hp} P_{el}(t)dt} \tag{III.12}$$

ADR indicators The ADR indicators used for evaluating explicit demand response originate from [27]. They consider active demand response (ADR) events, where from $t = 0$ to $t = t_{ADR}$, a deviation of the energy consumption is observed (e.g. requested by an aggregator at higher level), in comparison with a reference case where this ADR event does not occur. Before $t = 0$, it is assumed that the ADR scenario and the reference scenario are equal.

In this context, the first indicator C_{ADR} represents the available storage capacity during the ADR event, and is calculated with Equation III.13. It corresponds to the deviation in energy of the ADR case compared to the reference case, expressed in kWh. In the integrals, $Q_{th,ADR}$ and $Q_{th,ref}$ are respectively the thermal heating powers of the ADR case and the reference case. To obtain $Q_{th,ref}$, it is supposed that one can get the results for a reference case with the exact same boundary conditions, but without the flexibility activation, through a parallel simulation for instance. It was chosen to use the thermal power in the equations to have a result independent of the heating system. To get an insight more directly relevant for the grid side, the electrical power of the heat pump could be used instead in the same formulas. It should be noted that in the present work and contrary to [27], $Q_{th,ref}$ does not correspond to the case which minimizes the heating energy, but rather a case with average set-point temperature in the middle of the comfort range. In this way, both upwards and downwards modulation can be studied. In the case of an upwards modulation, C_{ADR} is positive and represents the additional energy stored within the building mass during t_{ADR}. In the case of a downwards modulation, C_{ADR} is negative and represents the energy "saved" compared to the reference case, during t_{ADR}.

$$C_{ADR} = \int_0^{t_{ADR}} (Q_{th,ADR}(t) - Q_{th,ref}(t))\, dt \tag{III.13}$$

Charging/discharging energy within the building thermal mass or storage tank comes at a certain cost, due to the extra losses caused by this operation. In order to take into account the effect of these losses, a storage efficiency is defined, as shown in Equation III.14.

$$\eta_{ADR} = 1 - \frac{\int_0^{\infty} (Q_{th,ADR}(t) - Q_{th,ref}(t))\, dt}{|\int_0^{t_{ADR}} (Q_{th,ADR}(t) - Q_{th,ref}(t))\, dt|} \tag{III.14}$$

By reorganizing this equation, the storage efficiency can alternatively be interpreted as the ratio between the "rebound effect" and the "ADR event". The rebound effect corresponds to what happens immediately after the end of the ADR event. This is illustrated in Figure III.9 for a downwards modulation: during the event, the building had to decrease its energy consumption (of 10 kWh in this case). Because of this prolonged reduction, once the modulation is no longer required, the building has to compensate and will use more energy just after the ADR event. The storage efficiency η_{ADR} thus consists in comparing the amplitude of the rebound effect with the actual capacity stored during

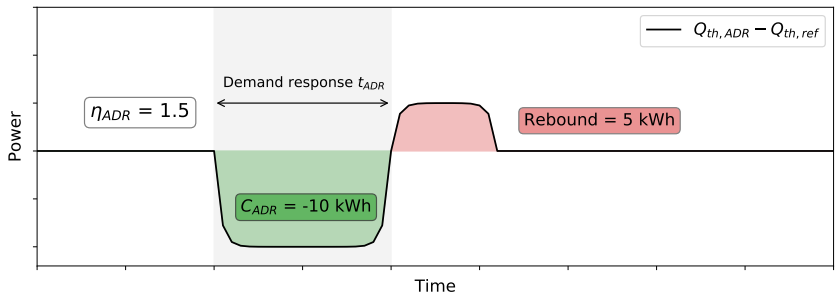

Figure III.9. Principle of the rebound effect, and example of calculation of the ADR efficiency η_{ADR}.

the event. In the case of an upwards modulation, it corresponds to the ratio between the energy saved after the ADR event and the surplus energy stored during the ADR event. In the case of a downwards modulation, it corresponds to the ratio between the surplus energy spent in the period after the ADR event and the energy saved during the ADR event.

The integrals used in the calculation of η_{ADR} are theoretically summed over an infinite period of time. In the present work, only the 24 hours ahead from the start of the ADR event have been considered. It is assumed that the ADR event has little to no effect on the behavior of the system after this limit.

2.2.3 Comfort indicators

To ensure that the control strategies do not affect the thermal sensations of the building occupants, thermal comfort indicators are evaluated over the considered simulation periods. The main variable examined for this purpose is the average operative temperature of the building. Indoor Environmental Quality (IEQ) is a vast topic including lighting and acoustics, and thermal comfort alone does also depend on many other parameters, such as the relative humidity, the air velocity and the clothing and activity levels. Since the controller manages and is aware only of the temperature (it does not take into account the humidity for instance), it was chosen to only analyze this parameter. Furthermore, temperature is the most relevant parameter in accounting for thermal sensations, therefore the comfort analysis focused on it. It should be added that the operative temperature is considered instead of the air temperature, therefore the radiation component is also taken into account, and in this way the results can be compared with the recommended ranges from the standard for buildings mechanically heated or cooled, which are also expressed in terms of operative temperature.

Table III.1. Comfort ranges as defined in the standard EN 15251.

Category	**Description**	**PPD**	**PMV**	**Range (heating season)**	**Range (cooling season)**
I	High level of expectation and is recommended for spaces occupied by very sensitive and fragile persons with special requirements	$< 6\%$	$\|PMV\| < 0.2$	21-25°C	23.5-25.5°C
II	Normal level of expectation and should be used for new buildings and renovations	$< 10\%$	$\|PMV\| < 0.5$	20-25°C	23-26°C
III	An acceptable, moderate level of expectation and may be used for existing buildings	$< 15\%$	$\|PMV\| < 0.7$	18-25°C	22-27°C
IV	Values outside the criteria for the above categories. This category should only be accepted for a limited part of the year	$> 15\%$	$\|PMV\| > 0.7$	-	-

The results are represented as the percentage of time where the operative temperature stays within the ranges defined in the European standard EN 15251 [140]. Those ranges are recalled in Table III.1: they correspond to different levels of PPD (percentage of people dissatisfied by the thermal conditions) or PMV (Predicted Mean Vote as a measure of the thermal sensation). These ranges of PPD/PMV are translated into different operative temperature ranges for the heating and cooling seasons. The percentage of time spent in each of the categories can be represented as in Figure III.10, as suggested by the standard and used in the analyses of this thesis.

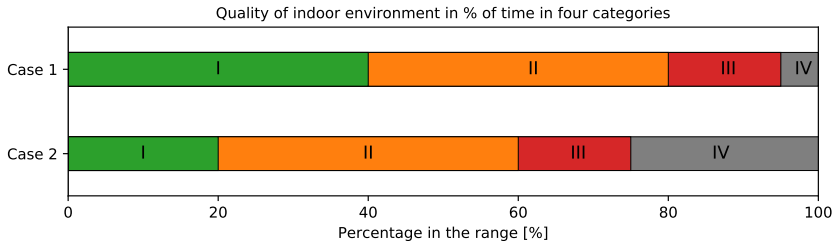

Figure III.10. Representation of the thermal comfort according to the European standard EN 15251.

2.3 Representations of energy flexibility

Using adapted KPIs enables to quantify the energy flexibility potential of buildings. However in certain contexts, a graphical representation can be more relevant, especially since the energy flexibility (and consequently most of the associated KPIs) can change over time. Since there is no clear consensus on how these results could be represented visually, the present section presents different proposals about how to create a daily profile showing the amount of flexibility available from a building. Such graphical content could be useful for several types of end-users: aggregators, utilities, electrical or mechanical engineers, designers. A standard representation could help them evaluate at a glance the available flexibility that a building can offer and at what cost, along the next day. This research question arose from internal discussions within the IEA EBC Annex 67, and it fits more in an explicit demand response scheme (therefore it stands out a little from the remaining of the thesis, which principally deals with implicit demand response).

The present section thus intends to perform an energy flexibility analysis on a test case, which is the same building than exposed later in section 4. The ADR indicators are used to assess the flexibility capacity and efficiency: in this case, the ADR events consist in modulating the room temperature set-point for a duration of t_{ADR}. The reference set-point is 21.5°C (or 20.5°C at night and when the building is unoccupied). From this reference, different amplitudes of the modulation are tested (1 or 2°C), and the upwards modulation means the set-point is increased, while a downwards modulation that the set-point is decreased by that value. The nomenclature is as follows: for a case 1D2H, the set-point is modulated of 1°C for a duration t_{ADR} of 2 hours. To obtain a full daily profile, a different simulation is carried out for every hour of the day: in each simulation, the ADR event starts at that hour, from hour 0 to hour 23. It is considered that only one ADR event can happen per day (therefore we discard the influence of successive events on each other).

From the obtained results, some examples of daily profile representations showing both the capacity C_{ADR} and the efficiency η_{ADR} of energy flexibility are proposed. The focus lies more on how to represent the results than on the actual values of the flexibility. For this reason, only one sample day, the 30th of January, was used for testing the proposed approach, and only in heating mode. The first proposed representation is shown in Figure III.11. In red are represented the results of the upwards modulations, and in green, the results of the downwards modulations; the bars represent the capacity C_{ADR} while the symbols represent the efficiency η_{ADR}. It should be noted that for the downwards case, the efficiency is plotted reversely, so as to obtain a symmetrical graph with regards to the zero horizontal axis (see the vertical axis on the right). When $C_{ADR} = 0$, η_{ADR} is not computed since an efficiency is meaningless when there is no actual capacity for flexibility.

The shape of the daily profile presented in Figure III.11 corresponds to the expectations, considering the occupancy profile. During the peak hours (5:00 to 8:00 and 18:00 to 20:00), the occupants are present in the building, and the set-point is thus already increased. Therefore, the heat pump is generally switched on already in the reference case. Increasing the set-point at these moments does not allow for supplementary upwards flexibility ($C_{ADR} = 0$ at 6:00 and 19:00). However, a downwards flexibility is logically available if the set-point is reduced during these hours: up to 8.5 kWh can be saved during the 2 hours of the ADR event (at 6:00 in the morning). Conversely, the system presents the opposite behavior during non-occupied and night hours, mainly from 0:00 to 4:00 and from 9:00 to 15:00. In these periods, the setback provokes a switching off of the heat pump already in the reference

scenario. The only available flexibility thus consists in forcing the heat pump to operate, by raising the set-point. In this way, a maximum of $C_{ADR} = 9.4$ kWh can be reached during the 2 hours ADR event (maximum reached at 3:00).

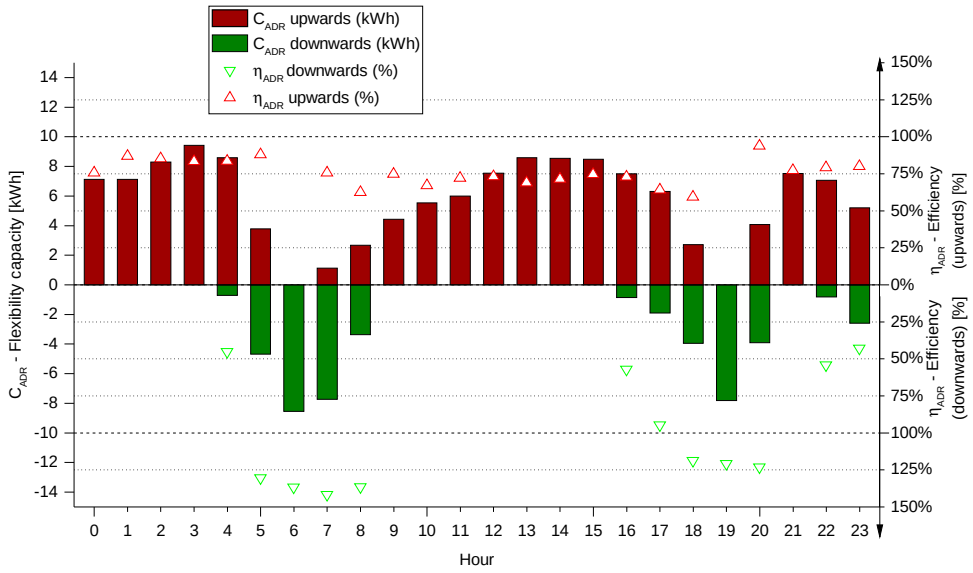

Figure III.11. Profile of the flexibility capacity and efficiency, in upwards and downwards modulations (case 1D2H).

The analysis of η_{ADR} shows some discrepancies between the upwards and the downwards modulation cases. The efficiency ranges from 59 to 94% in the upwards case, and is relatively stable. In the downwards cases, and more specifically those with a high capacity C_{ADR}, the efficiency reaches levels above 100%, up to 123%. Concretely, this means that the system saves energy that was not necessary to use in the first place: the energy saved during the ADR event is not compensated entirely by a posterior use of energy (rebound effect is thus limited). This operation causes obviously a slight decrease in the temperature, but since the reference case was not the case of minimum comfort, some margin still exists until the bottom comfort boundary is reached, and thus the comfort requirements are still met.

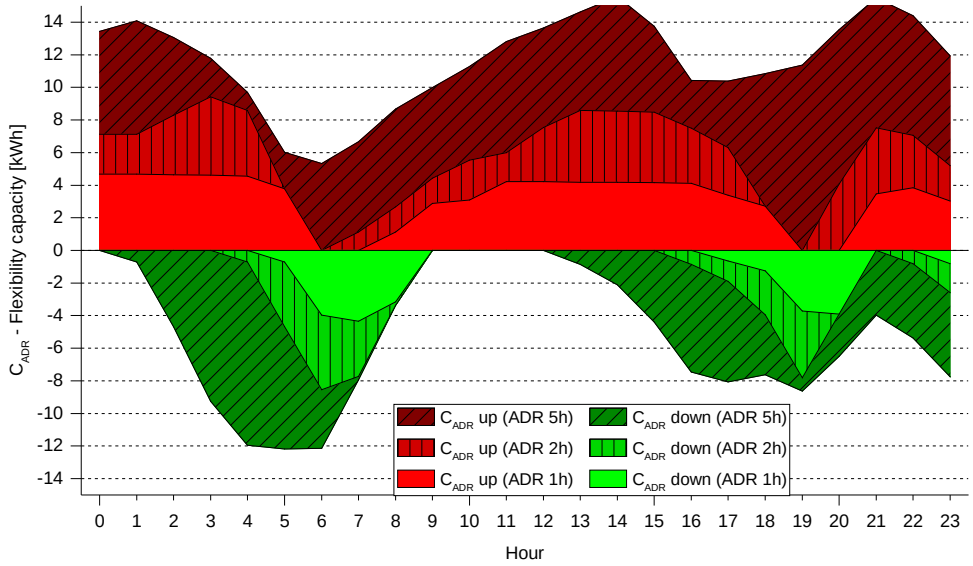

Figure III.12. Representation of the daily profile of C_{ADR} for different durations of the ADR event.

An alternative graphical representation of the daily C_{ADR} profile is proposed in Figure III.12, com-

paring different durations of the ADR event, keeping the same amplitude of the temperature variation (±1°C). In red, the upwards modulation is shown, and in green the downwards modulation. From lighter to darker color indicates a longer duration of the ADR event: 1h, 2h and 5h. With a longer ADR, the flexibility capacity obviously increases, and with a 5h event, there is a potential for flexibility all day long (while some hours presented little to no flexibility with an ADR event of only 1 or 2h). The interest of this representation is to show at a glance the comparison between different configurations of the ADR event. It does however not reveal the drop of efficiency due to the longer ADR events, which should be taken into account when actually using the flexibility.

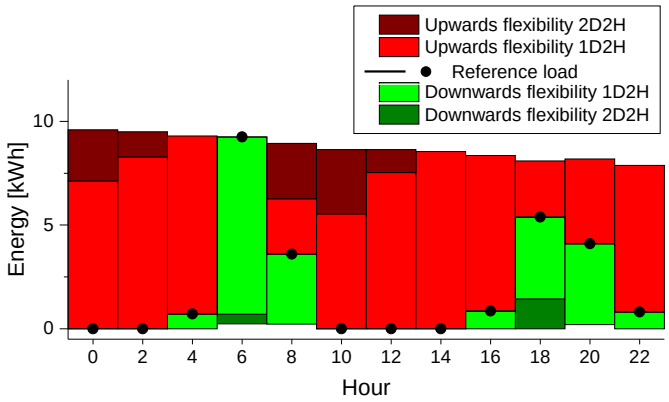

Figure III.13. Flexibility capacity profile including the reference load profile, aggregated per clusters of 2 hours (cases 1D2H and 2D2H).

Another suggestion for representation consists in additionally plotting the reference energy consumption, as shown in Figure III.13 (black solid line). This enables to put in relation the actual energy consumption with the flexibility potential. From the black line representing the load, the additional upwards flexibility is shown as a red area above the line, and the downwards flexibility is shown as a green area below the line. It can be seen that the periods of high energy consumption logically correspond to a downwards flexibility potential, while the periods with no consumption corresponds to upwards flexibility potential. This graph however does not provide information on the efficiency of the ADR event, therefore it should be complemented with another graph representing this aspect, so as to obtain a global overview of the flexibility potential. In the case of Figure III.13, ADR events of 2 hours duration are represented, and thus the reference load profile should be as well aggregated per clusters of 2 hours, to enable an easier comparison. Furthermore, events of different modulation amplitude are plotted in this graph: the flexibility capacity of a set-point modulation of ±1°C is shown in light green and red, while the modulation of ±2°C is shown in dark green and red. In this way, the additional benefits of amplifying the set-point modulation are revealed. It can be seen for example that further increasing the set-point provides greater upwards flexibility only in the early hours of the day (0:00 to 2:00) and after the morning occupancy (8:00 to 12:00). Further decreasing the set-point usually does not provide greater downwards flexibility, except at 18:00.

To summarize this study on the representations of flexibility, the first graph type enables to show graphically both the flexibility energy capacity and its storage efficiency along the day, and for both upwards and downwards flexibility. This representation thus gives a good overview of the different aspects of energy flexibility for a building in a single graph. When comparing different configurations of the ADR event, the area graph (second type) seems a better option for the flexibility capacity, but then the efficiency profiles should be plotted apart. In all representations, it was found that the existing occupancy schedule has a crucial influence on the flexibility potential: it actually shapes the daily profile of energy flexibility. Roughly, the occupancy periods (with already increased energy consumption) correspond to downwards flexibility potential, while the periods of unoccupancy or night correspond to upwards flexibility potential. Considering a flat temperature set-point of reference or a different occupancy schedule would considerably change the flexibility evaluation. Moreover, a set-point modulation of ±1°C during 2 hours enables to provide a maximum of 9.4 kWh in available flexibility capacity (upwards), and -8.6 kWh (downwards). Lengthening the duration of this ADR event enables to increase the capacity, but saturation is observed and the storage efficiency then tends to

decrease.

The relevance of the chosen KPIs can also be discussed. In this section, two distinct metrics have been used to quantify the different facets of energy flexibility, the flexibility capacity C_{ADR} and the flexibility efficiency η_{ADR}. They should be considered together, since one represents the amount of flexibility that can be offered, and the other which 'costs' the provision of this amount of flexibility would incur. Ideally, these two dimensions could be merged into a single indicator that would cover all the aspects of the energy flexibility. However, a loss of information would thus become inevitable. For instance, the other flexibility indicator used in this thesis, the Flexibility Factor, is a single indicator that provides information about the amount of load shifting, and also an estimation of the consequent losses or savings since it informs about the amount of energy used in the low-price hours. However, it is only a relative indicator (normalized between -1 and 1), and therefore does not give insights on the absolute savings. For instance, a certain scenario can present an excellent flexibility factor, but a shifting of very little energy in volume. So far, no common and global indicator has been found in the literature to cover all aspects of energy flexibility in a single metric. As a partial answer to this issue, the graphical representation presented here, with both the C_{ADR} and η_{ADR} parameters on the same graph thus provides a solution enabling to catch both information at the same time.

3 Heat pump system

The present thesis treats the subject of heat pump controls, hence it is deemed worthy to first provide in subsection 3.1 a short reminder of what is a heat pump system, how it operates and which components it is made of. To fully characterize the heat pump considered in this study, static tests were carried out in a laboratory setup: they are reported in subsection 3.2. Then, the simple models derived from the static tests measurements are described in subsection 3.3; such models will be used by the MPC controller. Furthermore, detailed models of the heat pump were developed to represent more accurately the dynamics of such systems in building simulation tools (TRNSYS), this modeling approach is finally presented in subsection 3.4.

3.1 Description of an air-to-water reversible heat pump system

A heat pump is a machine that enables to transfer heat from one fluid (the heat source) to another (the heat sink). This transfer is made possible through a closed circuit of refrigerant fluid which changes states along a cycle of compression/decompression. The heat source can consist of water (sea, lake etc...), earth (geothermal applications) or the ambient air. The heat sink can consist of water or air depending on the end application. In the present study, we consider an air-to-water heat pump. Heat pumps represent an ideal tool to couple the electrical and thermal networks, since they can cover thermal loads from electricity at a high efficiency. Their use within smart grids is therefore very promising and has already been largely studied in the literature [36].

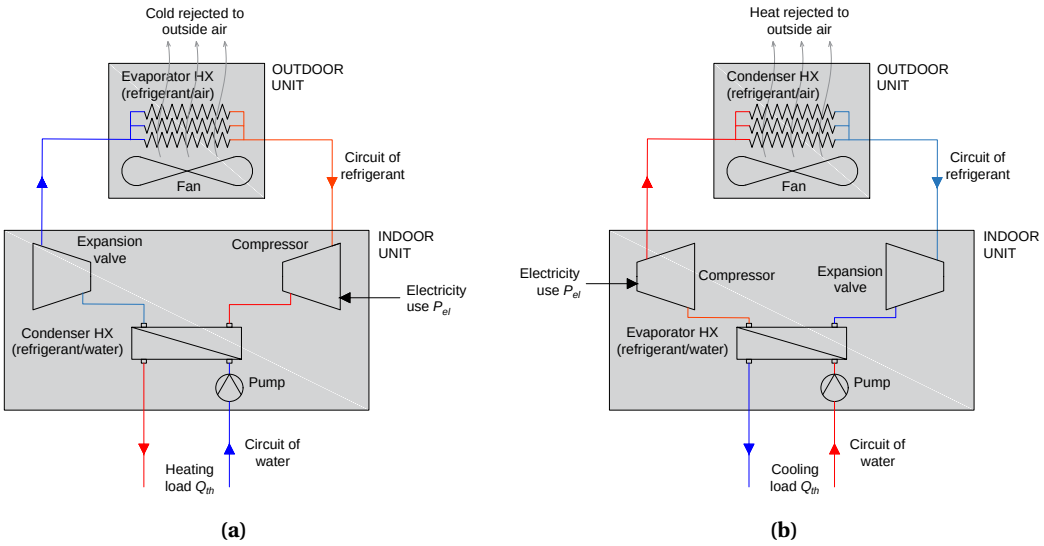

Figure III.14. Principle of the functioning of a heat pump in (a) heating and (b) cooling modes.

Figure III.14a represents the principle of the heat pump cycle for covering a heating load. The refrigerant fluid starts the cycle after the expansion valve as a cold liquid at low pressure. Passing through the evaporator heat exchanger (HX), it evaporates, absorbing heat from the air which is circulated through the heat exchanger by the circulating fans. The obtained gas is then compressed by an electrical compressor, which is the main source of energy use in the cycle. After the compressor, the refrigerant is a hot liquid: it passes through the condenser heat exchanger where it transfers the heat to the water circuit connected to the heating load. The pressure of the cold liquid refrigerant is then lowered in the expansion valve and the cycle resumes.

Some models of heat pumps are reversible, meaning they can either provide heating or cooling by inverting their cycle. The principle of a reversible heat pump in cooling mode is presented in Figure III.14b. It is similar than in heating mode, but the role of the heat exchangers has changed: the one placed in the outdoor unit now acts as the condenser while the one connected to the load now acts

as the evaporator. The place of the compressor and expansion valve is also inverted in the circuit. In practice, the inversion of the cycle is achieved by means of three-way valves.

The former description represents the basic operation of the heat pump at full load. If the load is reduced, the compressor (and hence the whole cycle) can be operated intermittently, and the heat pump thus presents an on-off behavior. Nowadays, most heat pumps on the market possess an additional inverter that enables to control the frequency of the compressor, and thus to reduce the heating or cooling load without stopping the whole cycle. Such devices are named variable speed heat pumps (VSHP) or inverter-controlled heat pumps.

To characterize the efficiency of a heat pump system, one commonly refers to the instantaneous Coefficient of Performance (COP), which is defined in Equation III.15 as the ratio between the thermal power Q_{th} produced by the heat pump and its electricity use P_{el} (which includes the power consumption of all the heat pump components, but excludes any system exterior to the heat pump). In cooling mode, the COP is called Energy Efficiency Ratio (EER), but the formula is the same: the thermal power Q_{th} is always considered positive, whether it represents a heating or cooling power. In the case of a water loop on the load side, Q_{th} is calculated with Equation III.16, where $\dot{m}$ is the water flow rate in the load circuit, c_p the specific capacity of water and ΔT the temperature difference between the supply and the return of the water loop.

$$COP = \frac{Q_{th}}{P_{el}} \tag{III.15}$$

$$Q_{th} = \dot{m} \cdot c_p \left(T_{sup} - T_{ret}\right) = \dot{m} \cdot c_p \Delta T \tag{III.16}$$

Among other important parameters that characterize the functioning of the heat pump, the frequency of the compressor f, expressed in Hz, informs on how fast is the machine running, since a VSHP can modulate its output. Another way to represent the modulation of the system is through the capacity ratio CR at part-load, defined in Equation III.17 as the ratio between the current thermal power Q_{th} and the maximum capacity of the machine $Q_{th,FL}$ at full load, in the same operating conditions. CR is expressed as a number between 0 and 1 or as a percentage: if it is running at full load, then $CR = 1$ or 100%. Moreover, Equation III.18 defines the part-load performance, which is the ratio between the COP in the current conditions and the COP of the machine at full load in the same conditions. A relationship normally exists between the CR and the PLF, see section 3.4.4 on this subject.

$$CR = \frac{Q_{th}}{Q_{th,FL}} \tag{III.17}$$

$$PLF = \frac{COP}{COP_{FL}} \tag{III.18}$$

A heat pump does not provide heat (or cold) like an electrical resistance would, it only transfers heat from one medium to another. This transfer process requires some energy but not as much as it provides, therefore the COP is normally higher than 1, and usually in the range of 2 to 6, depending on the operating conditions. Heat pumps are thus very efficient devices, and depending on where comes their electricity supply, can be considered as a sustainable option. For instance, considering an efficiency of the power system of 45.5% (value for 2010), a heat pump operating with a seasonal COP higher than 2.5 can be considered as renewable energy, as declared by the European Commission [141].

In the present thesis, a heat pump model available from the market was used to realize tests in both steady-state and dynamic operating conditions. The studied machine is an air-to-water, reversible VSHP from the series Yutaki S Combi of Hitachi. As a split system, it consists of both an outdoor unit and an indoor unit, which itself contains a 200 liters tank for storing DHW. The main specifications of the chosen heat pump are given in Table III.2.

Table III.2. Specifications of the studied Hitachi Yutaki S combi heat pump.

Parameter	Unit	Value
Nominal heating power [1]	kW	11
Nominal COP[1]	-	3.98
Nominal cooling power[2]	kW	7.2
Nominal EER[2]	-	3.3
DHW tank capacity	liters	200
Tank insulation polyurethane heat loss	kWh/day	1.4
Refrigerant	-	R-410A
Compressor type	-	Scroll DC inverter driven
Nominal air flow	m^3/min	80
Water flow rate range	m^3/h	1.0 to 2.7
Heating working range - Ambient temperature	°C	-25 to 25
Heating working range - Supply temperature	°C	20 to 60
Cooling working range - Ambient temperature	°C	10 to 46
Cooling working range - Supply temperature	°C	5 to 22
DHW working range - Ambient temperature	°C	-25 to 35
DHW working range - Tank temperature	°C	30 to 75

3.2 Static tests and experimental characterization of the heat pump

3.2.1 Principle for the static tests

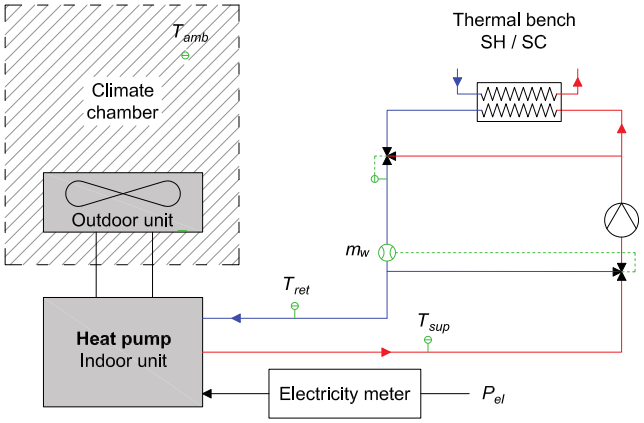

Figure III.15. (Schematic of the experimental setup for the measurement of the static tests points.

To fully characterize the heat pump and understand its functioning and performance under different conditions, static tests were realized in the laboratory setup previously described. These tests were performed in accordance to the European standards EN 14511 [142] and EN 14825 [143]. The schematic of the installation used for the steady-state tests is presented in Figure III.15: only the loop for space heating or cooling is used and connected to the corresponding thermal bench, while the DHW part of the machine is not activated.

[1]Standard rating conditions in heating mode [142]: outside air temperature 7°C, inlet water temperature 40°C, outlet water temperature 45°C

[2]Standard rating conditions in cooling mode [142]: outside air temperature 35°C, inlet water temperature 12°C, outlet water temperature 7°C

The static tests consist in fixing the triplet of temperatures $(T_{sup,SP}, T_{ret}, T_{amb})$: the supply set-point temperature $T_{sup,SP}$ is set in the local controller of the heat pump, the return water temperature T_{ret} is controlled in the thermal bench of the laboratory, and the ambient temperature T_{amb} is controlled by the climate chamber where the outdoor unit is situated. The values of these temperatures correspond to standard rating conditions according to EN 14511 [142], enabling to compare with the manufacturer's data. They are presented in Table III.3. In the heating case, a maximum ΔT of 8°C was sufficient to reach the maximum capacity of the machine, while in cooling mode it was necessary to reach the value of $\Delta T = 11°C$ for this purpose. It should be noted that we fix the set-points for those three temperatures, but the actual output might differ from that desired set-point (especially for T_{sup} where in certain conditions, the machine cannot reach the set-point $T_{sup,SP}$).

Table III.3. Combinations of temperatures tested in the steady-state experiments.

Parameter	Heating mode	Cooling mode
Ambient temperature	$T_{amb} \in \{-7°C, 2°C, 7°C, 12°C\}$	$T_{amb} \in \{20°C, 25°C, 30°C, 35°C\}$
Supply temperature	$T_{sup,SP} \in \{35°C, 45°C, 55°C\}$	$T_{sup,SP} \in \{7°C, 12°C, 18°C\}$
Temperature lift	$\Delta T \in [\![1°C, 8°C]\!]$	$\Delta T \in [\![1°C, 11°C]\!]$
Number of points	96	132

3.2.2 Static points

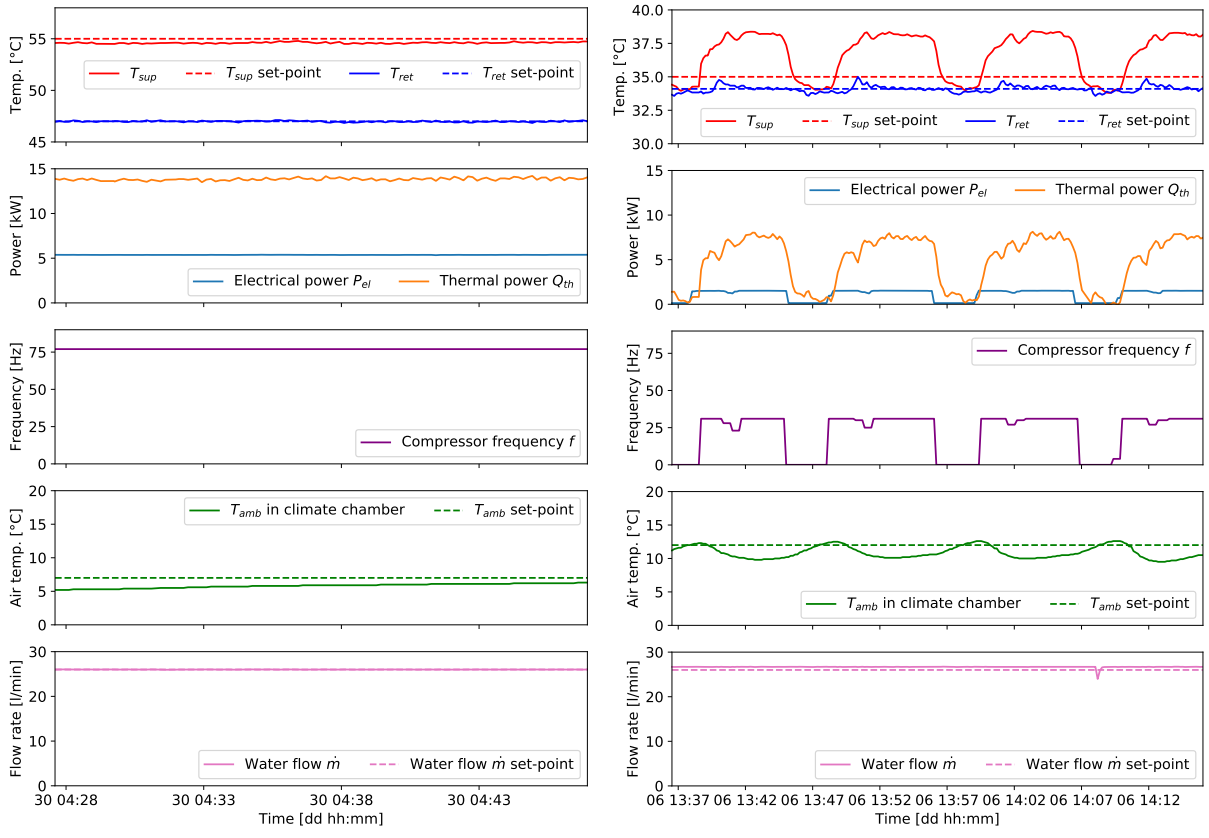

(a) **(b)**

Figure III.16. Measured parameters in two exemplary static points (a) at high load with constant parameters and (b) at lower load with a cyclic on-off behavior.

For each experimental point, at least 30 minutes of data were recorded in steady state, after leaving 20 minutes of transition between one point and the next one. It was ensured that no defrost operation

occurred during the measuring period, to avoid distorted measurements. The following parameters were measured and averaged over the measuring period of 30 minutes: supply and return temperatures T_{sup} and T_{ret}, water mass flow rate $\dot{m}$, thermal and electrical powers Q_{th} and P_{el}, air temperature T_{amb} in the climate chamber and frequency of the compressor f.

Two examples of static points in heating mode are presented in Figure III.16a and Figure III.16b. The first one represents a normal steady-state point at high load (high demand) where all parameters are almost constant. The second one represents a case where the load is very low: a temperature lift of only 1°C is imposed between the return water which is kept at 34°C and the supply water which is set to 35°C in the heat pump integrated controller. Even if the compressor speed is variable, it has a minimum below which it cannot operate. In the present case, this minimum has the value of 30 Hz. To avoid providing a load too much higher than the desired heating for this static point, the compressor has to switch on and off regularly: this cycling behaviour is clearly visible in Figure III.16b. The measured values of that static point correspond to the average of the parameters, and therefore they take into account the on-off cycling, which is a detail of importance when using such static points to form a model of the heat pump performance.

Figure III.17 shows the average temperature measured in the climate chamber for every static point. The control of the climate chamber is not perfect, especially in the heating mode (hence when

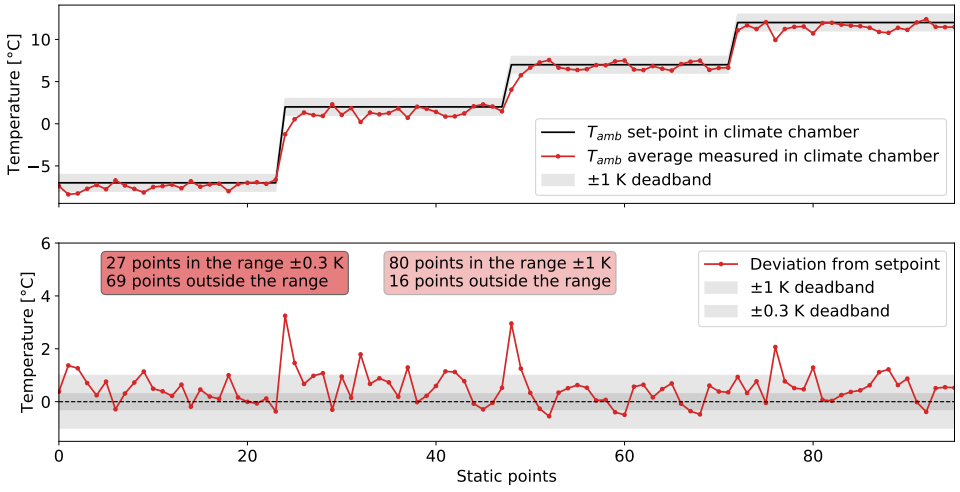

(a) Average air temperature in the climate chamber for the heating static points.

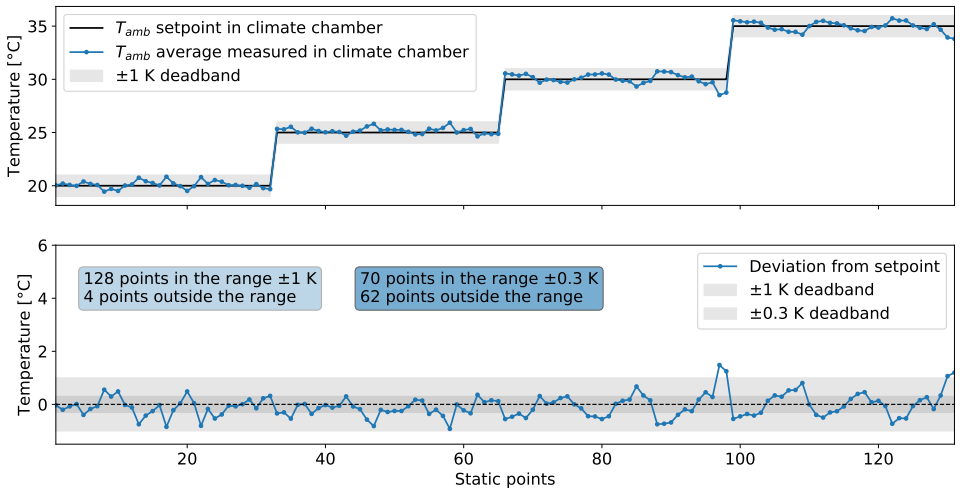

(b) Average air temperature in the climate chamber for the cooling static points.

Figure III.17. Average air temperature measured in the climate chamber during the static points in heating and cooling modes.

the climate chamber is cold) as seen in Figure III.17a. The standard EN 14511-2 [142] mentions that the arithmetic mean of the air temperature can deviate of a maximum of ± 0.3 K from the set-point. In the heating mode, only 27 points out of 96 belong to this allowed limit, and the deviation reaches 3.5 K in two extreme cases. Several reasons explain the large deviation in some cases: in heating configuration, defrosting operation occurs regularly (internally controlled by the heat pump) to avoid the formation of ice on the heat exchanger of the outdoor unit. Defrosting[1] consist in briefly inverting the heat pump cycle to melt the ice. The resulting water accumulates on the floor of the climate chamber below the outdoor unit, and complicates the task of the climate chamber controller which must maintain a certain level of humidity, temperature and air flow at the same time in the enclosed space. The deviation of the ambient temperature with respect to its set-point affects the comparison with the manufacturer's data, which are normally collected under the strict conditions defined in the standard [142]. Therefore when it is referred to "the experimental series at $T_{amb} = 7$ °C", the reader must understand that not all points of the series were performed at exactly 7°C, but with some deviations. However, even though the ambient temperature did not reach exactly the set value, these points are still valid for fitting adequate models, if we consider the measured value and not the set-point.

3.2.3 Results of the static tests in heating mode

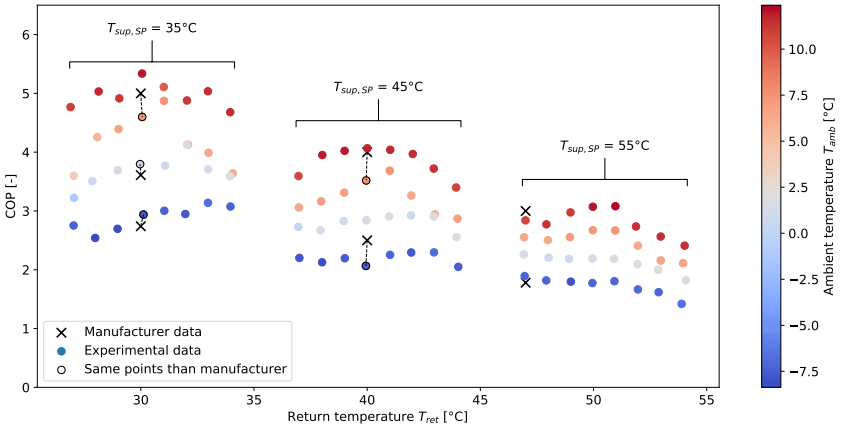

Figure III.18. COP in heating mode in function of the supply, return and ambient temperatures.

Coefficient of Performance The efficiency of the heat pump operation, i.e. the COP as defined in Equation III.15 is calculated for each static point and shown in both Figure III.18 and Figure III.19 with different representations. In Figure III.18, one can observe the degradation of COP which corresponds either to a higher supply temperature or a lower ambient temperature. In all the measured static points, the COP ranges from 1.4 to 5.3. Figure III.19 displays the same points, but the graph has been split in four subgraphs, one per series at a common ambient temperature set-point. Additionally, the error bars of COP calculation are represented, calculated with the precision of the measurements given in previous section 3.2.2: the points with low capacity have the highest error bars, given that a precision of 0.5 K in the temperature lift measurement has a great impact on the error of the thermal capacity (following Equation III.16). It is also observed that at low load ($\Delta T \leq 3$°C), the heat pump is not able to modulate and exhibits an on-off cycling behavior that induces a low COP. In the cases with a high load ($\Delta T \geq 6$°C) and low T_{amb}, the heat pump cannot reach the desired set-point despite the compressor running at full speed, and a lower COP is also generally observed[2].

[1] It should be noted that if defrosting occurred during the measurement of a static point, this experimental point was discarded and redone to avoid the influence of such specific behavior. None of the measured static points include defrosting operation, and thus they represent the behavior of the heat pump under normal operation.

[2] An additional figure is shown in Appendix B where both the supply and return temperatures are represented on the same graph, so as to appreciate when the set-point is reached or not.

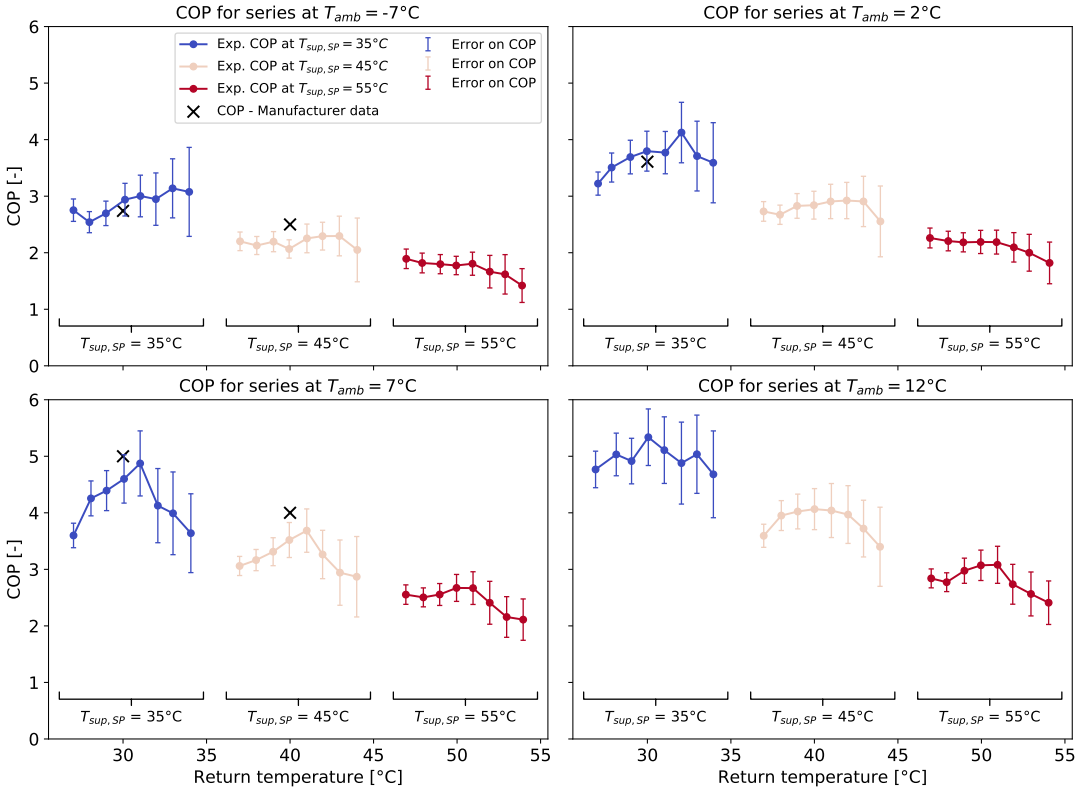

Figure III.19. COP in heating mode in function of the supply, return and ambient temperatures.

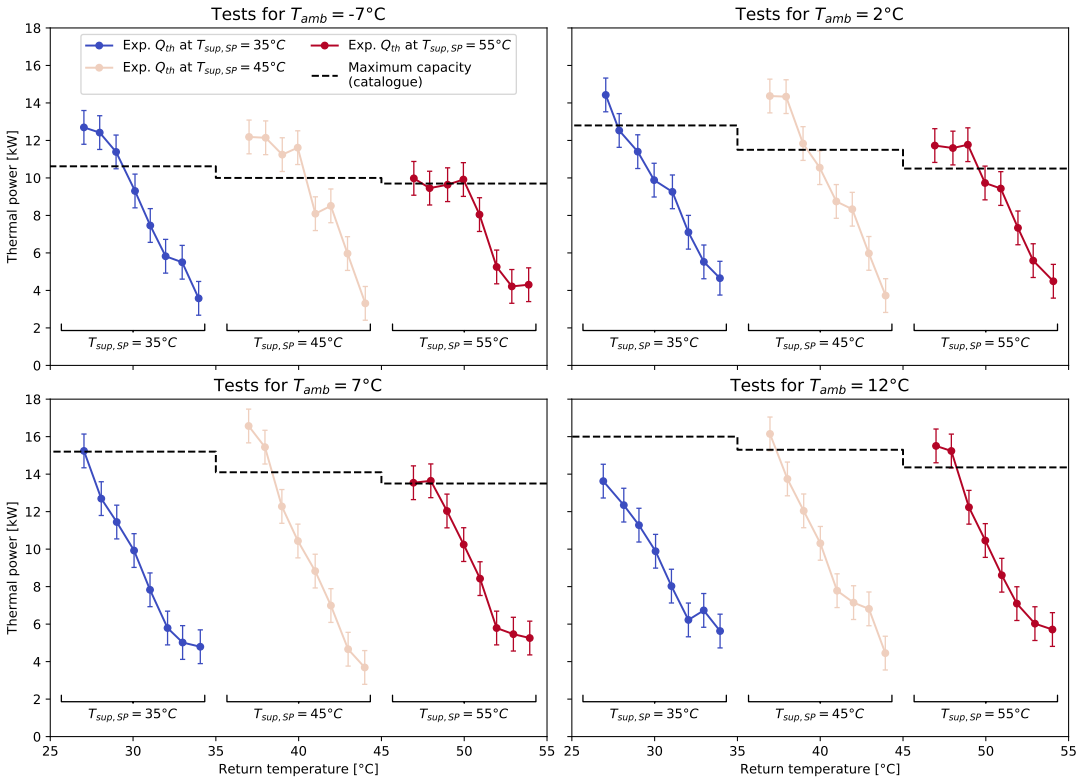

Figure III.20. Thermal capacity in heating mode, in function of the supply, return and ambient temperatures.

Thermal heating capacity The thermal capacity is calculated according to Equation III.16 and represented in Figure III.20. It is proportional to the temperature lift ΔT, therefore for a fixed supply temperature, Q_{th} follows normally a straight line when the return temperature decreases (i.e. ΔT increases). The dashed lines represent the maximum capacity declared in the manufacturer's catalogue for each operating conditions. In several cases, the experimental points reach a higher capacity than the theoretical maximum, revealing that the machine can be pushed to operate at higher capacity in certain conditions. However, as a precautionary measure, the maximum capacity declared in the catalogue was chosen as the upper boundary for the thermal power in the MPC framework, as further explained in section IV.2.3. A saturation plateau is observed for the high loads, especially when the supply temperature is higher ($T_{sup} = 55$°C), due to internal protections of the heat pump. At low loads, the capacity does not decrease linearly either: since the heat pump cannot modulate below a certain level, it cycles on and off, but still provides on average more capacity than required.

Compressor frequency Figure III.21 displays the average frequency of the compressor measured for all the experimental static points. Here the previously described limitation of the thermal capacity can clearly be correlated with the physical limitations of the compressor: its frequency is restricted to a maximum of 90 Hz. When the supply temperature is set to 55°C, the limit imposed by the heat pump local controller is even lower and set to 75 Hz. Such constraints explain the plateau observed for the thermal capacity at high loads. The graph of the heat pump electrical consumption was not plotted, although it would have a similar trend than the frequency graph of Figure III.21, since the compressor represents the principal consumer of electricity in the heat pump system.

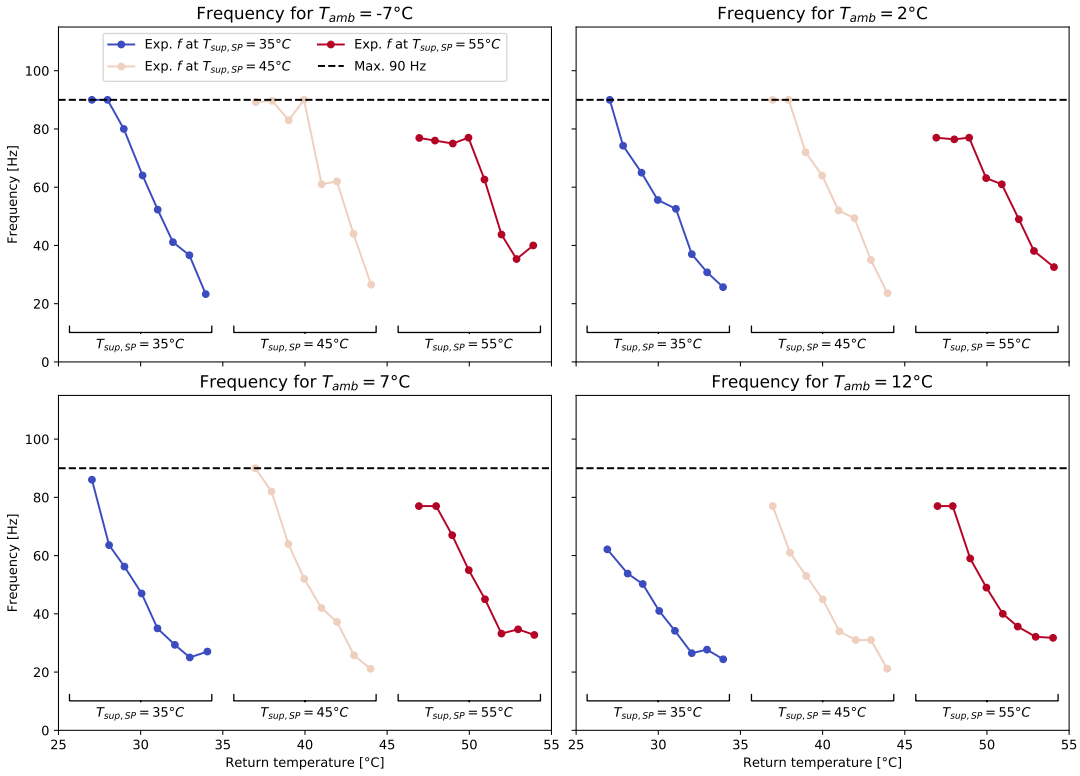

Figure III.21. Frequency in heating mode, in function of the supply, return and ambient temperatures.

3.2.4 Results of the static tests in cooling mode

Energy Efficiency Ratio The EER in cooling mode is represented in Figure III.22. The first notable difference with respect to the heating mode is that the efficiency of the heat pump depends much less on the outdoor conditions. The EER tends to be lower at high ambient temperature, but this

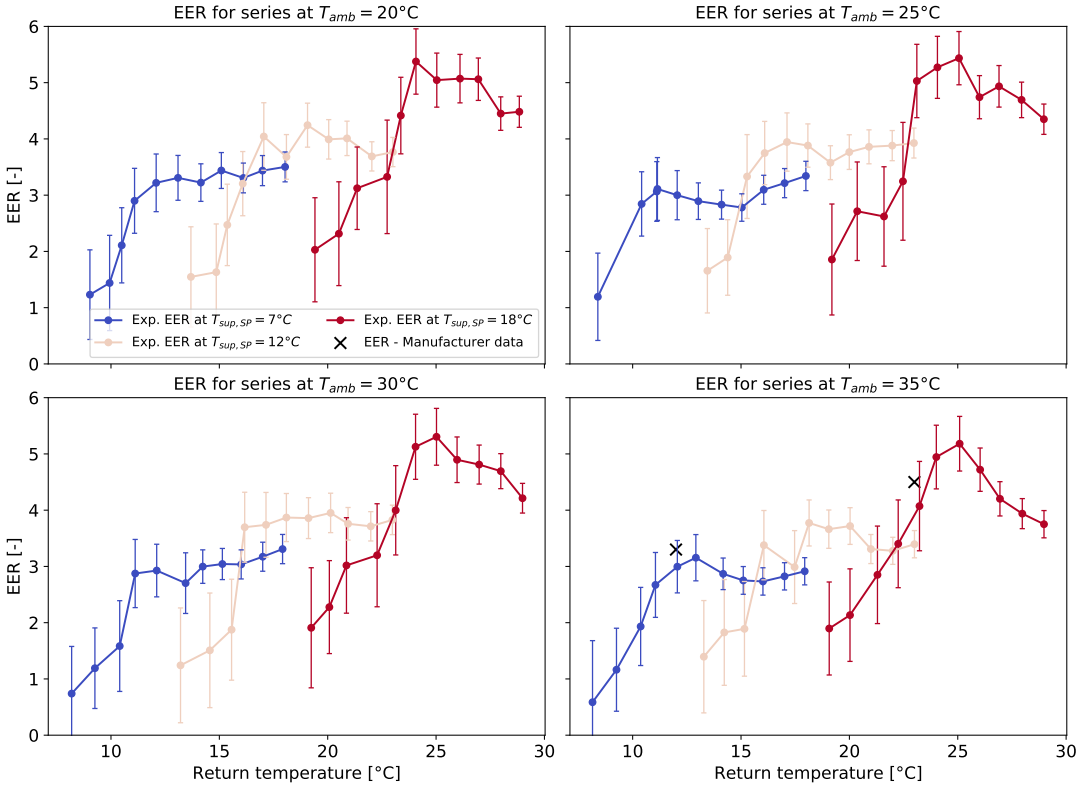

Figure III.22. EER in cooling mode in function of the supply, return and ambient temperatures.

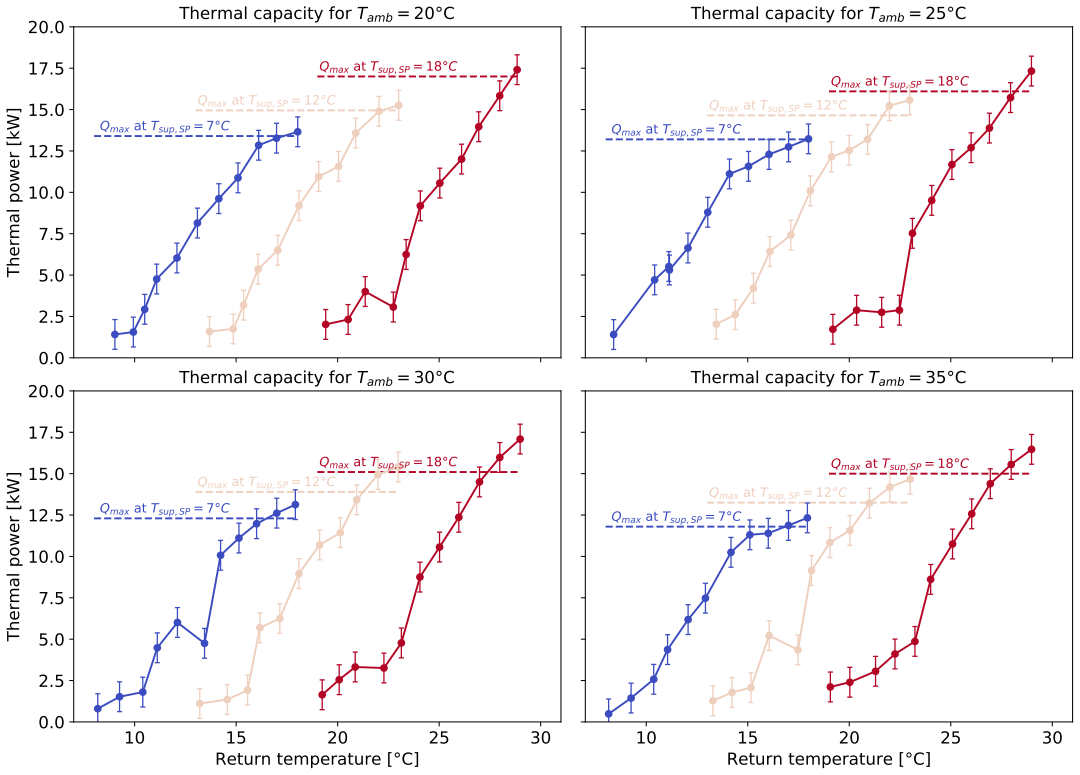

Figure III.23. Thermal capacity in cooling mode, in function of the supply, return and ambient temperatures.

degradation remains slender. The efficiency also starts at low values (below 1) when the load is low, due to the on-off cycling in such conditions. The EER then increases rapidly with the load, and reaches a maximum before to remain either constant or to decrease.

Thermal cooling capacity The thermal cooling capacity is represented in Figure III.23, with the maximum capacities declared in the catalogue plotted as colored dashed lines. In cooling mode, it was necessary to use a temperature lift of up to $\Delta T = 11$°C, since 8°C were not sufficient to reach the maximum capacity of the machine[1]. A similar linear behavior than in heating is observed, with Q_{th} being proportional to ΔT, except at low and high loads where the behavior is different. The capacity saturates at high loads with a bending of the cooling power curve, although not forming a clear plateau like in heating mode.

Compressor frequency The measured frequency of the static experimental points in cooling more is represented in Figure III.24. The compressor has an upper limit of 75 Hz in cooling (vs 90 Hz in heating mode), this limit is reached for all the experimental series, but at different moments: when ΔT reaches 11°C at $T_{sup} = 18$°C, when ΔT reaches 10°C at $T_{sup} = 12$°C and when ΔT reaches 8 or 9°C at $T_{sup} = 7$°C.

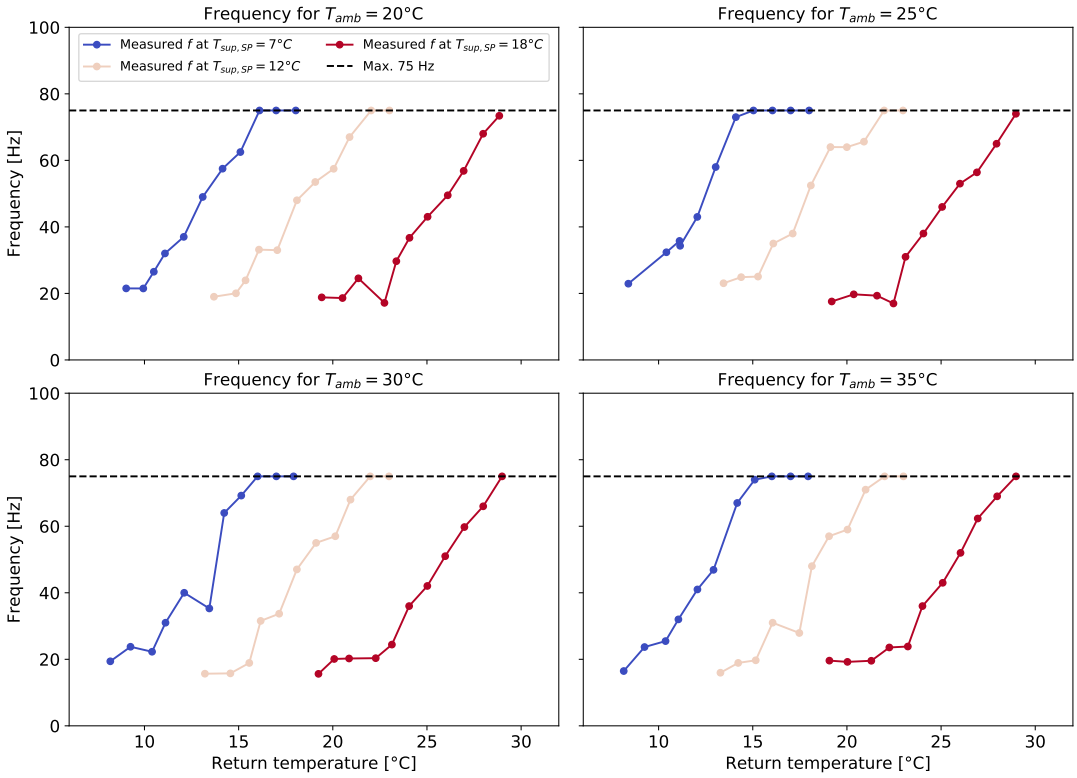

Figure III.24. Frequency in cooling mode, in function of the supply, return and ambient temperatures.

3.3 Simple black-box models of the heat pump

The experimental static tests previously described enable to have a comprehensive view of the heat pump performance in a wide range of operating conditions. Based on this performance map, black-box models can be derived, such as adequate polynomial regressions fitted using the average

[1] See also Appendix B to observe the thermal power in function of both the supply and return temperatures, in relation with the set-point $T_{sup,SP}$.

values of the different measured parameters. To characterize the performance of the system, the most interesting output is the final electricity consumption of the heat pump P_{el}, therefore we will derive models of P_{el} in function of the other parameters. Making a model of the COP instead could have been an alternative approach, as done in previous literature, however the MPC framework uses the electrical power of the heat pump in its cost function, therefore it appears more relevant to create directly a model of P_{el}. Among the other quantities that can be used as the model input parameters, the possible options are: T_{amb}, T_{sup}, T_{ret}, ΔT, $\dot{m}$, Q_{th}, CR, PLF and f. Most of these parameters are closely related to one another, therefore choosing a subset of them is sufficient for fitting an appropriate model.

The methodology for fitting a model is the following: a polynomial model structure is defined, with a certain set of coefficients. In the dataset of the experimental static tests, the points with saturation (i.e. where the frequency limit of the compressor is reached or where the set-point of T_{sup} cannot be met) are excluded, hence the model is only valid within these limits. The least square method is then used to fit the model to this restricted dataset, obtaining the optimal values of the polynomial coefficients.

If the fitted model is to be used within the MPC framework, some restrictions apply, since the model must be adapted to this specific final use. The following points must thus be considered:

- **Null consumption when the heat pump is off:** since the models are fitted only on points where the heat pump is functioning, it might happen that such models give $P_{el} \neq 0$ when $Q_{th} = 0$. The heat pump does have a residual electricity consumption when it is turned off, but it is small (around 95 W). It is preferred to approximate this standby consumption to 0 with the condition $P_{el}(Q_{th} = 0) = 0$, so that the MPC has more incentives to turn the heat pump off.
- **Parameters to include in the model:** the parameters chosen as inputs of the model must be easily accessible in the MPC framework, either as controllable inputs, as states of the building model, or as disturbance forecasts. Q_{th} is the main controllable inputs chosen in the current MPC, therefore this parameter must appear in the model. The on-off binary variables are excluded from the model since Q_{th} already contains the information of the on-off status. Additionally, the outdoor air temperature T_{amb} is included in the model (it is normally available as a weather forecast in the MPC), as well as the supply temperature T_{sup} (it can be derived from the state T_{dis}, which is the water temperature of the distribution circuit in the state-space model of the building). A different MPC framework could be envisioned, where the MPC controller can decide directly at which frequency f to operate the compressor. In such case, the heat pump model should include this parameter as an input, so as to reflect the influence of the decided control actions on the heat pump performance. However, such configuration is not possible with the chosen heat pump machine because the frequency is internally adjusted by its local controller and cannot be commanded from an external signal, therefore f is excluded from the model.
- **Linearity (or convexity):** to be used in the cost function of the MPC optimization problem, the heat pump must be represented by a convex function (with respect to the controllable variable Q_{th}), and preferably linear. This includes for example a quadratic function with a term in αQ_{th}^2 (if $\alpha > 0$). However, to limit even further the computational burden within the MPC calculation process, it is preferable to keep the heat pump model as a simple linear function.

Taking into account these constraints, the chosen model for the heat pump performance to be included in the MPC cost function is presented in Equation III.19.

$$P_{el,simpl} = [a_0 + a_1 T_{amb} + a_2 T_{sup}] \cdot Q_{th} = [1/COP\,(T_{sup}, T_{amb})] \cdot Q_{th} \tag{III.19}$$

It has the form of a polynomial in T_{sup} and T_{amb}, multiplied by the thermal capacity Q_{th}. The polynomial in fact represents the quantity 1/COP, or 1/EER in cooling mode. Models found in the literature usually represent the COP itself, since it is more easily interpretable. However, since it is the inverse of the COP that is used to obtain the electrical consumption of the heat pump, it makes more sense to directly create a model of the quantity 1/COP. Furthermore, 1/COP has a more linear behavior than the COP, which enables to fit a linear equation with lower error. This modeling strategy has not yet been found in the existing literature to the knowledge of the authors and thus constitutes a novel approach.

Most of the existing publications have developed similar models of the COP or the power P_{el}, but without the concern of the linearity. For instance in [144], Verhelst et al. derived polynomials of the COP, and includes the quantity $P_{el} = Q_{th}/COP$ in its objective function, later highlighting that the division of two optimization variables is a nonlinear operation which makes the overall optimal control problem (OCP) nonlinear. In their case, no binary variables were included in the OCP and therefore they could cope with these non-linearities in the objective function. In the case of the present thesis, with the presence of the on-off binary variables, the linearity concern becomes more imperative, and therefore the proposed 1/COP modeling constitutes the most promising approach.

It should be noted that the model of Equation III.19 does not take into account the part-load performance of the heat pump. Neither the compressor frequency f nor the capacity ratio CR at part-load are included as model parameters. The influence of the part-load operation on the performance of the heat pump will be discussed in further section 3.4.4. However, to justify this simplification, the conclusions of [144] provide interesting insights: the authors have compared a similar optimal control problem with or without including the part-load performance of the heat pump. They found that the OCP performed almost as good with or without this extra information.

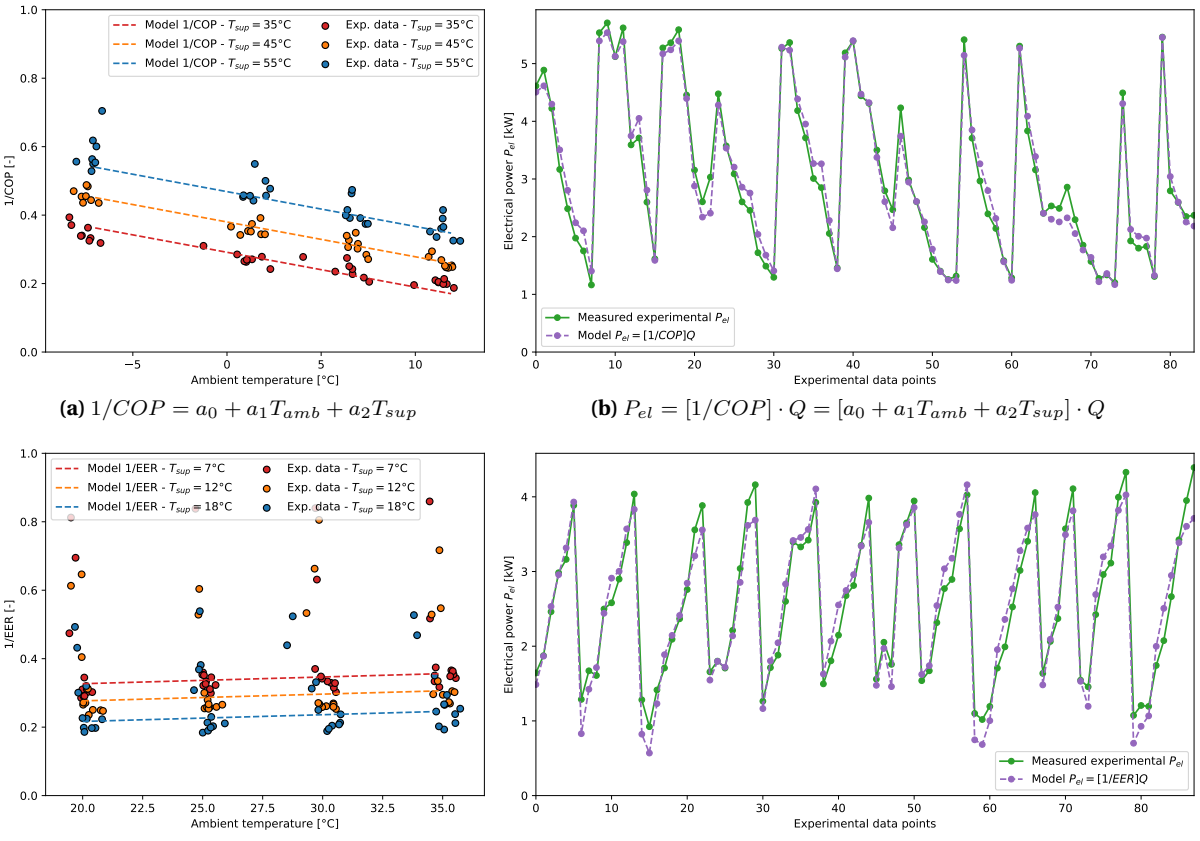

(a) $1/COP = a_0 + a_1 T_{amb} + a_2 T_{sup}$

(b) $P_{el} = [1/COP] \cdot Q = [a_0 + a_1 T_{amb} + a_2 T_{sup}] \cdot Q$

(c) $1/EER = a_0 + a_1 T_{amb} + a_2 T_{sup}$

(d) $P_{el} = [1/EER] \cdot Q = [a_0 + a_1 T_{amb} + a_2 T_{sup}] \cdot Q$

Figure III.25. Heat pump performance models based on static tests in heating mode (a)(b) and cooling mode (c)(d). Graphs (a) and (c) (left column) represent the quantities 1/COP and 1/EER respectively, in function of the ambient and supply temperatures. (b) and (d) (right column) represent the P_{el} models compared to the experimental data.

The model of Equation III.19 was fitted according to the aforementioned methodology with the static points both in heating and cooling modes. The obtained optimal values of the coefficients a_i are reported in Table III.4: with a NRMSE value of 6.44%, the heating model fits slightly better than the cooling model, which has a NRMSE of 8.76%. In Figure III.25, the models are represented along with the experimental points. On the left graphs, only the 1/COP part (or 1/EER) of the model is represented: it can clearly be observed that the hypothesis of the linear behavior is a good approximation in that case. Furthermore, the dependency of the heat pump performance with the ambient tempera-

Table III.4. Fitted coefficients and RMSEs of the heat pump performance black box models in heating and cooling modes.

Model	Mode	a_0	a_1	a_2	RMSE	NRMSE
1/COP	Heating mode	-0.01859	-0.01017	0.00886	0.1993 kW	6.44%
1/EER	Cooling mode	0.3576	0.00197	-0.01002	0.2236 kW	8.76%

ture can be appreciated: in heating mode, the curves present a clear slope, revealing that the efficiency drops (i.e. 1/COP increases) when it is colder outside. In cooling mode, the curves are almost flat, revealing that the outdoor conditions barely affect the heat pump efficiency in this configuration. This could also be observed from the coefficient a_1, associated with T_{amb} in the model, which is 5 times smaller in cooling mode than in heating mode (in absolute value). On the right graphs of Figure III.25, one can observe that the chosen models provide a satisfactory fitting over the experimental data. It should be noted that the cooling model performs slightly worse in the extreme ranges of powers, when the heat pump runs at very low or very high load, the model tends to underestimate the power consumption in both of these cases.

3.4 Modelling in TRNSYS

3.4.1 Overall detailed modeling in TRNSYS

In the co-simulation framework presented in subsection 1.1, a detailed model of the heat pump operation is needed to run the dynamic simulations. In TRNSYS, the existing models of heat pumps remain rather simple and do not capture the full dynamic behavior of heat pump systems, especially the variable speed sort. Type941 enables to reproduce an air-to-water heat pump, and resorts to a performance map of different points (usually derived from catalogue data) to determine the performance in the current conditions of the simulation, by interpolation of the existing points of the map. To the knowledge of the authors, no models of air-to-water VSHP currently exist as an available Type in TRNSYS libraries. In [145], the authors have created the new Type3254 to model a VSHP, but the considered system was air-to-air. It thus represents an opportunity to develop a similar approach for air-to-water variable speed systems, given that most heat pumps on the market are nowadays equipped with an inverter and no longer work only with on/off cycles.

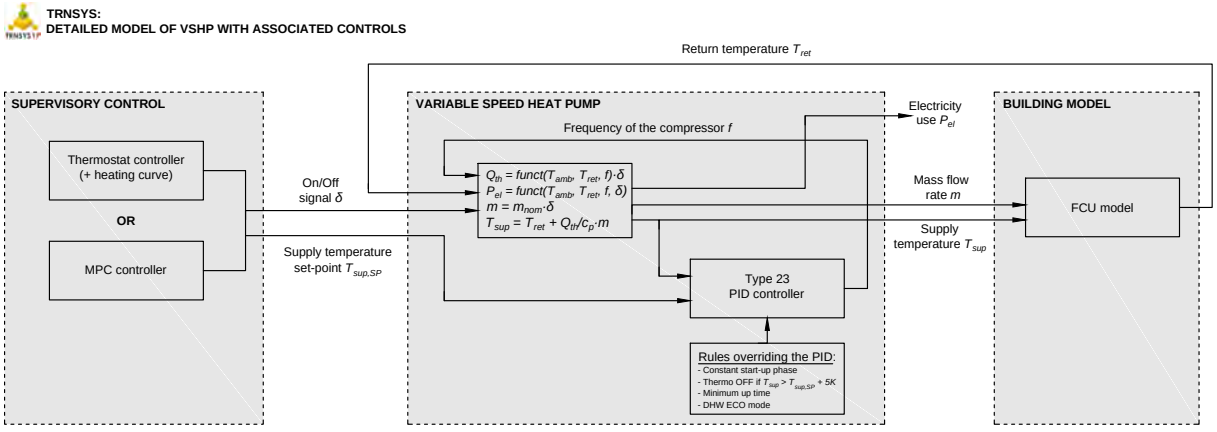

Figure III.26. Schematic of the detailed TRNSYS heat pump model.

Figure III.26 shows the principle of the adopted modeling strategy for the heat pump system. It mimics the actual operation of the heat pump, and especially the behavior of its local controller. For a standard user, this local controller normally acts as a black-box based on different rules and protections, but usually the manufacturers do not disclose any information about these rules or their parameters. Only by performing some tests or with direct information from the producer, one can guess the

rules adopted in the local controller, and try to reproduce them in the TRNSYS model. In the proposed configuration, the supervisory control sends a command of activation (on-off signal δ) and a supply temperature set-point $T_{sup,SP}$ (i.e. the supervisory control can be an RBC or MPC). The VSHP model receives these commands as well as the return temperature T_{ret} from the building FCU model. A PID controller then performs the set-point tracking on the supply temperature output, by controlling the frequency of the compressor. The performance of the heat pump is represented by two detailed black-box models of the thermal and electrical powers Q_{th} and P_{el}, which are in this case functions of the frequency f as well as the other operating conditions. Additional rules sometimes override the PID controller: these rules were determined based on observations made in the experiments, as well as from discussions with the manufacturer of the chosen heat pump. In the proposed approach, the frequency of the compressor is thus an actual visible variable[1], and it enables to reproduce the behavior of the heat pump with higher accuracy, since the output of a heat pump mostly depends on how fast the compressor is running. When this parameter did not exist as a variable within the formulation, as in the previous simpler models, this high accuracy could not be reached. After calculation, the overall VSHP model sends the actual supply temperature T_{sup} and the mass flow rate $\dot{m}$ to the model of the emission system, FCU in this case.

3.4.2 Detailed black-box polynomial models

The detailed black box models used in the TRNSYS VSHP framework are detailed in this section. The methodology is the same than in subsection 3.3, except that the restrictions due to the MPC no longer apply. For this reason, there are no constraints of linearity, the compressor frequency f can be integrated as an input to the model, and the model can give $P_{el} \neq 0$ when $f = 0$ (the heat pump can be "shut down" by other means in TRNSYS, like binary variables). The equations thus can present a higher degree of complexity, notably with quadratic and bilinear terms. The chosen polynomial functions, partially inspired from [144], are presented in equations III.20 and III.21. The coefficients were fitted on the experimental static points data: only the points without switching off of the compressor were considered to fit the $Q_{th,det}$ model, since the model will then switch the compressor on or off afterwards, while all the points were considered to fit the $P_{el,det}$ model, in order to still take into account the lower efficiency due to the on-off operation.

The obtained values and fitting results are presented in Table III.5, while Figure III.27 and Figure III.28 displays the models versus the experimental data points. Given the higher complexity of the detailed equations, a better fitting is obtained compared to the simple black-box models, especially concerning the electrical power P_{el}: its NRMSE decreased from 6.44% to 1.95% in heating, and from 8.76% to 2.72% in cooling. The curve of this model overlaps almost perfectly with the experimental data. The thermal power model displays a similar fitting, with satisfactory NRMSE values of 2.54% and 2.42% in heating and cooling respectively. It should be noted that the P_{el} model fits better than the Q_{th} model: this is due to the fact that the frequency of the compressor (a parameter of the model) is directly correlated with the electrical consumption of the heat pump, since the compressor represents

[1] An alternative approach was also developed, using the capacity ratio CR instead of the frequency as the variable regulated by the PID. This approach was used in [60], but not in the present thesis, therefore it is presented in Appendix C. In that alternative approach, the part-load performance characterization shown in subsubsection 3.4.4 is used as an input.

Table III.5. Fitted coefficients of the detailed heat pump polynomial models.

Coefficients of the thermal capacity Q_{th} model										
Mode	a_0	a_1	a_2	a_3	a_4	a_5	a_6	a_7	RMSE	NRMSE
Heat	2.04	9.19e2	-6.64e-2	1.94e-1	-3.57e-4	6.75e-4	2.13e-3	5.43e-5	0.267 kW	2.54%
Cool	-4.72	2.82e-3	1.36e-1	2.60e-1	-1.23e-3	1.25e-3	-1.07e-3	3.09e-3	0.256 kW	2.42%
Coefficients of the electrical power P_{el} model										
Mode	b_0	b_1	b_2	b_3	b_4	b_5	b_6	b_7	RMSE	NRMSE
Heat	-0.50	-4.21e-3	1.43e-2	1.42e-2	1.66e-4	2.44e-4	-1.01e-4	8.40e-4	0.0719 kW	1.95%
Cool	0.94	-1.59e-2	-2.34e-2	2.06e-2	2.71e-4	5.79e-4	2.45e-4	1.02e-4	0.0593 kW	2.72%

almost the entire electrical consumption of the system.

$$Q_{th,det} = a_0 + a_1 T_{amb} + a_2 T_{ret} + a_3 f + a_4 f^2 + a_5 T_{amb} T_{ret} + a_6 T_{amb} f + a_7 T_{ret} f \tag{III.20}$$

$$P_{el,det} = b_0 + b_1 T_{amb} + b_2 T_{ret} + b_3 f + b_4 f^2 + b_5 T_{amb} T_{ret} + b_6 T_{amb} f + b_7 T_{ret} f \tag{III.21}$$

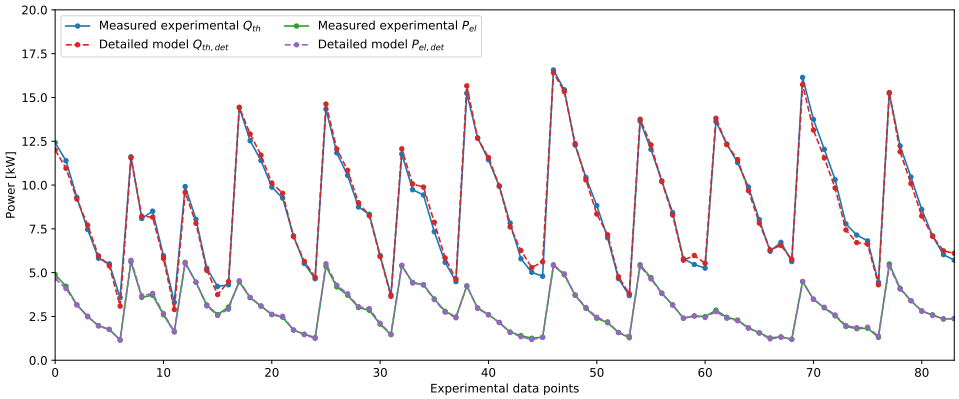

Figure III.27. Detailed Q_{th} and P_{el} models represented with the experimental data points, in heating mode.

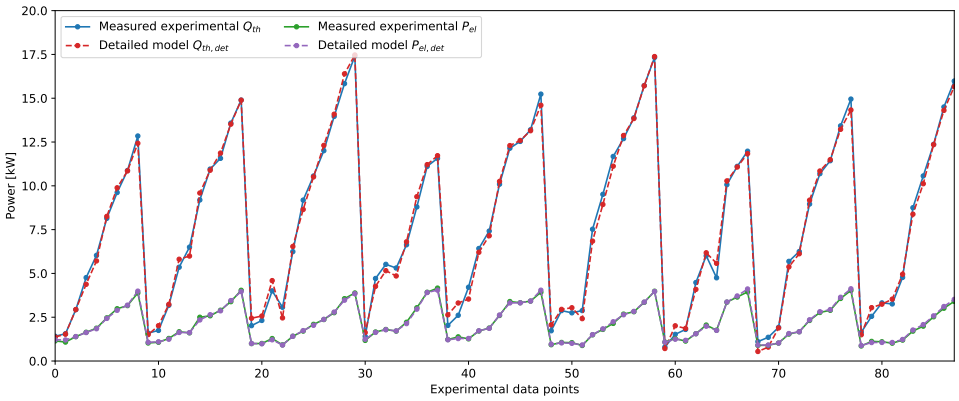

Figure III.28. Detailed Q_{th} and P_{el} models represented with the experimental data points, in cooling mode.

3.4.3 Tuning and performance of the detailed heat pump model

Once the detailed black-box models have been implemented, the local controller of the VSHP model in TRNSYS must be tuned appropriately. In particular, the values of the PID parameters must be adjusted so as to fit as good as possible with the dynamics observed in the experiments. The tuning methodology is explained in the following paragraphs.

Dataset used for the fitting process The PID values were fitted using an experimental dataset of the real heat pump operation. The dataset produced for the static tests was utilized for this purpose, however in this case all the transient phases were kept, as they reveal the reaction of the controller to changes in the inputs or in the set-point. This dataset contains regular changes of the T_{sup} set-point in the forms of steps, as well as regular steps of the input return temperature T_{ret}. The TRNSYS heat pump model is provided with the time series of the ambient temperature T_{amb} and the return temperature T_{ret} observed in the experimental tests, and tries to reproduce the same supply temperature T_{sup} by choosing the frequency f. The PID values must be adjusted so that the profiles of the frequency f,

temperature T_{sup}, powers Q_{th} and P_{el} match with the experimental measurement. The piece of the dataset chosen[1] lasts 4 hours, with time steps of 1 minute, as in the TRNSYS model.

Methodology To find the best PID parameters, a great number of simulations was run using the MOBO tool [146] with a brute-force algorithm. The gain constant K_p was varied between 1 and 10, and the integral time t_i between 0.005 and 0.2 h. The derivative time constant t_d was set to 0, as changing its value did not have an influence on the results, therefore it is in fact a PI controller. For each simulation, the RMSE of the frequency f was archived, because it is the output of the PID controller. The configuration with the minimal RMSE was chosen eventually.

Scope and limitations The tuning of the PID presents some limitations. In fact, the real heat pump does not operate with a PID controller, instead it updates the frequency of the compressor every minute following a set of rules of the form: `if` $T_{sup,SP} - T_{sup} > XX°C$ `then` $f = f + YY$ Hz. It was considered that these rules are highly specific to the chosen heat pump machine, therefore the PID modelling approach was chosen instead, as it represents a more general and common control approach. Furthermore, the behavior of the rules is very similar to a PID controller, as will be seen in the fitting results. The overall heat pump model was developed here in TRNSYS, but could be translated easily to other dynamic simulation tools, as polynomial functions and PID controllers are very usual components available in all software such as Modelica, EnergyPlus etc. However, the values of the PID parameters might need an adjustment if used in a different context, since a PID controller in TRNSYS with a 1 minute sampling time step does not necessarily correspond to the same values for a real PID controller, which would have a much smaller sampling time closer to real time.

Results of the tuning The best values for the PID parameters were $K_p = 3$ and $t_i = 0.025$ h. The profiles of temperatures, powers and frequency are represented in Figure III.29 for this configuration. The evolution of the compressor frequency is well reproduced by the controller, and thus all the simulated profiles match satisfactorily with the experimental data. The integrated values are also close: in the experiment, the heat pump delivered 54.1 kWh, and the simulation gives 53.2 kWh (-1.8% difference). On the other hand, the model slightly overestimates the electrical energy use: in the experiment, the heat pump used 18.8 kWh, while the model simulated an energy use of 20.3 kWh (+7.1 % difference). In cooling mode, the PID gain is negative ($K_p = -3$) and the model fits more neatly, as shown in Figure III.30. The model gives a fair representation of the electricity use, with 6.72 kWh simulated, a variation of -0.74% compared to the 6.77 kWh measured with the real heat pump. The thermal energy delivered is slightly overestimated, with 21.5 kWh simulated, a variation of +2.6% compared to the 21.0 kWh measured experimentally.

Additional control rules Additional rules override the decisions of the PID controller in some cases. The rules implemented follow the behavior observed experimentally or mentioned by the heat pump manufacturer:

- the compressor starts at a middle level of frequency (50 Hz) during 3 minutes, to reach stability in the system, and then starts to modulate with the PID controller,
- if the compressor switches off because of the low load, it must remain switched off for a minimum of 3 minutes (minimum down time),
- if the supply temperature reaches its set-point $T_{sup,SP} + 5$°C, the compressor is automatically shut down,

[1] A longer fragment of the dataset could have been used. However, since the model has no inertia contrary to the experimental setup, the periods of the dataset where T_{ret} was too close to T_{sup} were discarded: in such cases, the heat pump controller decisions also have an influence on the return temperature T_{ret} because of the on-off operation and the fact that the control of the thermal bench return loop is not perfect. We are not able to reproduce this behavior in the model without adding the inertia and connecting the supply and the return circuits, therefore it was preferred to keep only the periods where T_{ret} is more constant, to not disturb the identification process.

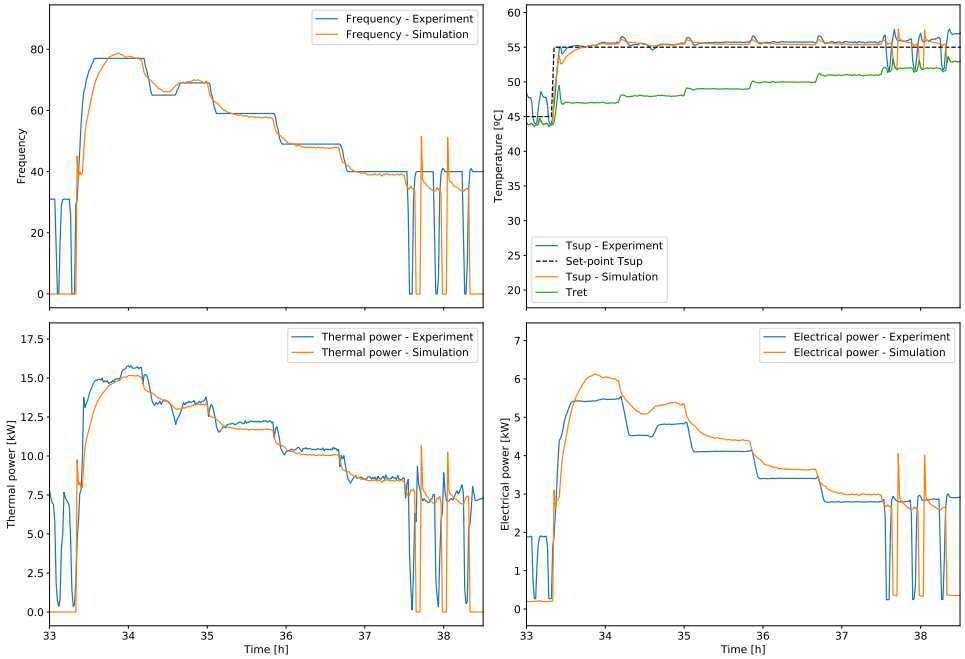

Figure III.29. Comparison between the experimental data with the real heat pump, and the simulation with the detailed HP in TRNSYS, in heating mode.

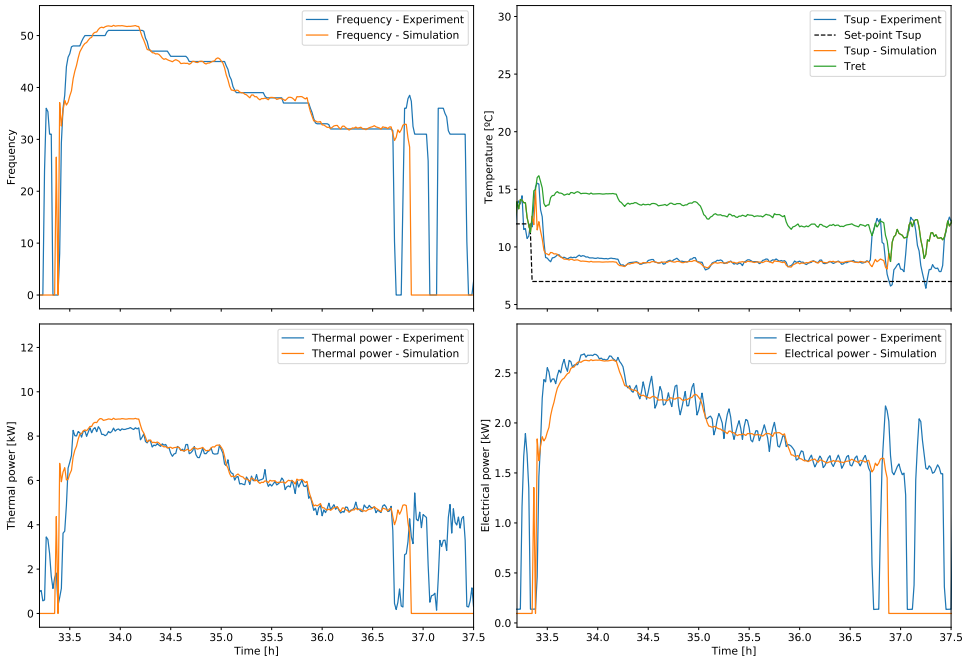

Figure III.30. Comparison between the experimental data with the real heat pump, and the simulation with the detailed HP in TRNSYS, in cooling mode.

- the reading of the T_{sup} temperature sensor was corrected by -0.4 K (-1.7 K in cooling), as this is the average offset observed between the heat pump internal data and the laboratory measurements.

- ECO mode for DHW: the frequency is limited to 40 Hz during the DHW charging, if this mode is activated.

3.4.4 Part-load performance characterization

Another interesting approach to characterize the heat pump consists in observing the variation of its efficiency at part-load. This is characteristic of variable-speed systems, able to modulate their output to run at a lower load without entering in on-off operation. Such characterization is useful for the alternative modeling approach presented in Appendix C, but also provides interesting insights in itself about the functioning of the heat pump. The characterization takes the form of a curve showing the change of performance at part-load, hence linking the part-load performance PLF with the capacity ratio CR. For VSHP systems, this relationship is not straightforward, and therefore it is explained here in details how such curve was obtained.

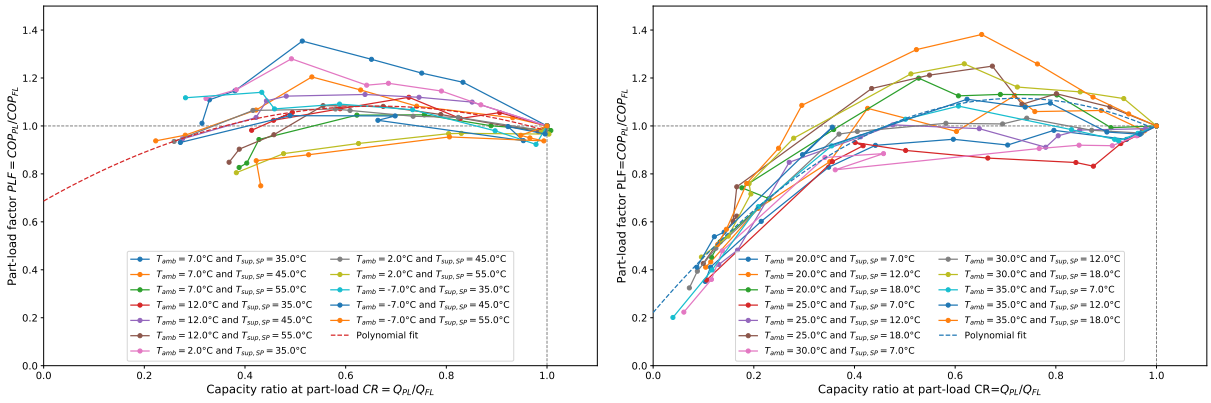

(a) **(b)**

Figure III.31. Experimental series of curves PLF=f(CR) in (a) heating and (b) cooling mode.

Figure III.31 shows the experimental values of the PLF / CR relation (taken from the static points data); all series clustered by values of $T_{sup,SP}$ and T_{amb} are represented independently. Hence for each curve, we first fix $T_{sup,SP}$ and T_{amb}, and consider the capacity of the heat pump at full load $Q_{th,FL}$ in these specific conditions, as well as the COP at full load COP_{FL}. This point is thus chosen as the reference for these fixed conditions, therefore both its PLF and its CR are equal to 1 ($CR = Q_{th,FL}/Q_{th,FL}$ and $PLF = COP_{FL}/COP_{FL}$). Then the load is being reduced, with lower values of thermal power: we can then calculate $CR = Q_{th}/Q_{th,FL}$ and $PLF = COP/COP_{FL}$ for every part load conditions, but still with $T_{sup,SP}$ and T_{amb} fixed. The reference point at full load therefore changes for each curve. To use these curves, it is thus necessary to know beforehand the full-load capacity in the current conditions (for instance using catalogue data or the relations developed later in Equation IV.16).

A quadratic function is then fitted to these experimental curves and additionally represented in the figure. As expected, when the load decreases, the efficiency of the system increases: this is characteristic of variable speed heat pumps. However, the increase is relatively small, since the PLF reaches only maximum values of 1.15 for the quadratic curve (1.4 in all the data). For low values of CR, the efficiency decreases rapidly since the heat pump enters in on-off operation, which degrades its COP.

The experimental curves of PLF in function of CR can be compared with other models found in the literature or derived from catalogue data, as shown in Figure III.32. The obtained quadratic fits are represented in red and blue for heating and cooling respectively. For reference, some models mentioned in [147] are plotted (straight dashed lines with the slopes mentioned in that article). Although these apply to water-to-water heat pumps, no other PLF/CR relations were found in the literature for air-to-water heat pumps. On the other hand, the green curve was created using the part-load data available in the datasheet of the manufacturer (some points at part-load in heating mode following standard EN 14825 [143]). The method used to obtained this curve was detailed in [60]. A large discrepancy is observed with the experimental curves. This is due to a different understanding of the notion of "part-load" in the standards and in dynamic simulations like TRNSYS. In TRNSYS, part-load simply refers to the machine itself, and how much it is producing relatively to its maximum capacity. In the standard EN 14825, part load refers to the overall system, hence including both the heat pump and the building load itself: therefore, this definition links the modulation of the machine with the

outdoor conditions (which define the load of the building). To explain this difference, an example is described hereafter: let us consider full load conditions (100%) of 10 kW thermal for a temperature of $T_{amb} = -10$°C. Per the definitions of the standard, a 30% load (CR=0.3) will for instance occur at $T_{amb} = +10$°C, hence the efficiency of the heat pump will obviously increase since the outdoor air is warmer. There is thus a inherent link between the CR and T_{amb}. This explains the high values of PLF (up to 2) in the green curve. On the other hand, as per the definitions of CR in TRNSYS, a 30% load can also occur at the same outdoor temperature $T_{amb} = -10$°C, if we only consider the machine.

This distinction is quite important when heat pumps are used in predictive control frameworks such as MPC. An MPC controller has the proper characteristic to operate the heat pump in an optimal way, but not necessarily following the normal "building load" corresponding to the current outdoor conditions. For instance, it might want to overheat the building just before a price increase, running the heat pump at 100% for a short period, while the outdoor temperature is mild and would normally require an operation of the heat pump at only 30%. For this reason, the PLF/CR curves obtained experimentally are more interesting to use for such applications.

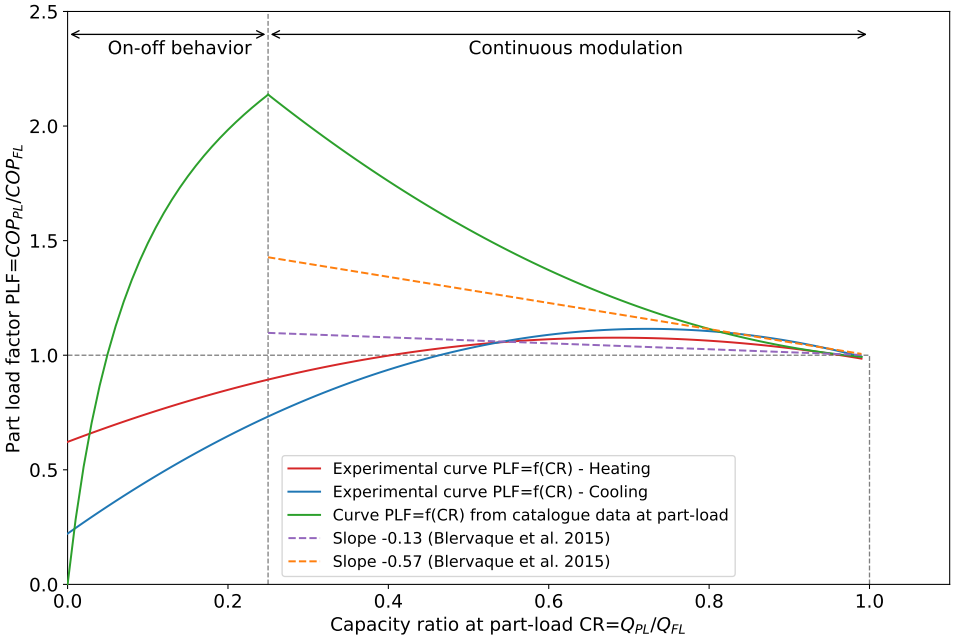

Figure III.32. Comparison of different models of PLF=f(CR) curves.

4 Using and modeling buildings as thermal energy storage

4.1 Residential building study case: white-box model

The present study focuses on the Mediterranean climate and the residential buildings constructed in this zone. They present the characteristics of having relatively balanced heating and cooling loads in winter and summer. Therefore such buildings can be used for demand response in both seasons. However, despite the great amount of literature on MPC and building energy flexibility published in the recent years, few studies have focused on cooling applications, and even less on study cases that make use of flexibility in both seasons [50]. Given this state of the art, the authors have deemed worthy to investigate in more details the potential of energy flexibility of Mediterranean buildings.

A typical block of flats of the region of Catalonia in Spain was chosen as a case study to analyze the benefits of the different control strategies. In particular, one flat situated on the first floor is studied in details. The apartment, where lives a family of four, comprises 4 bedrooms, a living room, kitchen and bathroom for a total surface of 110 m^2. The external walls contain 12 cm of insulation which represents a high insulation level for the Spanish climate. The HVAC systems comprise the air-to-water heat pump which provides heating or cooling to the Fan-Coil Units (FCU) situated in the rooms. The heat pump also contains an integrated 200 liters tank for storing DHW. The apartment is simulated in TRNSYS, with a detailed model that was previously validated with experimental metered data [148], [149]. This detailed model runs with a time step of 1 minute, enabling to capture short-term variations with sufficient accuracy. The main parameters of the building are summarized in Table III.6, and the building is represented in Figure III.33.

It should be noted that the detailed modeling of the building did not belong to the work of this thesis, an existing model was used and modified for this purpose. The building envelope, infiltration and occupancy were not changed from the original version of the TRNSYS model, and taken as is. Mostly the part of the HVAC systems has been modified, with the detailed heat pump model, the FCU, the distribution circuit and the tank.

Figure III.33. Sketch and photograph of the building.

Table III.6. Main parameters of the chosen building study case.

Parameter	Unit	Value
Location	-	Spain
Building date	-	1991-2007
Floor area	m^2	108.5
Window area	m^2	19.6
Protected volume	m^3	263.6
U-value walls	W/m^{2}K	0.2
U-value windows	W/m^{2}K	2.5 to 5.7
g-value windows		0.5 to 0.76
Infiltration n_{50}	h^{-1}	3
Emission system	-	Fan-coil units

4.2 Simplified modeling through thermal RC networks

4.2.1 RC model structure

For reasons of computation effort, simplified and linear models are necessary in the MPC framework to predict the dynamic behavior of the building [150]. A state-space model of the building study case was thus developed and identified through grey-box modeling techniques. The structure represented in Figure III.34 was chosen, with four temperature states $x = [T_{int}\ T_w\ T_{dis}\ T_{TES}]^T$: the indoor temperature, an intermediate temperature at the inside surface of the walls, the water temperature of the distribution circuit, and the average water tank temperature. It should be emphasized that such simplified models are developed only for control purposes, and not for matching exactly with the real building structure, therefore the level of details is kept to a minimum. Such simple models are broadly

used for similar applications, like for example in the thesis of Benedetelli on MPC [151].

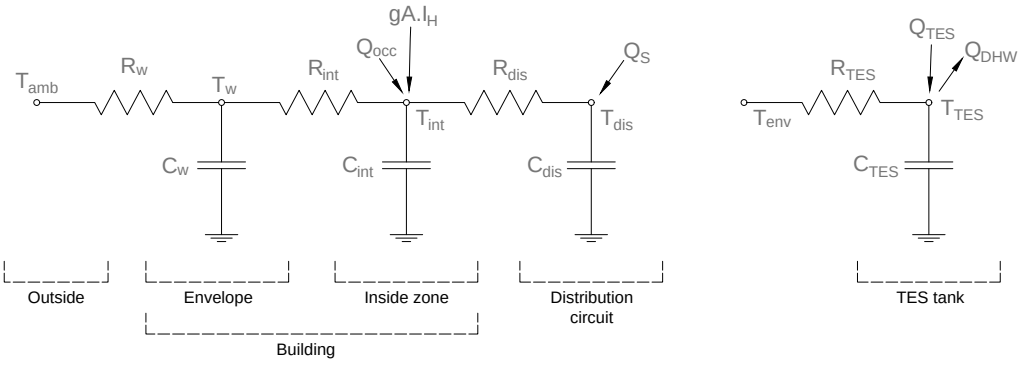

Figure III.34. RC model representation.

4.2.2 Description of the model states and parameters

The first state T_{int} lumps all the rooms of the apartment into one single operative temperature state, which is sufficient for MPC applications as shown for example in [152]. Its associated capacity C_{int} mostly represents the heat capacity of the air, furniture and internal partitions present within the entire inside zone, and considered as a single body [153], [154]. Lumping these elements of different thermal capacities into the single parameter C_{int} represents an important simplification, however the purpose of the simplified model is only to provide a general prediction of the building dynamics for the controller, and in this scope such assumption is valid, even if the physical phenomena are not represented in the most accurate manner. External heat inputs enter the building at the level of the state T_{int}: the heat naturally emitted by the occupants and the equipment Q_{occ}, the heat gains due to the ground horizontal solar irradiation I_H (buffered by the aperture area coefficient gA) and the heat coming from the heat pump through the distribution system. The differential equation governing the behavior or the state T_{int} is presented in Equation III.22.

$$C_{int} \cdot \dot{T}_{int} = \frac{1}{R_{int}} (T_w - T_{int}) + \frac{1}{R_{dis}} (T_{dis} - T_{int}) + gA \cdot I_H + Q_{occ} \tag{III.22}$$

The second state T_w represents an intermediate temperature at the surface of the external walls, and its associated capacity C_w covers the heat capacity of the massive walls. T_w is linked with the outside temperature T_{amb} through the resistance of the walls R_w. The different dynamics of the two states T_{int} and T_w are therefore both captured by this type of model. A first order model lumping all the thermal capacitances into a single parameter would not have been able to capture both the fast dynamics of the indoor zone and the slower dynamics of the massive structural elements. On the other hand, a third order model with an additional capacity accounting for internal walls and/or furniture could represent an alternative modeling approach, but adding unknown parameters increases the complexity of the obtained model and of the identification process. The second order modeling approach presented here (e.g. for the building part of the model) is thus considered sufficient for MPC applications [154], and was used in many previous works as shown in the introductory review of [155]. The differential equation governing the behavior or the state T_w is presented in Equation III.23.

$$C_w \cdot \dot{T}_w = \frac{1}{R_{int}} (T_{int} - T_w) + \frac{1}{R_w} (T_{amb} - T_w) \tag{III.23}$$

Apart from the two states of the building part of the model, an additional third state T_{dis} accounts for the distribution system (pipes and fan coil units). It acts as a small buffer between the heat pump output and the building zone, and enables to reproduce the inertia of this water circuit. The associated capacity C_{dis} represents the thermal capacity of the water contained in the pipes (around 40 liters), while the resistance R_{int} models the heat transfer of the FCU between the water circuit and the

indoor air. The distribution circuit receives directly the heat input from the heat pump Q_S (negative in case of cooling). The differential equation governing the behavior or the state T_{dis} is presented in Equation III.24.

$$C_{dis} \cdot \dot{T}_{dis} = \frac{1}{R_{dis}} (T_{int} - T_{dis}) + Q_S \tag{III.24}$$

Finally, the DHW tank constitutes the fourth state T_{TES}, which represents the average water temperature of the tank under a fully mixed tank assumption. The capacity C_{TES} covers the heat capacity of the 200 liters of water and the resistance R_{TES} takes into account the insulation of the tank. The DHW tank is charged through the heat Q_{TES} (positive term) coming from the heat pump circuit, and discharged with the heat tapped by the occupants Q_{DHW} (negative term, which follows the deterministic tapping program L from the standard [123]). Despite its insulation, the tank loses heat to its surrounding environment T_{env}. This environment temperature could differ according to the cases: if the DHW tank was placed in the conditioned space, for instance in the kitchen or the bathroom, then $T_{env} = T_{int}$, or if it was placed outside, then $T_{env} = T_{amb}$. In the present case, we consider that the tank is placed in a non-conditioned space like a utility room, basement or balcony, which temperature is approximated by $T_{env} = (T_{int} + T_{amb})/2$. The differential equation governing the behavior or the state T_{TES} is presented in Equation III.25.

$$C_{TES} \cdot \dot{T}_{TES} = \frac{1}{R_{TES}} (T_{env} - T_{TES}) + Q_{TES} - Q_{DHW} \qquad \text{with} \quad T_{env} = \frac{T_{int} + T_{amb}}{2} \tag{III.25}$$

4.2.3 State-space matrix format

To conform to the state-space model format, the model takes the form of Equation III.26, which stems from joining the differential equations III.22 to III.25 into a single system. For clarity, the matrix B is separated into B_u, which corresponds to the controllable inputs $u = [\,Q_S\ Q_{TES}\,]^T$, and B_e which corresponds to the exogenous, non-controllable inputs $e = [\,T_{amb}\ I_H\ Q_{occ}\ Q_{DHW}\,]^T$, also called disturbances. The considered relevant outputs are $y = [\,T_{int}\ T_{dis}\ T_{TES}\,]^T$, hence discarding the wall temperature T_w. The matrices and vectors forming the state-space model are described in equations III.27 to III.30.

$$\begin{cases} \dot{x} = A \cdot x + B_u \cdot u + B_e \cdot e \\ y = C \cdot x \end{cases} \tag{III.26}$$

With:

$$A = \begin{bmatrix} -\frac{1}{R_{int}C_{int}} - \frac{1}{R_{dis}C_{int}} & \frac{1}{R_{int}C_{int}} & \frac{1}{R_{dis}C_{int}} & 0 \\ \frac{1}{R_{int}C_w} & -\frac{1}{R_wC_w} - \frac{1}{R_{int}C_w} & 0 & 0 \\ \frac{1}{R_{dis}C_{dis}} & 0 & -\frac{1}{R_{dis}C_{dis}} & 0 \\ \frac{1}{2R_{TES}C_{TES}} & 0 & 0 & -\frac{1}{R_{TES}C_{TES}} \end{bmatrix} \quad \text{and} \quad x = \begin{bmatrix} T_{int} \\ T_w \\ T_{dis} \\ T_{TES} \end{bmatrix} \tag{III.27}$$

$$B_u = \begin{bmatrix} 0 & 0 \\ 0 & 0 \\ \frac{1}{C_{dis}} & 0 \\ 0 & \frac{1}{C_{TES}} \end{bmatrix} \quad \text{and} \quad u = \begin{bmatrix} Q_S \\ Q_{TES} \end{bmatrix} \tag{III.28}$$

$$B_e = \begin{bmatrix} 0 & \frac{gA}{C_{int}} & \frac{1}{C_{int}} & 0 \\ \frac{1}{R_w C_w} & 0 & 0 & 0 \\ 0 & 0 & 0 & 0 \\ \frac{1}{2R_{TES}C_{TES}} & 0 & 0 & -\frac{1}{C_{TES}} \end{bmatrix} \quad \text{and} \quad e = \begin{bmatrix} T_{amb} \\ I_H \\ Q_{occ} \\ Q_{DHW} \end{bmatrix} \tag{III.29}$$

$$C = \begin{bmatrix} 1 & 0 & 0 & 0 \\ 0 & 0 & 1 & 0 \\ 0 & 0 & 0 & 1 \end{bmatrix} \quad \text{and} \quad y = \begin{bmatrix} T_{int} \\ T_{dis} \\ T_{TES} \end{bmatrix} \tag{III.30}$$

This state space model is derived from the differential equations and thus has a continuous form. In the MPC scheme, the model must be discretized with the sampling time t_s, using the formulas of Equation III.31 and leading to the discrete state space model of Equation III.32. The transformed discrete matrices here have a superscript d to differentiate from their continuous form. However in the remaining of the thesis and to lighten the notation, we only use the general notation A, B, C without the superscript, assuming that the matrices have their discrete form in a discrete context and their continuous form in a continuous context. The choice of the discretization time step is further discussed in subsection 2.6 of chapter IV; the value of $t_s = 15$ minutes is chosen as a general rule.

$$A^d = e^{At_s}, \quad B^d = \left(\int_{t=0}^{t_s} e^{At} dt \right) B = A^{-1}(A^d - I)B, \quad \text{and} \quad C^d = C \tag{III.31}$$

$$\begin{cases} x(k+1) = A^d \cdot x(k) + B_u^d \cdot u(k) + B_e^d \cdot e(k) \\ y(k+1) = C^d \cdot x(k) \end{cases} \tag{III.32}$$

4.2.4 Parameter identification for the building part

The building part of this RC model was identified with data generated by the detailed model created and previously validated in TRNSYS [148]. The parameters to be identified were R_{int}, C_{int}, R_w, C_w and gA. The inputs were the outdoor temperature T_{amb}, the ground horizontal solar irradiation I_H and the total heat provided to the indoor zone $Q_{occ} + Q_S$. In order to have enough dynamic content in the generated data, the building model was excited following a Pseudo Random Binary Signal (PRBS) of the heating Q_S, similarly to the methodology described in [102] and the guidelines of the IEA EBC Annex 68 [156]. The PRBS contains on-off cycles at different frequencies so that both the fast and slow responses of the building are captured in the data, making the identification of the parameters easier and more reliable. Finally, the observation measurements consisted of the temperatures of the states T_{int} and T_w. The model identification was realized with the system identification toolbox of MATLAB [157] ("greyest" method which uses Gauss Newton least square search), and the data generated covered 1400 hours, with time steps of 3 minutes. The results for heating season are presented in Figure III.35 and Table III.7 (first row). The obtained fit reached 82.3%, which is satisfactory considering the low order of the simplified model.

The RC model preserves a certain structure which can be interpreted physically, therefore the resistance and capacity values can be compared to an order of magnitude expected for these parameters. Since a lot of smaller parameters are lumped into a limited number of R and C values (4 in this case), it can still result a difficult task to find suitable comparisons. Furthermore, the virtual intermediate state T_w can "move" within the thickness of the wall, which would modify the balance between the inside zone values (indexed int) and the wall values (indexed w). However, the overall resistance $R_{int} + R_w$ and the overall capacity $C_{int} + C_w$ should remain approximately at the same level. In the present case, the RC model gives $R_{int} + R_w = 10.1$ K/kW. When considering the resistance of the materials in all individual layers of the external walls, a parallel calculation gives $R_{eq} = 11.5$ K/kW, which is relatively

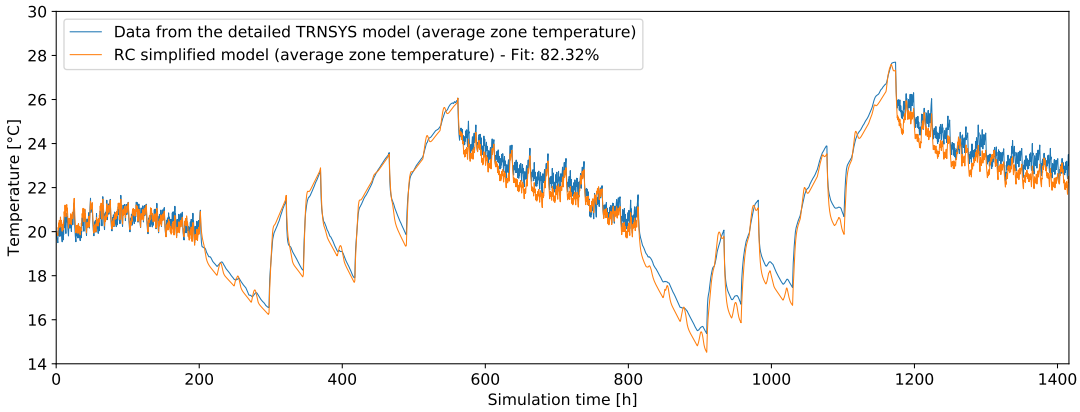

Figure III.35. Representation of the data (generated by a detailed model in TRNSYS) and the fitted RC model in heating mode.

close. For the capacities, we obtain $C_{int} + C_w = 26.0$ kWh/K. Summing all the capacities of the materials in the building gives $C_{eq} = 41$ kWh/K. However, only a part of the external walls mass is activated by the heating of the room (mostly until the insulation layer), the most external layers not being affected by a change of the indoor air temperature [153]. This concept is known as the effective capacity C_{eff}, and is calculated as a portion of C_{eq}. The ratio can vary in a great range and is not known precisely; values ranging from 1/2 to 1/3 are for example mentioned in [158]. Applying this rule to the present case $C_{eff} = 1/3 \cdot C_{eq} = 13.7$ kWh/K, which should be compared to 26.0 kWh/K. A discrepancy is observed, in fact the ratio in the present case is closer to 2/3: $C_{int} + C_w = 0.63 \cdot C_{eq}$. Since there does not exist any agreement in the literature about the calculation of the effective capacity, it is preferred to keep the values originating from the model identification process, given that they offer a good fit with the data, and that the primary goal of the model consists in predicting well rather than being physically meaningful. Furthermore, the balance between the wall and the inside zone values is conserved with the obtained values of R and C: R_w and C_w are much greater than R_{int} and C_{int} respectively, which is expected since the massive walls have a higher resistance and capacity than the air of the inside zone.

Table III.7. Parameters of the building RC model for heating and cooling.

Coefficient	$\mathbf{R_{int}}$	$\mathbf{R_w}$	$\mathbf{C_{int}}$	$\mathbf{C_w}$	**gA**
Unit	**K/kW**	**K/kW**	**kWh/K**	**kWh/K**	$\mathbf{m^2}$
Value (heating)	1.089	9.013	1.771	24.22	1.948
Value (cooling)	0.286	9.404	1.771	45.65	1.558

Theoretically, the values of resistances and capacities obtained in the heating case should also be valid for the cooling case, since they are intrinsic parameters of the building. However, they are subject to changes, for instance the thermal resistance or capacity of a material depend on its temperature, therefore the situation varies with the different boundary conditions in winter and summer. This is especially true for the aperture area gA, which represents the proportion of the outside solar irradiation entering the building, since the sun angle changes significantly between seasons. It can be observed in Figure III.36 that keeping the same parameters results in a poor model fit (38.5%) and the apparition of temperature peaks in the cooling season. It is assumed that another form of reduced-order model might be better suited for the cooling season, for instance differentiating the incoming solar irradiation from every façade instead of only considering one horizontal solar irradiation as the exogenous input. This would probably improve the model in cooling mode, since the solar gains have more importance in the summer period, with regards to the cooling demand. However this would also increase the number of parameters and complicate the identification process, therefore the same model structure than for heating is kept.

Even though the structure of the model is maintained, the model identification process is repeated in the cooling mode, so as to obtain a new set of the R and C parameter values that suits better the

summer period. This illustrates the limits of using simplified models. The methodology remains the same however: the building is virtually excited with a PRBS signal on the cooling parameter Q_S, which is negative in this case. The parameters obtained for the heating case are used as initial values of this identification process. The obtained values of the parameters for cooling are presented in the second row of Table III.7. The simulation results of this model are compared in Figure III.36 with the original TRNSYS model and with the simulation results the heating RC model would have given in the cooling scenario. The total resistance of the model $R_{int} + R_w = 9.69$ K/kW stays stable compared to the heating case (10.1 K/kW), although the internal resistance has decreased. On the other hand, the total capacity increases to $C_{int} + C_w = 47.4$ kWh/K (compared to 26.0 kWh/K in heating). One possible explanation resides in the fact that in reality, the solar irradiation also hits the wall directly (and thus affects the intermediate state T_w), and this phenomenon has greater amplitude in summer. Since this is not represented in the chosen RC model, the parameter estimation process instead decreased the resistance R_{int} between the two states, so that the external input I_H also affects the state T_w in a more direct manner. As a compensation for this reduced resistance, the capacity state C_w is increased to act as a buffer. Moreover, the aperture area gA has decreased in the cooling model, since the sun angle is higher and thus direct irradiation do not penetrate as deep into the building as in the heating case.

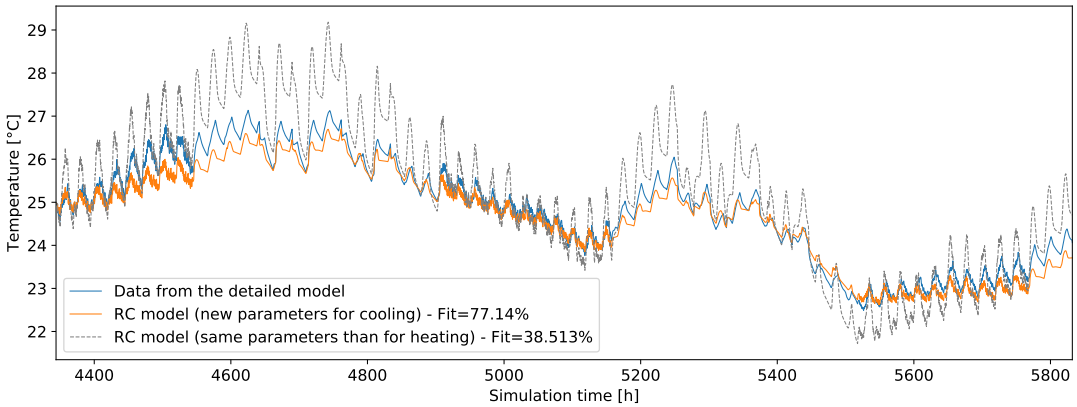

Figure III.36. Two different fittings of the RC model for cooling.

The parameter estimation process enabled to emphasize that simplified models for MPC applications in heating and cooling mode should be differentiated. In fact, the RC model simply is a linearization of a detailed model (or a real building) around an operation point; and since this operation point changes significantly between winter and summer, it is preferable to adapt the model as well. In the present case, the RC model was obtained from data created by another, more detailed model, but the identification process would be similar with monitoring data recorded from a real building, although some challenges would arise with the uncertainties of the input data, or if the wall temperature measurement is needed.

4.2.5 HVAC systems: TES and FCU

For the remaining of the system, the values of the RC parameters were mostly derived from manufacturer's datasheets and calculated data. The chosen values are presented in Table III.8. The two capacities C_{dis} and C_{TES} correspond to the thermal capacity of the water contained in the pipes of the FCU circuit and in the DHW storage tank, respectively. The tank contains 200 liters of water, while the pipes around 40 liters (the minimum being 38 liters specified in the heat pump manufacturer's datasheet). R_{TES} corresponds to the heat losses of the tank, considering its insulation layer, while R_{dis} corresponds to the heat transfer of the FCU from the water side to the air side.

Table III.8. Parameters of the system RC model.

Coefficient	$\mathbf{R_{dis}}$	$\mathbf{R_{TES}}$	$\mathbf{C_{dis}}$	$\mathbf{C_{TES}}$
Unit	**K/kW**	**K/kW**	**kWh/K**	**kWh/K**
Value (heating)	4.496	601	0.044	0.29
Value (cooling)	2.681	601	0.044	0.29

5 Conclusions on the methodologies

This chapter has reported in details the different methodologies used for the studies developed in the thesis. Although the methods and tools do not represent an actual goal or research question of the thesis on their own, they actually represent the most important part of the work, and their detailed description enables to understand later where do the obtained results stem from.

Firstly, the experimental and simulation frameworks have been described, and they are later used respectively in chapter V and VI. The experimental setup reproduces the hardware-in-the-loop testing principles, and the co-simulation framework enables to couple different pieces of software to investigate the effects of a controller on a specific study case. Those two frameworks developed in the mark of the thesis can be reused later, for instance to test further variations or configurations of the controllers and of the boundary conditions (building type, climate...).

Secondly, advances have been presented with regards to the penalty signals used to trigger the energy flexibility and the quantification or representation of this energy flexibility. The penalty signals play in particular a very important role, as they in fact contain the information on which the flexibility controllers will react. A significant part of the intelligence therefore consists in designing proper signals, so as to incite load shifting towards certain desired periods. Regarding this, a novel signal representing the marginal CO_2 emissions from the grid was created, with the aim to reduce the carbon footprint when such signal is used. An hourly price signal typical in Spain for small consumers was also chosen. These two signals are the ones later used to trigger the actions of the flexibility controllers, both the RBC and the MPC. Further than that, several KPIs have been selected and discussed, and graphical representation of the energy flexibility indicators have been proposed.

Finally, progress was made regarding the modelling of the different systems playing a part in the evaluation of energy flexibility in buildings. For the modelling of the building envelope, although the use of reduced order grey-box models is well-documented in existing literature, the use of such models for use in both heating and cooling modes has been investigated and reported in this chapter, and it constitutes an interesting outcome of the research. For the modelling of the heat pump systems, several advances have been made: a simplified model was first created, based on an experimental performance map, for use within the MPC framework. A detailed heat pump model was then developed in TRNSYS to be included in the simulation-only framework: this high-fidelity model reproduces well the control and dynamics of the real heat pump, and can thus be reused in a great variety of simulations.

All these elements, models and methods constitute in themselves valuable outputs of the work. Further than the reporting of their development, they are then used to produce the desired results which will be analyzed in the following chapters of the thesis.

Chapter IV

Development of controllers for energy flexibility

The main contribution of this thesis consist in developing and testing control strategies for heat pump systems in residential buildings. In this chapter, the development and tuning of those controllers is described in details: first in section 1, the rule-based controller is presented, and secondly in section 2 the MPC controller. Both of these controller types include different parameters that must be adjusted for an optimal performance. A special attention is thus given to the adequate methodology for tuning these parameters, since choosing proper values has a significant impact on the final results.

1 Rule-based controller

1.1 Description of the rule-based control methodology

To exploit the flexibility of heating or cooling loads, rule-based controls (RBC) constitute the simplest type of method to implement. RBC can for example aim at avoiding peak periods with fixed schedules [42], reducing the peak power exchange between buildings and the grid [43], reducing the energy cost [44] or increasing the consumption of RES [45]. In the case described in this thesis, the focus lies on reducing the costs or emissions linked to covering the thermal loads of the building. In this way, the RBC can later be compared with the MPC: both types of controllers react to the same input signals, them being the time-varying price of electricity or the marginal emissions of the grid, as explained in the previous chapter.

Before to explain the principle of the chosen RBC controller, let us describe first the reference control strategy. It simply consists in applying fixed set-points to maintain in the indoor space (i.e. controlling the indoor temperature T_{int}) and in the DHW tank (i.e. controlling the water temperature T_{TES}). A set-point of $T_{TES,SP} = 45$°C is fixed for the DHW tank, with a negative deadband of 5°C, hence the temperature oscillates between 40 and 45°C. For the room thermostat, the reference set-points are chosen based on the recommendations from standard EN15251 [140]: $T_{int,SH,SP} = 21$°C in the winter season, and $T_{int,SC,SP} = 25$°C in the summer season. These values were chosen so that the operative temperature stays within comfort Category II (normal level of expectation), considering a deadband of ± 1°C.

Starting from this reference with fixed set-points, the implemented RBC consists in modulating the set-points according to the current value of a penalty signal (e.g. electricity price or emissions). This method was partly inspired from [137], and it is illustrated in Figure IV.1. The dashed lines shown in Figure IV.1 show the common lower or upper bound for the temperature: the same values are chosen as constraints in the MPC controller, so that the three control strategies can be compared (reference, RBC and MPC).

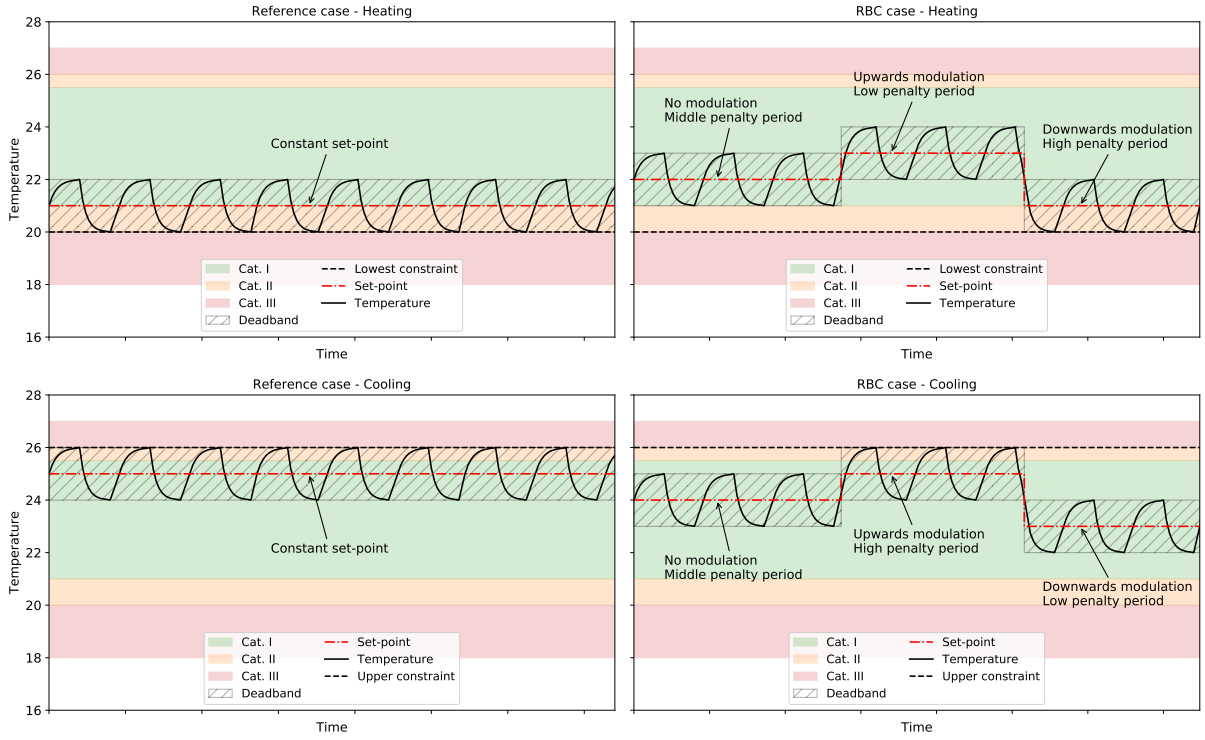

Figure IV.1. Principles of the RBC set-point modulation, for space heating and space cooling.

Firstly, thresholds representing the limits of the high and low penalty are defined. At a given moment, the data of the varying penalty signal c of the next 24 h is collected. These data are treated as follows: the 40$^{\text{th}}$ percentile of the distribution constitutes the threshold for low price c_{low} and the 60$^{\text{th}}$ percentile constitutes the threshold for high price c_{high}. These values of the percentiles have shown to be the best compromise; the methodology for choosing them is discussed in subsection 1.2. At every time step, the calculation of c_{low} and c_{high} is repeated, and the current penalty signal c is compared with the thresholds; if it falls below c_{low}, the set-point T_{SP} is increased to store thermal energy in the mass of the building while energy is cheap (decreased in the case of cooling). If the current value of the penalty is above c_{high}, the set-point is decreased to discharge the stored thermal energy instead of using active systems while energy is expensive (set-point increased in case of cooling). To realize these variations, a modulation factor r is introduced, as shown in Equation IV.1. The calculation of the temperature set-points is then summarized in equations IV.2 and IV.3. The amplitude of the modulation is $\delta T_{SH} = \delta T_{SC} = 1$°C for space heating and cooling, and $\delta T_{TES} = 5$°C for DHW, in comparison with the reference case aforementioned. It should be noted that the flexibility control strategy could be applied either to only one set-point, either for both the indoor temperature and the TES set-points at the same time. Overall, the strategy aims at shifting the loads towards periods of lower penalty.

$$r = \begin{cases} +1 & \text{if } c < c_{low} \\ 0 & \text{if } c_{low} < c < c_{high} \\ -1 & \text{if } c > c_{high} \end{cases} \tag{IV.1}$$

$$T_{int,SP} = \begin{cases} T_{int,SH,0} + r \cdot \delta T_{SH} & \text{in heating mode} \\ T_{int,SC,0} - r \cdot \delta T_{SC} & \text{in cooling mode} \end{cases} \tag{IV.2}$$

$$T_{TES,SP} = T_{TES,0} + r \cdot \delta T_{TES} \tag{IV.3}$$

1.2 Tuning of the RBC

The core of the RBC intelligence lies in how to choose the thresholds for the low and high penalty c_{low} and c_{high}, since they will determine when to modulate the set-points. The tuning of the thresholds was performed on a study case, and reported in [159]. Only the electricity price was used as penalty signal in this process, hence in this subsection, c corresponds to the electricity price only, but the same would apply for other signals like the CO_2 emissions from the grid.

Let us define the k-th percentile of the price data for the next day: $c_{low,k}$ represents the lower threshold, while $c_{high,100-k}$ represents the high threshold, the $(100-k)$-th percentile. For the tuning, k is varied between 10 to 50 and the effect on the performance of the controller is studied. The performance indicator chosen for this parametric analysis is the flexibility factor FF, as defined in subsection 2.2: it enables to quantify the actual load-shifting provoked by the RBC controller. This flexibility factor also depends on the thresholds of low and high price. It should be noted that the control strategy can be implemented using the percentile k but analyzed with a different percentile i: let us then define the i-th percentile of the price data, which will be used in the FF calculation. The modulation factor r in function of the k-th percentile and the flexibility factor in function of the i-th percentile are recalled in equations IV.4 and IV.5.

$$r_k = \begin{cases} +1 & \text{if } c < c_k \\ 0 & \text{if } c_k < c < c_{100-k} \\ -1 & \text{if } c > c_{100-k} \end{cases} \tag{IV.4}$$

$$FF_k = \frac{W_{lowprice} - W_{highprice}}{W_{lowprice} + W_{highprice}} = \frac{\int_{c<c_i} P_{el}(t)dt - \int_{c>c_{100-i}} P_{el}(t)dt}{\int_{c<c_i} P_{el}(t)dt + \int_{c>c_{100-i}} P_{el}(t)dt} \tag{IV.5}$$

Where W corresponds to the integrated energy used by the heat pump during low or high price periods.

Simulations of one week were carried out in TRNSYS, with time steps of three minutes, on the same residential study case. The weather data was retrieved from a weather station situated in Terrassa (Barcelona, Spain) during the year 2015. A selected week in January 2015 was chosen (cold season), as well as one in April 2015 (mid-season). The corresponding price profile of the same weeks was retrieved from the Spanish TSO (PVPC tariff). The simulated cases of this parametric analysis are summarized in Table IV.1.

Table IV.1. Simulation cases for the parametric analysis of the RBC controller.

Case	Percentile for modulation	Percentile for FF analysis	Price and weather input
0a	Reference case	k =10 to 50	January 2015
1a	k =10	i =10 to 50	January 2015
2a	k =20	i =10 to 50	January 2015
3a	k =30	i =10 to 50	January 2015
4a	k =40	i =10 to 50	January 2015
5a	k =50	i =10 to 50	January 2015
0b	Reference case	i =10 to 50	April 2015
1b	k =10	i =10 to 50	April 2015
2b	k =20	i =10 to 50	April 2015
3b	k =30	i =10 to 50	April 2015
4b	k =40	i =10 to 50	April 2015
5b	k =50	i =10 to 50	April 2015

The flexibility factor analysis is presented in Figure IV.2 for cases 1 to 5. On the horizontal axis, the different simulated cases correspond to different values of k (10 to 50) used to define the thresholds for the control; the different series show the different values of i used to define the thresholds of the

flexibility factor. The flexibility factor highly depends on both values. It can be observed in January (Figure IV.2 (a)) that for a fixed case, the value of $i = k$ shows the highest flexibility factor, which is only logical since the evaluation factor then coincides with the actual control implemented. The overall highest flexibility factor of 0.69 is obtained in case 4a, with $k = i = 40$. In spring season (Figure IV.2 (b)), this tendency is less clear, but in most cases, the configurations $k = i$ also present the highest flexibility. The highest values of the flexibility factor are obtained with $k = 50$ (case 5b) and i=10 and 50. As the heating needs are reduced in mid-season, and thus provide less interest in load-shifting, the control strategy is preferably optimized for the winter season. Therefore, the values $k = i = 40$ are chosen for later studies, which means the 40-th percentile is the low threshold while the 60-th percentile is the high threshold. An example applied on a real case with the electricity price is shown in Figure IV.3, with two different tariffs, the calculated thresholds and the resulting modulation factor r.

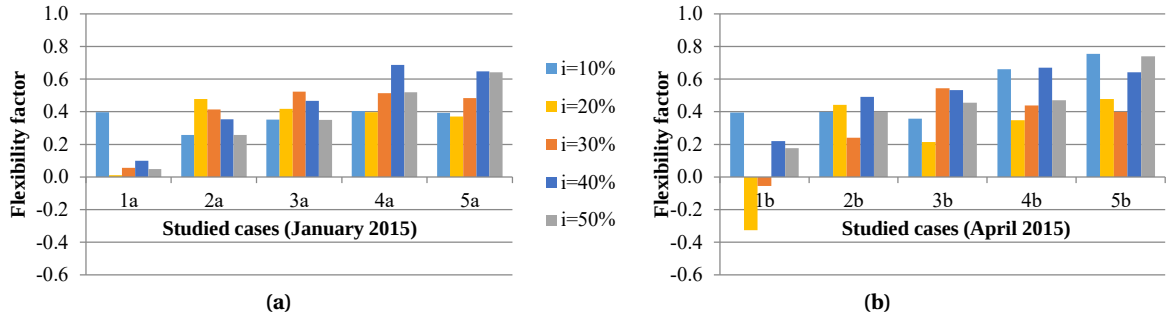

Figure IV.2. Flexibility factor computed for the total electricity use of the heat pump in cases 1 to 5, both in January 2015 (a) and April 2015 (b). Cases 1 to 5 correspond respectively to values of the percentiles k=10 to 50, applied to the price thresholds for the control strategy.

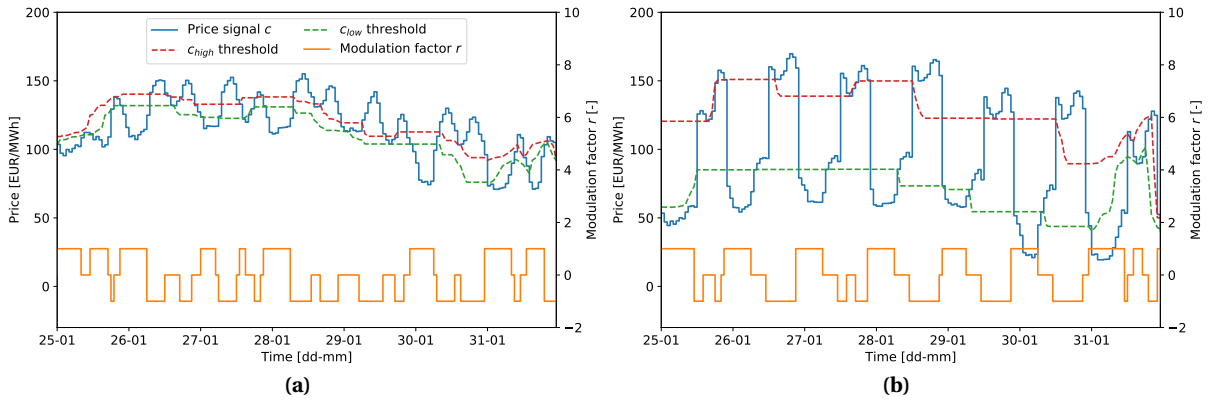

Figure IV.3. Electricity price for end-users contracted on the PVPC tariff in Spain in January 2015 (standard tariff (a) and 2-periods tariff (b)). The calculated thresholds and the resulting modulation factor are additionally represented.

This tuning process enabled to find the best calculation method for the thresholds of high and low penalty. The chosen percentile values have shown to be appropriate for the considered price signal, and the same values were used for other penalty signals, such as the CO_2 emissions from the grid, even though these signals can have a different shape. The tuning was only carried out with data of the heating season, however the shape of the price signal is very similar across the entire year, since it is constructed 'artificially' with a high price period in the afternoons and a low-price period in the mornings. For this reason, it is considered that the tuning is also valid in the cooling season, since the values of the appropriate percentiles would be identical.

Apart from the thresholds of the high and low penalty, other parameters can be tuned in the RBC controller. Notably the amplitude of the set-point modulation can also be modified: higher values of

$\delta T_{SH} = 2$°C and $\delta T_{TES} = 10$°C were tested, but they resulted in a considerable increase of the energy use, although comfort was not significantly impacted [159]. The original values $\delta T_{SH} = \delta T_{SC} = 1$°C and $\delta T_{TES} = 5$°C were thus conserved.

2 Development of a model predictive controller

2.1 MPC algorithm

The overall MPC control algorithm was developed to manage the heating and cooling loads of the building, and to exploit their flexibility. The mathematical formulation of this problem is presented in Algorithm 1; it consists of a classical optimization problem with constraints. The controller intends to minimize a certain objective function J over the time horizon N, by choosing the values of the following variables: $\delta = [\delta_S, \delta_{TES}]^T$ is the vector of the two binary variables which activate respectively the space heating or cooling mode and the DHW production mode, $u = [Q_S, Q_{TES}]^T$ is the vector of the continuous variables which represent the thermal power to deliver either to the building space or to the TES tank. The constraints ruling these control inputs are clarified in subsection 2.3. Different forms of the objective function have been tested: they are detailed in subsection 2.2, along with the tuning of the weighting coefficients in the multi-objective cost function. During the optimization, the controller must take into account the dynamics of the building through a simplified state-space model as previously described in chapter III. Finally, some constraints on the output temperatures $y = [T_{int}, T_{TES}]^T$ must be met to guarantee the satisfaction of the users, these comfort constraints are detailed in subsection 2.4.

Algorithm 1 - MPC controller

$$\underset{u,\delta}{\text{minimize}} \quad J = \alpha_\varepsilon \cdot J_\varepsilon + \alpha_{\Delta u} \cdot J_{\Delta u} + (1 - \alpha_\varepsilon - \alpha_{\Delta u})\, J_{obj} \tag{IV.6}$$

$$\text{subject to} \quad \forall k \in 1, \ldots, N :$$

$$\text{Model of the building dynamics:} \quad \begin{cases} x(k+1) = & A \cdot x(k) + B_u \cdot u(k) + B_e \cdot e(k) \\ y(k+1) = & C \cdot x(k) \end{cases} \tag{IV.7}$$

$$\text{Constraints on the control inputs}^1\text{:} \quad \begin{cases} \delta \odot \underline{u} \leq u(k) \leq \delta \odot \overline{u} \\ \|\delta\|_1 \leq 1 \\ \text{Minimum up and down times} \end{cases} \tag{IV.8}$$

$$\text{Comfort constraints on the control outputs:} \quad \begin{cases} \underline{y}(k) - \varepsilon(k) \leq y(k) \leq \overline{y}(k) + \varepsilon(k) \\ \varepsilon(k) \geq 0 \end{cases} \tag{IV.9}$$

[1] Where $\odot$ is the Hadamard product (matrix product term by term).

2.2 Objectives and tested MPC configurations

As seen in Algorithm 1, the MPC algorithm intends to minimize a certain objective over the prediction horizon. In the present case, the objective comprises in fact three aspects, weighted by the corresponding coefficients α :

- maintaining the comfort level with the objective J_ε, as shown in Equation IV.10. In fact, it consists in limiting the discomfort, or in other words, avoid the excursions outside the defined temperature boundaries. ε is a slack variable that enables to soften the constraints on the output temperatures. In principle $\varepsilon = 0$, but exceptionally, the temperature is allowed to trespass the boundaries ($\varepsilon > 0$); the cost of this constraint violation is reflected in the objective J_ε, as shown in Equation IV.10. As another advantage, this formulation avoids infeasibility of the MPC in the case where the initial states are found outside the boundaries (which typically happens at start-up for instance, or due to discrepancies of the model when operating close to the boundaries).

$$J_\varepsilon = \sum_{k=1}^{N} \varepsilon(k) \tag{IV.10}$$

- smoothing the control actions to avoid too frequent on-off switching with the objective $J_{\Delta u}$, as shown in Equation IV.11.

$$J_{\Delta u} = \sum_{k=2}^{N} \|u(k) - u(k-1)\|_1 \tag{IV.11}$$

- an actual objective J_{obj} which can be the minimization of the thermal energy delivered to the building J_{en}, the minimization of the cost of the electricity used by the heat pump for delivering this energy J_{cost}, or the minimization of the CO_2 emissions related to this electricity use J_{CO2}. The formulation of these objectives is detailed in the next subsections 2.2.1 to 2.2.4, while the global multi-objective function is summarized in Table IV.2 for the different configurations.

Table IV.2. Multi-objective function for the different MPC configurations.

MPC configuration	**Main objective** J_{obj}	**Full objective function** J
MPC ThEnerg	Minimizing the thermal energy $J_{obj} = J_{en}$	$J = \alpha_\varepsilon \cdot J_\varepsilon + \alpha_{\Delta u} \cdot J_{\Delta u} + (1 - \alpha_\varepsilon - \alpha_{\Delta u})\, J_{en}$
MPC Cost	Minimizing the monetary costs $J_{obj} = J_{cost}$	$J = \alpha_\varepsilon \cdot J_\varepsilon + \alpha_{\Delta u} \cdot J_{\Delta u} + (1 - \alpha_\varepsilon - \alpha_{\Delta u})\, J_{cost}$
MPC CO_2	Minimizing the CO_2 emissions $J_{obj} = J_{CO2}$	$J = \alpha_\varepsilon \cdot J_\varepsilon + \alpha_{\Delta u} \cdot J_{\Delta u} + (1 - \alpha_\varepsilon - \alpha_{\Delta u})\, J_{CO2}$

2.2.1 Minimization of the thermal energy (MPC ThEnerg)

In this configuration, the quantity minimized by the MPC over the control horizon is the thermal energy delivered to the building (in addition to the smoothing and discomfort terms), hence without taking into account the variable efficiency of the heat pump system. The mathematical formulation with $J_{obj} = J_{en}$ is written in Equation IV.12.

$$J_{en} = \sum_{k=1}^{N} \|u(k)\|_1 = \sum_{k=1}^{N} \left(Q_S(k) + Q_{TES}(k)\right) \tag{IV.12}$$

In the overall objective of the MPC, J_{en} is combined with two other objectives (comfort and smoothing of the control). To determine the weighting coefficients α between these different quantities, Pareto fronts are plotted, where several values of the coefficients are tested on simulations. The results are plotted separating the different components of the objective function, as can be seen in Figure IV.4. In this graph, the J_ε objective is represented on the y-axis, J_{en} on the x-axis, and $J_{\Delta u}$ through color mapping of the points. The different lines correspond to different values of α_u, while the different points of a line correspond to different values of α_ε.

To choose appropriate values of the weighting coefficients, one must remain in the right horizontal part of the lines, where the discomfort J_ε is at its minimum. At the same time, it is preferable to minimize the thermal energy J_{en}, therefore to stay as much on the left of the graph as possible. Furthermore, one must also avoid unreasonably high computation times and high values of $J_{\Delta u}$ (yellow colors on the present graph), even though this is the least relevant parameter (with a time step of 15 minutes, a cyclic on-off behavior would not cause many problems). As a compromise between all these considerations, the values chosen are $\alpha_{\Delta u} = 0.05$ and $\alpha_\varepsilon = 0.8$ for the J_{en} objective in heating mode; $\alpha_{\Delta u} = 0.05$ and $\alpha_\varepsilon = 0.6$ in cooling mode. The same approach is repeated for every MPC configuration.

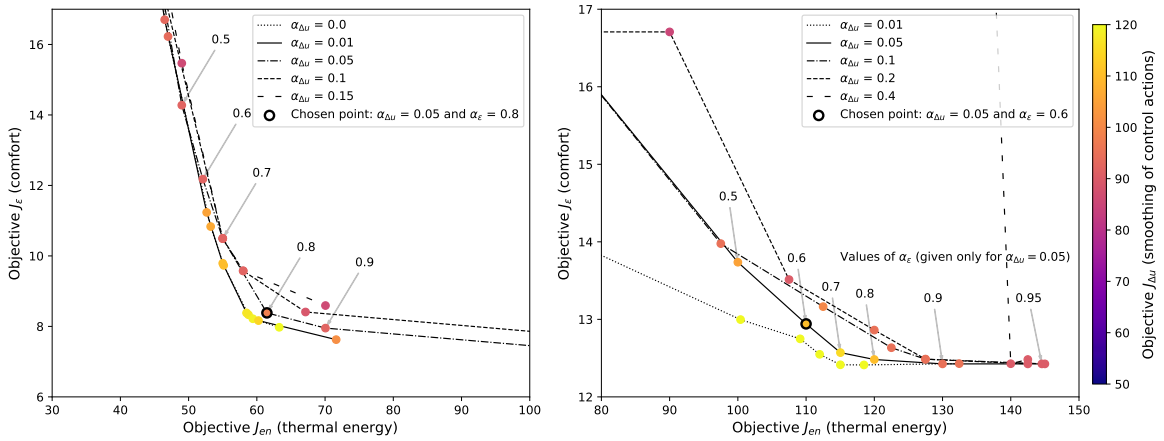

(a) **(b)**

Figure IV.4. Pareto fronts for the J_{en} configuration, in (a) heating and (b) cooling modes.

2.2.2 Minimization of the operational costs (MPC Cost)

In this configuration, the cost of the electricity used by the heat pump is minimized by the MPC. This configuration presents an increased complexity, since the electricity use P_{el} is introduced in the equation (and not only the delivered heat as previously), and therefore the heat transmission by the emitter and the performance of the heat pump must both be taken into account into the objective function. For this purpose, the simplified models detailed in subsection 3.3 of chapter III are utilized. The electricity used by the heat pump is then multiplied at every time step by a time-varying cost of electricity c_{el} (in EUR/MWh, changing every hour), normalized by $c_{el,max}$. The value of $c_{el,max} = 200$€/MWh is chosen reasonably above the highest price observed in the whole year, so that the ratio $c_{el}/c_{el,max}$ stays between 0 and 1. Normalizing all the subobjectives facilitates the subsequent balancing of the multi-objective function with the weighting coefficients. In the present case, the Spanish PVPC tariff is used, since its historical data and forecasts are public [132]. More information on the price signals is given in subsection 2.1 of chapter III. Introducing such a penalty signal helps the decision-making process of the MPC since it already predefines favorable or non-favorable periods for when to operate the systems. The formulation of J_{cost} is presented in Equation IV.13.

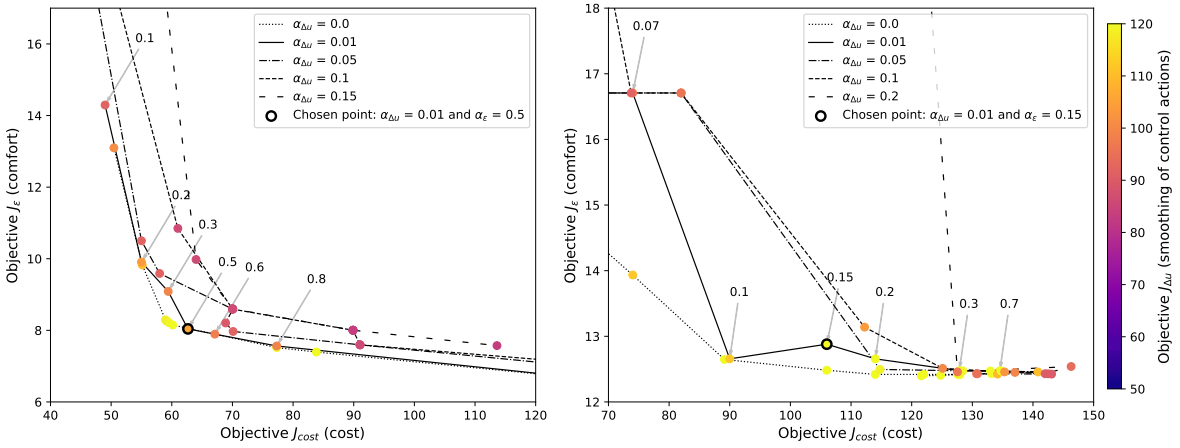

(a) **(b)**

Figure IV.5. Pareto fronts for the J_{cost} configuration, in (a) heating and (b) cooling modes.

The costs related to the FCU (which are synchronized with the space heating/cooling operation) can be considered or not in the equation (the term $P_{el,FCU}$). If they are, a constant electricity consumption for the FCU is used when the SH/SC circuit is activated, amounting to 30 W per each of the eight FCUs (Equation IV.14). It should be noted that the other non-shiftable electricity costs of the building are not included in the cost objective J_{cost}, since they would not influence the calculation of the optimal MPC plan for the heat pump. The Pareto fronts for J_{cost} are presented in Figure IV.5. In this configuration, the chosen values are $\alpha_{\Delta u} = 0.01$ and $\alpha_{\varepsilon} = 0.15$ for cooling, $\alpha_{\Delta u} = 0.01$ and $\alpha_{\varepsilon} = 0.5$ for heating.

$$J_{cost} = \sum_{k=1}^{N} [P_{el,S}(k) + P_{el,TES}(k) + P_{el,FCU}(k)] \cdot \frac{c_{el}(k)}{c_{el,max}} \tag{IV.13}$$

$$P_{el,FCU} = \delta_S(k) \cdot P_{FCU,on} \text{ (with } P_{FCU,on} = 0.24 \text{ kW)} \tag{IV.14}$$

2.2.3 Minimization of the CO_2 emissions (MPC CO2)

This formulation resembles the previous J_{cost}, except that the monetary cost c_{el} is replaced by a cost in terms of CO_2 emissions c_{MEF} (in $kgCO_2/kWh$). The marginal emissions factor (MEF) is used for this purpose, and normalized by the value $c_{MEF,max} = 0.5$ $kgCO_2/kWh$. This parameter estimates the emissions savings that can be realized from a change in the load (i.e. a demand response action), given the state of the electrical grid. It differs from the average emissions factor since it considers the supposed merit order in which the different sources of electricity generation are activated. The MEF is computed for every hour according to the model and calculations described in section 2 of chapter III. The formulation with $J_{obj} = J_{CO2}$ is presented in Equation IV.15. The Pareto curves for J_{CO2} are plotted on Figure IV.6. In this configuration, the chosen values are $\alpha_{\Delta u} = 0.05$ and $\alpha_{\varepsilon} = 0.15$ for heating, $\alpha_{\Delta u} = 0.01$ and $\alpha_{\varepsilon} = 0.15$ for cooling.

$$J_{CO2} = \sum_{k=1}^{N} [P_{el,S}(k) + P_{el,TES}(k) + P_{el,FCU}(k)] \cdot \frac{c_{MEF}(k)}{c_{MEF,max}} \tag{IV.15}$$

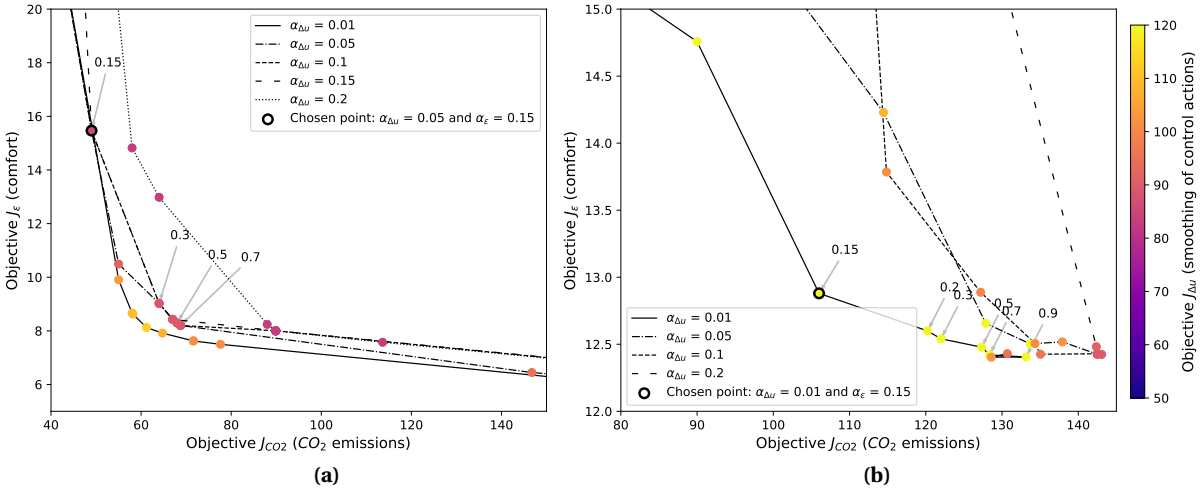

Figure IV.6. Pareto fronts for the J_{CO2} configuration, in (a) heating and (b) cooling modes.

2.2.4 Summary of the MPC configurations

The summary of the previously determined coefficients for the multi-objective function are recalled in Table IV.3.

Table IV.3. Summary of the weighting coefficients in heating and cooling modes for the different objectives.

	HEATING			COOLING		
Objective	J_{en}	J_{cost}	J_{CO2}	J_{en}	J_{cost}	J_{CO2}
Value of α_ε	0.8	0.5	0.15	0.6	0.15	0.15
Value of $\alpha_{\Delta u}$	0.05	0.01	0.05	0.05	0.01	0.01
Value of $\alpha_{obj} = 1 - \alpha_\varepsilon - \alpha_{\Delta u}$	0.15	0.49	0.8	0.35	0.84	0.84

2.3 Constraints on the control inputs

Continuous variables (i.e. the thermal powers Q_S and Q_{TES} delivered respectively to the building and the tank) were chosen as the inputs controllable by the MPC. They enable to represent the variable speed characteristic of the studied system, which can modulate its delivered capacity within a certain range. In order to switch from the space heating/cooling to the DHW production mode, it is however necessary to introduce the additional binary variables δ_S and δ_{TES}. They equal 1 when their respective mode is activated, 0 otherwise. The heat pump can only operate in one mode at a time, so the binary variables are constrained by $\|\delta\|_1 \leq 1$, which is equivalent to $\delta_S + \delta_{TES} \leq 1$. Introducing binary variables transforms the nature of the control problem, and thus the MPC must resort to Mixed Integer Linear Programming (MILP) instead of simpler Linear Programming (LP) to solve it [160].

The binary variables also enable to limit the heating power Q in a certain range $[\underline{Q};\overline{Q}]$ when the heat pump is turned on. With only the continuous variables Q_S and Q_{TES} and simple constraints of the form $0 \leq Q \leq \overline{Q}$, the MPC could have decided to provide very low values of the thermal capacity Q, without turning it off. In reality, a heat pump system has a minimum power below which it cannot operate; for instance with the considered equipment, the frequency of the compressor cannot drop below 31 Hz, if the load is still too low for that frequency, the heat pump would switch off. The binary variables and the ranges of heating power enable to reproduce this behavior. The general constraints expressed in Equation IV.8 can therefore be reformulated as follows:

$$\text{Constraints on the control inputs at each time step k:} \quad \begin{cases} \delta_S \cdot \underline{Q_S(k)} \leq Q_S(k) \leq \delta_S \cdot \overline{Q_S(k)} \\ \delta_{TES} \cdot \underline{Q_{TES}(k)} \leq Q_{TES}(k) \leq \delta_{TES} \cdot \overline{Q_{TES}(k)} \\ \delta_S(k) + \overline{\delta_{TES}(k)} \leq 1 \end{cases}$$

Two approaches exist when considering the values of the maximum and minimum values of the capacity Q_{th}. The first approach considers that the range of operation is constant. In that case, the chosen values correspond to the manufacturers specifications and the range of operation observed in static tests:

- $[\underline{Q_{SC}};\overline{Q_{SC}}] = [-8\text{ kW} ; -2.5\text{ kW}]$ in cooling mode,
- $[\underline{Q_{SH}};\overline{Q_{SH}}] = [3\text{ kW} ; 10\text{ kW}]$ in heating mode,
- $[\underline{Q_{TES}};\overline{Q_{TES}}] = [5\text{ kW} ; 5\text{ kW}]$ in DHW production mode. In fact, the charging power of the internal loop of the DHW tank charging cannot be controlled independently. Furthermore, when using the ECO mode for DHW production as is the case here, the compressor is limited to work at 40 Hz and for this reason it is assumed that DHW is always produced at a constant load of the heat pump.

This first approach represents a simplification, since the capacity range of the machine depends on the operating conditions, and more specifically on the ambient temperature T_{amb} and the chosen supply temperature T_{sup}. This dual dependency is illustrated in Figure IV.7, where the maximum capacity of the heat pump is represented in function of the two parameters. To take into account the variation of the maximum capacity in function of the operating conditions, a second approach is developed: the maximum capacity is modeled with a quadratic function which will serve as the upper constraint of the MPC. The constraint cannot depend on T_{sup}, which depends itself on the decision of the MPC, so the quadratic expression is only function of T_{amb}. For conservative reasons, the model takes into

account only the extreme supply temperatures: $T_{sup} = 55°C$ in heating mode and $T_{sup} = 7°C$ in cooling mode. In this way, it is guaranteed that the heat pump can deliver the thermal capacity within this bound, even though in theory it could deliver more, if the supply temperature is milder than these extreme values (as shown by the scatter points above the plotted curves in Figure IV.7)

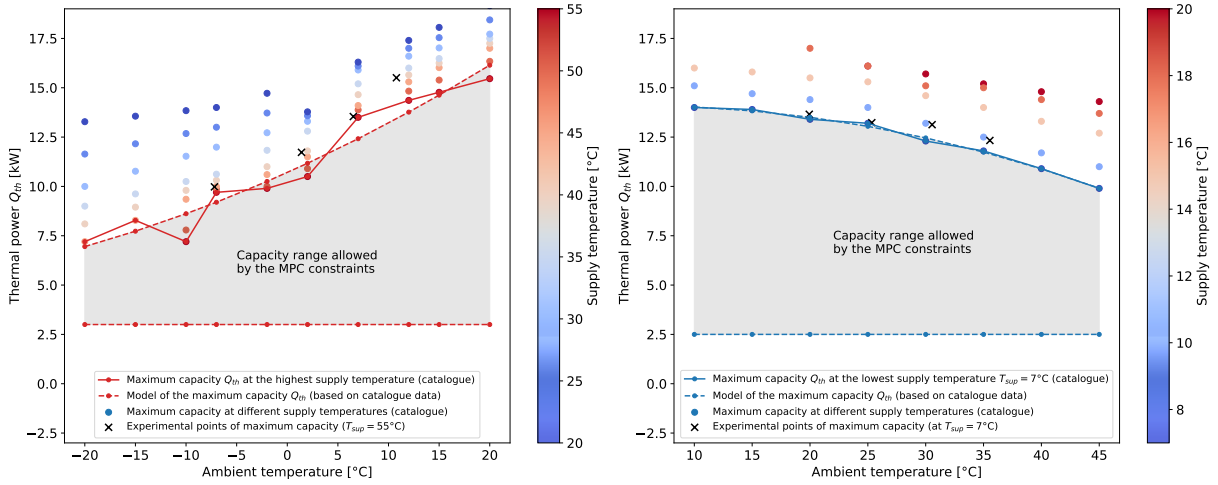

(a) **(b)**

Figure IV.7. Quadratic model of the maximum thermal capacity based on catalogue data in (a) heating and (b) cooling mode.

The quadratic function of the maximum capacity is shown in Equation IV.16 and the fitted coefficients for heating and cooling are presented in Table IV.4. The minimum capacity is kept as a constant in the second approach, as in the first one. The results presented in this thesis consider the second approach, hence with the upper constraint dependent on the ambient temperature.

$$\overline{Q_S}(k) = a_0 + a_1 \cdot T_{amb}(k) + a_2 \cdot T_{amb}(k)^2 \tag{IV.16}$$

Table IV.4. Coefficients of the fitted quadratic models for the capacity constraints in heating and cooling models.

Mode	$\mathbf{a_0}$	$\mathbf{a_1}$	$\mathbf{a_2}$
Heating	10.70	0.2298	0.00211
Cooling	14.02	0.02646	-0.00262

Finally, additional constraints must be set to impose minimum operation times of the heat pump. As an alternative to the smoothing objective, such constraints avoid the heat pump to switch on and off too often from one time step to the next. For this purpose, let us define the binary variable $\sigma(k) = \delta(k) - \delta(k-1)$: in this way, $\sigma(k)$ is equal to 1 if the heat pump is switched on at instant k, to -1 if the heat pump is switched off, and 0 if the heat pump remains in the same state. We would like to impose that if the heat pump is switched on (i.e. $\sigma(k) = 1$), it stays activated during at least L_{up} time steps (i.e. $\delta = 1$ in the interval $[k, k + L_{up}]$). The constraint is thus formulated mathematically as in Equation IV.17. In a similar fashion, a minimum down-time constraint can be enforced with Equation IV.18: if the heat pump is switched off ($\sigma(k) = -1$), then it has to remain in this state during at least L_{down} time steps (i.e. (i.e. $\delta = 0$ in the interval $[k, k + L_{down}]$). The value of L_{up} was chosen as 3 time steps for the space heating/cooling circuit: as observed in the experiments, 2 time steps of 15 minutes were required to reach a steady-state, hence the constraint ensures that the heat pump enters and functions in this steady state phase for some time. For DHW tank charging, the value of $L_{up} = 2$ time steps was also deducted from experimental observations: a single time step did not allow the system to reach temperatures sufficiently high to actually warm the tank. L_{down} was chosen as 2 time steps for both circuits.

$$\delta(k : k + L_{up}) \geq \sigma(k) \tag{IV.17}$$

$$\delta(k:k+L_{down}) \leq 1+\sigma(k) \tag{IV.18}$$

2.4 Comfort constraints on the control outputs

For comfort reasons, additional constraints are set to the two outputs of the MPC controller. For the indoor conditions, the room temperature T_{int} must stay within the boundaries $\left[\underline{T_{int}};\overline{T_{int}}\right]$. The ranges are chosen from the standard [140] according to the season and for a normal level of acceptation of the occupants for comfort (Category II):

- $\left[\underline{T_{int}};\overline{T_{int}}\right] = [20°\text{C}; 24°\text{C}]$ in winter season,
- $\left[\underline{T_{int}};\overline{T_{int}}\right] = [22°\text{C}; 26°\text{C}]$ in summer season.

These constraints are relaxed with the slack variable ε : in this way, small excursions outside the hard constraints are permitted at a certain cost (see also section 2.2 about the comfort objective).

Regarding the tank storing DHW, its temperature T_{TES} must stay in the range:

- $\left[\underline{T_{TES}};\overline{T_{TES}}\right] = [40°\text{C}; 55°\text{C}]$, regardless of the season.

To avoid the spread of the Legionnaire's disease, an additional anti-legionella protection (rising the temperature of the tank to 70°C for 10 minutes) is normally activated every week for more safety, but this feature is not studied in the present work since the considered simulations only last 3 days and the anti-legionella setting make use of an additional electrical resistance to reach 70°C, not the heat pump itself[1]. Finally, the output constraints can be reformulated as follows:

$$\text{Constraints on the control outputs at each time step k:} \quad \begin{cases} \underline{T_{int}} - \varepsilon(k) \leq T_{int}(k) \leq \overline{T_{int}} + \varepsilon(k) \\ \underline{T_{TES}} - \varepsilon(k) \leq T_{TES}(k) \leq \overline{T_{TES}} + \varepsilon(k) \\ \varepsilon(k) \geq 0 \end{cases}$$

2.5 Compensating the computational delay

2.5.1 Principles of computational delay

MPC controllers belong to the class of computer-based control systems. As such, they always require a certain finite time period for processing the computation of the next control actions, as well as for performing analog-to-digital conversions in the case of exchanging information with sensors and actuators [162]. In the case of the studied system, its inertia is large and the considered time steps are long (15 minutes), but the optimization calculation of the MPC is computationally expensive and time consuming, therefore the time delays for such systems are not negligible. According to [163] there are two different ways to deal with this computational delay:

- if the delay h is small enough in comparison with the time step t_s, the next steps are followed: the controller receives the inputs at time step k, computes the control actions as quickly as possible during the time h, and sends them to the plant. These control actions will be applied for the remaining of the time step, until next control actions are computed and sent. This approach somehow neglects the influence of the computational delay.
- if the delay h cannot be neglected as is the present case, a delay of one time step can be introduced. The next steps are thus followed: the controller receives the inputs at time step k, and will use the whole time step t_s to perform the calculations. At the time step $k+1$, the controller

[1] On this topic, some research was carried out by Bleys et al. [161], on how and at which frequency to use these anti-legionella thermal shocks in a flexible manner.

sends the obtained control actions to be applied to the plant immediately and during the entire next time step. However in this configuration, the process model must include a delay equal to t_s to take into account the fact that the control actions arrive to the plant with a delay of one time step.

The principle of these two approaches is presented in Figure IV.8. Other works have already considered including the computational time delay for model predictive controllers in the control systems literature [164], but it has seldom been studied within the field of heat pumps and HVAC systems. For this reason the adopted approach is reported in the following subsection.

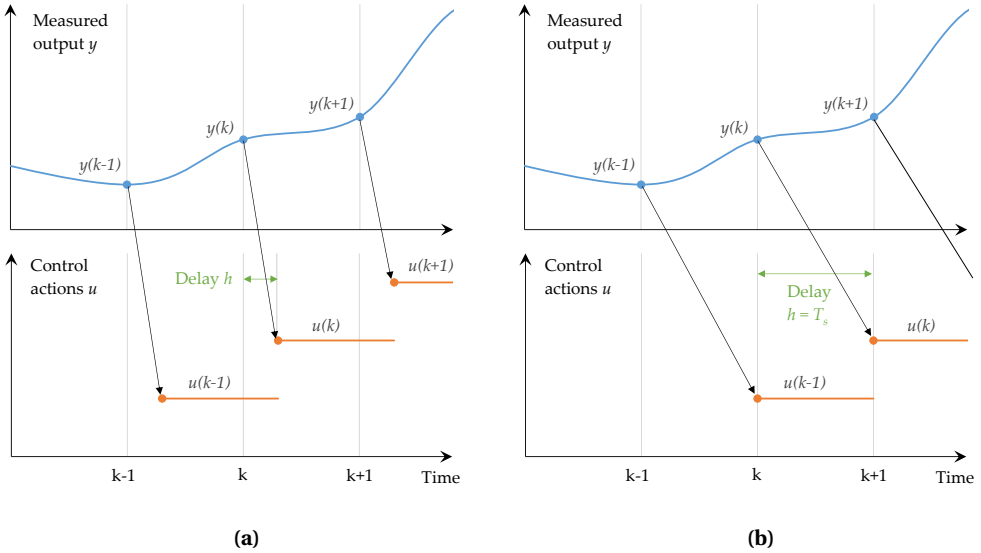

Figure IV.8. Including the computational delay according to the two proposed approaches (inspired from [163]): (a) if the delay is small compared to t_s and therefore its effects are neglected, or (b) if the delay is fixed to one entire time step for the MPC to reach its solution.

2.5.2 Compensation of computational delay in the state-space model

To compensate for the computational delay, the second approach is adopted: an entire time step is left for the MPC to calculate the control actions before to send them to the heat pump. To account for this delay in the state-space model, we operate a change of variables: instead of declaring the control variables $u(k)$, we declare directly the control variables $v(k) = u(k+1)$ shifted by one time step. The variables of u become new states to be included in the states vector x. The new vector of spaces is thus noted $\tilde{X}$ and concatenates the previously considered states x as well as the variables u. The other inputs which are not controllable should not be delayed, therefore the vector of the exogenous disturbances remains unchanged: $\tilde{E} = e$. All the new variables after the change of variables are noted with a tilde (˜). The new vectors are presented in Equation IV.19 in their short version and in Equation IV.20 in their expanded version. The new matrices of the state space model are presented in Equation IV.21, leading to the complete new state space formulation of Equation IV.22.

$$\tilde{X}(k) = \begin{bmatrix} x(k) \\ u(k) \end{bmatrix} \quad , \quad \tilde{U}(k) = v(k) \quad , \quad \tilde{E}(k) = e(k) \quad and \quad \tilde{Y}(k) = y(k) = \begin{bmatrix} x_1(k) \\ x_2(k) \end{bmatrix} \tag{IV.19}$$

$$\tilde{X}(k) = \begin{bmatrix} T_{int}(k) \\ T_w(k) \\ T_{TES}(k) \\ Q_S(k) \\ Q_{TES}(k) \end{bmatrix}, \tilde{U}(k) = \begin{bmatrix} Q_S(k+1) \\ Q_{TES}(k+1) \end{bmatrix}, \tilde{E}(k) = \begin{bmatrix} T_{amb}(k) \\ I_H(k) \\ Q_{occ}(k) \\ Q_{DHW}(k) \end{bmatrix} and \quad \tilde{Y}(k) = \begin{bmatrix} T_{int}(k) \\ T_{TES}(k) \end{bmatrix} \tag{IV.20}$$

$$\tilde{A} = \begin{bmatrix} A & B_u \\ (0) & (0) \end{bmatrix} \quad , \quad \tilde{B_u} = \begin{bmatrix} (0) \\ I_2 \end{bmatrix} \quad , \quad \tilde{B_e} = \begin{bmatrix} B_e \\ (0) \end{bmatrix} \quad and \quad \tilde{C} = \begin{bmatrix} 1 & 0 & 0 & 0 & 0 \\ 0 & 0 & 1 & 0 & 0 \end{bmatrix} \tag{IV.21}$$

$$\begin{cases} \tilde{X}(k+1) = & \tilde{A} \cdot \tilde{X}(k) + \tilde{B_u} \cdot \tilde{U}(k) + \tilde{B_e} \cdot \tilde{E}(k) \\ \tilde{Y}(k+1) = & \tilde{C} \cdot \tilde{X}(k) \end{cases} \tag{IV.22}$$

After the computation of the MPC, the first control actions $v(1)$ are retrieved and applied to the heat pump, and the model has already taken into account that they will be applied with a delay of one time step. This configuration compensating for the computational delay is useful for real-time applications, such as the experiments reported in chapter V. However it is not necessary for co-simulation only studies, where the time of the simulation can be "stopped" until the computation of the MPC is finished, therefore the co-simulations of chapter VI do not include this correction.

2.6 Time parameters, formulation and solving of the MPC

Further than the constraints and objectives, several other parameters have an important influence on the outcome of an MPC controller.

Discretization time step First of all, the discretization time step t_s should be chosen with care. In the MPC configurations, a value of t_s =15 minutes was chosen. Given the inertia of the system, choosing a shorter time step does not bring further interest: the heat pump has a warm up period that lasts a few minutes when it is started, therefore enabling short activations does not make sense since only the warm up period would occur, without exploiting the subsequent steady-state operation afterwards. Furthermore, most heat pumps actually integrate minimum runtime protections to avoid too frequent switching that would damage the machine in the long term. Choosing a discretization time step long enough enables to reflect such behavior. In the considered machine, the minimum up and down times are parameters than can be set in the local controller of the heat pump, between a value of 0 to 15 minutes. A larger time step also reduces the amount of decision variables for the MPC (for the same time horizon), and thus limits the computational burden of the optimization process. However, the time step should also be also short enough to enable a precise control of the heat pump in an optimal way and to receive feedback frequently to be able to react in case of unexpected disturbances. The chosen value of 15 minutes correspond to a satisfactory tradeoff between these different aspects for the considered system. Moreover, 15 minutes is the smallest time interval in which the aggregator market enables biddings for demand response, therefore in the view of utilizing the flexibility of buildings, the value of 15 minutes is preferred for the discretization time step of the MPC.

Prediction horizon The prediction horizon N, expressed as a number of time steps, constitutes another important parameter in the MPC framework. In the present work, a value of 24 hours ahead was chosen (i.e. $N = 96$ time steps of 15 minutes). A very long prediction horizon would in theory enable to better anticipate the changes of the disturbances on the long term, but it also increases the computational complexity (the longer the horizon, the more control variables to optimize, for the same time step). Furthermore, the quality of the forecasts decreases with time, therefore choosing a prediction horizon of more than several days presents little interest. On the other hand, a shorter prediction horizon would simplify the optimization problem but also reduce its power of anticipating future changes of the external disturbances. As a balance, a value of 24 hours for the prediction enables to capture the daily patterns occurring in the occupancy, weather and grid status evolutions. It was shown in [165] that 24 hours is the most common prediction horizon for MPC in buildings; longer horizons might be better suited if the time constant of the building is large (e.g. TABS applications), but are not necessary otherwise.

Software and solvers Finally, the software tools to write and solve the code of the MPC algorithm are briefly described in this paragraph. MATLAB was utilized to write the core of the MPC code. MATLAB possesses built-in functions that enable to easily write and identify state-space models, as well as

tools for performing optimization. Furthermore, MATLAB can be coupled with TRNSYS through the Type155 for carrying out co-simulations (see subsection 1.1 in chapter III). Within MATLAB, YALMIP [120] constitutes a powerful tool for optimization based algorithm development. YALMIP provides a general framework for writing optimization problems in a control context, and simplifies the interfacing with different available solvers for the resolution of said problems. The optimization problems considered in the present thesis include both binary and continuous variables, and therefore require mixed-integer linear programming algorithms to solve them. The commercial solver GUROBI [121] was used to solve the MPC problem. YALMIP formulates the optimization problem and calls GUROBI to solve it. GUROBI resorts to the branch-and-bound algorithm to find the solution [84].

2.7 Final tested formulation

To summarize, and given the precisions made in the previous sections, the full final formulation of the MPC controller is shown in the following algorithm. Several remarks should be noted:

- The inclusion of the computational delay was implemented for the version of the controller used in the experimental setup, but not in the version for the simulation-only framework, where it was not necessary since the time can artificially be paused until the calculation of the OPC is finished.

- Regarding the objectives, although the configuration $J_{obj} = J_{en}$ was developed, it was not tested in the experimental nor in the simulation setup. Only the configurations with penalty signals, minimizing the costs or the emissions were tested, with $J_{obj} = J_{cost}$ and $J_{obj} = J_{CO2}$ respectively, since they present more interest in terms of energy flexibility.

- To avoid too frequent switching operation on and off, it was mentioned that several strategies can be utilized: the smoothing objective $J_{\Delta U}$, or the minimum up and down constraints, or both at the same time. To limit the computation time of the controller, it was chosen to only keep the constraints but not the smoothing objective, so that there is one objective less in the multi-objective cost function.

Algorithm of the MPC controller

$$\underset{u,\delta}{minimize} \quad J = \alpha_\varepsilon \cdot J_\varepsilon + (1-\alpha_\varepsilon)\, J_{obj}$$

subject to $\quad \forall k \in 1,\dots,N:$

Model of the building dynamics:
$$\begin{cases} x(k+1) = & A \cdot x(k) + B_u \cdot u(k) + B_e \cdot e(k) \\ y(k+1) = & C \cdot x(k) \end{cases}$$

Constraints on the control inputs:
$$\begin{cases} \delta_S(k) \cdot \underline{Q_S} \le Q_S(k) \le \delta_S(k) \cdot \overline{Q_S}(k) \\ \delta_{TES}(k) \cdot \underline{Q_{TES}} \le Q_{TES}(k) \le \delta_{TES}(k) \cdot \overline{Q_{TES}} \\ \delta_S(k) + \delta_{\overline{TES}}(k) \le 1 \\ \sigma(k) = \delta(k) - \delta(k-1) \\ \delta(k : k + L_{up}) \ge \sigma(k) \\ \delta(k : k + L_{down}) \le 1 + \sigma(k) \end{cases}$$

Comfort constraints on the control outputs:
$$\begin{cases} \underline{T_{int}}(k) - \varepsilon(k) \le T_{int}(k) \le \overline{T_{int}}(k) + \varepsilon(k) \\ \underline{T_{TES}}(k) - \varepsilon(k) \le T_{TES}(k) \le \overline{T_{TES}}(k) + \varepsilon(k) \\ \varepsilon(k) \ge 0 \end{cases}$$

3 Conclusions on the development of the controllers

In this chapter, the development and tuning of two different controllers for exploiting the energy flexibility in buildings has been reported. Following the outcome of the state-of-the-art presented in chapter II, both a rule-based and a model predictive controller have been created. The literature review had outlined the advantages and drawbacks of those two types of controllers, therefore one of each has been developed in this thesis for further testing. In particular, the process of their development was reported in this chapter with a level of details seldom seen in previous literature, which enabled notably to highlight the parts which require more development work.

The RBC strategy consisted in a modulation of the room temperature set-point triggered by the considered penalty signal. Its development therefore did not require a significant amount of work. However, an appropriate tuning was necessary to obtain a better performance. This tuning process enabled to highlight the sensitivity of the considered strategy to the design parameters of the controller (here the percentiles of the penalty signal that define the high and low thresholds of the penalty).

The design of the MPC required significantly more work. In particular, the models needed within its formulation and reported in chapter III represent a large part of its development efforts. Apart from the models, the MPC created in this thesis was designed specifically for the control of heat pump systems, and therefore it took into account their intrinsic particularities. In the existing literature on automatic control, heat pumps are often considered with very simplified models, like a constant COP for instance, or without considering operational constraints representative of a real heat pump system functioning. For instance, the formulation of the MPC optimization algorithm in this thesis includes binary variables to enable the MPC to decide whether to operate the heat pump in space heating or cooling, or for the production of DHW. Such variables also permit to impose lower constraints on the operating load of the heat pump, when it is switched on. Without those, the MPC could decide to operate the heat pump at very low load, which is not realistic and would result in a poor performance. Additional elements in the formulation, such as the inclusion of the computational delay, the minimum up and down constraints, the tuning of the multi-objective function, the adaptations needed between the heating and the cooling mode, complete the range of novelties brought to the developed MPC controller in the present work. Overall, this MPC is entirely adapted for the control of heat pump systems, taking into account real-life constraints and performance, which makes it quite advanced and thus constitutes a real contribution from this thesis to the research in this domain.

The two developed controllers are then tested in different frameworks in Chapters V (experiments) and VI (simulations). They are fed with the exact same penalty signals and are tested with the same boundary conditions, to enable a thorough comparison of their performance. Such repetitive tests are made possible by the experimental and co-simulation frameworks described in chapter III.

Chapter V

Results of the experimental studies

In this chapter, the results of the experimental tests of the proposed controllers are reported. They were carried out in the semi-virtual environment laboratory setup previously described (see chapter III). Firstly, the considered boundary conditions for the tests are exposed, as well as the references cases considered in heating and cooling. Then, all the experimental cases are analyzed jointly, using the Key Performance Indicators defined in chapter III: integrated energy values, heat pump performance, energy flexibility and comfort. Finally, conclusions and discussions that arose from the practical implementation of MPC with the heat pump are reported.

1 Boundary conditions, reference cases and tested configurations

The boundary conditions used in the simulation setup are the same for all the experimental cases, respectively in heating and cooling seasons. They come from real data or assumptions, and are synchronized (e.g. the weather data corresponds to the price data of the exact same day). A duration of 3 days was chosen for performing each experiment, as a trade-off between the constraints of the laboratory installation and having long enough tests to obtain significant results. In heating mode, the chosen period is from the 24^{th} to the 26^{th} of February 2018 (both days included), and in cooling mode from the 8^{th} to the 10^{th} of July 2016 (both days included). The boundary conditions are represented graphically in Figure V.1 and detailed in the subsequent paragraphs. They were chosen for different reasons: firstly, they represent periods of high heating and cooling loads, which means the outdoor temperature is low in the first case, and high in the second case, given the considered climate. Having a high thermal load ensures that the flexibility action will be visible in comparison with the reference case. In the opposite case of a period of low load, the heat pump would be activated very few times, and thus the effects of the flexibility strategies might have been less evident (although such cases of mid-season would be worth investigating too in further work). However, choosing periods of high load might result in an overestimation the estimated flexibility, since a larger amount of energy consumption can potentially be shifted in time if the base consumption is already high. This effect should be kept in mind when analyzing the results, and extrapolation to the annual potential of flexibility should not be performed without special care. Secondly, the chosen periods present a degree of variety in the weather conditions, which enable to see the effects of flexibility activation in different contexts. For instance, the two first days of the chosen winter period are very sunny, with an ambient temperature peak at noon, while the third day is very cloudy with an almost constant temperature and low solar irradiation. In the chosen summer period, the two first days are slightly cloudy while the third day is entirely sunny, resulting in a prolonged period with temperatures above 30°C.

Weather data The weather data was collected from a weather station situated in Tarragona (Spain). The measurements include the ambient air temperature, the relative humidity, the total and diffuse horizontal solar irradiation, the wind velocity and direction. In the experiments, the air temperature and humidity conditions are reproduced dynamically in the climate chamber. It can be observed in

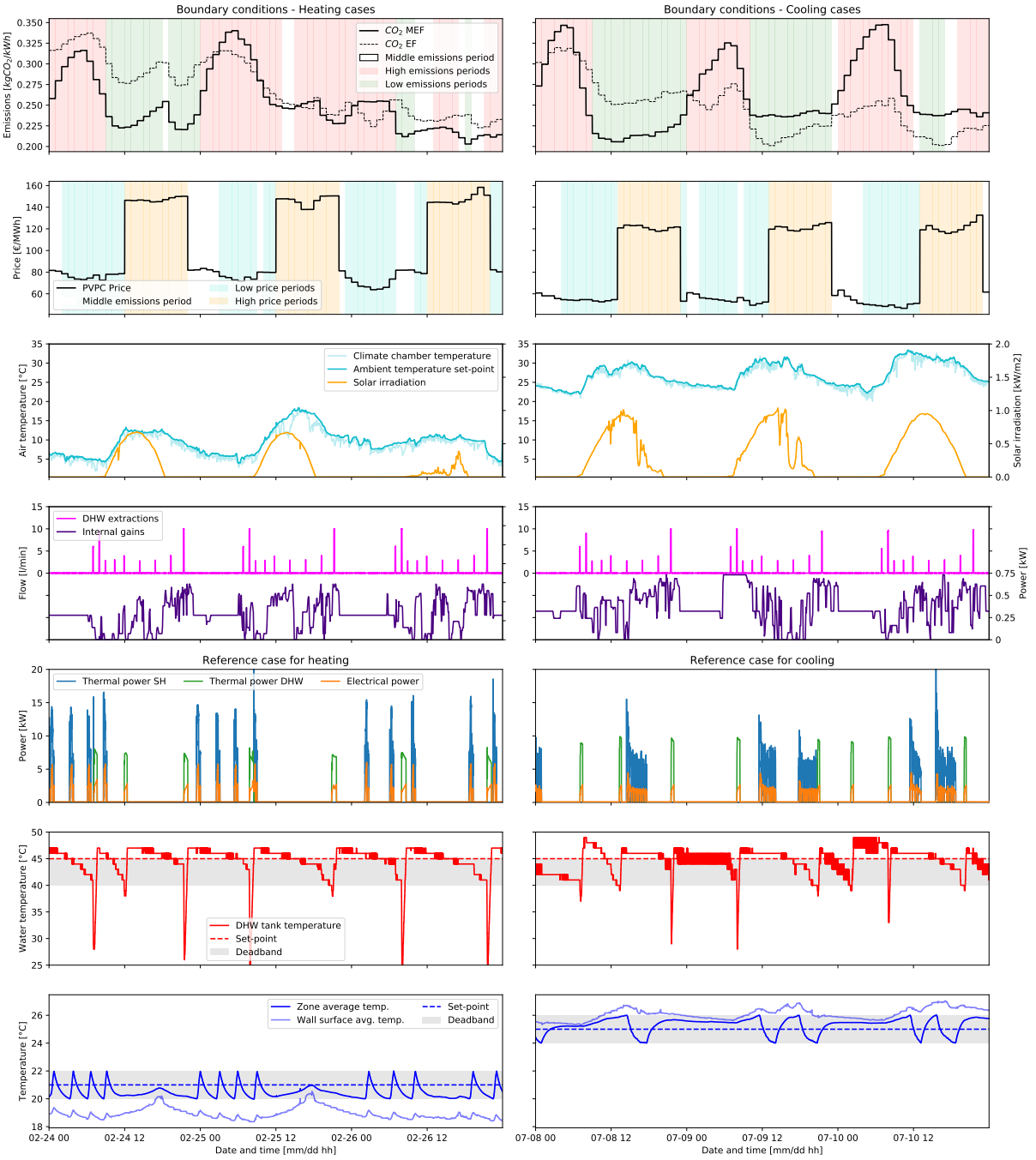

Figure V.1. Boundary conditions and measurement of the reference cases in heating (left) and cooling (right).

Figure V.1 that the climate chamber temperature is not exactly equal to the tracked set-point, due to the difficulties of the internal controller of the chamber, however the temperature always stays in a close range around the desired value. The three days in winter and summer were chosen because of their high heating/cooling load and variety of weather conditions (cloudy and sunny days among the three days).

Penalty signals The penalty signals used for triggering the activation of the demand-side flexibility were already described in chapter III. As a reminder, the price signal (PVPC 2 periods) is downloaded from the official website of the Spanish TSO Red Eléctrica de España [132]. The marginal emissions

factor for the Spanish grid is calculated with the methodology of section III.2.1.2, using the hourly energy mix of Spain also downloaded from the TSO. In Figure V.1, the periods of high and low penalty have been highlighted with colors; they were determined using the calculated high and low thresholds.

Occupancy and DHW extractions The occupancy profile was generated using a stochastic tool, taking into account the probability of the 4 occupants to be present in the dwelling at each moment, and to be active or not. However, once the stochastic profile has been generated, the same one is used for all the experiments covering the same period, to enable the comparison across cases. The resulting heat gains from the occupancy profile are shown on the middle graph of Figure V.1. They are implemented in the TRNSYS model of the apartment previously described in chapter III. For the DHW extraction profile, a deterministic profile is used, originating from the standard EN 12976-2 [123]. The profile includes 9 draws representing showers and small draws for washing and cleaning, summing up to 7.647 kWh per day, and with a maximum flow rate of 10 l/min for the showers. The same profile is repeated for every day of the experiments, both in winter and summer. The temperature of the water mains is set to 10°C in winter and 19°C in summer.

Reference cases in winter and summer The reference cases are represented in the 3 bottom graphs of Figure V.1, both in heating and cooling modes. In the reference case, the controller is a room thermostat, set to a constant value of 21°C in winter and 25°C in summer, with a deadband of $\pm$1°C around this set-point. In the storage tank, the set-point is 45°C with a negative deadband of 5°C. These two thermostats determine whether to activate or not the heat pump, with priority for the DHW. At the level of the heat pump, the supply temperature set-point is then determined by a heating or cooling curve, which enables to adapt the supply temperature to the ambient temperature (e.g. when the outdoor temperature is higher in winter, the supply temperature can be reduced). This type of control, available in most heat pumps on the market, enables to operate the heat pump at higher efficiency when the outdoor conditions are milder. A sensor measuring the ambient temperature is needed for that purpose; it is included in the outdoor unit. The utilized heating and cooling curves are represented in Figure V.2: their extreme values correspond to the operating range of the FCU in heating and cooling modes.

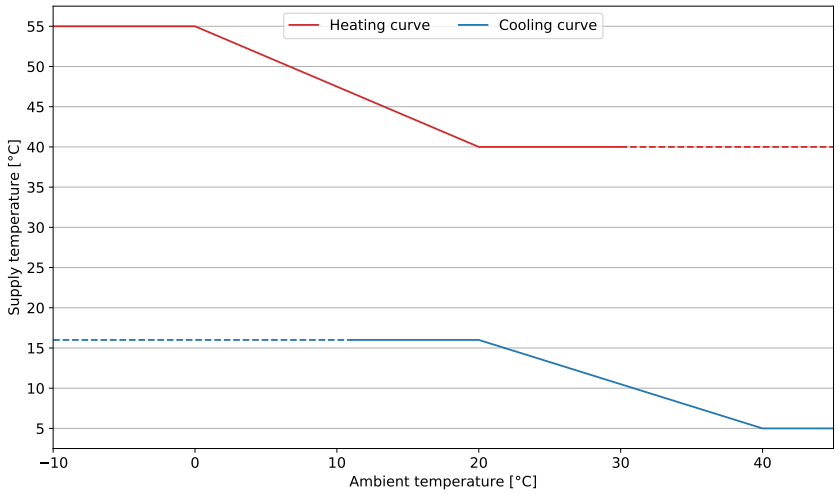

Figure V.2. Heating and cooling curve.

The integrated energy values for the two reference cases are presented in Table V.1. The other flexibility cases will then be analyzed in comparison with these values.

Tested flexibility cases After running the two reference experimental cases, the different flexibility controllers have been used one by one. The RBC controller and the MPC controller are tested, both

Table V.1. Summary table of the integrated energy values for the reference cases in heating and cooling.

Experimental case			**Ref. Heating**	**Ref. Cooling**
Electrical energy use	$P_{el,\Sigma}$	[kWh]	38.3	35.8
Thermal energy produced for SH/SC	$Q_{th,\Sigma,SH/SC}$	[kWh]	63.5	65.6
Thermal energy produced for DHW	$Q_{th,\Sigma,TES}$	[kWh]	29.1	23.4
Total thermal energy produced	$Q_{th,\Sigma}$	[kWh]	92.6	89.1
COP (only space heating/cooling)	$COP_{avg,SH/SC}$	[-]	2.74	2.69
Thermal energy change in the "storage"	ΔQ_{th}	[kWh]	-8.47	-21.1
Total thermal energy used	$Q_{th,use}$	[kWh]	101.0	110.2
Cost of electricity use	$c_{el,\Sigma}$	[€]	3.61	3.33
CO_2 emissions	$c_{MEF,\Sigma}$	[kgCO_2]	10.7	8.39
Primary energy	$c_{PEF,\Sigma}$	[kWh]	84.6	77.0

with the objectives of reducing the costs or the emissions related to the heat pump use. It should be noted that the MPC controller also requires data to forecast the future behavior of the systems. The same time series as previously described were utilized for this purpose (weather, penalty signals, occupancy), hence we consider here an MPC with a perfect forecast, which is perfectly aware of the future. For the MPC controller, the data are sampled every 15 minutes, which is the discretization time step of the optimization problem. To summarize, there are 8 flexibility experimental cases: the 4 configurations MPC Cost, MPC CO_2, RBC Cost and RBC CO_2 are tested both in heating and cooling modes.

2 Integrated energy and cost values

A fair overview of the performance of the control strategies can already be concluded from observing the integrated energy values presented in Tables V.2 and V.3. It is first observed that the MPC configurations all achieve their objectives of cost or emissions reductions compared to the reference case, while the RBC controller, in its current configuration, does not manage to reduce them.

In heating mode, MPC Cost actually induces a very small cost reduction of less than 1%. The reference heating case is already close to optimal regarding electricity costs, leaving little room for improvement. The MPC Cost configuration still manages to keep the costs at a constant level, while slightly improving the flexibility (see next section). In cooling mode on the other hand, the reference case shows an adverse behavior with regards to cost optimization, using most of the energy in the afternoon where the price is high. In that case, the MPC can really display its full optimization potential by effectively shifting most of the load towards periods of lower prices, and thus achieving a cost reduction of 37.4%, similar to the levels observed in the literature [36].

MPC CO2 performs well both in the winter and summer configurations, reaching marginal CO_2 emissions savings of 11% and 22% respectively in both seasons. These results are however mostly achieved thanks to a reduction of the energy use which leads to a slight degradation of the occupant's thermal comfort, especially in cooling mode (see next section on this topic).

The RBC configurations do not perform satisfactorily when only looking at the costs or emissions reductions. In fact, by keeping the same lower bound for the temperature set-point than in the reference case, the modulation has to operate at higher levels, which causes an increase in the energy use and in the overall temperature levels in the dwelling. RBC Cost thus increases the costs by almost 50% in heating mode, although it performs very well in shifting all the loads to lower price periods. In cooling mode, since the reference case is far from the cost optimal, RBC Cost manages to keep the cost increase at +7%, even though the increase in electricity use is actually +64%. All RBC configurations improve considerably the comfort conditions, therefore a reduction of the set-point is considered as further improvement and will be tried out with simulations in the next chapter.

Table V.2. Integrated energy values of the heating experimental cases.

HEATING		**Ref.**	**MPC Cost**	**MPC CO2**	**RBC Cost**	**RBC CO2**
Electrical energy use	[kWh]	*38.3*	38.5	35.2	60.8	48.7
	[%]		+0.56%	-8.16%	+58.9%	+27.3%
Thermal energy produced for SH	[kWh]	*63.5*	72.5	61.6	126.7	100.7
	[%]		+14.2%	-2.93%	+99.7%	+58.6%
Thermal energy produced for DHW	[kWh]	*29.1*	22.7	25.3	31.2	27.5
	[%]		-21.9%	-13.0%	+7.0%	-5.6%
Total thermal energy produced	[kWh]	*92.6*	95.2	86.9	157.8	128.1
	[%]		+2.8%	-6.1%	+70.5%	+38.4%
$COP_{avg,SH}$	[-]	*2.74*	3.41	3.50	2.77	2.94
	[%]		+24.5%	+27.7%	+1.2%	+7.3%
Total thermal energy used	[kWh]	*101.0*	100.9	88.6	127.2	122.6
	[%]		-0.1%	-12.3%	+25.9%	+21.4%
Cost of electricity use	[€]	*3.61*	**3.58**	3.51	**5.39**	4.87
	[%]		**-0.84%**	-2.64%	**+49.4%**	+35.1%
Marginal CO_2 emissions savings	[$kgCO_2$]	*10.7*	+0.23	**-1.16**	+6.32	**+2.21**
	[%]		+2.11%	**-10.9%**	+59.2%	**+20.7%**
Primary energy	[kWh]	*84.6*	85.9	76.7	136.0	106.8
	[%]		+1.6%	-9.3%	+60.8%	+26.3%

Table V.3. Integrated energy values of the cooling experimental cases.

COOLING		**Ref.**	**MPC Cost**	**MPC CO2**	**RBC Cost**	**RBC CO2**
Electrical energy use	[kWh]	*35.8*	31.8	27.8	58.8	64.1
	[%]		-11.2%	-22.4%	+64.3%	+79.2%
Thermal energy produced for SC	[kWh]	*65.6*	58.5	36.2	129.3	143.5
	[%]		-10.9%	-44.8%	+96.9%	+118.7%
Thermal energy produced for DHW	[kWh]	*23.4*	21.8	21.6	22.7	22.5
	[%]		-6.7%	-7.7%	-3.0%	-3.8%
Total thermal energy produced	[kWh]	*89.1*	80.3	57.8	152.0	166.1
	[%]		-9.8%	-35.1%	+70.6%	+86.5%
$COP_{avg,SC}$	[-]	*2.69*	3.07	2.96	2.57	2.55
	[%]		+14.0%	+10.0%	-4.6%	-5.4%
Total thermal energy used	[kWh]	*110.2*	108.5	105.1	148.2	134.5
	[%]		-1.6%	-4.6%	+34.5%	+22.1%
Cost of electricity use	[€]	*3.33*	**2.09**	2.56	**3.58**	6.05
	[%]		**-37.4%**	-23.1%	**+7.4%**	+81.5%
Marginal CO_2 emissions savings	[$kgCO_2$]	*8.39*	-0.70	**-1.87**	+7.24	**+6.51**
	[%]		-8.3%	**-22.3%**	+86.3%	**+77.6%**
Primary energy	[kWh]	*77.0*	69.5	59.8	132.6	136.9
	[%]		-9.7%	-22.3%	+72.3%	+77.9%

It should be noted that the thermal energy produced by the heat pump for DHW is an estimation, since it could not be measured directly. In fact, when the heat pump operates in this mode, it only uses its internal circuit to warm up the TES tank (see Figure III.3), and therefore no sensors can be placed in the laboratory to record what is happening. The own sensors of the heat pump do record the temperatures at the supply and return side as well as the water flow rate, but these measurements are highly uncertain to obtain a reliable thermal power measurement (temperature measurement with a resolution of ± 1°C). For this reason, thermal energy produced for DHW is estimated along the three days of the experiment with a thermal energy balance, as shown in Equation V.1.

$$Q_{th,DHW,\Sigma} = Q_{extr} + Q_{losses} + \Delta Q_{th,TES} \tag{V.1}$$

Where Q_{extr} is the extracted heat from the tank, measured accurately in the DHW thermal bench of the laboratory, Q_{losses} are the thermal losses of the tank, estimated to a constant 47.3 W as per catalogue data, and $\Delta Q_{th,TES}$ is the difference of energy content in the tank between the end and the beginning of the experiment.

3 Efficiency of the heat pump operation

Next, the efficiency of the heat pump operation is analyzed in details. On Figure V.3, the thermal energy produced and the electrical energy used for space heating/cooling[1] are represented, as well as their ratio, the average COP or EER. The MPC configurations operate the heat pump at a higher efficiency for space heating and cooling, reaching around 3.5 for the heating COP and around 3 for the cooling EER, while the RBC configurations operate at a same level of efficiency than the reference case.

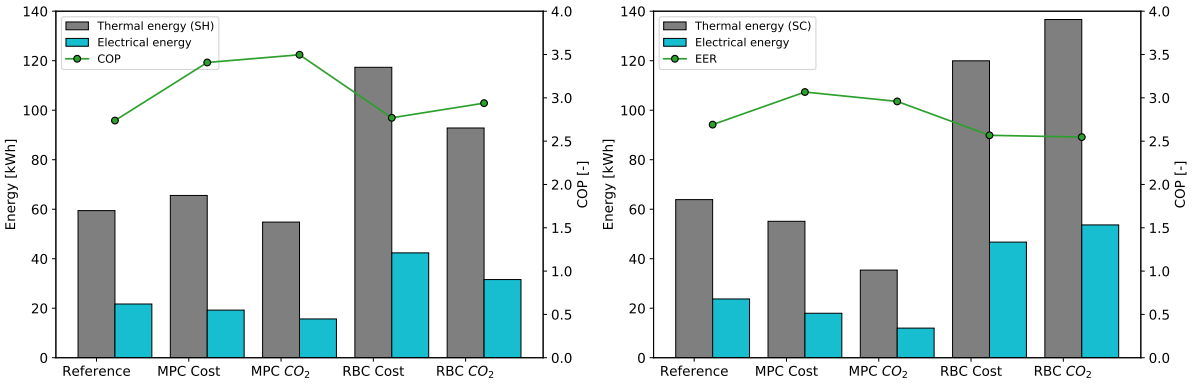

Figure V.3. Thermal energy produced, electrical energy used and COP/EER during space heating/cooling operation.

The MPC controller can make use of its knowledge about the future to operate the heat pump in the moments where the efficiency is potentially higher. This is illustrated in Figure V.4 where the box plots of the supply temperature and the ambient temperature during the space heating/cooling operation are represented. In heating mode, the MPC controller operate the heat pump at a lower supply temperature, with a median of around 43°C, while the RBC controller on the other hand operates it at higher supply temperature of median 50°C. This explains partly the better COP observed in these experiments. Furthermore, the MPC controller chooses periods where the ambient temperature is warmer, especially for MPC CO2, with a median around 8°C while the reference case median is around 6°C. The RBC configurations operate in a very similar manner than the reference case. As

[1]The analysis is constrained to space heating and cooling because of the uncertainty regarding the thermal energy produced in DHW mode.

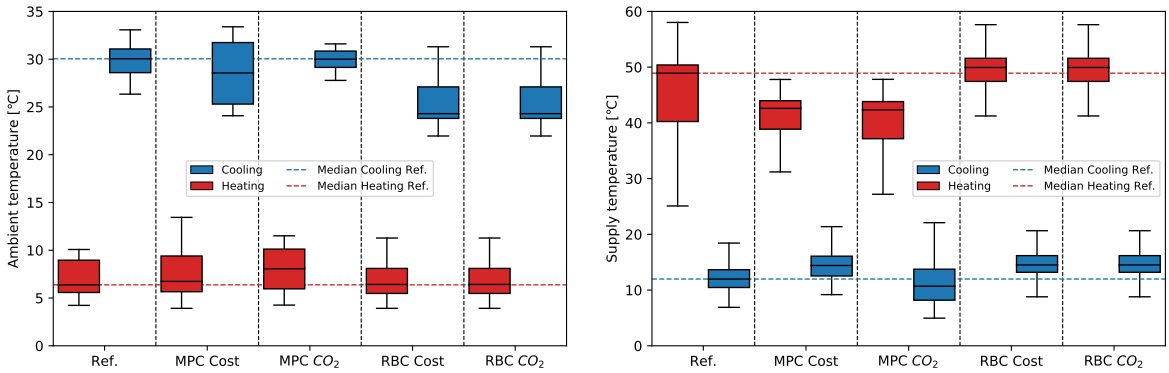

(a) **(b)**

Figure V.4. (a) Box plots of the ambient temperature distribution, only during space heating/cooling operation. (b) Box plots of the supply temperatures distribution, only during space heating/cooling operation.

previously shown in chapter III, both a lower supply temperature and a milder outdoor temperature have a positive effect on the COP.

The analysis differs a little in cooling mode: in that case, MPC Cost and the RBC controllers operate at a slightly higher supply temperature, which is beneficial. On the other hand, MPC CO2 uses a slightly lower supply temperature, which explains why its efficiency is not as high as MPC Cost. The ambient temperature has little effect on the efficiency in cooling mode as shown in chapter III, although the RBC configurations operate the heat pump when the outside temperature is cooler.

4 Energy flexibility and load shifting

The core of the implemented flexibility control strategies consists in shifting the thermal loads of the building towards periods of lower electricity price or grid CO_2 emissions. To analyze if this shifting effectively occurs and in which proportion, Figure V.5 is plotted: it represents the breakdown of the electricity use of the heat pump according to the low, medium or high penalty periods (price or emissions). Additionally, the consumption is split between the operation modes of the heat pump: space heating (SH) or cooling (SC), DHW and standby mode (SB). In this way, the load shifting can be analyzed in details.

Firstly, it is observed that in heating mode, the reference case uses most of the electricity in the low price periods. MPC Cost manages to increase a little the energy use in these hours, while RBC Cost increases it significantly, while reducing especially the DHW operation in high price hours. The reference case also uses most of the energy in high emissions periods, and MPC CO2 reduces this amount, although without increasing the energy used in low emissions periods. On the other hand, RBC CO2 increases the energy use in low emissions periods without decreasing the high emissions periods consumption.

In cooling mode, the reference case uses most electricity at high price hours (afternoon periods, where the cooling demand is highest but also the price). MPC Cost effectively transfers this energy use to the low price hours, almost eliminating space cooling operation when the price is high. RBC Cost also provides this effective load shifting, although dramatically increasing the energy use in the low-price hours and resulting in a higher energy use in total. The reference cooling case also uses most energy in low emissions hours. MPC CO2 nonetheless manages to eliminate the space cooling operation in high emission hours, without increasing the low emissions periods operation. RBC CO2 on the other hand increases dramatically the energy use in low emissions hours, while also slightly increasing it in the high emissions hours, resulting in a poor performance.

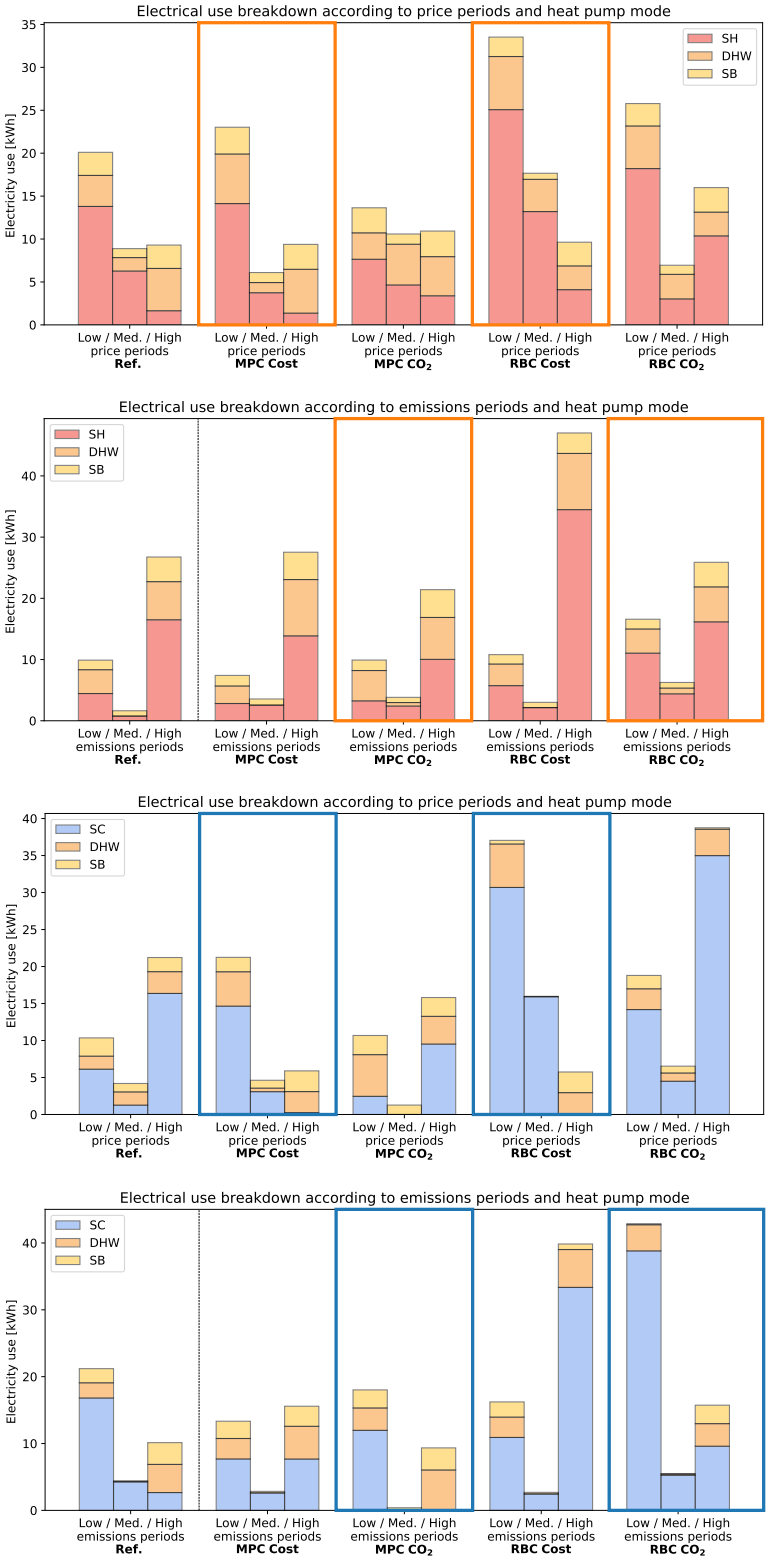

Figure V.5. Breakdown of the electricity use according the the price or emissions periods. The most relevant graphs have been highlighted by color rectangles: MPC Cost and RBC Cost when analyzing the price periods, MPC CO2 and RBC CO2 when analyzing the emissions periods.

These observations are reflected in the analysis of the flexibility factors, as shown in Figure V.6. In heating mode, FF_{cost} is increased from 0.37 in the reference case, to 0.42 by MPC Cost, and to 0.55 by RBC Cost. Similarly, FF_{CO_2} is increased from -0.46 in the reference case to -0.37 by MPC CO2 and -0.22 by RBC CO2. All strategies therefore operate a load shifting in their desired directions (i.e. towards periods of lower penalty), with a higher amplitude achieved by the RBC controllers.

In cooling mode, the reference case has a low FF_{cost} of -0.34. MPC Cost manages to increase this value to 0.57, and RBC Cost to 0.73: both controllers thus achieve a significant load shifting, with a higher performance for the RBC. On the other hand, $FF_{CO2} = 0.35$ in the reference case, and MPC CO2 fails to increase this value, instead it slightly decreases it at 0.32. RBC CO2 manages to increase it but by a small margin, reaching the value of 0.46.

In summary, it is observed that the RBC configurations operate a more radical load shifting, which results in a general increase of the energy use, while the MPC configurations have a milder but more controlled effect. It is also noted that the control strategies have opposite behaviors: when FF_{cost} is increased, FF_{CO_2} is decreased, and vice-versa. This is due to the fact that the two penalty signals have symmetric shapes, the peaks of the price signal corresponding approximately to the valleys of the CO_2 signal. Hence shifting the loads to the low price hours also means shifting them to the high emission hours, and it will thus result very difficult to reach both objectives at the same time.

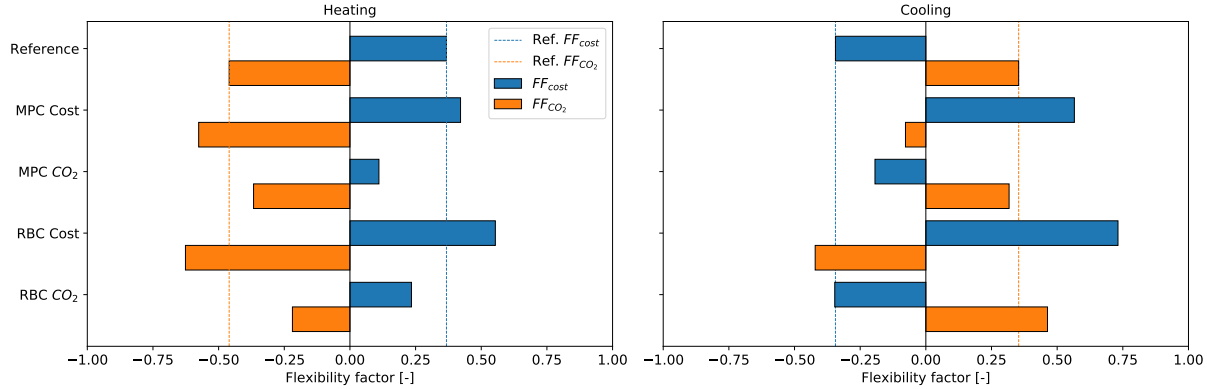

Figure V.6. Flexibility factors relative to cost or emissions, both in heating and cooling modes. The flexibility factors of the reference cases are highlighted with dashed lines to clearly display in which direction each controller modifies the factor.

5 Comfort

Thermal comfort is guaranteed in the RBC configurations by the deadband zone around the set-point, and in the MPC framework by the introduction of temperature range constraints on the indoor temperature. These constraints are softened to increase the robustness of the controller, therefore it is important to verify that comfort is not jeopardized during the actual operation of the systems. The comfort analysis is represented in Figure V.7, with the percentages of time where the indoor operative temperature stays within the bounds defined in the standard [140]. These bounds take different values seasonally: Cat.I corresponds to the interval 21-25°C in winter, and 23.5-25.5°C in summer, Cat.II to the interval 20-25°C in winter and 23-26°C in summer.

It can be firstly observed that all the RBC configurations provide a great increase of the comfort conditions, with 100% of the time spent in Cat.I in all cases except RBC CO2 in heating mode with 70% of the time. This partly explains the poor performance of the RBC controller in the other aspects, notably the reduction of the costs or emissions.

The MPC configurations have a more mitigated effect on the thermal comfort of the occupants: in heating mode, MPC Cost does show some improvements, with 35% of the time spent in Cat.I (against 15% in the reference case) while MPC CO2 remains at a similar level than the reference case. In cooling

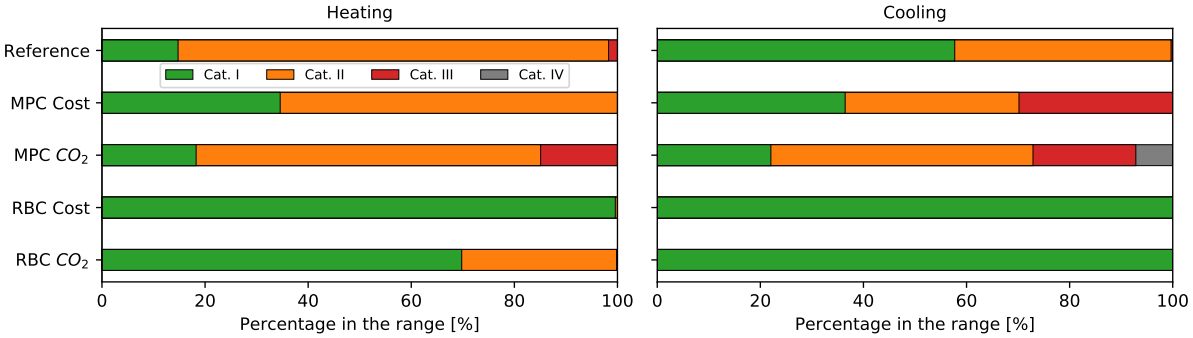

Figure V.7. Comfort analysis of the experimental cases.

mode, the MPC configurations cause a slight degradation of the comfort conditions, with around 30% of the time spent in Cat. III, against 0% in the reference case. In the case of MPC CO2, 7% of the time is even spent in Cat. IV, which is an unacceptable level of comfort. This suggests that the weighting coefficient for the comfort objective in the MPC cost function should be increased a little. In the cooling mode, it can be concluded that the excellent results of MPC in terms of flexibility were achieved at the cost of some degradation in the thermal sensations of the occupants. The difficult trade-off between the comfort of the occupants and the increased flexibility, as reflected in the multi-objective function of the MPC, is thus perfectly illustrated by these results.

6 Conclusions and discussions on the practical implementation of MPC

6.1 Conclusions on the experimental results

Each of the studied controller have some positive and negative effects, depending with which KPIs they are evaluated. To have a more complete overview, each case is now analyzed as a whole, and suggestions for improvements are drawn.

In heating mode, the 4 controllers performed as follows:

- **MPC Cost**: although this configuration operates some load shifting and improves both the efficiency of the heat pump and the comfort conditions, it barely managed to reduce the costs. It is therefore suggested to reduce the α_2 coefficient for comfort, since more flexibility can only be obtained by being less strict on the comfort constraints.

- **MPC CO2**: this configuration performed well, it managed to reach 11% lower CO_2 emissions than the reference case. This result was achieved by shifting the loads towards low emission periods, which coincidentally also correspond to the periods where the operation of the heat pump is more efficient (higher ambient temperature inducing a higher COP). The controller had little effect on the comfort conditions and can thus be kept in its current configuration.

- **RBC Cost**: this configuration operated a radical load shifting towards periods of lower prices. To avoid using energy during the high price periods, it had to compensate by overcharging the building during the low price hours, which resulted in an increased energy consumption, and for this reason the costs were not decreased but instead increased by 49%. Furthermore the comfort conditions were largely improved which is not necessarily needed, therefore the overall set-point of this configuration should be decreased.

- **RBC CO2**: very similarly, this configuration shifted almost all the loads towards periods of low carbon emissions, but still increased the energy use, and consequently the emissions by 20.7%.

Its set-point should thus also be decreased since the occupants do not require a comfort of Cat.I for 100% of the time.

In cooling mode, the 4 controllers performed as follows:

- **MPC Cost**: since the reference cooling case was largely suboptimal with regards to the energy costs, MPC Cost managed to efficiently produce a load shifting towards periods of cheap electricity, reaching a very satisfactory value of 37% cost savings. Part of this performance also derives from operating the heat pump at a higher efficiency, namely when the outdoor temperature was cooler and at higher supply temperatures. Only a slight degradation of comfort was observed, therefore this configuration can be kept as is.
- **MPC CO2**: this controller also performed well, reaching 22% savings in the carbon emissions, even though its load-shifting was limited. However, some incursions of the zone temperature occurred outside of the acceptable comfort range (Cat. IV during 7% of the time), therefore the α_2 coefficient for comfort should be slightly raised to always stay within at least comfort Category III.
- **RBC Cost**: this configuration produced a radical load shifting, eliminating the space cooling load during the high price hours. This provision of energy flexibility caused an important increase of the electricity use of 64%. This extra energy use mostly occurred during low price hours, therefore the energy costs was only increased by 7%: the "value for money" of the heat pump was improved, but without reducing the absolute costs. The comfort conditions were significantly improved (100% of the time in Category I), suggesting that there is some margin to increase the zone temperature set-point in order to improve the performance in terms of flexibility.
- **RBC CO2**: this controller performed relatively poorly, because the reference cooling case was already close to optimal regarding the CO_2 emissions. The energy use was significantly increased during low emission hours, which resulted in a better FF_{CO2} value, but the absolute emissions were increased by 77% compared to the reference case. The set-point for room temperature should be frankly decreased to hope for a better performance in terms of flexibility, since the comfort conditions were again at 100% in Category I.

Overall, the analyzed results revealed that the RBC controllers could be improved. On the other hand, the implemented MPC strategies had a positive performance, although with a lower effectiveness than expected. In fact, in some cases the savings were not as important as expected from similar studies in the literature, where savings of 7 to 35% have been reported [36]. For instance in the MPC Cost for heating, the savings were almost nonexistent. The MPC configurations can of course be improved, as will be seen in the next chapter with co-simulations.

However, there are also other reasons which can explain the discrepancies observed between the experimental results and the expected performance. In fact, the present study implemented the MPC with an actual heat pump, while most of the existing literature relied only on simulations. Working with real systems enables to obtain more realistic results and to reveal certain bottlenecks that appear when interfacing the supervisory controller with the physical system, which includes its own local controller. Two of these effects are discussed in the following sections: the DHW tank charging control and the transient effects (ramping especially). Such practical challenges could only be brought up by experimental studies (or alternatively simulation studies with very detailed transient models), and they are therefore considered as valuable learnings and part of the work output.

6.2 Practical implementation of MPC - DHW tank charging

It was seen in the flexibility analysis that the MPC strategies sometimes failed to shift the DHW load to the low penalty periods (see Figure V.5), and even sometimes shifted this load to high penalty periods. This adverse effect can partly be explained by the interfacing between the supervisory and the local controllers of the heat pump. The command to activate the DHW tank charging through the Modbus gateway is called "Control DHW Run/Stop" in the manufacturer manual. Sending a 0 to this

input effectively prevents the DHW operation of the heat pump. However, sending a 1 does not automatically provoke the tank charging: it only corresponds to an "availability" of the DHW operation, the built-in controller then determines if it needs to be activated, based on the temperature in the tank. The local controller considers the actual set-point and a negative deadband of 5°C which can be set in the local controller (5°C is the minimum): for instance, if the set-point is 55°C and the water in the tank is 51°C when the activation signal for DHW is sent, the heat pump will not start. This is problematic if the MPC intends to precharge the tank at some times where the local controller would not deem it necessary. The principle of MPC to utilize the TES by overheating it in some favorable periods and discharging it at others periods is thus hindered by the interaction with the local controller. This problem does not occur in the other circuit of the heat pump which supplies SH/SC: the equivalent command is called "Control Circuit 1 Run/Stop", and sending a 1 to this input always results in an activation of the heat pump.

An example of the DHW charging bottleneck is illustrated in Figure V.8. On the top graph, the SC binary command is represented, on the second graph the DHW binary command, on the third graph the response of the heat pump in terms of its compressor frequency, and in the bottom graph the tank temperature. One can observe that the first 5 activation requests (4 of SC, 1 of DHW) are correctly followed by an activation of the heat pump compressor. The 6th requested activation (DHW) does not result in an actual operation of the heat pump: the water temperature at that moment was 50°C, therefore not sufficiently low for the built-in controller to order the DHW tank charging. As a result, the MPC must reschedule the tank charging at the subsequent iterations, and two later DHW activations are thus observed. This can pose a problem to the performance of the MPC: if the tank charging was initially planned at a low-penalty period, the reschedule could occur at less favorable periods in terms of price or CO_2 emissions. This partly explains the poor performance of the DHW load shifting and the fact that it is sometimes shifted to high penalty periods.

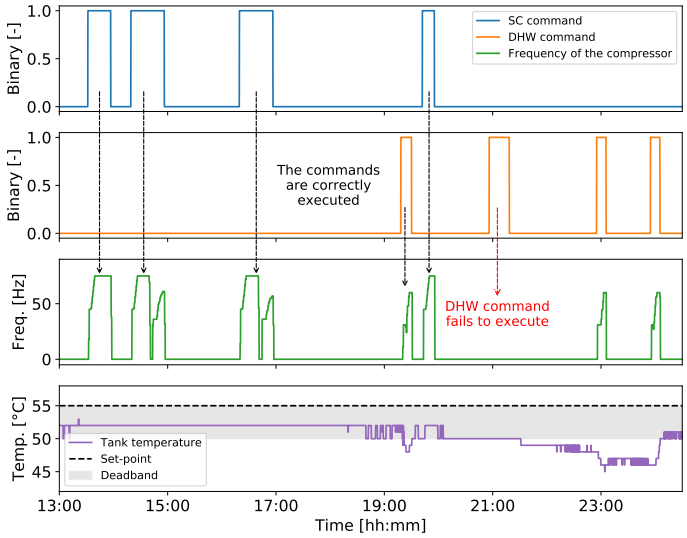

Figure V.8. Example of non-execution of the DHW production command. This particular case comes from [52], where the set-point for DHW was higher, at 55°C.

On average, the charging of the DHW tank occurred 17 times over the studied periods of 3 days. A DHW command was sent on average 12 additional times and ignored by the local controller of the heat pump. This situation thus occurred quite frequently, which explains why the MPC struggled to shift the DHW loads. This offers as valuable learning that the implementation of an MPC controller with a real heat pump is not a straightforward process. Oftentimes, the functioning of the local controllers built in the machine are not described clearly by the manufacturer, and the developer must therefore consider the heat pump as a black box and realize tests to observe its behavior in-situ. This increases the development costs of the controller and its implementation, while they are already high due to the required modelling (60% of the costs mentioned in [165]).

Potential solutions to overcome the DHW charging limitation include:

- Instead of using the set-point determined by the MPC solution, always set it to the maximum (55°C for instance). The modulation potential of the MPC would be lost, and the tank might be overheated for its actual use, but the DHW charging should occur with more probability.
- The deadband could also be reduced. In the present case, the minimum is 5°C so it is not possible, but other heat pump models might let the installer set smaller values. Such protection enables to avoid too many switching of the DHW charging mode, but this can be managed in other ways by an MPC controller.
- Another possibility would be to choose a heat pump where an explicit control of the DHW charging is possible, or to use other inputs (such as the booster or the anti-legionella setting, but these are made for other purposes and generally use the electrical resistance to provide fast heating at high temperatures).

6.3 Practical implementation of MPC - Transient and dynamic effects

The transitory phases constitute another aspect proper to the dynamics of a real heat pump operation. The MPC controller computes an optimal plan considering that the heat pump will effectively deliver heat at the correct set-point, with the desired constant thermal power. However, many dynamic effects occur in reality which make the actual operation differ from the MPC scheduled plan.

To illustrate this point, Figure V.9 is plotted. On the top graph, the plan of the MPC is shown: the controller scheduled to operate space heating during 48 minutes, at a thermal power of around 6 kW. The measured thermal power (calculated with the temperature lift and the mass flow rate) is also represented, and a clear discrepancy can already be observed. On the second graph, the supply and return temperatures are plotted, on the third graph the frequency of the heat pump compressor and on the bottom graph, the zone temperature in the building (both predicted by the MPC and as happened in the actual simulation) is represented.

In this example, the operation of the space heating activation is separated in 5 phases highlighted by different background colors. The last phase is the quasi steady-state during which the heat pump operate according to plan: the measured and planned thermal powers coincide, and the heat pump supplies water at a temperature close to the desired set-point of 48°C. This operation confirms that the heat pump performance has been represented correctly, since its model was based on points measured in steady-state too. However, before to reach this steady-state operation, the systems go through other successive phases, which are not anticipated by the MPC.

Firstly, a delay is observed before the heat pump reacts, and the compressor only starts few minutes after the commands are sent. Secondly, after the compressor has started running, a ramping phase occurs: the heat pump starts with a plateau due to its internal control, and then increases its power gradually. Since the water had cooled down since the last activation, the system starts a lower temperature and must ramp progressively to achieve the desired set-point. However, this increase is slow and takes at least 15 minutes in the present case. Contrary to a boiler, the temperature lift of a heat pump is rather limited (around 5°C normally), and thus the system must “wait” for the return temperature to also increase so that the supply temperature can reach the desired value. At the end of the ramping phase, the compressor frequency has reached a maximum and therefore the actual thermal power is significantly higher than anticipated by the MPC. This observation partly explains why the delivered thermal energy is increased in most MPC cases. During the third phase, an overshoot effect occurs: the supply temperature overcomes the desired set-point and thus the heat pump starts to decrease the compressor frequency. However, due to the inertia of the systems and the delayed internal control of the machine, the supply temperature still reaches the value of a protection deadband (+5°C above the set-point), causing a shutdown of the compressor, which is the fourth phase. The shutdown lasts around 5 minutes, and then the compressor is switched on again and starts the steady-state phase.

The transient phases partly explain why the MPC strategies have a relatively limited performance. For instance, if the space heating activations are short, the heat pump stays in the transient phases

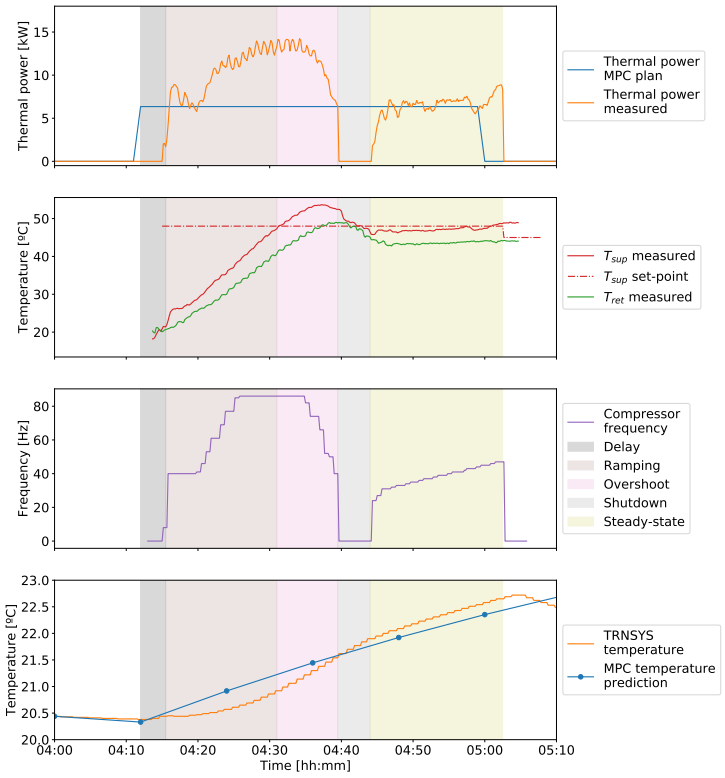

Figure V.9. Example of an activation of space heating, where the delay and the ramping effects can clearly be observed.

and do not reach the steady state, therefore its delivered power is higher than anticipated and this causes the final increase in thermal energy observed in most cases. The fluctuations in power could also cause trouble for direct control schemes of demand response with heat pumps: if an aggregator or utility requires a certain level of power from the heat pump load during a fixed period, they must be aware that this power might be delayed or not guaranteed during the whole period (shutdown or cycling).

These transient phases only explain partly the performance, other phenomena can play a role in the observed effects. Notably, the heat pump operates at milder temperatures as demonstrated in Figure V.4 and this displacement of the operating point to another region of the performance map can also cause an increase of the thermal power with respect to the reference case. The inability of the compressor to modulate its output below 30 Hz additionally participates in increasing the on-off cycling and to generate discrepancies compared to the desired MPC plan.

To quantify the actual effect of the thermal power overshoot on the overall dynamic behavior, Figure V.10 is plotted. It represents the thermal powers (planned by the MPC and measured) in the MPC Cost case over 24 hours, compared to the reference case. The increase of thermal energy compared to the MPC plan is clearly visible: the MPC solution required to deliver only 16.7 kWh during this day, while 24.4 kWh were actually supplied to the building, which represents an increase of 45%. Furthermore, in this case space heating is activated 4 times in the reference case, and 8 times in the MPC case: doubling the number of cycles results in a higher impact of the overshooting effect on the overall performance.

The overshoot and transient phases also occur in the reference case, however since the thermostat controller do not work in a predictive manner, this mismatch does not affect it as much as in the MPC cases. For that case, the thermostat shuts down the heating when the delivered energy equals what is needed to reach the desired set-point, thus if the heat pump delivers more heat, the thermostat will stop before. On the other hand, a predictive controller makes a plan beforehand and expects it to be complied with, therefore the unexpected transient effects have a greater influence on it.

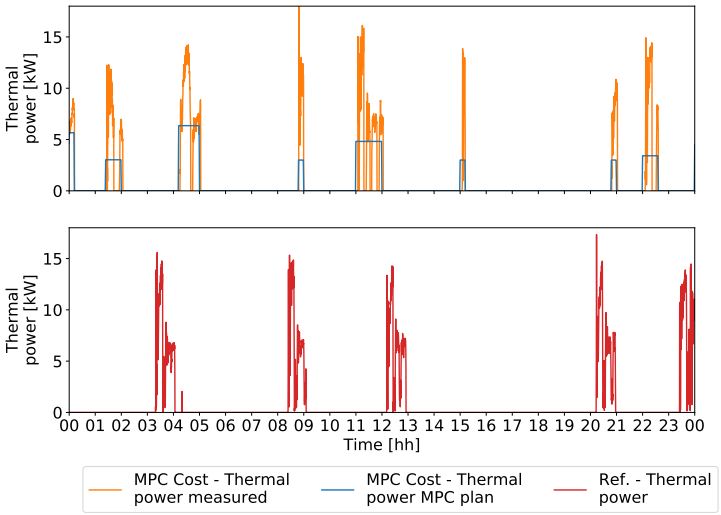

Figure V.10. Comparison over one day between the reference case and one MPC case (MPC cost).

The main issue regarding the start-up phase is that it is difficult to model within the MPC framework. The model is correct in steady-state as previously mentioned, only a correction is needed to account for the successive transient phases when the heat pump is switched on. Potential solutions include:

- Applying a constant coefficient to consider the excess thermal power of the start-up transitory phases. This coefficient should reflect the ratio between the delivered energy during a total activation period and the planned energy (integrals of the two curves on the top graph of Figure V.9). In this way, the set-point sent to the heat pump will be slightly lower, and the delivered thermal energy should match better with the MPC plan.
- Increasing the discretization time step of the MPC might also improve the performance: in this way, the heat pump will stay activated during longer periods and thus the start-up phase will have a lesser importance overall.
- Encouraging longer periods of heat pump activation can also be enforced in several ways, for example increasing the minimum up time constraint, or increasing the relative importance of the smoothing term in the multi-objective function. The latter would provoke the heat pump to operate for longer periods since too many switching will be highly penalized. The steady-state will thus last longer and take a larger proportion compared to the transient phases, reducing the influence of the latter.

Chapter VI

Results of the co-simulation studies

After having performed the experimental tests, simulation-only studies have been carried out. As a first step, the heat pump model developed in chapter III was further validated against the data of the experimental cases. After that, different configurations of the flexibility controllers were explored and tuned, and they were subsequently tested within the co-simulation framework. The boundary conditions and the performance indicators used in these analysis were the same than for the experimental cases of the previous chapter, enabling a thorough comparison.

1 Boundary conditions, reference cases and tested configurations

The boundary conditions used for the co-simulation tests are the exact same than in the experimental ones. The operation of the heat pump is simulated over the same three days in winter and summer, from the 24th to to the 26th of February 2018 and from the 8th to the 10th of July 2018 respectively, with the corresponding weather and penalty signals. The description of these boundary conditions is thus not repeated here, the reader is referred to section 1 of chapter V for further details.

1.1 Reference cases

The reference cases for heating and cooling were simulated similarly to the experimental reference cases. This gives an opportunity to perform a second validation of the heat pump detailed model, by comparing the values obtained in the co-simulation with the ones obtained in the laboratory setup. This comparison is presented in Figure VI.1, where the left part of each graph shows side to side the co-simulation values and the experimental values in heating mode, and in cooling mode on the right side.

Analyzing the heating case, it appears that the model underestimates slightly the energy use compared to the heat pump in the experiment. Both the thermal energy and the electrical energy have a little lower values, but stay in the same order of magnitude than what was observed experimentally. As a consequence, the costs and emissions are also slightly lower. It should be noted that a perfect fit is difficult to attain, since the model, and particularly the building envelope part, are not found exactly in the same state at the beginning of the simulation and of the experiment. In fact, a few days of simulation are always run beforehand, to bring the building to a preconditioned state at the start of the analyzed period. The heat pump model is different also during this pre-simulation, therefore when the experiment/simulation starts, the temperature states might differ. However, it is observed that the efficiency of the heat pump operation, displays very similar values than in the experiments.

In cooling, the underestimation of the energy levels is more severe. The amount of produced cooling is slightly lower than in the experiment (-5%), however the electricity needed presents an even higher reduction, of around 15%. This means that the model slightly overestimates the efficiency of the heat pump, as can be seen in the bottom right graph of Figure VI.1. Two main factors can ex-

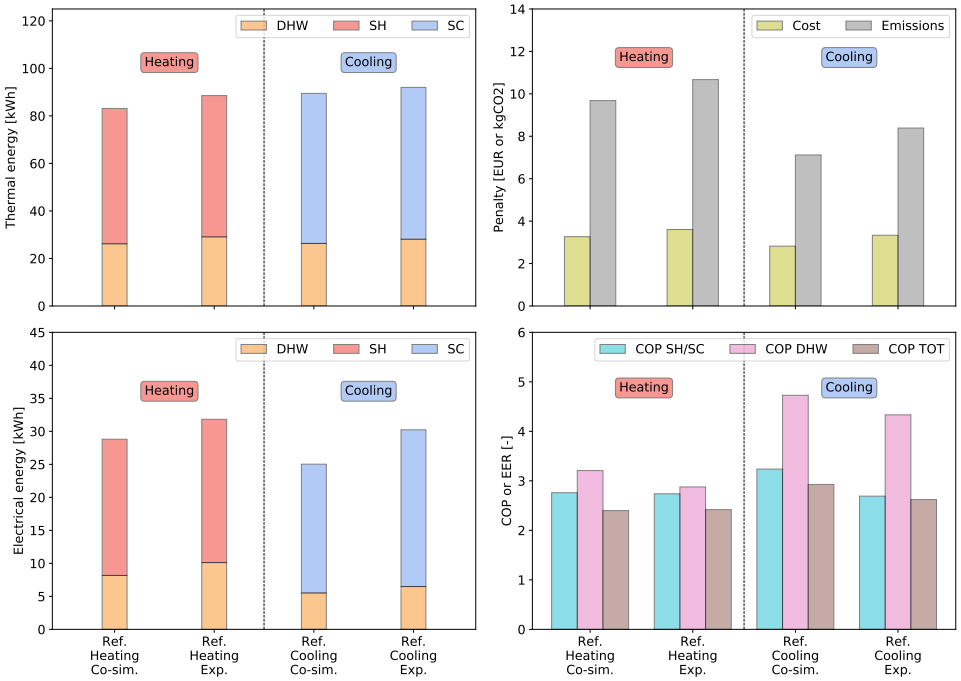

Figure VI.1. Validation of the model with the experimental data in the two reference cases.

plain this. The first reason concerns the model for the production of DHW: for this part, the model of the heat pump made for the heating mode was used. However this model was fitted using the static points data of cold season, with outdoor temperatures ranging from -7 to 12°C, according to the standard [142]. The model is therefore valid mainly in this range of outdoor temperatures. Roughly, the model shows that the COP increases with the outdoor temperature. However in the cooling season, the outdoor temperature reaches 20 to 35°C, and the heat pump still runs in heating mode to produce DHW. In this range of outdoor conditions, the COP does not increase as much with the ambient temperature, it tends to saturate and to still increase, but in different proportions. The extrapolation of the model for warmer weather thus provokes this overestimation of the COP. The second reason concerns the operation in space cooling mode: it was observed in the experiment that since the cooling demand is relatively small, the compressor of the heat pumps turns on and off frequently when the machine operates in this mode. This provokes a reduction of the efficiency in the experimental results. In theory, this efficiency degradation is also included in the model, since the static points at low load presented this on/off behavior and were averaged to take it into account. It appears that the frequent on/off cycling causes a higher degradation of the COP in cooling mode for the real heat pump, due to the losses at every start-up and the uninterrupted pumping operation during the off periods of the compressor. An additional degradation coefficient $C_c = 0.9$ could be implemented to reflect this behavior: this is the default value suggested by the standard EN14825 [143]. This correction was not implemented, as the present work focuses on the improvements of certain control strategies relatively to a reference case, less so on the absolute values of the efficiency.

Despite the small discrepancies observed between the simulation and the real heat pump experiments, the overall dynamics of the system are well captured by the model. Selected time series are represented in Figure VI.2 to illustrate this point. The operation of the heat pump is sometimes shifted a bit in time, notably because of the different initial state. However, it is observed that the simulated compressor works at levels of frequency close to the experimental cases, that the activations of the heat pump occur at similar moments and for the same duration, and the evolution of the temperatures is also very similar. These observations enable to consider the detailed heat pump model as satisfactory for the purpose of the present work, and it will thus be used for the further co-simulation case studies.

1.2 Tested configurations

The detailed model of heat pump in TRNSYS has been validated both as a stand-alone model in chapter III, and as a system integrated in the overall building model in the previous section. This double validation provides guarantees about the reliability of the model, and ensures that said model reproduces the behavior of the real heat pump in a satisfactory manner, at least for the purpose of the present thesis. Co-simulations can then be run without the costs and physical limits of laboratory testing, in a wider range of configurations than in the experimental tests presented so far.

Looking back at the experimental results, it appeared that the most difficult task in tuning the controller resides in adjusting the balance between the comfort and the provision of flexibility. For this reason, in the co-simulation studies, this trade-off has been improved, and the comfort conditions were further tuned in relation with the flexibility objective. In the case of RBC, this can be adjusted by the "normal" set-point during the periods of no modulation. In the case of MPC, it is the weighting coefficient α_2 associated with discomfort that plays this role. Varying these parameters, the selected cases for the co-simulations are presented in Table VI.1.

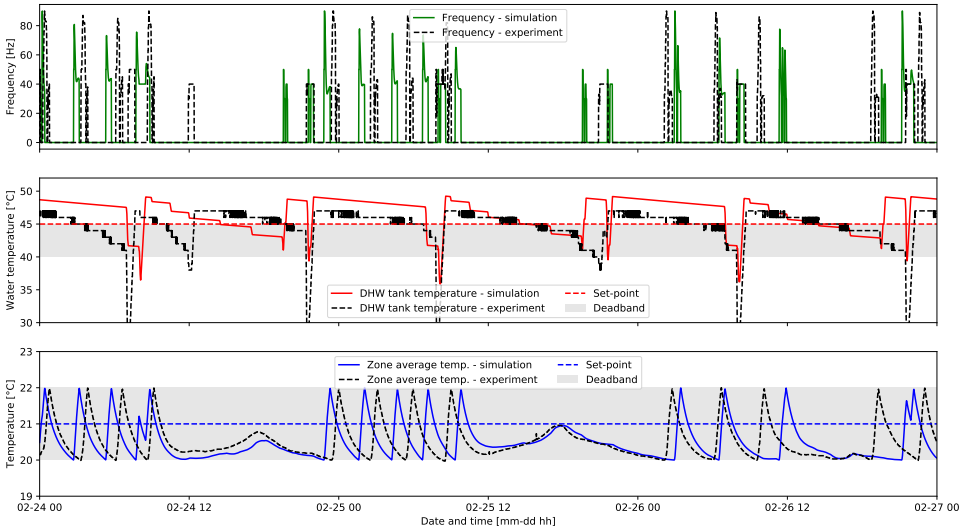

(a) Heating reference case.

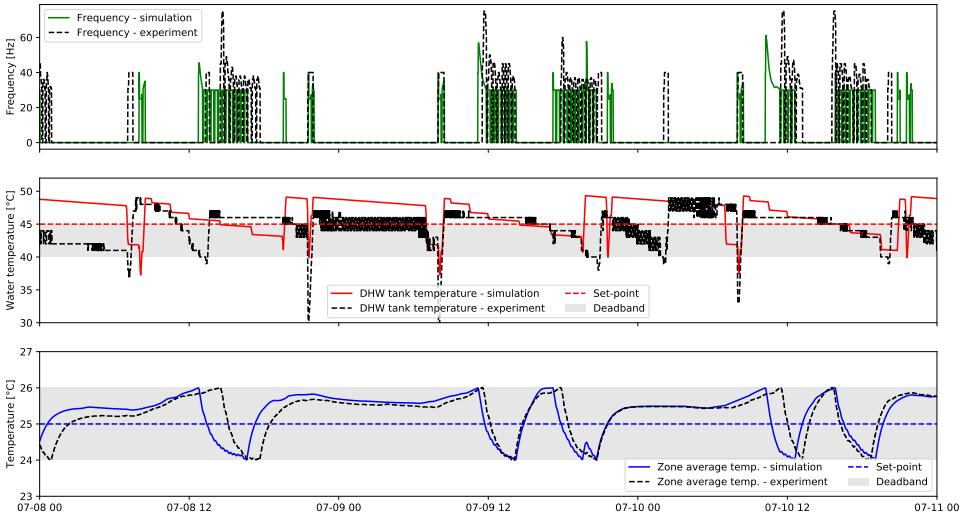

(b) Cooling reference case.

Figure VI.2. Time series comparing the reference cases in the experiments and in the simulation-only framework, in terms of compressor frequency and temperatures in the room and the tank.

In heating mode, for the MPC Cost case, the weighting coefficient for comfort α_ε was decreased from 0.5 tested in the experimental case, to 0.4, since that configuration had barely managed to reduce the costs while improving the comfort conditions. For the MPC CO2, the coefficient was unchanged at 0.15 since this value provided good results in the experiments. In cooling mode, the coefficient was slightly raised for MPC CO2 from 0.15 to 0.155, to avoid degrading too much the comfort conditions as observed in the experiments, where some incursions in the comfort Category IV were observed. The coefficient was unchanged at 0.15 for the MPC Cost configuration.

For the RBC configurations, the adjustment can be made by choosing the "normal" set-point, in the periods where there is no modulation. In the reference cases, this set-point is fixed to 21°C in winter and 25°C in summer, with a symmetric deadband of $\pm$1°C. The thermostat forces the temperature to stay within this deadband. In the RBC cases, so as to provide a certain amount flexibility, it is necessary to widen the bounds between which the temperature is allowed to evolve. "Bounds" here refers to the maximum and minimum temperature that are allowed in a certain configuration. Amplifying the range defined by the lower and the upper bounds can be done in different manners. Three different RBC configurations are thus tested, numbered from 1 to 3:

- RBC1: the critical bound is kept at the same value than in the reference case. The critical bound is the lower one in winter (20°C) and the upper one in summer (26°C), in other words the bound to which the temperature must stay close in order to minimize the energy use. The other bound is moved of 2°C. These bounds are the same one than used in the MPC configurations. This is a very conservative option, since it only allows the temperature to move in a more energy-using direction. RBC1 is the configuration that was previously tested in the experiments.

- RBC2: both temperature bounds are moved symmetrically. The upper bound is raised of 1°C while the lower bound is decreased of 1°C.

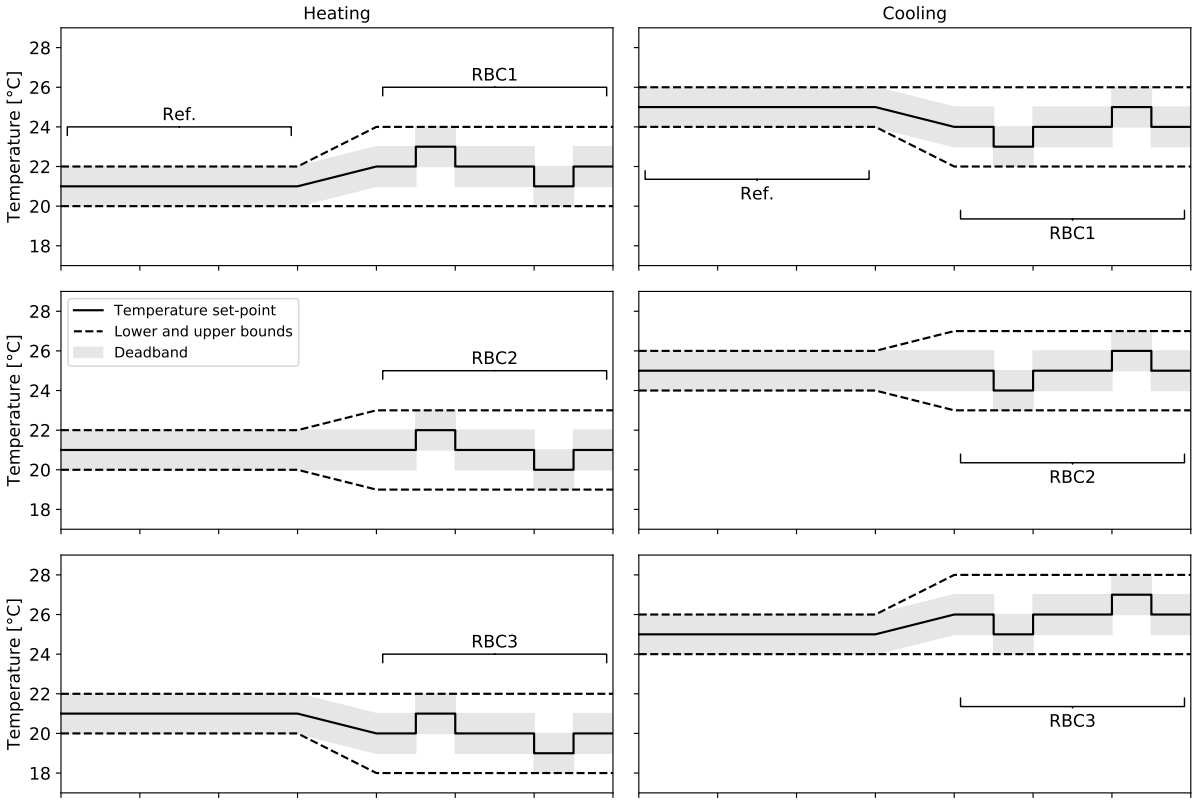

Figure VI.3. Set-points, deadbands and bounds for the tested RBC configurations, in heating (top) and cooling mode (bottom). The notches correspond to the possible upwards and downwards set-point modulation occurring with the RBC controller.

Table VI.1. Cases studied in the co-simulation framework.

Case	HEATING			COOLING		
	"Normal" set-point[1] [°C]	**Lower and upper bounds**[2] [°C]	**Weighting coefficient** α_ε [-]	**"Normal" set-point**[1] [°C]	**Lower and upper bounds**[2] [°C]	**Weighting coefficient** α_ε [-]
Ref.	21	[20, 22]	-	25	[24, 26]	-
MPC Cost	-	[20, 24]	0.4	-	[22, 26]	0.15
MPC CO2	-	[20, 24]	0.15	-	[22, 26]	0.155
RBC1 Cost	22	[20, 24]	-	24	[22, 26]	-
RBC2 Cost	21	[19, 23]	-	25	[23, 27]	-
RBC3 Cost	20	[18, 22]	-	26	[24, 28]	-
RBC1 CO2	22	[20, 24]	-	24	[22, 26]	-
RBC2 CO2	21	[19, 23]	-	25	[23, 27]	-
RBC3 CO2	20	[18, 22]	-	26	[24, 28]	-

[1] The normal set-point when there is no modulation.

[2] In RBC, this interval corresponds to the absolute lower and upper bounds, considering the extreme cases of upwards/downwards modulation plus the deadband of ±1°C. In MPC, it corresponds to the interval of constraints imposed on the output room temperature, which can sometimes be violated depending on the discomfort objective.

- RBC3: the critical bound is moved of 2°C, while the other bound stays at the same value than in the reference case. The upper bound is then 28°C in cooling and the lower bound 18°C in heating mode.

The concept of the three RBC configurations is illustrated in Figure VI.3 for more clarity. All the configurations are then analyzed in the following sections, using the same indicators than in the previous chapter about the experiments.

2 Integrated energy and cost values

The integrated energy values are presented in Table VI.2 for the heating cases. It is observed that the improved version of MPC Cost performed slightly better, reaching cost savings of 4.5%, however the order of magnitude of these savings remain small. As for the RBC Cost configurations, none of them managed to actually reduce the energy costs compared to the reference case, the best one being RBC3 Cost, with only a 4.6% increase. The results of RBC1 Cost can be compared with the experimental results, since the controller had the same configuration: the 55% cost increase observed here in the simulations is coherent with the 49% cost increase seen in the experimental part.

The "CO_2" controllers performed better in the heating season. MPC CO2 managed to reduce the marginal emissions by 15%. RBC1 CO2 did increase them by 19.8% (20.7% in the experiment with the same configuration), while RBC2 CO2 reached an almost similar level of emissions savings than MPC, with namely 11.8% decrease compared to the reference case. RBC3 CO2 achieved the highest level of CO_2 emissions saved, with 35.7%, although this great performance came at the cost of comfort degradation as will be seen later on.

The integrated energy values for the cooling season are presented in Table VI.3. It is first observed that all the cost controllers managed to actually reduce the costs. The savings reach 31.8% for the MPC Cost controller, and from 1.5 to 41.2% for the three RBC Cost configurations. The RBC Cost thus can reach a similar performance than the MPC in that case, although the 41.2% savings of RBC3 Cost are attained at the cost of some comfort degradation.

Regarding the performance of the CO_2 controllers, a clear difference can be seen between the MPC configuration and the three RBC configurations. MPC CO2 reduces the carbon emissions by 10% while none of the the RBCs manages to reach a reduced carbon footprint compared to the reference case.

Table VI.2. Integrated energy values of the heating simulated cases. Firstly the reference case values are presented, then the values for the "cost" controllers (MPC and RBCs), and finally the values for the "CO_2" controllers (MPC and RBCs).

HEATING		**Ref.**	**MPC Cost**	**RBC1 Cost**	**RBC2 Cost**	**RBC3 Cost**	**MPC CO2**	**RBC1 CO2**	**RBC2 CO2**	**RBC3 CO2**
Electrical energy use	[kWh]	*34.7*	36.2	56.0	45.2	35.9	32.2	44.5	32.3	23.1
	[%]		+4.4%	+61.5%	+30.4%	+3.6%	-7.1%	+28.3%	-6.8%	-33.3%
Thermal energy produced for SH	[kWh]	*57.0*	53.4	113.5	83.9	55.1	40.3	88.8	50.9	21.9
	[%]		-6.3%	+99.2%	+47.3%	-3.3%	-29.2%	+55.9%	-10.6%	-61.5%
Thermal energy produced for DHW	[kWh]	*26.2*	31.6	29.0	29.1	29.1	30.6	27.9	28.0	28.0
	[%]		+20.5%	+10.7%	+10.9%	+11.1%	+16.9%	+6.4%	+6.7%	+6.9%
Total thermal energy produced	[kWh]	*83.2*	85.0	142.5	113.0	84.2	79.9	116.7	78.9	50.0
	[%]		+2.1%	+71.3%	+35.8%	+1.2%	-4.0%	+40.3%	-5.1%	-39.9%
COP_{avg}	[-]	*2.40*	2.35	2.54	2.50	2.34	2.48	2.62	2.44	2.16
	[%]		-2.1%	+6.1%	+4.1%	-2.3%	+3.3%	+9.3%	+1.8%	-9.9%
Total thermal energy used	[kWh]	*98.9*	104.7	111.8	102.3	92.1	93.7	112.4	102.5	90.9
	[%]		+5.9%	+13.0%	+3.4%	-6.9%	-5.2%	+13.6%	+3.6%	-8.2%
Cost of electricity use	[€]	*3.27*	**3.12**	**5.08**	**4.25**	**3.42**	3.46	4.60	3.31	2.41
	[%]		**-4.5%**	**+55.5%**	**+30.1%**	**+4.6%**	+5.8%	+40.8%	+1.3%	-26.4%
Marginal CO_2 emissions savings	[$kgCO_2$]	*9.7*	+0.3	+5.8	+2.8	+0.3	**-1.5**	**+1.9**	**-1.1**	**-3.5**
	[%]		+3.2%	+59.8%	+29.3%	+3.5%	**-15.1%**	**+19.8%**	**-11.8%**	**-35.7%**
Primary energy	[kWh]	*76.8*	80.0	125.0	100.4	79.5	68.9	97.3	70.6	50.2
	[%]		+4.2%	+62.8%	+30.8%	+3.5%	-10.2%	+26.8%	-8.0%	-34.5%

Table VI.3. Integrated energy values of the cooling simulated cases. Firstly the reference case values are presented, then the values for the "cost" controllers (MPC and RBCs), and finally the values for the "CO_2" controllers (MPC and RBCs).

COOLING		**Ref.**	**MPC Cost**	**RBC1 Cost**	**RBC2 Cost**	**RBC3 Cost**	**MPC CO2**	**RBC1 CO2**	**RBC2 CO2**	**RBC3 CO2**
Electrical energy use	[kWh]	*30.4*	28.5	44.1	34.1	24.3	27.7	51.7	43.0	31.3
	[%]		-6.3%	+45.1%	+12.1%	-19.9%	-9.0%	+69.9%	+41.3%	+3.0%
Thermal energy produced for SC	[kWh]	*64.4*	55.1	104.7	74.1	42.2	52.1	128.5	100.8	64.6
	[%]		-14.5%	+62.6%	+15.1%	-34.4%	-19.2%	+99.5%	+56.5%	+0.3%
Thermal energy produced for DHW	[kWh]	*25.8*	30.3	28.7	28.5	28.2	31.3	28.8	28.7	28.9
	[%]		+17.6%	+11.2%	+10.5%	+9.4%	+21.2%	+11.6%	+11.4%	+12.1%
Total thermal energy produced	[kWh]	*90.2*	85.4	133.4	102.7	70.5	83.3	157.3	129.5	93.5
	[%]		-5.3%	+47.9%	+13.8%	-21.9%	-7.6%	+74.4%	+43.6%	+3.6%
COP_{avg}	[-]	*2.97*	3.00	3.02	3.01	2.90	3.01	3.04	3.01	2.98
	[%]		+1.1%	+1.9%	+1.6%	-2.4%	+1.5%	+2.6%	+1.6%	+0.6%
Total thermal energy used	[kWh]	*105.1*	110.6	100.3	117.8	119.2	116.2	83.3	100.8	110.3
	[%]		+5.2%	-4.6%	+12.1%	+13.4%	+10.6%	-20.8%	-4.1%	+4.9%
Cost of electricity use	[€]	*2.78*	**1.90**	**2.74**	**2.16**	**1.63**	2.71	4.94	3.98	2.88
	[%]		**-31.8%**	**-1.5%**	**-22.2%**	**-41.2%**	-2.5%	+77.9%	+43.4%	+3.6%
Marginal CO_2 emissions savings	[$kgCO_2$]	*7.1*	+0.0	+4.7	+1.8	-1.0	**-0.7**	**+6.2**	**+4.1**	**+1.5**
	[%]		+0.2%	+65.9%	+25.5%	-14.7%	**-10.0%**	**+87.1%**	**+57.9%**	**+21.0%**
Primary energy	[kWh]	*65.2*	63.1	99.8	76.7	53.8	59.4	110.2	91.6	66.9
	[%]		-3.2%	+53.1%	+17.6%	-17.5%	-9.0%	+69.0%	+40.4%	+2.7%

In fact, the best RBC configuration still increases the emissions by 21%, which is a quite poor performance.

3 Efficiency of the heat pump operation

The efficiency of the heat pump operation is represented in Figure VI.4, with the summed energy values and the resulting COP/EER, only in space heating/cooling mode (i.e. the DHW mode is not

studied here). In heating mode, the cost controllers present a COP very similar to the reference one. The CO_2 controllers however all present an increase of the COP. These controllers naturally move the heat pump loads towards periods of low emissions, typically the afternoons, where the outdoor temperature is higher which also improves the efficiency of the heat pump. This can be further observed in Figure VI.5 where the ambient temperature recorded during space heating operation is represented as box plots. All the CO_2 configurations operated the heat pump when the outdoor air was warmer. MPC CO2 performed especially well, reaching a COP of 3.19 during the space heating operation. This good performance was also attained thanks to lowering the supply temperature, as seen in Figure VI.5b.

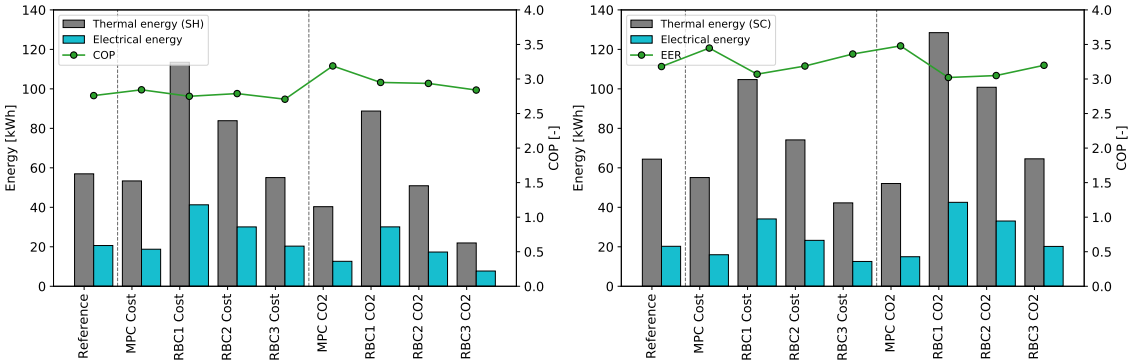

Figure VI.4. Thermal energy produced, electrical energy used and COP/EER during space heating/cooling operation.

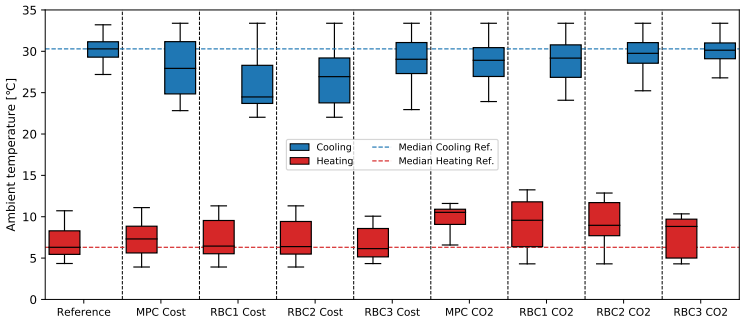

(a) Ambient temperature box plots during the space heating/cooling operation.

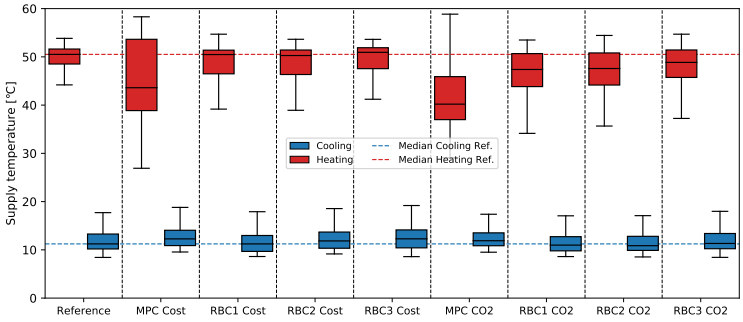

(b) Supply temperature box plots during the space heating/cooling operation.

Figure VI.5. Box plots of the ambient and supply temperatures distribution during space heating/cooling operation.

In cooling mode, it is mostly the MPC controllers that provide a better efficiency of the heat pump. They both reach EER values of 3.45 for MPC Cost and 3.48 for MPC CO2, while the reference case was at 3.18. The reasons for this improvement are less evident than in cooling, given that the EER depends less on the outdoor conditions than the COP. For instance RBC1 Cost is the configuration that operates

the heat pump at periods of lowest levels of outdoor temperature, which should be beneficial for the efficiency, and still presents the lowest EER of 3.07. The supply temperature varies very slightly among all the cooling configurations, as seen in Figure VI.5. The RBC controllers also provide satisfactory heat pump efficiencies, with EER values of 3.36 for RBC3 Cost and 3.20 for RBC3 CO2.

4 Energy flexibility and load shifting

Similarly as in the analysis of the experiments, the energy flexibility is first evaluated looking at the graphs of the energy used in the low, medium and high penalty periods, presented in Figure VI.6.

Observing firstly the cost controllers in heating mode, MPC Cost managed to eliminate the space heating operation during high price hours, while raising the energy use in low price hours, which corresponds to its expected behavior. The RBC configurations also increased significantly the energy use in low price hours, without managing to also reduce it in high price hours. RBC3 presents in fact a very similar distribution than the reference case.

Still in heating mode, the load shifting of the CO_2 controllers is analyzed (second graph of Figure VI.6). It appears that the reference case used most of the energy in the high emissions periods, therefore the CO_2 controllers manage to reverse this tendency and to reduce significantly the energy use in those high emission hours. MPC CO2 and RBC3 CO2 both do a good job in this regard.

Now analyzing the cost controllers in cooling mode (third graph of Figure VI.6), all of them manage to eliminate the use of space cooling during high price hours. However, this is compensated by a severe increase of the energy use in low price hours for RBC1 Cost and RBC2 Cost, while MPC Cost and RBC3 Cost manage to keep this increase at a reasonable level.

Finally the CO_2 controllers in cooling mode are analyzed. RBC1 and RBC2 CO2 both increase very significantly the energy use in low emissions periods, which gives positive results in terms of flexibility factors, but negative results in terms of absolute emissions savings. MPC CO2 and RBC3 CO3 have a very similar distribution that the reference cooling case, only with a slightly lower energy use for all periods. Thus they only operated a limited load shifting, which resulted in actual emissions savings only for the MPC controller.

The previous analysis in terms of load-shifting is reflected in the values of the flexibility factors, as shown in Figure VI.7. Firstly analyzing the factors in heating mode, MPC Cost shows the best results in terms of FF_{cost}: it manages to reach the value of 0.62 compared to the reference case with 0.36. On the other hand, the RBC cases barely improve this value, their FF_{cost} ranging from 0.34 to 0.45, the best being RBC1 Cost. In terms of CO_2 flexibility factor, the MPC and RBC controllers perform in a very similar way: their FF_{CO_2} values are contained in a small range, from -0.22 to -0.15, while the reference case presented a much lower value of -0.64.

In cooling mode, the RBC controllers present better values of flexibility factors than the MPC controller. Regarding the cost flexibility, FF_{cost} took the value of -0.22. The MPC Cost controller managed to increase this value to 0.51 which is already a great improvement, and RBC1 Cost to an even greater value of 0.69. Regarding the CO_2 flexibility, the reference case had a FF_{CO_2} value of 0.36: MPC CO2 stayed at the same level with 0.33, and the RBC configurations reached the value of 0.52 (RBC1 and 2).

It should be noted that increasing the flexibility factors can be achieved in two ways: by decreasing the energy use in the high penalty periods, or by increasing it during the low penalty periods, and oftentimes with a combination of both. The MPC controllers tend to use the first approach, while the RBC controllers resort more to the second one. However, this latter strategy - increasing too much the load during the low penalty periods - often leads to a significantly increased energy use overall, even though it gives positive results in terms of flexibility factors. This effect might offset the benefits of using energy during low penalty periods, and cause in the end a failure in reducing the summed penalties, as seen in some of the RBC cases.

Figure VI.6. Breakdown of the electricity use according the the price or emissions periods. The most relevant graphs have been highlighted by color rectangles: MPC Cost and the RBCs Cost when analyzing the price periods, MPC CO2 and the RBCs CO2 when analyzing the emissions periods.

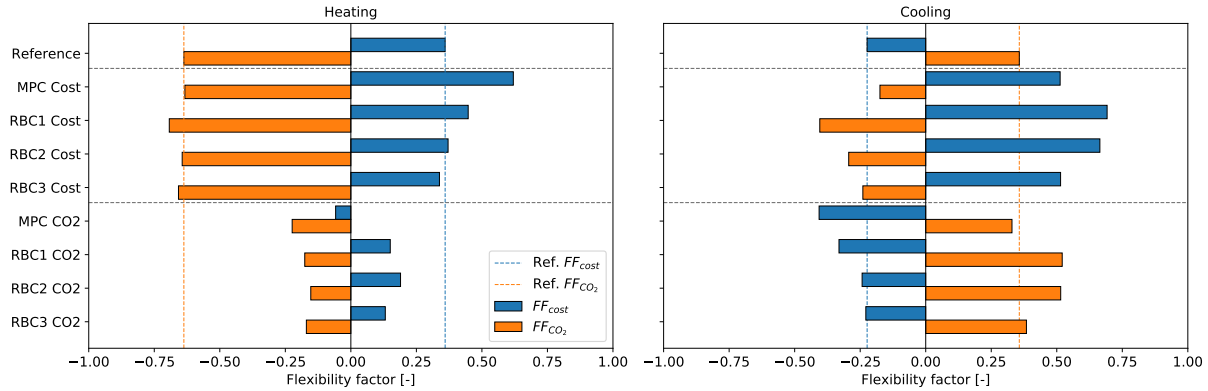

Figure VI.7. Flexibility factors relative to cost or emissions, both in heating and cooling modes. The flexibility factors of the reference cases are highlighted with dashed lines to clearly display in which direction each controller modifies the factor.

5 Comfort

The comfort analysis is presented for all cases in Figure VI.8. The configurations presenting the best results in terms of energy flexibility logically all present a degradation of the comfort conditions to some extent. The main question then consists in deciding how much degradation is acceptable. Some flexibility in the comfort conditions is almost inevitable to harvest the benefits of energy flexibility, although this should be limited and barely noticeable by the occupants.

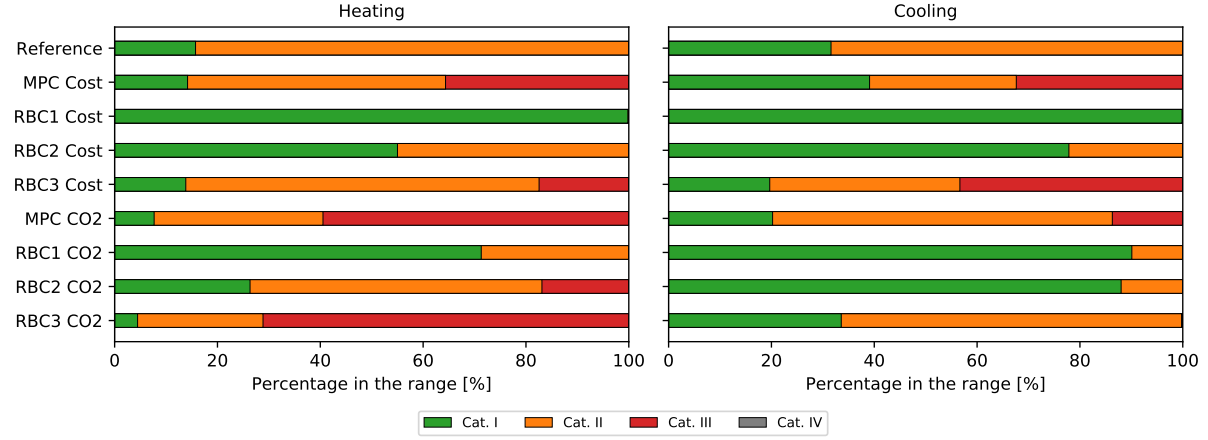

Figure VI.8. Comfort analysis of the simulated cases.

For the cost controllers in heating mode, MPC Cost and RBC3 Cost present similar levels of thermal comfort, however MPC Cost would be the preferred option since it provided better performance in terms of energy flexibility and cost savings. For the CO_2 still in heating mode, both MPC CO2 and RBC3 CO2 display a large percentage of time in Category III, between 60 and 70%. In relation to their emission savings, RBC2 CO2 or MPC CO2 could be chosen as a preferred controller.

In cooling mode, the cost controllers MPC Cost and RBC3 Cost both degrade the comfort conditions with respectively 32 and 43% of the time spent in Category III. RBC2 Cost manages to improve the comfort conditions compared to the reference, while still decreasing the costs. One of those three options are possible, depending on the desired level of comfort. For the CO_2 controllers, MPC CO2 slightly degrades comfort with 14% in Category III, however it is the only configuration that manages to provide emissions savings and therefore should constitute the favored option, compared to the RBCs that all increase the time spent in Category I.

6 Conclusions from the co-simulation cases

After having tested various configurations, and in particular balancing the comfort conditions with the provision of energy flexibility, general conclusions can be drawn about the performance of the energy flexibility controllers. The first learning from this process was the high sensitivity of the controller to their tuning parameters. In particular for MPC, slightly modifying the weighting coefficient had a great impact on the results: this could be seen when changing the α_ε coefficient for comfort from 0.15 in the experimental MPC CO2 case for cooling, to 0.155 in the simulated case. This slight change of 0.005 in the coefficient modified the emissions savings from -22.3% to -10.0%, which is a consequent difference, probably due to the passing of a certain threshold between one case and the other. This highlights the necessity of an appropriate tuning for the controllers.

To summarize the performance of the RBC and MPC controllers, the results can be analyzed in relation to their reference case. When the reference case is far from optimal or showing an adverse behavior with regards to the considered objective, the MPC and RBC controller can both manage to generate consequent savings. For instance, in winter the reference case is not optimal with regards to the carbon emissions, since most of the energy is used at night, when outdoor temperatures are lower, COP is also lower and the emissions are high. In that case, the RBC CO2 or MPC CO2 enable to save at least around 15% on the emissions. Similarly in summer, the reference case is far from optimal regarding the costs, since it uses most of the energy for cooling during the afternoons, when the price is high. In that case, RBC Cost or MPC Cost can reach cost savings of around 30%. On the other hand, when the reference case already approaches the optimal, MPC really takes advantage of its prediction capacities, and reaches a better performance than RBC. In winter, the reference case is already cheap, therefore RBC CO2 fails to provide further savings in the studied configurations, while this context brings out the best of the MPC CO2 which manages to reach small cost savings of around 5%. Likewise in summer, the reference case already causes relatively low emissions, therefore the RBC CO2 only causes a deterioration of the carbon footprint, while MPC CO2 can displays its full optimization potential and manages to provide emission savings of around 10%.

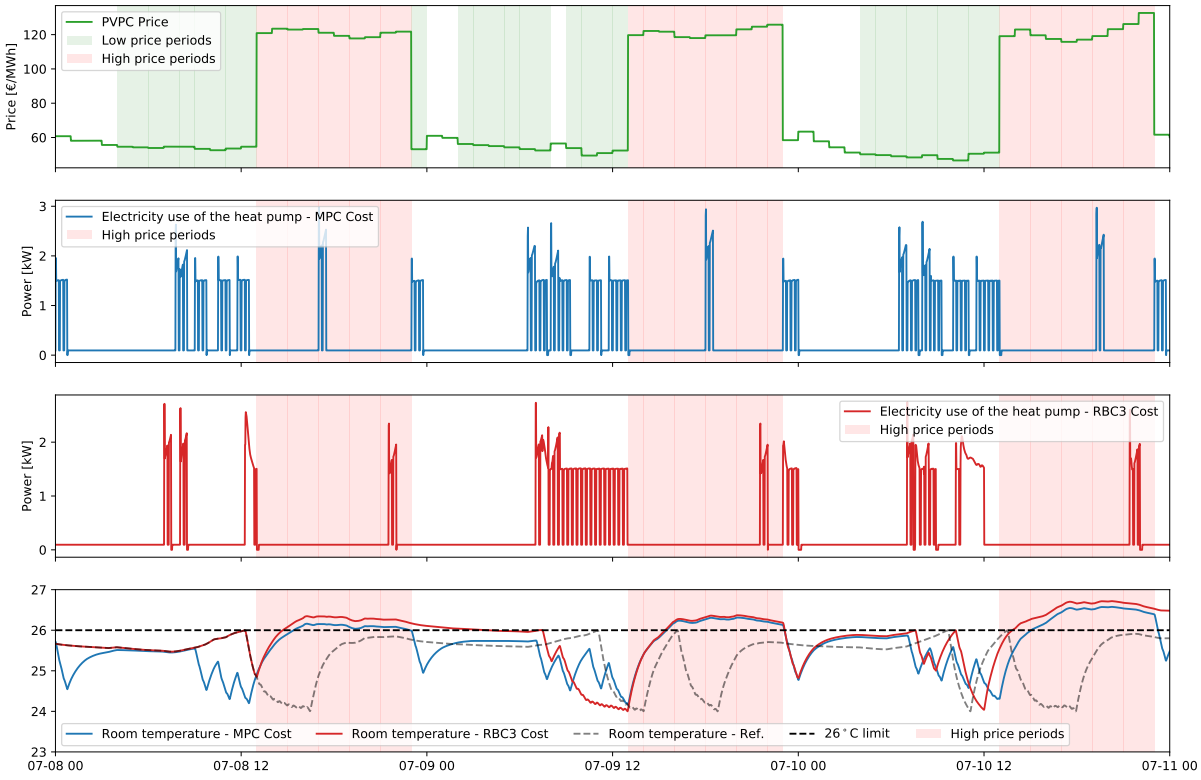

Figure VI.9. Time series comparing the MPC Cost and the RBC3 Cost configurations in cooling mode.

Choosing an RBC or MPC controller therefore depends on the season and the objective one wants to achieve. MPC guarantees a good performance in all cases, but has an extra development cost. In some cases, RBC performs as well as MPC, therefore these extra costs are not necessary and the RBC controller might be sufficient. It should be noted that the two controllers have slightly different ways to reach their objective. The RBC controllers increase in general the consumption during low penalty periods, but do not necessarily decrease it during the high penalty periods. This might still result in a positive impact on the flexibility factors, but not necessarily on the overall savings, since the overall energy use will increase significantly. The MPC controller on the other hand tried to reduce the energy use during the high penalty hours, but also tries to limit its transfer to the low penalty hours. This strategy is normally smarter and more subtle; it benefits from the prediction and optimization features of the MPC, to operate the heat pump in more favorable periods and when it is more energy-efficient.

The different dynamics of RBC and MPC are also illustrated with an example of time series in Figure VI.9. It can be seen on the two middle graphs, representing the heat pump power draw in the MPC Cost and one of the RBC Cost configurations that both controllers tend to avoid the high price hours, by shifting the load before or after them. MPC presents this behavior more systematically than the RBC: it precools the building until the last moment before the price increases so as to fully rely on the pre-cooling effect and avoid the heat pump operation during all the periods of expensive electricity. It also provokes a rebound effect every time the price drops, therefore the cooling load is spread both before and after the high price period. RBC has a generally similar behaviour, but since it does not have any knowledge of the future, it does not act as efficiently: for example during the third and last day, before the high price period, the RBC pre-cools the building, but stops one hour before the price increase. During that last hour, the temperature in the zone increases, while the heat pump could have continued to provide cheap cooling, and thus could have limited the subsequent comfort violations during the high price hours. This reveals the superiority of MPC due to its prediction and anticipation abilities.

Chapter VII

Discussions, conclusions and outlook on further research

1 Discussions

The obtained results are put into perspective and discussed in this section. In particular, the development, tuning and computational efforts of the flexibility controllers are discussed, as well as as the differences between costs or emissions optimization, and the practical barriers still hindering the large-scale deployment of such controllers.

1.1 Development efforts

Along this thesis, and more specifically in chapter III and IV, the whole development process of the flexibility controllers has been reported in details. The costs of elaboration of the controller are not negligible and should be considered in balance with their performance, to have a global overview of their potential.

The development of the RBC controller is not particularly complicated. It requires the choice and obtaining of an input signal, and the calculation of the adapted thermostat set-point. The latter would represent the most effort-intensive task: the thermostat must be programmable, and some hardware piece is needed to receive the input penalty signals and calculate the thresholds and adapted set-point automatically. Other than that, the RBC is a rather straightforward controller, which actually only acts on the thermostat, and not directly on the heat pump.

On the other hand, the development of the MPC is a more complex and expensive process. It requires precise models of both the specific building and heat pump on which the controller will be implemented, otherwise its performance might deteriorate. Because it is so case-specific, an MPC controller can hardly be bought "off-the-shelf", an almost new controller must be developed practically every time. The required modelling is responsible for this situation in large proportions [166]: it represents around 60% of the total development costs for MPC controllers [165].

However, given the superior performance of MPC over other types of controllers, as demonstrated in this thesis, efforts are made to reduce their development costs and make them more accessible. Regarding the building modelling, a lot of research has focused on how to obtain reliable RC models in a simple way [102], [154], [167], [168]. For instance, De Coninck et al. developed a toolbox to help automatize the process of the parameter estimation [49]. These methods could be used to produce a bank of simplified RC models, based on the few building archetypes encountered in each country as classified from the TABULA project [169]. Since creating a building model, even simplified, requires a lot of meta-information that is sometimes not available, a database of several standard RC building models would be useful in this regard. The advantage of grey-box models here is that the parameters still have a certain level of physical interpretation and thus can be modified by the designer of

the controller: for instance, starting from a standard RC model, if the designer knows that the building has more insulation than the standard building of this archetype, they can increase the resistance parameter of the external walls R_w accordingly. The same principle could be adapted for the heat pump models, with the creation of database of simplified models for different kinds of heat pumps (air-source, water-source, ground-source etc.). When inserting such model in an MPC scheme, the designer would only need to inform the capacity of the real heat pump to make it function. Making these models scalable and easily configurable thus constitutes the key to facilitate an easier implementation of MPC at a larger scale.

Another path to minimize the modelling efforts consists in relying on online parameter estimation. Since the MPC constantly records the operation of the heat pump and the response of the building, these data could be used as training dataset to correct the models automatically at regular time intervals. Starting from a common standard model, the MPC controller would thus learn from the functioning of the systems, and adapt the model parameters given the response of the specific building to heating or cooling excitation found in its past data. Such methods are being investigated and represent promising research paths [170], [171]. It would be particularly relevant in the context of Mediterranean climate studied in the present thesis, where the model would need changes notably between the heating and cooling seasons: an online parameter estimation method would adapt the model little by little as time passes by, instead of an abrupt transition.

1.2 Controller tuning: balancing energy flexibility and comfort

Once the controller is operational, it still requires an appropriate tuning to reach an optimal performance. The tuning principally consists in balancing the comfort of the users with the provision of the energy flexibility, which is the main objective of the controller. It represents a crucial step, and aside from the modelling part, another resource-intensive task. The development process of the controllers revealed this difficult task of finding a trade-off between the different aspects of building energy flexibility, so that it benefits all involved parties (utilities, end-users and society as a whole). In general, the controller manages to find a balance between the sometimes contradictory objectives (cost, comfort, carbon footprint, flexibility etc.), although they sometimes emphasize one aspect at the cost of another one.

In the case of RBC, the tuning consisted in finding the appropriate values of the percentiles for the thresholds of the penalty signals. This process should in theory not be repeated, although if the shape of the signal is very different or irregular, other percentiles might result in a better performance. Once the calculation method of the thresholds is fixed, the base set-point (i.e. when there is no modulation) also needs to be adapted, as shown in the co-simulation chapter. This process is rather straightforward and should be fixed for a given controller (with a certain objective and during a certain season). The choice of the base set-point also influences greatly the outcome of the controller.

In the case of the MPC, the fine-tuning consisted in finding the appropriate values of the weighting coefficients in the multi-objective cost function, through the Pareto analysis. This process revealed that different values of the coefficients were required for every configuration, and that the outcome of the controller was very sensitive to their values. In particular, the value of the coefficient α_ε, associated with the objective J_ε determines whether the controller will rather emphasize comfort or the flexibility objective; it should thus be chosen with specific care. Its sensitivity was evidenced in the thesis, notably with the MPC CO2 configuration in cooling: a significant change was observed in the results by passing from a value of $\alpha_\varepsilon = 0.15$ to a value of $\alpha_\varepsilon = 0.155$. Considering hard constraints rather than soft ones (hence eliminating the discomfort term J_ε in the objective function) could solve this sensitivity issue, however the J_ε objective considerably improves the robustness of the controller [46] and therefore it remains interesting to keep it.

Since it remains complicated to find a priori the satisfactory tradeoff between comfort and energy flexibility, it is proposed to leave a certain margin of action to the users to adapt this trade-off in a more dynamic manner. This was performed in a similar way by Wood et al. [172], where the occupants were provided with feedback on their energy consumption and indoor environmental conditions, so that they could make informed decisions about the operation of the systems. A suggestion for a potential

future implementation would be a visual interface with a slider that can be moved by the user, either towards better comfort, either towards a cheaper or a more environmentally-friendly operation of the systems. An graphical example is shown on Figure VII.1. After some period, the occupants might decide to move the cursor in one direction or the other, for instance if they experienced discomfort for their taste, or if they consider that their energy bill became too expensive. The occupants should not be bothered with numbers, but the position of the cursor should be translated back-end into a more concrete input usable by the controller. For the RBC, the slider's position would determine the level of the normal room temperature set-point, and for the MPC, the value of the weighting coefficient, which gives more or less importance to the comfort objective relatively to the reduction of the costs or the emissions.

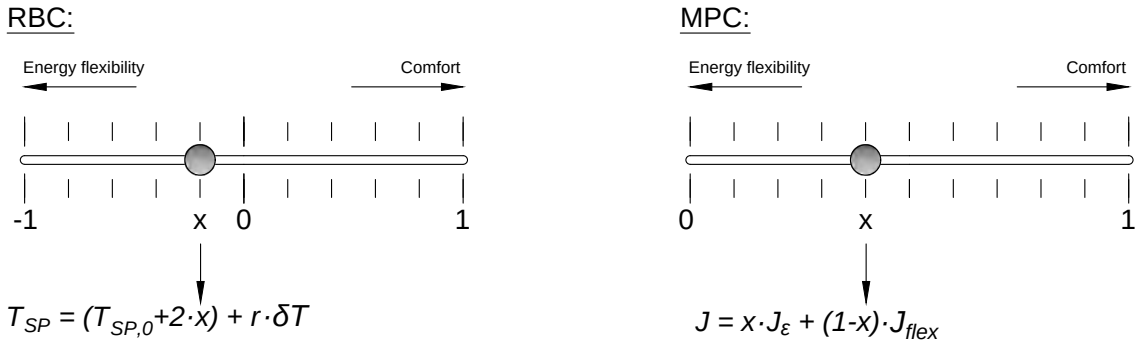

Figure VII.1. Example of possible implementation for a user-friendly interface, where the users can tune themselves if they would rather emphasize comfort or energy flexibility. In the case of RBC, the position of the slider x would change the level of the normal set-point $T_{SP,0} + 2 \cdot x$ (before the modulation $r \cdot \delta T$ for flexibility). For MPC, the position of the slider would determine the weighting coefficient α_ε which balances the comfort objective J_ε and the other flexibility objective J_{flex}.

1.3 Computational burden of the MPC

The computational burden of the controllers should also be examined in details. RBC does not require any complex calculations, therefore this is not a limitation for this type of controller. On the other hand, MPC by nature consists in solving an optimization problem at regular time intervals. This causes an important computational burden, which should also be put in balance with the significant advances brought by this type of controller, since it could represent a barrier to their implementation. Furthermore, the computational efforts have rarely been reported in details in the literature on MPC for building climate control. Additionally, such complex control strategies could actually backfire by taking on a more important part of a building's energy use than what they enable to save, notably for nZEB (for instance, up to 39% of the energy use was reportedly use for control and monitoring in a prototype nZEB [173], although they did not use MPC).

For these reasons, the calculation process of the MPC is discussed here. Especially for the experimental part, the calculation time was limited to 600 seconds, since the OCP must be solved within one time step of 15 minutes. 15 minutes are 900 seconds, but the lower value of 600 seconds was chosen as a safety measure to also allow some time for the precalculations and data communication in the experimental setup. If the solver finds a solution to the OCP within these 600 seconds, the calculation is flagged as a success, and its actual calculation time is collected. If the solver fails to find a solution in the allotted time, the calculation is stopped, and the last solution is kept as the output of the MPC, as if it was the optimal solution. In fact, after a certain time in the calculation, the progression becomes very slow, because the objective function is flat near the optimum [144]. It is therefore preferable to stop the computation and retrieve the current best solution found by the solver, which is oftentimes not very far from the optimal one.

On average, it was observed that MPC Cost took the same amount of time to solve the OCP in the winter and summer configurations: 224 and 214 s respectively. MPC CO2 presents larger differences:

it took it 391 s on average to solve the OCP in the winter configuration, while only 5 s in the summer configuration. These durations are not negligible, but in the present case, they do not cause issues since the controlled plant has a large inertia and its discretization time step is large, enabling sufficient time for the calculation (especially considering the delay within the model, see subsection 2.4 in chapter IV). The reason for the long computation time of the present optimal control problem resides in its nature: it mixes integer and continuous variables, and thus the problem must be solved numerically through Mixed Integer Linear Programming, which increases significantly the computation effort [84].

The MILP formulation is however necessary, because the binary variables enable to reproduce more accurately the behavior of the heat pump, notably its minimum capacity and the switch between DHW and space heating or cooling modes. The high computational burden of MPC might raise concerns about whether it is reasonable to have a computer or small hardware device constantly computing the new optimal trajectory, and how much energy use this would represent. To the knowledge of the author, no studies so far have studied the potential impact of the energy use caused by these repeated computations of MPC. Ideally, this extra consumption should be put into perspective with the additional savings provided by the MPC. It is hoped that with the ever increasing calculation capacities of computers nowadays, the computation barrier becomes less and less of an obstacle. Furthermore, the solving of the OCP might be decentralized through cloud-based services so that the energy use due to calculation would occur in a remote server with high energy efficiency.

1.4 Penalty signals: cost vs carbon footprint optimization

The penalty signals play an important role in the activation of building energy flexibility. In the present work, two different signals have been used: the time-varying electricity price and the marginal CO_2 intensity of the grid. Both normalized signals can be seen in Figure VII.2 for comparison. From the analyzed cases, it appears that they often display opposite behavior: the high penalty occurs in the afternoons for the price (the grid operators want to incentivize peak shaving in this way), while it corresponds to the low penalty for CO_2 (due to the high share of solar and renewable energy at this moment). For this reason, it results complicated to optimize both objectives at the same time: increasing the cost flexibility will provoke a decrease of the CO_2 flexibility and vice-versa. This was clearly observed with the analysis of the flexibility factors: when FF_{cost} moves in one direction, FF_{CO2} generally moves in the other direction. It is however expected that the price signal will evolve in the future to better reflect the carbon footprint of the power generation, so that eventually, both signals will tend to present the same shape, making economical and environmental benefits coincide. This could be achieved for instance through a global carbon tax.

The patterns of these signals also affect the outcome of the flexibility controllers: the price signal presents large day-night variations, and thus already provides a pre-defined pattern for the electricity use, which facilitates the consequent optimization of the MPC. On the other hand, the CO_2 signal presents smaller variations, and therefore gives less prior information to the MPC as to which periods are more interesting for operating the systems. The marginal emissions signal was chosen precisely because it varies more than the average emissions signal. Some seasonal changes in the signals can also be observed: the average price was for example 22% lower in the cooling case than in the heating case. This is one reason behind the different weighting coefficients obtained by the Pareto analysis in heating and cooling mode for the MPC configurations; it compensated for the lower price difference by decreasing accordingly the α_ε coefficient. A more meticulous sensitivity analysis could be conducted on these weighting parameters as a further research topic, for instance trying to obtain coefficients independent from the utilized penalty signal. This could be done by dynamically adapting the coefficients to the level of the input signal, or a prior normalization of the input signal realized in a more dynamic way than the present study (i.e. not considering a fixed maximum cost c_{max}).

As already mentioned earlier, other penalty signals could be used by the controllers to activate the flexibility, such as the residual load of the grid, the primary energy factor, or the percentage of renewables in the energy mix. The principle of the controllers, either RBC or MPC, would not change since conceptually and from a pure control viewpoint, it does not really matter what represents the penalty signal. Only a further tuning might be required. Furthermore, whichever signal is used to

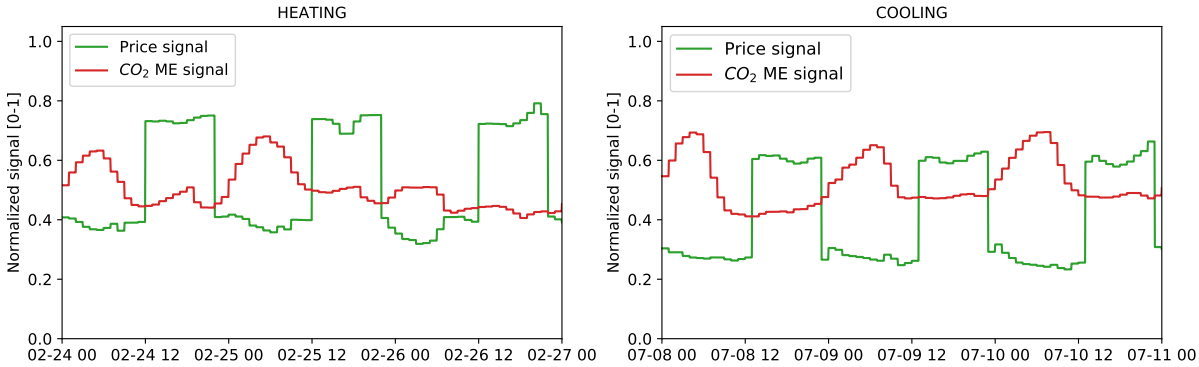

Figure VII.2. Normalized penalty signals (price and marginal emissions) in heating and cooling seasons.

trigger the energy flexibility, it is anticipated that their variations will increase in the future, notably due to the higher penetration of RES in the grid. The prices might become more volatile for instance. Klein et al. also demonstrated that the residual load will have very large daily variations in 2030, especially in Spain with negative residual load at midday due to the high share of solar power [78]. In this context, MPC might become an even more profitable option in the future, since it can benefit from its optimization and prediction features to operate the systems optimally in any situation, even with important changes from one day to the next.

1.5 Practical implementation and barriers for flexibility controllers

As partly discussed already, several barriers still hinder the deployment of flexibility controllers at a large scale, and especially for MPC. The implementation of RBC does not represent particular challenges since it acts only on the thermostat and not on the heat pump. It requires the possibility to act on this room thermostat and the availability of a communication channel to automatically receive the predictions of the penalty signals. For this reason, RBC can constitute a cheap and promising solution in some cases, reaching satisfactory results in many cases, sometimes as good as MPC.

In view of its higher level of complexity, MPC presents more challenges in its implementation, as shown notably in the conclusion section of the chapter on the experimental results. Technological barriers notably appear when interfacing the MPC controller with the heat pump. Difficulties were encountered during this thesis work with the real heat pump system, for instance when attempting to control the DHW production loop, while the local controller was overriding the MPC decisions. Finding the inputs of the heat pump which can be controlled, and understanding their exact effects requires prior work. For instance in the present studies, the level of thermal power delivered was controlled by adapting the supply temperature of the heat pump. It would be preferable to control directly the frequency of the compressor for a VSHP system, since all the functioning of the heat pump mainly depends on this variable (thermal output and electricity use notably). However, the frequency of the compressor is not controllable directly for most heat pumps available on the market, it is regulated by a robust internal controller installed by the manufacturer for safety purposes, and which cannot be overridden. Hu et al. notably considered in their study [174] an MPC scheme that could directly control the frequency of an air conditioner, but this work was based on simulations and did not contemplate this practical barrier: most probably, their strategy cannot be implemented in reality, unless with a close collaboration with the heat pump manufacturer. Other ways to control the operation of the heat pump exist: for instance one can ”trick” the controller by modifying the input for the sensor which is supposed to measure the outdoor temperature. In this way, the heat pump internal controller believes it is colder or warmer outside, and adapts its supply temperature according to its programmed heating or cooling curve (weather compensation control). This is a convoluted manner of controlling a black-box system which leaves little options for supervisory control.

Additionally to the operation of the heat pump, the MPC faces other technical challenges, such as the lack of measurements needed for a proper functioning of the controller. The MPC controller

requires feedback about the building status and the current operation of the heat pump: sometimes sensors are not available to provide these data. In most residential buildings, only one temperature sensor is placed in the living room. If the states of the building are not known, they can still be estimated [152]. Other times, they are measured but with a very low precision: for instance in the present work, the temperature of the water in the tank is recorded by a sensor of the heat pump internal unit, but its resolution is only ± 1 K, making this measurement not much accurate for the controller. Furthermore, a single temperature measurement at the middle height of the tank is little representative of the state of charge of this tank, given the stratification that can occur between its top and bottom parts.

Apart from the technological aspects, other barriers which belong more to the sociological side also slow down the deployment of MPC. Killian and Kozek [166] have notably mentioned several of them:

- engineering efforts needed for modelling and design: this was already discussed in previous section,
- lack of qualification of control engineers: MPC requires certain qualifications and few experts in the field of the building sector know how to set up or maintain such complex controller,
- industry's reluctance to innovation: the building automation sector being fairly conservative, MPC faces difficulties to compete with traditional control methods which are tried, tested and known in the big companies.

Despite these barriers, a number of encouraging trends also promise a bright future for MPC technology in the building automation sector. The heat pump market is getting ready for enabling demand response in its products: for instance, the label "Smart-Grid Ready" or "SG-ready" has emerged in Germany, with most heat pumps on the European market now presenting this label [175]. The principle of SG-ready consists in implementing 2 binary inputs in the heat pump controller, which makes a total of 4 possible combinations. These 4 inputs can be activated to enable demand-response as follows:

- Input 1 (positions 1:0): the heat pump must be switched off,
- Input 2 (positions 0:0): the heat pump runs in an energy-efficient mode,
- Input 3 (positions 0:1): the heat pump runs at an increased level (for instance at an increased temperature set-point),
- Input 4 (positions 1:1): the heat pump is forced to operate at full load (within its operational limits).

Some research has already been carried out about using such standardized inputs to facilitate DSM with heat pumps, notably by Fischer et al. who investigated the use of SG-ready from the perspective of an aggregator of energy flexibility [176]. In the US, the OpenADR protocol has also been developed: it is meant as a Smart Grid standard, to "standardize the message format used for DSM" and so that "communication signals can be exchanged in a uniform and interoperable fashion among utilities, grid operators and energy management and control systems" [177]. These important progresses in standardization will solve the issues of compatibility and communications, and establish a common ground for enabling DR in buildings.

Furthermore, the increased use of home automation systems provides a favorable context for the development of MPC controllers [166]. With the boom of the Internet of Things (IoT), wireless sensors can easily be deployed to obtain the additional measurements needed for the good functioning of the MPC. In addition, smart home automation products have shown an important increase in sales number: this represents a great opportunity for MPC solutions, as they can fit neatly as integrated parts of such products. For instance, smart home automation systems can take the form of a user-friendly app which gives feedback to the occupants about their comfort and energy management, let them control remotely certain systems and decide which objectives they would like to emphasize. Such app could

leverage the full potential of an MPC controller, notably thanks to their adaptive features which reduce the prior work in developing control models.

To summarize, MPC is only at its premises in the building automation sector: 15 years ago only, this type of control was barely known in this industry, while nowadays, most of the research about intelligent climate control schemes includes MPC. The recent progresses in standardization, modelling techniques, inclusion in home automation systems, availability of sensors and data, computing power, suggest that MPC will see an important development in the coming years, including in smaller residential buildings.

2 Conclusions and further research

2.1 General conclusions - Activating flexibility in residential heating and cooling loads

Along this thesis, control strategies have been developed for enhancing the energy flexibility of residential buildings equipped with heat pumps. From development and modelling, to tuning, application and testing, all the process has been documented, and the results analyzed in details from different angles. All the steps enable to have a complete overview of not only the performance of the controllers, but also the workload necessary to their development. The work focused on implicit demand response with two types of controllers: a rule-based controller and a model predictive controller.

Energy flexibility can be triggered by different penalty signals: such signals incite the operation of the heat pump at the times where the signal is low, and discourage it otherwise. The hourly-varying price of electricity, widely spread for small consumers in Spain, was used for this purpose, leading to a cost optimization strategy, as done in most research in energy-flexible buildings. In addition, a new penalty signal reflecting the marginal CO_2 emissions of the grid was developed. This novel approach enables the controller to focus instead on the minimization of the carbon footprint of the heat pump use. It was found that these two objectives (cost or emissions minimization) were contradictory, and improving one aspect generally leads to the deterioration of the other, since the variations of the two signals have opposite behaviors.

RBC and MPC had both been largely studied in the existing literature about energy flexibility for HVAC control. However, little research had previously investigated such in details MPC for controlling heat pump systems. In particular, the present thesis includes a large part of experimental work, where the strategies were tested on a real heat pump in a laboratory setup. The full dynamics of the heat pump functioning could thus be observed. This hardware-in-the-loop process enabled to highlight interesting insights regarding the practical implementation of such controllers, notably communication challenges and discrepancies between predicted and actual behavior. It also gives more credibility and reliability to the presented results: in the existing literature, a number of articles made important simplifications regarding the heat pump behavior, while in this thesis this bias could be eliminated thanks to the experimental nature of the studies.

Further than the experimental part, advances in modelling have also been achieved in the mark of this thesis. Regarding the building simplified model for the MPC controller, a grey-box RC model was adjusted with a satisfactory fit of 77 to 82% with a much more detailed white-box model. It was shown that it is preferable to adapt the model and change the values of resistance and capacities for use in cooling or heating modes. Regarding the heat pump models, two types of models were developed: simplified polynomial models for use in the MPC, and detailed transient model in TRNSYS. Both models were based on a performance map obtained experimentally with the heat pump functioning in a wide variety of operation points, therefore they represent the actual behavior of the heat pump, and are not only based on catalogue data. Especially the detailed VSHP model, which includes its local PID controller, is a novelty since such model did not exist thus far in the existing TRNSYS libraries. Assembled together, the building and heat pump models together with the controllers form a complete co-simulation framework which was used to test different control configurations. It con-

stitutes a trustworthy test benchmark, which can be reused for further research in the same domain, for instance to perform sensitivity analysis on the numerous parameters present in the flexibility controllers.

Applying the controllers on the heat pump in the experimental and simulation frameworks, their benefits were demonstrated. When optimizing the energy costs, monetary savings of around 5% were achieved in heating mode, and around 30% in cooling mode, compared to a reference thermostat control. When optimizing the CO_2 emissions, savings of around 15% were reached in heating mode, and around 10% in cooling mode. The amplitude of these savings depended a lot on whether the reference case already performed close to optimally regarding the costs or emissions. Minimizing the costs in winter and the emissions in summer result a more complicated task, since these respective reference cases already operated the heat pump in favorable periods. The most important savings were achieved when minimizing the costs in summer and the emissions in winter. Globally, in all seasons and all configurations, an improvement of the energy flexibility could be achieved. The differences between the RBC and the MPC will be discussed in the next section. Furthermore, the performance of the controllers was also analyzed in terms of flexibility factors (comprised between -1 and 1), which reveal the amount of energy use that was shifted to the low-penalty periods. The CO_2 flexibility factor was increased by +0.15 in summer and by +0.45 in winter, while the cost flexibility factor was increased by +0.75 in summer and +0.25 in winter. These results confirm that the flexibility controllers effectively managed to shift the operation of the heat pump towards the periods of lesser penalty, and this load-shifting correspond to the energy flexibility effect sought after in this work.

To conclude, the present thesis has covered many aspects of energy-flexibility control strategies for heat pump systems in residential buildings: trigger input signals, models and formulation required for MPC, implementation on a real heat pump, adaptations needed for heating and cooling modes, practical bottlenecks, results in experimental and simulation setups. The positive performance of RBC and MPC observed along the work of this thesis confirm the potential of such controllers to actively exploit the thermal mass of buildings and water tanks, which can be considered as thermal energy storage widely available at low cost. Through this sort of DSM strategy, the thermal loads of buildings can be made more flexible, and thus help the smart grids of the future to integrate larger shares of RES.

2.2 Pros and cons of the energy flexibility controllers: RBC and MPC

The performance of the RBC and the MPC has been analyzed in details in the thesis. A more direct comparison is proposed here, to highlight the pros and cons of both controllers in the light of different criteria.

Regarding the development efforts, it was already clearly stated that this still represents a large obstacle for MPC. RBC only consists in an adaptation of a classical thermostatic control, therefore it does not represent a particular challenge. On the other hand, the creation of adequate control models represents a large workload before the MPC can be operational, and it also means that an MPC can hardly be sold as a ”plug-and-play” solution. It is hoped that with the accumulated experience and the development of this sector, the costs associated with the development of MPC will decrease in the future. RBC still possess a strong advantage in this regard thanks to its simplicity: it only needs plugging to the thermostat, and does not require to act directly on the heat pump, which limits the communication problems and uncertainties.

About the formulation of MPC more specifically, some innovative features have been developed in this thesis. Firstly, the performance of the heat pump was included as a model based on experimental data, providing the optimizer with a more accurate representation of its behavior. Secondly, a mixed-integer formulation was implemented, where the introduction of binary variables enabled to reproduce the dynamics of the heat pump, as seldom done in existing literature. In fact, a variable-speed heat pump has a lower threshold below which it switches off, and the binary variable enables to constrain the heat pump power between its minimum and maximum capacity to reproduce that. The binary variable also permits to switch between the operation in DHW production mode, or provision of space heating/cooling. However, the mixed-integer nature of the optimization problem increases the complexity and the solving time needed, but it is hoped that the computation barriers will be-

come less limiting with the ever increasing calculation capacities. Computational burden is on the other hand not an issue for RBC.

Both types of controllers require some amount of tuning to reach an optimal performance. The tuning process is probably more complex and resource-costly in the case of MPC, but also exists in RBC. It mainly consists in balancing the comfort of the occupants vs the optimization of energy flexibility. It was shown that a preliminary fixing of this trade-off is complicated to achieve, and letting the users make this decision in a more dynamic manner could constitute a good solution.

Regarding the performance, MPC clearly outperforms RBC, since it manages to operate effective load-shifting in all cases, while RBC only in some of the cases. Both controllers have a rather distinct way of improving the energy flexibility of the building: RBC tends to increase the heat pump use during the low penalty periods, without necessarily decreasing it in the high penalty periods. MPC tends to decrease the energy use during high penalty periods, and to limit the consequent increase in low-penalty periods. The results in terms of flexibility factors might be equal, but would lead to a generally higher thermal energy use in the RBC case.

Operating a building flexibly is a subtle compromise between different aspects that are all related and sometimes contradictory. RBC can only manage this balance to a certain extent, limited by its predefined rules. The strength of MPC is that such control is capable to explicitly quantify and balance different objectives, and to benefit from its knowledge of the future. Furthermore, it can sometimes lead to improving several objectives at a time: for instance, certain configurations enable simultaneously to realize some load shifting towards low-penalty periods, to reduce the electricity bill of the users, while maintaining comfortable conditions indoors. These findings are of utmost importance since the deployment of flexibility at a large scale will require the acceptance of all parties involved: the occupants of the buildings (interested in their comfort and energy bills), the grid stakeholders (interested in load shifting and the moments when electricity is consumed) and the society as a whole (which should be concerned about the reduction of the CO_2 emissions and climate change).

A thorough comparison between an RBC and MPC controller in the exact same experimental setup had not been performed so far, to the knowledge of the author. To sum up, it can be stated that MPC is a preferred option for any of the configurations studied, since it will enable to always reach a certain level of savings, thanks to its finer optimization features and ability to predict the future behavior. However, its development, tuning and implementation costs are considerable, and might hinder its deployment on a large scale. In some cases where a radical load-shifting is required (namely for reducing the emissions in winter or the costs in summer), RBC performs just as good as MPC, and can provide similar services for a much simpler and cheaper implementation. In these cases, RBC should be preferred since its simplicity and low-cost provide higher chances of implementation in the field, and thus higher chances to eventually make an impact. It is also anticipated that the penalty signals (price or emissions) are bound to become more volatile in the future: MPC might have better abilities to cope with these rapid changes and therefore remains a very promising type of controller for energy flexibility in buildings.

2.3 Contributions of the thesis

The present thesis brought several contributions to the knowledge area of energy flexibility in buildings. The principal contribution represents the development of the flexibility controllers, a process which has been reported with a high level of details. The first step consisted in identifying different penalty signals to inform the decisions of the controllers regarding the best periods when to operate the heat pump. In addition to the price of electricity, traditionally used for this purpose, a novel penalty signal representing the marginal CO_2 emissions of the power grid has been created following a new methodology. This signal better estimates the effects of DSM actions in terms of carbon footprint than an average emissions factor would. The cost reduction objective was in fact found to be conflicting with the reduction of the emissions in the considered context. Secondly, a rule-based controller was developed and tuned: it consisted in a set-point modulation triggered by thresholds set on the penalty signal. A high sensitivity of the RBC was observed regarding the base set-point and the thresholds of high and low penalty. Thirdly, a model predictive controller was also developed. To this

end, simplified models of both the building envelope and the heat pump performance were fitted. It was shown that these models needed adaptations between heating and cooling operation, so that they could be used in the winter and the summer seasons. The necessity of a mixed integer formulation of the MPC was also highlighted, to represent better the real operation of a variable speed heat pump used for DHW and space conditioning. Considering the computational delay constitutes another novelty of the developed MPC. Similarly than for the RBC, the importance of tuning and the sensitivity to the tuning parameters in the MPC was evidenced, showing that considering too restrictive constraints on the comfort side does not enable to provide energy flexibility. Further than the controllers themselves, the simulation frameworks developed for their testing are another valuable output of this work, since they can be reused to test additional configurations.

To evaluate the benefits brought by the developed controllers, certain performance indicators have been chosen, such as the flexibility factors, the costs and marginal emissions savings. Additionally, graphical representations of the flexibility potential have been proposed, to be used for example by aggregators of flexibility. The RBC and MPC controllers showed the ability to provide cost savings of 5% and emissions savings of 15 % in heating mode, and in cooling mode, 30% cost savings and 10% emissions savings. These results were achieved by shifting the heat pump loads to periods of lesser penalty, increasing the flexibility factors by up to +0.7 in the best scenario. It was shown that in certain contexts (i.e. when the reference control is far from optimal regarding the considered objective), the RBC controller could perform as well as the MPC, which suggests that the development costs of MPC are not worth it in such cases. When the reference case is already close to optimal, the MPC could perform better, which justifies the efforts put into fitting appropriate models and implementing the optimization framework of the MPC. The better abilities of MPC to anticipate and optimize the heat pump operation have been highlighted as strong advantages for its development in the future.

Another strong contribution of the thesis is the testing of the flexibility controllers in an experimental setup with a real heat pump. In addition to the experiments, a high-fidelity heat pump model was created based on the observed behavior of the real heat pump in the laboratory. Both frameworks thus conferred a high reliability to the reported results, even if these results showed sometimes lower claimed savings than reported in literature studies where much simpler heat pump models have been used. Moreover, the implementation on a real heat pump enabled to highlight some practical challenges such as the MPC model mismatch, and conflicts of communication, control and connection with the local controller of the heat pump, which also constitute valuable learnings obtained from this thesis work.

Overall, the thesis evidenced the potential of using RBC or MPC controllers to provide energy flexibility in a residential context under a Mediterranean climate in Spain. In particular, the capacities for flexibility offered in the heating and the cooling season have been differentiated, with for example a higher potential for cost savings in the summer season, and for emissions savings in the heating season. Reversible heat pumps can thus be used as enablers of implicit demand response in both seasons for residential buildings. In this way, the thermal loads of such buildings can be made more flexible, and eventually permit a larger integration of renewable energy sources in the power grid.

2.4 Recommendations for further research

The energy flexibility of buildings is a relatively new field, which means a lot of potential further research could be carried out to cover unexplored aspects.

Firstly, the field of application can be broadened: this thesis has focused on residential buildings of the nZEB type in a Mediterranean climate. Other building typologies and climates could be included in the study, reusing the testing framework developed in this thesis. In particular, investigating the other building archetypes of Spain, trying different levels of insulation/refurbishment, including the production of a local PV system and comparing the results in terms of energy flexibility would provide interesting insights. Furthermore, a single building can only provide a little amount of flexibility, therefore research should now also focus on aggregation of demand-side flexibility and scaling existing strategies at the higher level of building clusters [178]. A new Annex project following IEA EBC Annex 67 might look closely into these research topics. Regarding the climate, more research would be

needed regarding shoulder seasons (spring and autumn), where the needs for heating or cooling are very limited, or where the system might switch from one mode to the other. In these seasons, the flexibility capacity for load-shifting should be low, but its efficiency high, since it would be easier to retain heat (or cold) over long periods if the losses to the outside are lower (milder outdoor temperatures). A better understanding of these phenomena would enable to have a more representative overview of the energy flexibility potential all year round, since this thesis only focused on short periods of the most extreme weather in the considered climate.

The formulation of the MPC also constitutes a subject for further research. It has already been detailed in this thesis, but only one configuration of the controller was then tested. Possible variations of the controller includes for example time-varying temperature constraints: instead of considering a constant comfort range all day long, the constraints can be adapted to the presence of the occupants, relaxing them when the inhabitants are absent, or introducing a night setback to allow for lower temperatures at night in heating mode. The constraints on the inputs can also be improved: we have here considered a conservative option, where the capacity of the heat pump is limited to a maximum calculated from a certain model (see Equation IV.16). In reality, the capacity of the heat pump can happen to be greater in certain conditions of supply temperature, therefore amplifying the range would give more possibilities to the optimization problem. Additionally, the MPC studied in the thesis has only been tested in conditions of perfect forecast: the controller had a perfect knowledge of the future weather and penalty signal. Functioning in real time, such controller would need to rely on imperfect weather predictions obtained from forecast services. Introducing this level of uncertainty and comparing with the perfect predictions base case is an interesting topic, to evaluate if the controller can get close enough to this ideal base case.

Finally, mainly implicit demand response has been studied in this thesis, since it was the only possibility for enabling energy flexibility in buildings in Spain. Recent political changes and evolutions in the market might enable also explicit demand response and aggregation of flexible loads in the future, therefore this other type of DSM should also be studied for small consumers. Explicit demand response consists in actively requesting a customer to change its consumption patterns in exchange for a direct reward. This was only touched on in the thesis in section III.2.3, with active rule-based DR events and how to represent their potential graphically. Further research is certainly needed in this field regarding how to make such explicit DR strategies viable both for a potential aggregator and the final users.

To sum up, there are plenty of new topics and facets of existing topics to be investigated further, and this is a booming field of research. It will be very exciting to see what is coming in this sector in the upcoming years, and in which directions the markets and research will move.

Bibliography

[1] Intergovernmental Panel on Climate Change (IPCC), "Special Report on Global Warming of 1.5ºC," Incheon, Republic of Korea, Tech. Rep., 2018 (Cited on pages 1, 2).

[2] Copernicus Climate Change Service, *Climate bullletins*, 2019. [Online]. Available: https://climate.copernicus.eu/ (Cited on page 1).

[3] J. Duncombe, *Greenland Ice Sheet Beats All-Time 1-Day Melt Record*, Aug. 2019. DOI: 10.1029/2019EO130349. [Online]. Available: https://eos.org/articles/greenland-ice-sheet-beats-all-time-1-day-melt-record (Cited on page 1).

[4] Climate Emergency Declaration and Mobilisation in Action, *Call to declare a climate emergency*, 2019. [Online]. Available: https://climateemergencydeclaration.org/ (visited on 08/13/2019) (Cited on page 1).

[5] UNFCC Conference of the Parties (COP), *Adoption of the Paris Agreement. Proposal by the President*. Geneva (Switzerland), 2015. [Online]. Available: http://unfccc.int/documentation/documents/advanced%7B%5C_%7Dsearch/items/6911.php?priref=600008831 (Cited on page 2).

[6] European Commission - Directorate-General for Energy, *Clean energy for all Europeans*, Luxembourg, 2019. DOI: 10.2833/21366 (Cited on page 2).

[7] B. Johnson, P. Denholm, B. Kroposki, and B.-m. Hodge, "Achieving a 100% Renewable Grid," *IEEE Power and Energy Magazine*, no. april, pp. 61–73, 2017, ISSN: 1540-7977. DOI: 10.1109/MPE.2016.2637122 (Cited on page 2).

[8] IRENA, IEA, and REN21, *Renewable Energy Policies in a Time of Transition*. 2018, p. 112, ISBN: 9789292600617 (Cited on page 2).

[9] REN21, *Renewables - Global Status Report 2019*. 2019, p. 336, ISBN: 9783981891140. [Online]. Available: https://wedocs.unep.org/bitstream/handle/20.500.11822/28496/REN2019.pdf?sequence=1%7B%5C&%7DisAllowed=y%7B%5C%%7D0Ahttp://www.ren21.net/cities/wp-content/uploads/2019/05/REC-GSR-Low-Res.pdf (Cited on page 2).

[10] IRENA, *Renewable energy auctions: Status and trends beyond price (preliminary findings)*. Abu Dhabi, 2019, ISBN: 978-92-9260-136-2 (Cited on page 2).

[11] J. R. Martín, *Portugal reveals winners of record-breaking solar auction*, Aug. 2019. [Online]. Available: https://www.pv-tech.org/news/portugal-reveals-winners-of-record-breaking-solar-auction (Cited on page 2).

[12] P. D. Lund, J. Lindgren, J. Mikkola, and J. Salpakari, "Review of energy system flexibility measures to enable high levels of variable renewable electricity," *Renewable and Sustainable Energy Reviews*, vol. 45, pp. 785–807, 2015, ISSN: 13640321. DOI: 10.1016/j.rser.2015.01.057 (Cited on pages 3, 5).

[13] S. Chatzivasileiadis, D. Ernst, and G. Andersson, "The Global Grid," *Renewable Energy*, vol. 57, pp. 372–383, 2013, ISSN: 09601481. DOI: 10.1016/j.renene.2013.01.032 (Cited on page 4).

[14] C. Mitchell, "Momentum is increasing towards a flexible electricity system based on renewables," *Nature Energy*, vol. 1, no. 2, p. 15 030, 2016, ISSN: 2058-7546. DOI: 10.1038/nenergy.2015.30 (Cited on page 5).

[15] A. Morch and O. Wolfang, *Post-2020 framework for a liberalised electricity market with a large share of renewable energy sources*, 2016 (Cited on page 5).

[16] International Energy Agency, "The Power to Choose. Demand Response in Liberalised Electricity Markets," *Promotion {&} Education*, vol. 11, p. 156, 2003, ISSN: 1025-3823. DOI: 10.1177/10253823040110040101 (Cited on page 5).

[17] Smart Energy Demand Coalition SEDC, "Explicit Demand Response in Europe - Mapping the Markets 2017," Tech. Rep., 2017, p. 223. [Online]. Available: http://www.smarten.eu/wp-content/uploads/2017/04/SEDC-Explicit-Demand-Response-in-Europe-Mapping-the-Markets-2017.pdf (Cited on pages 5, 36).

[18] CNMC Comisión Nacional de los Mercados y la Competencia, "INF/DE/180/18 - Acuerdo por el que se emite informe sobre el cumplimiento del último hito del plan de sustitución de contadores," CNMC, Madrid, Spain, Tech. Rep., 2019, pp. 1–63 (Cited on pages 5, 37).

[19] European Commission, "Directive 2010/31/EU of the European Parliament and of the Council of 19 May 2010 on the energy performance of buildings (recast)," *Official Journal European Communities*, vol. L 153, pp. 13–35, 2010 (Cited on pages 5, 6).

[20] IEA DSM Task 17, "Conclusions and Recommendations – Demand Flexibility in Households and Buildings," Tech. Rep., 2016. [Online]. Available: http://www.ieadsm.org/publications/key-publications/ (Cited on page 5).

[21] R. D'Angiolella, M. De Groote, and M. Fabbri, "NZEB 2.0: interactive players in an evolving energy system," *REHVA Journal*, vol. 53, no. 3, pp. 52–55, 2016 (Cited on page 5).

[22] VITO, "Interim Report July 2019 of the 2nd Technical Support Study on the Smart Readiness Indicator for Buildings," VITO, Mol, Belgium, Tech. Rep., 2019, p. 281. [Online]. Available: https://smartreadinessindicator.eu (Cited on page 6).

[23] S. Ø. Jensen, A. Marszal-Pomianowska, R. Lollini, W. Pasut, A. Knotzer, P. Engelmann, A. Stafford, and G. Reynders, "IEA EBC Annex 67 Energy Flexible Buildings," *Energy and Buildings*, vol. 155, pp. 25–34, Aug. 2017, ISSN: 03787788. DOI: 10.1016/j.enbuild.2017.08.044 (Cited on page 6).

[24] Y. Chen, P. Xu, J. Gu, F. Schmidt, and W. Li, *Measures to improve energy demand flexibility in buildings for demand response (DR): A review*, 2018. DOI: 10.1016/j.enbuild.2018.08.003 (Cited on page 6).

[25] A. Arteconi, N. J. Hewitt, and F. Polonara, "State of the art of thermal storage for demand-side management," *Applied Energy*, vol. 93, pp. 371–389, 2012, ISSN: 03062619. DOI: 10.1016/j.apenergy.2011.12.045 (Cited on page 6).

[26] J. Heier, C. Bales, and V. Martin, "Combining thermal energy storage with buildings - A review," *Renewable and Sustainable Energy Reviews*, vol. 42, pp. 1305–1325, 2015, ISSN: 13640321. DOI: 10.1016/j.rser.2014.11.031 (Cited on page 6).

[27] G. Reynders, J. Diriken, and D. Saelens, "Generic characterization method for energy flexibility: Applied to structural thermal storage in residential buildings," *Applied Energy*, vol. 198, pp. 192–202, 2017, ISSN: 03062619. DOI: 10.1016/j.apenergy.2017.04.061 (Cited on pages 6, 42, 43).

[28] D. I. Mendoza-Serrano, D. J. Chmielewski, and Ieee, "Controller and System Design for HVAC with Thermal Energy Storage," *2012 American Control Conference*, pp. 3669–3674, 2012, ISSN: 0743-1619. DOI: 10.1109/ACC.2012.6315658 (Cited on page 6).

[29] K. Amarasinghe, D. Wijayasekara, H. Carey, M. Manic, D. He, and W. P. Chen, "Artificial neural networks based thermal energy storage control for buildings," *IECON 2015 - 41st Annual Conference of the IEEE Industrial Electronics Society*, pp. 5421–5426, 2015. DOI: 10.1109/IECON.2015.7392953 (Cited on page 6).

[30] B. Venkatesh, "Thermal Energy Storage for Homes," in *2018 IEEE International Conference on Smart Energy Grid Engineering (SEGE)*, IEEE, 2018, pp. 36–39, ISBN: 9781538664100 (Cited on page 6).

[31] A. J. Marszal, P. Heiselberg, J. S. Bourrelle, E. Musall, K. Voss, I. Sartori, and A. Napolitano, "Zero Energy Building - A review of definitions and calculation methodologies," *Energy and Buildings*, vol. 43, no. 4, pp. 971–979, 2011, ISSN: 03787788. DOI: 10.1016/j.enbuild.2010.12.022 (Cited on page 6).

[32] I. Sartori, A. Napolitano, and K. Voss, "Net zero energy buildings: A consistent definition framework," *Energy and Buildings*, vol. 48, pp. 220–232, 2012, ISSN: 03787788. DOI: 10.1016/j.enbuild.2012.01.032 (Cited on page 6).

[33] F. Noris, E. Musall, J. Salom, B. Berggren, S. Ø. Jensen, K. Lindberg, and I. Sartori, "Implications of weighting factors on technology preference in net zero energy buildings," *Energy and Buildings*, vol. 82, pp. 250–262, 2014, ISSN: 03787788. DOI: 10.1016/j.enbuild.2014.07.004 (Cited on page 7).

[34] E. Rodriguez-Ubinas, C. Montero, M. Porteros, S. Vega, I. Navarro, M. Castillo-Cagigal, E. Matallanas, and A. Gutierrez, "Passive design strategies and performance of Net Energy Plus Houses," *Energy and Buildings*, vol. 83, pp. 10–22, 2014, ISSN: 03787788. DOI: 10.1016/j.enbuild.2014.03.074 (Cited on page 7).

[35] T. Péan, L. Gennari, O. B. Kazanci, and B. W. Olesen, "Evaluation of the Energy and Comfort Performance of a Plus- Energy House under Scandinavian Summer Conditions," *Proceedings of the 12th World REHVA Conference - CLIMA 2016, Aalborg, Denmark*, 2016 (Cited on page 7).

[36] D. Fischer and H. Madani, "On heat pumps in smart grids: A review," *Renewable and Sustainable Energy Reviews*, vol. 70, no. October 2016, pp. 342–357, 2017, ISSN: 18790690. DOI: 10.1016/j.rser.2016.11.182 (Cited on pages 7, 15, 29, 49, 94, 101).

[37] European Copper Institute and T. Nowak, *Heat Pumps - Integrating technologies to decarbonise heating and cooling*, European Copper Institute, Ed. European Copper Institute, 2018 (Cited on page 7).

[38] International Energy Agency, *Tracking Clean Energy Progress - Cooling*, 2019. [Online]. Available: https://www.iea.org/tcep/buildings/cooling/ (visited on 08/18/2019) (Cited on page 7).

[39] European Heat Pump Association, *EHPA stats*, 2019. [Online]. Available: http://stats.ehpa.org (visited on 08/18/2019) (Cited on page 7).

[40] T. Nowak and P. Westring, "Growing for good ? The European Heat Pump Market - Status and outlook," in *12th IEA Heat Pump Conference 2017*, Rotterdam, Netherlands, 2017, pp. 1–10 (Cited on page 7).

[41] International Energy Agency, *Energy Technology Perspectives 2017: Catalysing Energy Technology Transformations*. 2017, p. 371, ISBN: 9789264208001. DOI: 10.1787/energy_tech-2014-en. [Online]. Available: https://webstore.iea.org/download/summary/237?fileName=English-ETP-2017-ES.pdf (Cited on page 8).

[42] A. D. Carvalho, P. Moura, G. C. Vaz, and A. T. De Almeida, "Ground source heat pumps as high efficient solutions for building space conditioning and for integration in smart grids," *Energy Conversion and Management*, vol. 103, pp. 991–1007, 2015, ISSN: 01968904. DOI: 10.1016/j.enconman.2015.07.032 (Cited on pages 9, 17, 18, 20, 75).

[43] U. I. Dar, I. Sartori, L. Georges, and V. Novakovic, "Advanced control of heat pumps for improved flexibility of Net-ZEB towards the grid," *Energy and Buildings*, vol. 69, pp. 74–84, 2014, ISSN: 03787788. DOI: 10.1016/j.enbuild.2013.10.019 (Cited on pages 9, 16–20, 75).

[44] L. Schibuola, M. Scarpa, and C. Tambani, "Demand response management by means of heat pumps controlled via real time pricing," *Energy and Buildings*, vol. 90, pp. 15–28, 2015, ISSN: 03787788. DOI: 10.1016/j.enbuild.2014.12.047 (Cited on pages 9, 18, 19, 28, 75).

[45] R. De Coninck, R. Baetens, D. Saelens, A. Woyte, and L. Helsen, "Rule-based demand-side management of domestic hot water production with heat pumps in zero energy neighbourhoods," *Journal of Building Performance Simulation*, vol. 7, no. 4, pp. 271–288, 2014, ISSN: 1940-1493. DOI: 10.1080/19401493.2013.801518 (Cited on pages 9, 17–21, 23, 28, 30, 36, 75).

[46] G. Masy, E. Georges, C. Verhelst, and V. Lemort, "Smart grid energy flexible buildings through the use of heat pumps and building thermal mass as energy storage in the Belgian context," *Science and Technology for the Built Environment*, vol. 4731, no. August, pp. 800–811, 2015, ISSN: 2374-4731. DOI: 10.1080/23744731.2015.1035590 (Cited on pages 9, 17, 23–28, 36, 120).

[47] R. Halvgaard, N. K. Poulsen, H. Madsen, and J. B. Jorgensen, "Economic Model Predictive Control for building climate control in a Smart Grid," *2012 IEEE PES Innovative Smart Grid Technologies (ISGT)*, pp. 1–6, 2012. DOI: 10.1109/ISGT.2012.6175631 (Cited on pages 9, 23–27, 36).

[48] J. Ma, S. J. Qin, and T. Salsbury, "Application of economic MPC to the energy and demand minimization of a commercial building," *Journal of Process Control*, vol. 24, no. 8, pp. 1282–1291, 2014, ISSN: 09591524. DOI: 10.1016/j.jprocont.2014.06.011 (Cited on pages 9, 23–27).

[49] R. De Coninck, F. Magnusson, J. Åkesson, and L. Helsen, "Toolbox for development and validation of grey-box building models for forecasting and control," *Journal of Building Performance Simulation*, no. July, pp. 1–16, 2015, ISSN: 1940-1493. DOI: 10.1080/19401493.2015.1046933 (Cited on pages 9, 27, 29, 119).

[50] T. Péan, J. Salom, and R. Costa-Castelló, "Review of control strategies for improving the energy flexibility provided by heat pump systems in buildings," *Journal of Process Control*, vol. 74C, no. Special Issue on Efficient Energy Management, pp. 35–49, Apr. 2019, ISSN: 09591524. DOI: 10.1016/j.jprocont.2018.03.006 (Cited on pages 9, 12, 68, 149).

[51] T. Péan, J. Ortiz, and J. Salom, "Impact of Demand-Side Management on Thermal Comfort and Energy Costs in a Residential nZEB," *Buildings*, vol. 7, no. 2, p. 37, 2017, ISSN: 2075-5309. DOI: 10.3390/buildings7020037 (Cited on pages 12, 20).

[52] T. Péan, R. Costa-Castello, E. Fuentes, and J. Salom, "Experimental testing of variable speed heat pump control strategies for enhancing energy flexibility in buildings," *IEEE Access*, vol. 7, no. 1, pp. 37 071–37 087, 2019, ISSN: 2169-3536. DOI: 10.1109/ACCESS.2019.2903084 (Cited on pages 12, 37, 102).

[53] T. Péan, R. Costa-Castelló, and J. Salom, "Price and carbon-based energy flexibility of residential heating and cooling loads using model predictive control," *Sustainable Cities and Society*, vol. 50, Oct. 2019, ISSN: 22106707. DOI: 10.1016/j.scs.2019.101579 (Cited on pages 12, 37).

[54] T. Péan, J. Ortiz, and J. Salom, "Potential and optimization of a price-based control strategy for improving energy flexibility in Mediterranean buildings.," in *Proceedings of CISBAT 2017 International Conference – Future Buildings and Districts – Energy Efficiency from Nano to Urban Scale (under review)*, Lausanne, Switzerland, 2017 (Cited on page 12).

[55] T. Péan, E. Fuentes, J. Ortiz, and J. Salom, "Performance of a gas boiler under dynamic operation conditions: experimental studies in semi-virtual environment," in *COBEE2018 - Conference On Building Energy & Environment*, Melbourne, Australia, 2018 (Cited on page 12).

[56] T. Péan, B. Torres, J. Salom, and J. Ortiz, "Representation of daily profiles of building energy flexibility," in *eSim 2018, the 10th Conference of IBPSA-Canada*, Montréal (QC), Canada, 2018, pp. 153–162, ISBN: 9782921145886 (Cited on page 13).

[57] T. Péan, J. Salom, and J. Ortiz, "Environmental and Economic Impact of Demand Response Strategies for Energy Flexible Buildings," in *Building Simulation and Optimization BSO 2018, 11-12th September 2018, Cambridge (UK)*, Cambridge, United Kingdom, 2018, pp. 277–283 (Cited on pages 13, 38).

[58] T. Péan, J. Salom, and R. Costa-Castelló, "Configurations of model predictive control to exploit energy flexibility in building thermal loads," in *57th IEEE Conference on Decision and Control*, Miami Beach, FL, USA, 2018 (Cited on page 13).

[59] T. Péan and J. Salom, "Laboratory facilities used to test energy flexibility in buildings - A technical report from IEA EBC Annex 67 Energy Flexible Buildings," IEA EBC Annex 67, Tech. Rep., 2019. [Online]. Available: http://annex67.org/media/1708/laboratory-facilities-used-to-test-energy-flexibility-in-buildings-2nd-edition.pdf (Cited on pages 13, 32).

[60] R. Toffanin, T. Péan, J. Ortiz, and J. Salom, "Development and Implementation of a Reversible Variable Speed Heat Pump Model for Model Predictive Control Strategies," in *Building Simulation 2019 - 16th IBPSA International Conference*, Rome, Italy, 2019 (Cited on pages 13, 62, 66, 153).

[61] C. Finck, P. Beagon, J. Clauß, T. Péan, P. Vogler-Finck, K. Zhang, and H. Kazmi, "Review of applied and tested control possibilities for energy flexibility in buildings - A technical report from IEA EBC Annex 67 Energy Flexible Buildings," International Energy Agency - Energy in Buildings and Communities, Tech. Rep., 2018, p. 61. [Online]. Available: http://annex67.org/media/1551/review-of-applied-and-tested-control-possibilities-for-energy-flexibility-in-buildings-technical-report-annex67.pdf (Cited on page 13).

[62] J. Salom and T. Péan, "Experimental facilities and methods for assessing energy flexibility in buildings - Deliverable of the Annex 67 - Energy Flexible Buildings," International Energy Agency - Energy in Buildings and Communities, Tech. Rep., 2019, p. 111 (Cited on page 13).

[63] Y. J. Kim, E. Fuentes, and L. K. Norford, "Experimental Study of Grid Frequency Regulation Ancillary Service of a Variable Speed Heat Pump," *IEEE Transactions on Power Systems*, vol. 31, no. 4, pp. 3090–3099, 2016, ISSN: 08858950. DOI: 10.1109/TPWRS.2015.2472497 (Cited on page 15).

[64] A. Afram and F. Janabi-Sharifi, "Theory and applications of HVAC control systems - A review of model predictive control (MPC)," *Building and Environment*, vol. 72, pp. 343–355, 2014, ISSN: 03601323. DOI: 10.1016/j.buildenv.2013.11.016 (Cited on page 15).

[65] E. Atam and L. Helsen, "Ground-coupled heat pumps: Part 1 - Literature review and research challenges in modeling and optimal control," *Renewable and Sustainable Energy Reviews*, vol. 54, pp. 1653–1667, 2016, ISSN: 18790690. DOI: 10.1016/j.rser.2015.10.007. [Online]. Available: http://dx.doi.org/10.1016/j.rser.2015.10.007 (Cited on pages 15, 29).

[66] K.-H. Lee, M.-C. Joo, and N.-C. Baek, "Experimental Evaluation of Simple Thermal Storage Control Strategies in Low-Energy Solar Houses to Reduce Electricity Consumption during Grid On-Peak Periods," *Energies*, vol. 8, no. 9, pp. 9344–9364, 2015, ISSN: 1996-1073. DOI: 10.3390/en8099344 (Cited on pages 16–18, 20, 21, 28).

[67] J. Hong, C. Johnstone, J. Torriti, and M. Leach, "Discrete demand side control performance under dynamic building simulation: A heat pump application," *Renewable Energy*, vol. 39, no. 1, pp. 85–95, 2012, ISSN: 09601481. DOI: 10.1016/j.renene.2011.07.042 (Cited on pages 16–18, 20, 21).

[68] H. Madani, J. Claesson, and P. Lundqvist, "A descriptive and comparative analysis of three common control techniques for an on/off controlled Ground Source Heat Pump (GSHP) system," *Energy and Buildings*, vol. 65, pp. 1–9, 2013, ISSN: 03787788. DOI: 10.1016/j.enbuild.2013.05.006 (Cited on pages 16, 17).

[69] M. Miara, D. Günther, Z. L. Leitner, and J. Wapler, "Simulation of an Air-to-Water Heat Pump System to Evaluate the Impact of Demand-Side-Management Measures on Efficiency and Load-Shifting Potential," *Energy Technology*, vol. 2, no. 1, pp. 90–99, 2014, ISSN: 21944288. DOI: 10.1002/ente.201300087 (Cited on pages 16, 18–20, 36).

[70] C. Kandler, P. Wimmer, and J. Honold, "Predictive control and regulation strategies of air-to-water heat pumps," *Energy Procedia*, vol. 78, pp. 2088–2093, 2015, ISSN: 18766102. DOI: 10.1016/j.egypro.2015.11.239. [Online]. Available: http://dx.doi.org/10.1016/j.egypro.2015.11.239 (Cited on page 16).

[71] C. Verhelst, "Model Predictive Control of Ground Coupled Heat Pump Systems for Office Buildings," PhD thesis, Katholieke Universiteit Leuven, 2012, ISBN: 9789460184970 (Cited on pages 16, 23, 36).

[72] ISO, *ISO 7726: Ergonomics of the thermal environment – Instruments for measuring physical quantities*, 2001 (Cited on page 16).

[73] R. De Coninck, R. Baetens, B. Verbruggen, J. Driesen, D. Saelens, and L. Helsen, "Modelling and simulation of a grid connected photovoltaic heat pump system with thermal energy storage using Modelica," *8th International Conference on System Simulation in Buildings*, no. June, pp. 1–21, 2010, ISSN: 1600051X (Cited on pages 16–18, 20, 28).

[74] G. Reynders, T. Nuytten, and D. Saelens, "Potential of structural thermal mass for demand-side management in dwellings," *Building and Environment*, vol. 64, pp. 187–199, 2013, ISSN: 03601323. DOI: 10.1016/j.buildenv.2013.03.010 (Cited on pages 17, 18, 21, 24, 28).

[75] J. Le Dréau and P. Heiselberg, "Energy flexibility of residential buildings using short term heat storage in the thermal mass," *Energy*, vol. 111, no. 1, pp. 1–5, 2016, ISSN: 03605442. DOI: 10.1016/j.energy.2016.05.076. arXiv: arXiv:1011.1669v3 (Cited on pages 18–20, 28).

[76] G. R. Newsham and B. G. Bowker, "The effect of utility time-varying pricing and load control strategies on residential summer peak electricity use: A review," *Energy Policy*, vol. 38, no. 7, pp. 3289–3296, 2010, ISSN: 03014215. DOI: 10.1016/j.enpol.2010.01.027 (Cited on page 19).

[77] O. Corradi and H. Ochsenfeld, "Integration of fluctuating energy by electricity price control," MSc Thesis, Technical University of Denmark (DTU), 2011 (Cited on page 19).

[78] K. Klein, S. Killinger, D. Fischer, C. Streuling, J. Salom, and E. Cubi, "Comparison of the future residual load in fifteen countries and requirements to grid-supportive building operation," in *Eurosun 2016*, Palma de Mallorca, Spain, 2016, pp. 11–14 (Cited on pages 19, 21, 36, 40, 123).

[79] F. Oldewurtel, A. Parisio, C. N. Jones, D. Gyalistras, M. Gwerder, V. Stauch, B. Lehmann, and M. Morari, "Use of model predictive control and weather forecasts for energy efficient building climate control," *Energy and Buildings*, vol. 45, pp. 15–27, 2012, ISSN: 03787788. DOI: 10.1016/j.enbuild.2011.09.022 (Cited on pages 20, 22, 30).

[80] D. Fischer, J. Bernhardt, H. Madani, and C. Wittwer, "Comparison of control approaches for variable speed air source heat pumps considering time variable electricity prices and PV," *Applied Energy*, vol. 204, pp. 93–105, 2017, ISSN: 03062619. DOI: 10.1016/j.apenergy.2017.06.110 (Cited on pages 20, 29).

[81] M. d. M. Castilla, J. D. Álvarez, F. Rodríguez, and M. Berenguel, *Comfort Control in Buildings*, ser. Advances in Industrial Control September. London: Springer London, 2014, p. 221, ISBN: 978-1-4471-6346-6. DOI: 10.1007/978-1-4471-6347-3 (Cited on page 21).

[82] Y. Zong, L. Mihet-Popa, D. Kullmann, A. Thavlov, O. Gehrke, and H. W. Bindner, "Model predictive controller for active demand side management with PV self-consumption in an intelligent building," *IEEE PES Innovative Smart Grid Technologies Conference Europe*, pp. 1–8, 2012, ISSN: 2165-4816. DOI: 10.1109/ISGTEurope.2012.6465618 (Cited on page 22).

[83] C. Verhelst, D. Degrauwe, F. Logist, J. V. Impe, and L. Helsen, "Multi-objective optimal control of an air-to-water heat pump for residential heating," *Building Simulation*, vol. 5, no. 3, pp. 281–291, 2012, ISSN: 1996-3599. DOI: 10.1007/s12273-012-0061-z (Cited on pages 22, 23).

[84] E. F. Camacho and C. Bordons, *Model Predictive control*, ser. Advanced Textbooks in Control and Signal Processing. London: Springer London, 2007, vol. 53, pp. 1689–1699, ISBN: 978-1-85233-694-3. DOI: 10.1007/978-0-85729-398-5 (Cited on pages 22, 25, 26, 89, 122).

[85] F. Tahersima, J. Stoustrup, H. Rasmussen, and S. a. Meybodi, "Economic COP optimization of a heat pump with hierarchical model predictive control," *2012 IEEE 51st IEEE Conference on Decision and Control (CDC)*, no. Cdc, pp. 7583–7588, 2012, ISSN: 01912216. DOI: 10.1109/CDC.2012.6425810 (Cited on page 23).

[86] X. Li and A. Malkawi, "Multi-objective optimization for thermal mass model predictive control in small and medium size commercial buildings under summer weather conditions," *Energy*, vol. 112, pp. 1194–1206, 2016, ISSN: 03605442. DOI: 10.1016/j.energy.2016.07.021 (Cited on pages 23, 26, 27, 36).

[87] T. S. Pedersen, P. Andersen, and K. M. Nielsen, "Central control of heat pumps for smart grid purposes tested on single family houses," *2013 10th IEEE International Conference on Networking, Sensing and Control, ICNSC 2013*, pp. 118–123, 2013. DOI: 10.1109/ICNSC.2013.6548722 (Cited on page 23).

[88] M. U. Kajgaard, J. Mogensen, A. Wittendorff, A. T. Veress, and B. Biegel, "Model predictive control of domestic heat pump," *2013 American Control Conference*, pp. 2013–2018, 2013. DOI: 10.1109/ACC.2013.6580131 (Cited on pages 23, 36).

[89] R. M. Santos, Y. Zong, J. Sousa, L. Mendonça, and A. Thavlov, "Nonlinear Economic Model Predictive Control Strategy for Active Smart Buildings," in *2016 IEEE PES Innovative Smart Grid Technologies Conference Europe*, Ljubljana, Slovenia, 2016, ISBN: 9781509033584. DOI: 978-1-5090-3358-4/ (Cited on pages 23, 25–27).

[90] G. Bianchini, M. Casini, A. Vicino, and D. Zarrilli, "Demand-response in building heating systems: A Model Predictive Control approach," *Applied Energy*, vol. 168, pp. 159–170, 2016, ISSN: 03062619. DOI: 10.1016/j.apenergy.2016.01.088 (Cited on pages 23, 27, 28, 36).

[91] M. Dahl Knudsen and S. Petersen, "Demand response potential of model predictive control of space heating based on price and carbon dioxide intensity signals," *Energy and Buildings*, vol. 125, pp. 196–204, 2016, ISSN: 03787788. DOI: 10.1016/j.enbuild.2016.04.053 (Cited on pages 23, 25–27, 36, 37).

[92] S. M. Sichilalu and X. Xia, "Optimal power dispatch of a grid tied-battery-photovoltaic system supplying heat pump water heaters," *Energy Conversion and Management*, vol. 102, pp. 81–91, 2015, ISSN: 01968904. DOI: 10.1016/j.enconman.2015.03.087 (Cited on pages 23, 27, 28, 36).

[93] D. I. Mendoza-Serrano and D. J. Chmielewski, "Smart grid coordination in building HVAC systems: EMPC and the impact of forecasting," *Journal of Process Control*, vol. 24, no. 8, pp. 1301–1310, 2014, ISSN: 09591524. DOI: 10.1016/j.jprocont.2014.06.005. [Online]. Available: http://dx.doi.org/10.1016/j.jprocont.2014.06.005 (Cited on pages 23, 28).

[94] J. Salpakari and P. Lund, "Optimal and rule-based control strategies for energy flexibility in buildings with PV," *Applied Energy*, vol. 161, pp. 425–436, 2016, ISSN: 03062619. DOI: 10.1016/j.apenergy.2015.10.036 (Cited on page 23).

[95] H. A. Toersche, V. Bakker, A. Molderink, S. Nykamp, J. L. Hurink, and G. J. M. Smit, "Controlling the heating mode of heat pumps with the TRIANA three step methodology," *2012 IEEE PES Innovative Smart Grid Technologies, ISGT 2012*, pp. 1–7, 2012. DOI: 10.1109/ISGT.2012.6175662 (Cited on pages 23, 25).

[96] D. Sturzenegger, D. Gyalistras, M. Gwerder, C. Sagerschnig, M. Morari, and R. S. Smith, "Model Predictive Control of a Swiss office building," in *11th REHVA World Congress*, 2013, p. 10. [Online]. Available: http://www.opticontrol.ethz.ch/Lit/Stur%7B%5C_%7D13%7B%5C_%7DProc-Clima2013.pdf (Cited on pages 23–27).

[97] F. Oldewurtel, D. Sturzenegger, G. Andersson, M. Morari, and R. S. Smith, "Towards a standardized building assessment for demand response," *Proceedings of the IEEE Conference on Decision and Control*, pp. 7083–7088, 2013, ISSN: 01912216. DOI: 10.1109/CDC.2013.6761012 (Cited on pages 23, 26, 27, 42).

[98] R. De Coninck and L. Helsen, "Quantification of flexibility in buildings by cost curves - Methodology and application," *Applied Energy*, vol. 162, pp. 653–665, 2016, ISSN: 03062619. DOI: 10.1016/j.apenergy.2015.10.114. [Online]. Available: http://dx.doi.org/10.1016/j.apenergy.2015.10.114 (Cited on pages 23, 25, 27, 28).

[99] Z. Váňa, J. Cigler, J. Široký, E. Žáčeková, and L. Ferkl, "Model-based energy efficient control applied to an office building," *Journal of Process Control*, vol. 24, no. 6, pp. 790–797, 2014, ISSN: 09591524. DOI: 10.1016/j.jprocont.2014.01.016 (Cited on pages 23, 25, 27, 28).

[100] ASHRAE, *ANSI/ASHRAE Standard 55: Thermal Environmental Conditions for Human Occupancy*. Atlanta, USA, 2013. DOI: ISSN1041-2336 (Cited on page 26).

[101] UNE, *ISO 7730: Ergonomics of the thermal environment - Analytical determination and interpretation of thermal comfort using calculation of the PMV and PPD indices and local thermal comfort criteria*. 2006 (Cited on page 26).

[102] P. Bacher and H. Madsen, "Identifying suitable models for the heat dynamics of buildings," *Energy and Buildings*, vol. 43, no. 7, pp. 1511–1522, 2011, ISSN: 03787788. DOI: 10.1016/j.enbuild.2011.02.005 (Cited on pages 27, 29, 71, 119).

[103] R. Juhl, J. K. Møller, and H. Madsen, "ctsmr – Continuous Time Stochastic Modeling in R," *The R Journal*, vol. XX, pp. 1–11, 2015. arXiv: 1606.00242 (Cited on pages 27, 29).

[104] A. Pawlowski, J. L. Guzman, F. Rodríguez, M. Berenguel, and J. Sanchez, "Application of time-series methods to disturbance estimation in predictive control problems," *IEEE International Symposium on Industrial Electronics*, pp. 409–414, 2010. DOI: 10.1109/ISIE.2010.5637867 (Cited on page 28).

[105] R. Ooka and S. Ikeda, "A review on optimization techniques for active thermal energy storage control," *Energy and Buildings*, vol. 106, pp. 225–233, 2015, ISSN: 03787788. DOI: 10.1016/j.enbuild.2015.07.031. [Online]. Available: http://dx.doi.org/10.1016/j.enbuild.2015.07.031 (Cited on page 28).

[106] A. Arteconi, N. J. Hewitt, and F. Polonara, "State of the art of thermal storage for demand-side management," *Applied Energy*, vol. 93, pp. 371–389, 2012, ISSN: 03062619. DOI: 10.1016/j.apenergy.2011.12.045. [Online]. Available: http://dx.doi.org/10.1016/j.apenergy.2011.12.045 (Cited on page 28).

[107] D. Six, J. Desmedt, J. V. A. N. Bael, and D. Vanhoudt, "Exploring the Flexibility Potential of Residential Heat Pumps," *21st International Conference on Electricity Distribution*, no. 0442, pp. 6–9, 2011 (Cited on page 28).

[108] D. Vanhoudt, D. Geysen, B. Claessens, F. Leemans, L. Jespers, and J. Van Bael, "An actively controlled residential heat pump: Potential on peak shaving and maximization of self-consumption of renewable energy," *Renewable Energy*, vol. 63, pp. 531–543, 2014, ISSN: 09601481. DOI: 10.1016/j.renene.2013.10.021 (Cited on page 28).

[109] H. Wolisz, H. Harb, P. Matthes, R. Streblow, and D. Müller, "Dynamic simulation of thermal capacity and charging / discharging performance for sensible heat storage in building wall mass," in *13th Conference of International Building Performance Simulation Association*, 2013, pp. 2716–2723 (Cited on page 28).

[110] J. Kensby, A. Trüschel, and J.-O. Dalenbäck, "Potential of residential buildings as thermal energy storage in district heating systems – Results from a pilot test," *Applied Energy*, vol. 137, pp. 773–781, 2015, ISSN: 03062619. DOI: 10.1016/j.apenergy.2014.07.026 (Cited on page 28).

[111] N. J. Hewitt, "Heat pumps and energy storage - The challenges of implementation," *Applied Energy*, vol. 89, no. 1, pp. 37–44, 2012, ISSN: 03062619. DOI: 10.1016/j.apenergy.2010.12.028 (Cited on page 28).

[112] European Parliament, *Directive 2009/72/EC of the European Parliament and of the Council of 13 July 2009 concerning common rules for the internal market in electricity*, Strasbourg, France, 2009 (Cited on pages 29, 36).

[113] Spain, *Real Decreto 1110/2007, de 24 de agosto, por el que se aprueba el Reglamento unificado de puntos de medida del sistema eléctrico*. 2007 (Cited on pages 29, 36).

[114] A. Vandermeulen, L. Vandeplas, and D. Patteeuw, "Flexibility offered by residential floor heating in a smart grid context : the role of heat pumps and renewable energy sources in optimization towards different objectives .," in *12th IEA Heat Pump Conference 2017*, 2017, pp. 1–12 (Cited on page 29).

[115] E. Mlecnik, "Goodbye Passive House, Hello Energy Flexible Building?" In *Proceedings of PLEA 2016 36th International Conference on Passive and Low Energy Architecture*, Los Angeles, USA, 2016 (Cited on page 29).

[116] R. A. Lopes, A. Chambel, J. Neves, D. Aelenei, and J. Martins, "A Literature Review of Methodologies Used to Assess the Energy Flexibility of Buildings," *Energy Procedia*, vol. 91, pp. 1053–1058, 2016, ISSN: 18766102. DOI: 10.1016/j.egypro.2016.06.274 (Cited on pages 29, 42).

[117] A. Arteconi, D. Patteeuw, K. Bruninx, E. Delarue, W. D'haeseleer, and L. Helsen, "Active demand response with electric heating systems: Impact of market penetration," *Applied Energy*, vol. 177, no. October, pp. 636–648, Sep. 2016, ISSN: 03062619. DOI: 10.1016/j.apenergy.2016.05.146 (Cited on page 30).

[118] S. Klein, W. Beckman, J. Mitchel, J. Duffie, N. Duffie, and T. Freeman, *TRNSYS - A transient systems simulation program - TRNSYS 17 Users Manual*, U. of Wisconsin-Madison, Ed., Madison, WI, USA, 2009 (Cited on page 31).

[119] N. Alibabaei, A. S. Fung, and K. Raahemifar, "Development of Matlab-TRNSYS co-simulator for applying predictive strategy planning models on residential house HVAC system," *Energy and Buildings*, vol. 128, pp. 81–98, 2016, ISSN: 03787788. DOI: 10.1016/j.enbuild.2016.05.084 (Cited on page 32).

[120] J. Lofberg, "YALMIP : a toolbox for modeling and optimization in MATLAB," *2004 IEEE International Conference on Robotics and Automation (IEEE Cat. No.04CH37508)*, pp. 284–289, 2004, ISSN: 03014215. DOI: 10.1109/CACSD.2004.1393890 (Cited on pages 32, 89).

[121] Gurobi Optimization, *Gurobi*, 2018. [Online]. Available: http://www.gurobi.com (Cited on pages 32, 89).

[122] D. Fischer, T. Wirtz, K. D. Zerbe, B. Wille-Haussmann, and H. Madani, "Test Cases for Hardware In The Loop Testing of Air To Water Heat Pump Systems in A Smart Grid Context," in *24th IIR International Congress of Refrigeration*, Yokohama, Japan, 2015, p. 584. DOI: 10.13140/RG.2.1.1657.3843 (Cited on page 32).

[123] CEN, *EN 12976-2 - Thermal solar systems and components - Factory made systems - Part 2: Test methods*, Brussels, Belgium, 2017 (Cited on pages 33, 70, 93).

[124] R. Grønborg Junker, R. Relan, R. Amaral Lopes, G. Renders, K. Byskov Lindberg, and H. Madsen, "Characterizing the Energy Flexibility of Buildings and Districts," *Applied Energy*, vol. 225, no. April, pp. 175–182, 2018, ISSN: 0306-2619. DOI: 10.1016/j.apenergy.2018.05.037 (Cited on pages 36, 42).

[125] M. Barbero, L. Igualada, and C. Corchero, "Overview of the regulation on aggregator agents in Europe," *2018 15th International Conference on the European Energy Market (EEM)*, no. 3, pp. 1–5, 2018, ISSN: 21654093. DOI: 10.1109/EEM.2018.8470015 (Cited on page 36).

[126] California Independent System Operator (CAISO), *What the duck curve tells us about managing a green grid*, 2016. [Online]. Available: https://www.caiso.com/Documents/FlexibleResourcesHelpRenewab
7B%5C_%7DFastFacts.pdf (Cited on page 36).

[127] R. De Coninck and L. Helsen, "Quantification of flexibility in buildings by cost curves - Methodology and application," *Applied Energy*, vol. 162, pp. 653–665, 2016, ISSN: 03062619. DOI: 10.1016/j.apenergy.2015.10.114 (Cited on page 36).

[128] Gobierno de España. Ministerio de Industria Energía y Turismo, *Real Decreto 216/2014, de 28 de marzo, por el que se establece la metodología de cálculo de los precios voluntarios para el pequeño consumidor de energía eléctrica y su régimen jurídico de contratación*, 2014. [Online]. Available: https://www.boe.es/boe/dias/2014/03/29/pdfs/BOE-A-2014-3376.pdf (Cited on page 37).

[129] J. Clauß, S. Stinner, I. Sartori, and L. Georges, "Predictive rule-based control to activate the energy flexibility of Norwegian residential buildings: Case of an air-source heat pump and direct electric heating," *Applied Energy*, vol. 237, no. December 2018, pp. 500–518, Mar. 2019, ISSN: 03062619. DOI: 10.1016/j.apenergy.2018.12.074 (Cited on page 37).

[130] P. Vogler-Finck, R. Wisniewski, and P. Popovski, "Reducing the carbon footprint of house heating through model predictive control – A simulation study in Danish conditions," *Sustainable Cities and Society*, vol. 42, no. January, pp. 558–573, 2018, ISSN: 22106707. DOI: 10.1016/j.scs.2018.07.027 (Cited on page 37).

[131] A. Hawkes, "Estimating marginal CO2 emissions rates for national electricity systems," *Energy Policy*, vol. 38, no. 10, pp. 5977–5987, 2010, ISSN: 03014215. DOI: 10.1016/j.enpol.2010.05.053 (Cited on pages 38, 39).

[132] Red Electrica de España, *ESIOS – Sistema de información del operador del sistema.* 2018. [Online]. Available: https://www.esios.ree.es/en%20(accessed%2007/03/2018) (visited on 04/04/2017) (Cited on pages 38, 82, 92).

[133] IPCC Working Group III, "Annex III: Technology-specific cost and performance parameters - IPCC," in *Climate Change 2014: Mitigation of Climate Change*, 5th Assess, IPCC, 2014 (Cited on page 38).

[134] U. R. Fritsche and H.-W. Greß, "Development of the Primary Energy Factor of Electricity Generation in the EU-28 from 2010-2013," IINAS, Darmstadt, Germany, Tech. Rep. March, 2015 (Cited on page 41).

[135] M. Lu and A. Hasan, "Literature Review on Metrics and Indicators for Energy Flexibility in Single Buildings, Internal Report of IEA EBC Annex 67 Activity A.2.1.," Tech. Rep., 2016 (Cited on page 42).

[136] J. Clauß, C. Finck, P. Vogler-Finck, and P. Beagon, "Control strategies for building energy systems to unlock demand side flexibility – A review," in *15th International Conference of the International Building Performance Simulation Association, San Franciso, USA*, San Francisco, USA, 2017 (Cited on page 42).

[137] J. Le Dréau and P. Heiselberg, "Energy flexibility of residential buildings using short term heat storage in the thermal mass," *Energy*, vol. 111, no. 1, pp. 1–5, 2016, ISSN: 03605442. DOI: 10.1016/j.energy.2016.05.076 (Cited on pages 42, 75).

[138] R. De Coninck and L. Helsen, "Quantification of flexibility in buildings by cost curves - Methodology and application," *Applied Energy*, vol. 162, pp. 653–665, 2016, ISSN: 03062619. DOI: 10.1016/j.apenergy.2015.10.114 (Cited on page 42).

[139] G. Reynders, R. Amaral Lopes, A. Marszal-Pomianowska, D. Aelenei, J. Martins, and D. Saelens, "Energy flexible buildings: An evaluation of definitions and quantification methodologies applied to thermal storage," *Energy and Buildings*, vol. 166, pp. 372–390, 2018, ISSN: 03787788. DOI: 10.1016/j.enbuild.2018.02.040 (Cited on page 42).

[140] CEN, *EN 15251: Indoor environmental input parameters for design and assessment of energy performance of buildings addressing indoor quality, thermal environment, lighting and acoustic*, Brussels, Belgium, 2007 (Cited on pages 44, 75, 86, 99).

[141] European Commission, *2013/114/EU Commission Decision of 1 March 2013 establishing the guidelines for Member States on calculating renewable energy from heat pumps from different heat pump technologies pursuant to Article 5 of Directive 2009/28/EC of the European Parliament an*, 2013 (Cited on page 50).

[142] CEN, *EN 14511-2: Air conditioners, liquid chilling packages and heat pumps with electrically driven compressors for space heating and cooling - Part 2: Test conditions*, Brussels, Belgium, 2012 (Cited on pages 51, 52, 54, 108).

[143] ——, *EN 14825: Air conditioners, liquid chilling packages and heat pumps, with electrically driven compressors, for space heating and cooling - Testing and rating at part load conditions and calculation of seasonal performance*, Brussels, Belgium, 2013 (Cited on pages 51, 66, 108).

[144] C. Verhelst, F. Logist, J. Van Impe, and L. Helsen, "Study of the optimal control problem formulation for modulating air-to-water heat pumps connected to a residential floor heating system," *Energy and Buildings*, vol. 45, pp. 43–53, 2012, ISSN: 03787788. DOI: 10.1016/j.enbuild.2011.10.015 (Cited on pages 60, 62, 121).

[145] G. St-Onge, M. Kummert, and M. Kegel, "Variable capacity mini-split air source heat pump model for TRNSYS," in *eSim 2018, the 10th Conference of IBPSA-Canada*, Montréal (QC), Canada, 2018, ISBN: 9782921145886 (Cited on page 61).

[146] M. Palonen, M. Hamdy, and A. Hasan, "MOBO A New Software for Multi-Objective Building Performance Optimization," in *Proceedings of the 13th Conference of International Building Performance Simulation Association (IBPSA)*, Chambéry, France, 2013, pp. 2567–2574. [Online]. Available: http://www.ibpsa.org/proceedings/bs2013/p%7B%5C_%7D1489.pdf (Cited on page 64).

[147] H. Blervaque, P. Stabat, S. Filfli, M. Schumann, and D. Marchio, "Variable-speed air-to-air heat pump modelling approaches for building energy simulation and comparison with experimental data," *Journal of Building Performance Simulation*, vol. 1493, no. July 2015, pp. 1–16, 2015, ISSN: 1940-1493. DOI: 10.1080/19401493.2015.1030862 (Cited on page 66).

[148] J. Ortiz, F. Guarino, J. Salom, C. Corchero, and M. Cellura, "Stochastic model for electrical loads in Mediterranean residential buildings: Validation and applications," *Energy and Buildings*, vol. 80, pp. 23–36, 2014, ISSN: 03787788. DOI: 10.1016/j.enbuild.2014.04.053 (Cited on pages 68, 71).

[149] P. Taddeo, J. Ortiz, J. Salom, E. Lucas Segarra, V. Gutiérrez González, G. Ramos Ruiz, and C. Fernández Bandera, "Comparison of experimental methodologies to estimate the air infiltration rate in a residential case study for calibration purposes," in *39th AIVC 2018 - Smart Ventilation for Buildings - 18-19th September 2018*, Antibes, France, 2018 (Cited on page 68).

[150] C. Ghiaus and I. Hazyuk, "Calculation of optimal thermal load of intermittently heated buildings," *Energy and Buildings*, vol. 42, no. 8, pp. 1248–1258, 2010, ISSN: 03787788. DOI: 10.1016/j.enbuild.2010.02.017 (Cited on page 68).

[151] M. Benedettelli, "Optimization of building performance via model-based predictive control," PhD thesis, Università Politecnica delle Marche, 2018. [Online]. Available: http://hdl.handle.net/11566/252888 (Cited on page 69).

[152] R. De Coninck and L. Helsen, "Practical implementation and evaluation of model predictive control for an office building in Brussels," *Energy and Buildings*, vol. 111, pp. 290–298, 2016, ISSN: 03787788. DOI: 10.1016/j.enbuild.2015.11.014 (Cited on pages 69, 124).

[153] H. Johra and P. Heiselberg, "Influence of internal thermal mass on the indoor thermal dynamics and integration of phase change materials in furniture for building energy storage: A review," *Renewable and Sustainable Energy Reviews*, vol. 69, no. May 2016, pp. 19–32, 2017, ISSN: 18790690. DOI: 10.1016/j.rser.2016.11.145 (Cited on pages 69, 72).

[154] G. Reynders, J. Diriken, and D. Saelens, "Quality of grey-box models and identified parameters as function of the accuracy of input and observation signals," *Energy and Buildings*, vol. 82, pp. 263–274, Oct. 2014, ISSN: 03787788. DOI: 10.1016/j.enbuild.2014.07.025 (Cited on pages 69, 119).

[155] H. Viot, A. Sempey, L. Mora, J. C. Batsale, and J. Malvestio, "Model predictive control of a thermally activated building system to improve energy management of an experimental building: Part I—Modeling and measurements," *Energy and Buildings*, vol. 172, pp. 94–103, 2018, ISSN: 03787788. DOI: 10.1016/j.enbuild.2018.04.055 (Cited on page 69).

[156] H. Madsen, P. Bacher, G. Bauwens, A.-H. Deconinck, G. Reynders, S. Roels, E. Himpe, and G. Lethé, "Thermal Performance Characterization using Time Series Data - IEA EBC Annex 58 Guidelines," Tech. Rep., 2015. DOI: 10.13140/RG.2.1.1564.4241 (Cited on page 71).

[157] L. Ljung, *MATLAB System Identification Toolbox - Getting Started Guide R2016a*, Mathworks, Ed. Mathworks, 2016 (Cited on page 71).

[158] K. Antonopoulos and E. Koronaki, "Apparent and effective thermal capacitance of buildings," *Energy*, vol. 23, no. 3, pp. 183–192, Mar. 1998, ISSN: 03605442. DOI: 10.1016/S0360-5442(97)00088-1 (Cited on page 72).

[159] T. Péan, J. Salom, and J. Ortiz, "Potential and optimization of a price-based control strategy for improving energy flexibility in Mediterranean buildings," *Energy Procedia*, vol. 122, pp. 463–468, Sep. 2017, ISSN: 18766102. DOI: 10.1016/j.egypro.2017.07.292 (Cited on pages 77, 79).

[160] J. Maciejowski, *Predictive control with constraints*. Jun. 2002, ISBN: 0-201-39823-0 PPR (Cited on page 84).

[161] B. Bleys, O. Gerin, and K. Dinne, "The risk of Legionella development in sanitary installations," in *REHVA Annual Meeting Conference 2018 - Low Carbon Technologies in HVAC*, Brussels, Belgium, 2018, pp. 1–8 (Cited on page 86).

[162] S. Benett, *Real-Time Computer Control: An Introduction*, Prentice H. Prentice Hall, 1993, ISBN: 978-0137641765 (Cited on page 86).

[163] K. J. Åström and B. Wittenmark, *Computer-Controlled Systems: Theory and Design*, Prentice H. Tom Robbins, 1997, ISBN: 0-13-314899-8 (Cited on pages 86, 87).

[164] Y. Su, K. K. Tan, and T. H. Lee, "Computation delay compensation for real time implementation of robust model predictive control," in *IEEE 10th International Conference on Industrial Informatics*, IEEE, 2012, pp. 242–247, ISBN: 9781467303118. DOI: 10.1109/INDIN.2012.6301174 (Cited on page 87).

[165] H. Thieblemont, F. Haghighat, R. Ooka, and A. Moreau, "Predictive control strategies based on weather forecast in buildings with energy storage system: A review of the state-of-the art," *Energy and Buildings*, vol. 153, pp. 485–500, 2017, ISSN: 03787788. DOI: 10.1016/j.enbuild.2017.08.010 (Cited on pages 88, 102, 119).

[166] M. Killian and M. Kozek, "Ten questions concerning model predictive control for energy efficient buildings," *Building and Environment*, vol. 105, pp. 403–412, 2016, ISSN: 03601323. DOI: 10.1016/j.buildenv.2016.05.034 (Cited on pages 119, 124).

[167] F. Ferracuti, A. Fonti, L. Ciabattoni, S. Pizzuti, A. Arteconi, L. Helsen, and G. Comodi, "Data-driven models for short-term thermal behaviour prediction in real buildings," *Applied Energy*, vol. 204, pp. 1375–1387, 2017, ISSN: 03062619. DOI: 10.1016/j.apenergy.2017.05.015 (Cited on page 119).

[168] S. Prívara, J. Cigler, Z. Váňa, F. Oldewurtel, C. Sagerschnig, and E. Žáčeková, "Building modeling as a crucial part for building predictive control," *Energy and Buildings*, vol. 56, pp. 8–22, 2013, ISSN: 03787788. DOI: 10.1016/j.enbuild.2012.10.024 (Cited on page 119).

[169] Institute for Housing and Environment (Germany), *TABULA project*, 2016. [Online]. Available: http://episcope.eu/ (visited on 08/20/2019) (Cited on page 119).

[170] S. Rouchier, M. J. Jiménez, and S. Castaño, "Sequential Monte Carlo for on-line parameter estimation of a lumped building energy model," *Energy and Buildings*, vol. 187, pp. 86–94, 2019, ISSN: 03787788. DOI: 10.1016/j.enbuild.2019.01.045 (Cited on page 120).

[171] P. Radecki and B. Hencey, "Online Model Estimation for Predictive Thermal Control of Buildings," *IEEE Transactions on Control Systems Technology*, vol. 25, no. 4, pp. 1414–1422, 2017, ISSN: 10636536. DOI: 10.1109/TCST.2016.2587737 (Cited on page 120).

[172] G. Wood, R. Day, E. Creamer, D. van der Horst, A. Hussain, S. Liu, A. Shukla, O. Iweka, M. Gaterell, P. Petridis, N. Adams, and V. Brown, "Sensors, sense-making and sensitivities: UK household experiences with a feedback display on energy consumption and indoor environmental conditions," *Energy Research and Social Science*, vol. 55, no. April, pp. 93–105, 2019, ISSN: 22146296. DOI: 10.1016/j.erss.2019.04.013 (Cited on page 120).

[173] O. B. Kazanci and B. W. Olesen, "Sustainable Plus-energy Houses (Baeredygtige Energi-Plus huse) Final Report," Elforsk, Tech. Rep., 2014. [Online]. Available: https://elforsk.dk/sites/elforsk.dk/files/media/dokumenter/elforsk/Slutrapport%7B%5C_%7D344-060%7B%5C%%7D2520med%7B%5C%%7D2520bilag.pdf (Cited on page 121).

[174] M. Hu, F. Xiao, J. B. Jørgensen, and S. Wang, "Frequency control of air conditioners in response to real-time dynamic electricity prices in smart grids," *Applied Energy*, vol. 242, no. March, pp. 92–106, 2019, ISSN: 03062619. DOI: 10.1016/j.apenergy.2019.03.127 (Cited on page 123).

[175] Bundersverband Wärmepumpe, *Regularium für das Label "SG Ready" für elektrische Heizungs- und Warmwasserwärmepumpen*, Berlin, Germany, 2013 (Cited on page 124).

[176] D. Fischer, T. Wolf, and M.-A. Triebel, "Flexibility of heat pump pools: The use of SG-Ready from an aggregator's perspective," *12th IEA Heat Pump Conference*, pp. 1–12, 2017 (Cited on page 124).

[177] OpenADR Alliance, *OpenADR*, 2019. [Online]. Available: https://www.openadr.org/ (visited on 08/19/2019) (Cited on page 124).

[178] SMS-PLC, *SmArt BI-directional multi eNergy gAteway*, 2019. [Online]. Available: https://sabina-project.eu/mission-objectives/ (visited on 09/15/2019) (Cited on page 128).

List of Figures

List of Tables

Appendices

Appendix A

Detailed table of the MPC objective functions

Table A.1, found in the next page, shows the comparison of the objective functions found in existing literature about MPC for the control of heat pumps. It is an extended version of Table II.2 in chapter II. The table is also available in [50].

Appendix

Table A.3. Detailed table of the objective functions.

Reference	Objective function	Economic term	Energy term	Peak shaving term	CO_2 term	Robustness term/slack variable	Flexibility term	(Dis)comfort term
Masy et al. (2015)	$J =$	$\sum_k P_{el}(k) \cdot W_{hp}(k)$					$+\alpha \cdot$	$\sum_k \theta_{occ}(k) \cdot (\varepsilon_{min}(k) + \varepsilon_{max}(k))$
Tahersima et al. (2012)	$J =$	$\sum_k P_{el}(k) \cdot T_{sup}(k)$					$+$	$\sum_k \lvert T_{zon}(k) - T_{set}(k) \rvert$
Li and Malkawi (2016)	$J =$	$\sum_k G_g(k) P_g(k) + P_{el}(k) W_{hp}(k)$					$+\alpha$	$\sum_k (\theta_{occ}(k) \cdot PMV(k))^2$
Verhelst et al. (2012)	$J = (1-\alpha) \cdot$	$\sum_k P_{el}(k) \cdot W_{hp}(k)$					$+\alpha$	$\sum_k (T_{zon}(k) - T_{set}(k))^2$
Pedersen et al. (2013)	$J =$	$\sum_{k=1}^{24} E_{hp}(k) \mathrm{P}_{el}(k)$					$+$	$\sum_{k=1}^{24} \lvert T_{ref}(k) - T(k) \rvert \alpha(k)$
Kajgaard et al. (2011)	$J =$	$\alpha \sum_k P_{el}(k) \cdot W_{hp}(k)$	$+$			$\sum_k l_{int}(x(k))$	$+$	$\sum_k l_{comf}(T_{zon}(k) - T_{set})$
Halvgaard et al. (2012)	$J =$	$\sum_k c(k) \cdot u(k)$	$+$			$\sum_k \rho \cdot v(k)$		
Santos et al. (2016)	$J =$	$\sum_k c(k) \cdot u(k)$	$+$			$\sum_k \rho \cdot v(k)$		
Bianchini et al. (2016)	$J =$	$\sum_k P_{el}(k) \cdot W_{hp}(k)$	$-$				$\sum_j \gamma_j R_j$	
Knudsen and Petersen (2016)	$J = (1-\alpha) \cdot$	$\sum_k c(k) \cdot u(k)$	$+\beta \cdot$		$\sum_k e(k) \cdot u(k)$			
Sichilalu et al. (2015)	$J =$	$\sum_k (\alpha \cdot P_{el}(k) \cdot W_{cons}(k) - \beta \cdot P_{el} \cdot W_{prod}(k))$						
Mendoza-Serrano et al. (2014)	$J =$	$\sum_k P_{el}(k) \cdot W_{hp}(k) \cdot \Delta t$						
Salpakari and Lund (2015)	$J =$	$\sum_k P_{el,net}(k) \cdot W_{net}(k)$						
Toersche et al. (2012)	$J =$			$\sum_{k=2}^{N} \left\lvert \sum_{j=1}^{H} W_{hp}(k,j) - \sum_{j=1}^{H} W_{hp}(k-1,j) \right\rvert$				
Ma et al. (2014)	$J =$	$\sum_k P_{el}(k) \cdot W_{hp}(k) \cdot \Delta t$	$+$	$P_p \cdot \max\{W(k)\}$				
Sturzenegger et al. (2013)	$J =$		$\sum_k c(k) \cdot u(k)$					
Oldewurtel et al. (2013)	$J =$		$\sum_k c(k) \cdot u(k)$					
De Coninck et al. (2016)	$J =$	$\sum_k G_g(k) P_g(k) + P_{el}(k) W_{hp}(k)$	$+\alpha \cdot$				$(E - E_{target})^2$ $+\beta \cdot$	$\sum_k \theta_{occ}(k) \cdot (T_{zon}(k) - T_{set}(k))^2$
Vana et al. (2014)	$J =$	$\sum_k c(k) \cdot u(k)$	$+$			$\sum_k \beta \cdot \lvert u(k) - u(k-1) - v(k) \rvert_2^2$		$+$ $\sum_k (\lvert A(y(k) - z(k)) \rvert_2^2 + \lvert A^c(y(k) - z^c(k)) \rvert_2^2)$

Table A.1. Objective functions used in the MPC in existing literature.

As far as possible, the terms used in each referenced article were homogenized using the common nomenclature. However some terms were not introduced in the text:

- α's and β's are weighing factors to balance between the different objectives
- In Masy et al. (2015)[31], $\varepsilon_{\mathrm{low}}$ and $\varepsilon_{\mathrm{high}}$ are used to soften the constraints as follows: $T_{min} - \varepsilon_{min} \leq T_{zon} \leq T_{max} + \varepsilon_{max}$
- In Pedersen et al. (2013)[48], $\alpha(k)$ is a vector of factors that weight between cost and discomfort
- In Kajgaard et al. (2011)[49], l_{comf} and l_{int} are convex cost functions used for comfort (the former uses the temperature error, the latter the integral of that error).
- In Bianchini et al. (2016)[52], $\gamma_j \mathrm{R}_j$ represents the fulfillment of j-th DR request (=1 if the request was fulfilled). The cost function tries to minimize the opposite of that quantity, so that to maximize the number of fulfilled DR requests.
- In Toersche et al. (2012)[57], the double sum corresponds to the successive changes in the energy use. Minimizing this term enables to flatten the energy use profile.
- In Vana et al. (2014)[62], A and A^c define two different comfort ranges: one that can be violated from time to time (with a low cost), and a stricter one that should not be violated at almost any time (with a high cost).

Appendix B

Thermal power of the heat pump in function of the supply and return temperatures

Figure B.1 shows the thermal power levels observed in the static tests both in heating and cooling modes. In heating mode, the left point of each line correspond to the return temperature, and the right point the supply temperature. In cooling mode, they are reversed. In these graphs, the actual value of T_{sup} can be compared with its set-point $T_{sup,SP}$. In heating mode, mostly when $T_{sup,SP}$ is set to high values like 55 or 45°C, and when the outdoor temperature is colder (-7 or 2°C), the heat pump cannot reach the desired set-point. In cooling mode, it is mostly when $T_{sup,SP}$ is set to low values like 7°C that the heat pump cannot reach this value. Furthermore, an offset can be observed in the "normal cases", especially in cooling mode: the internal heat pump sensor must measure a lower supply temperature than the one of the laboratory (the one represented in the graphs), which explains why it seems that the heat pump never reaches the set-point.

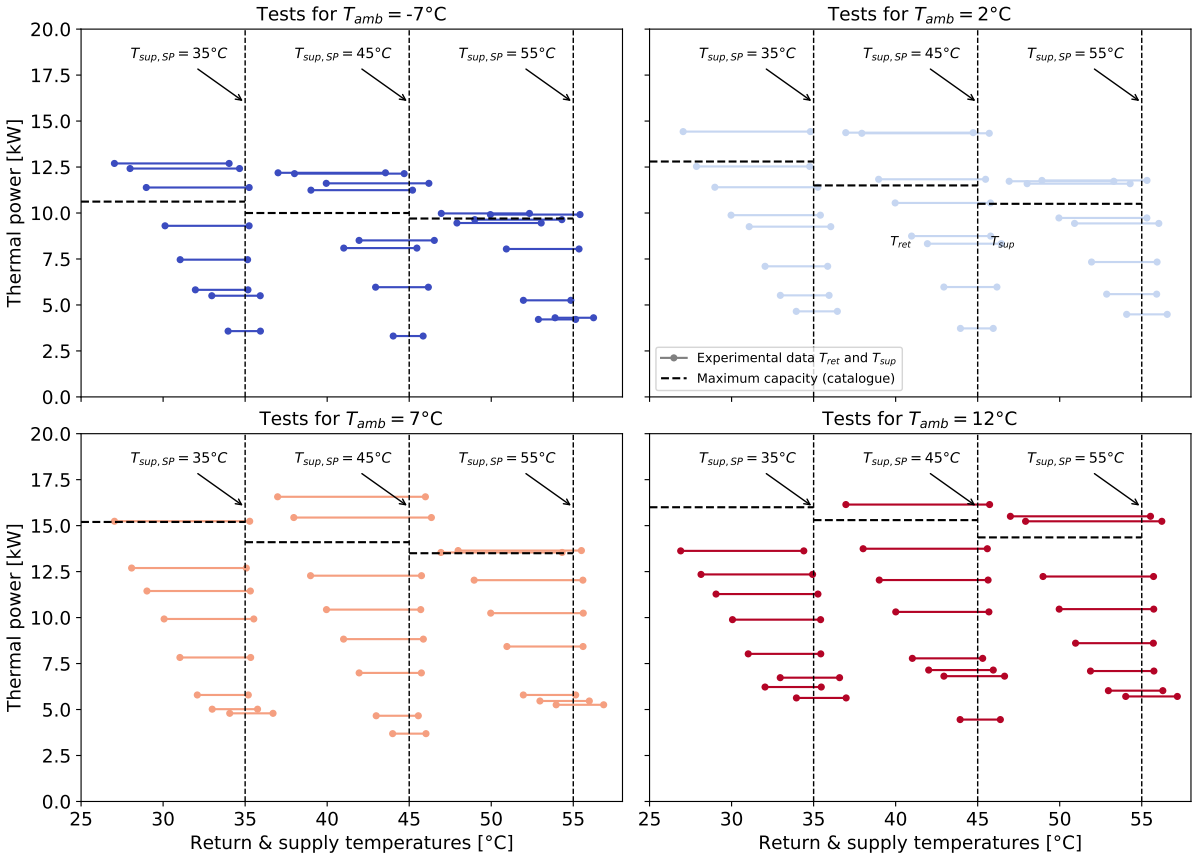

(a)

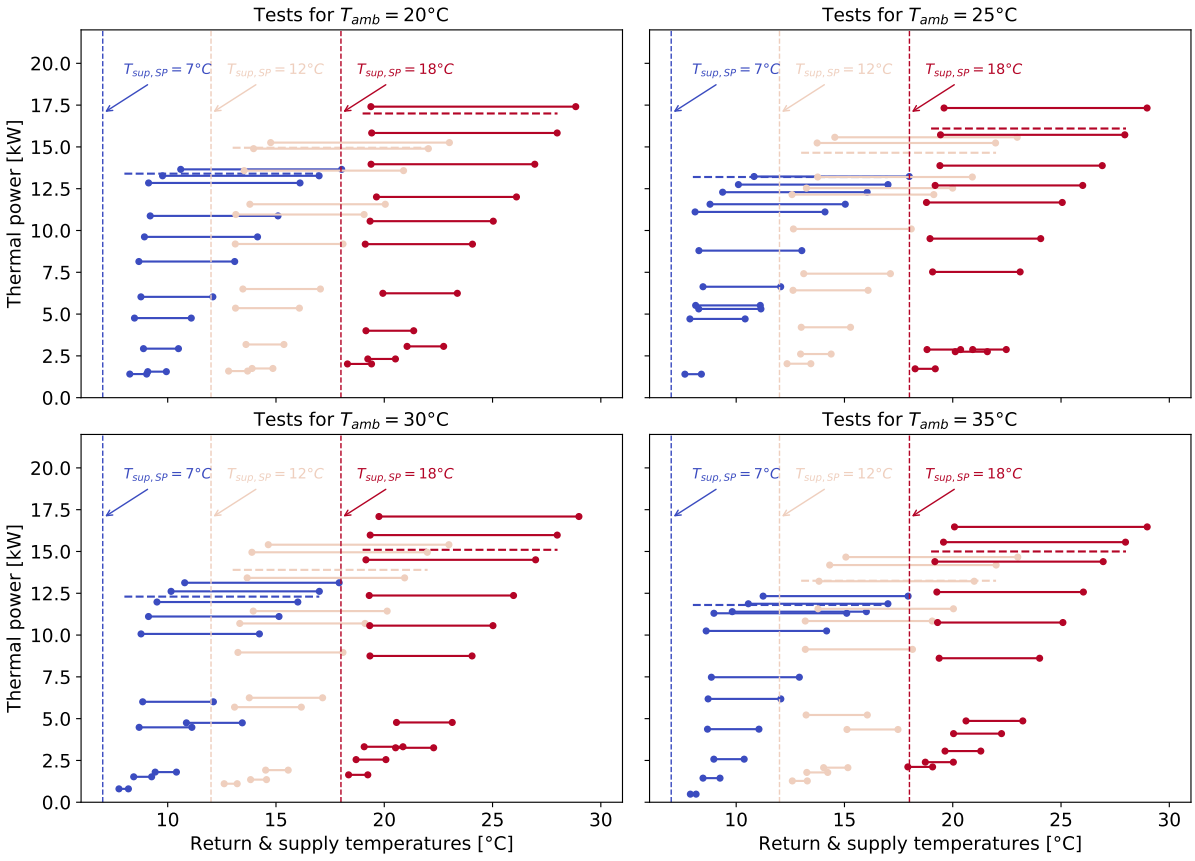

(b)

Figure B.1. Thermal power of the heat pump in the heating (a) and cooling (b) static tests, showing both the supply and return temperatures.

Appendix C

Alternative modeling approach for VSHP in TRNSYS

In the thesis, the chosen approach for developing a detailed heat pump model in TRNSYS was through black-box polynomial models and a PID controller regulating the frequency of the compressor. An alternative approach would consist in combining existing Types of TRNSYS in order to obtain a reliable VSHP model: Type941 gives the performance at full-load, and Type43 enables to modulate that performance at part-load, with a curve obtained from experimental or catalogue data. In that case, the PID controller determines the capacity ratio at part-load (CR), or in the other words, the percentage of the full capacity at which the heat pump has to operate.

This approach is presented here in Figure C.1. This model was used in [60], but not in the co-simulations of the present thesis; for this reason it is mentioned as an appendix. Two TRNSYS types require some input about the specific heat pump system used in the simulation for such model. Type 941 needs to be provided with a map of different points describing the performance in different conditions, at full load capacity. These data can usually be retrieved from manufacturer catalogues, where the points following the testing standard for heat pumps must be reported. Type 43 uses the part-load performance data reported in section 3.4.3 of Chapter III, namely the curve linking the part-load performance PLF with the capacity ratio CR.

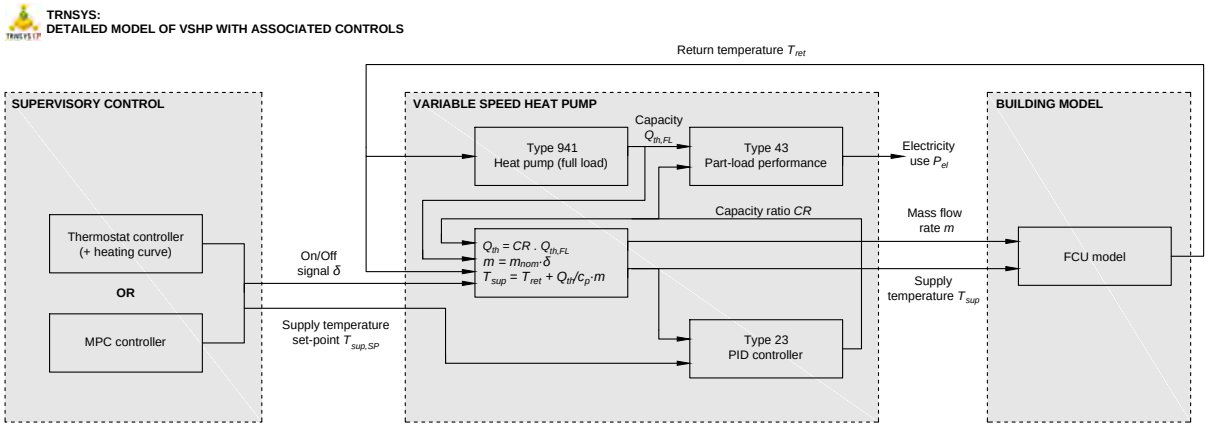

Figure C.1. Schematic of the alternative detailed TRNSYS heat pump model.